SOUTHWEST RESEARCH INSTITUTE®

Internal Research and Development 2014

The SwRI IR&D Program exists to broaden the Institute's technology base and to encourage staff professional growth. Internal funding of research enables the Institute to advance knowledge, increase its technical capabilities, and expand its reputation as a leader in science and technology. The program also allows Institute engineers and scientists to continually grow in their technical fields by providing freedom to explore innovative and unproven concepts without contractual restrictions and expectations.

- Space Science
- Materials Research & Structural Mechanics
- Intelligent Systems, Advanced Computer & Electronic Technology, & Automation
- Measurement & Nondestructive Evaluation of Materials & Structures
- Engines, Fuels, Lubricants, & Vehicle Systems
- Geology & Nuclear Waste Management
- Fluid & Machinery Dynamics
- Electronic Systems & Instrumentation
- Chemistry & Chemical Engineering

SOUTHWEST RESEARCH INSTITUTE®

SwRI IR&D 2014 – Space Science

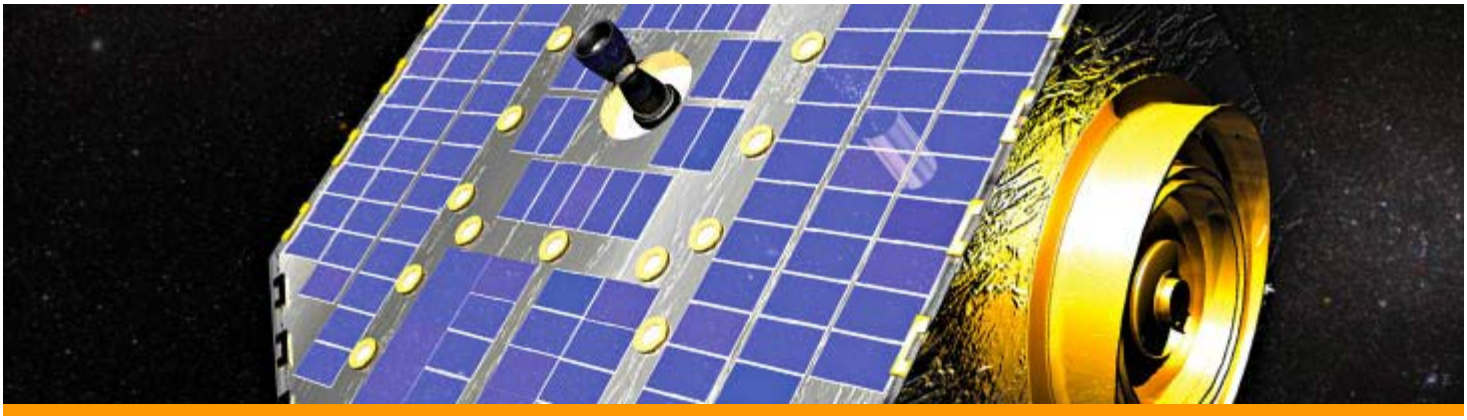

- Critical Technology for Next Generation Neutral Atom Imaging Instruments for Space Research, 15-R8298
- Capability Development for Extreme Ultraviolet Imaging and Calibration, 15-R8322
- An Advanced UV Spectrograph Concept for the JUICE Ganymede Orbiter Mission, 15-R8324
- Carbon Foils Properties for Space Plasma Instrumentation, 15-R8340
- Developing Mission Operations Center Capabilities, 15-R8366
- Development of High Voltage Optocoupler for Space Applications, 15-R8388
- Development of a Compact Raman Visible Spectrograph Design for a NASA Mars 2020 Rover Instrument Proposal, 15-R8416
- Validation of SwRI Suborbital Program Experiments Through Zero-g Flight Demonstration of Flight-Ready Hardware, 15-R8417
- Modeling of an Europan Exosphere with Plumes, 15-R8453
- Space-Based Communications Processing, 15-R8469
- Testing of Prototype Mass Spectrometer for Earth Atmospheric Studies, 15-R8475

SOUTHWEST RESEARCH INSTITUTE®

SwRI IR&D 2014 – Materials Research & Structural Mechanics

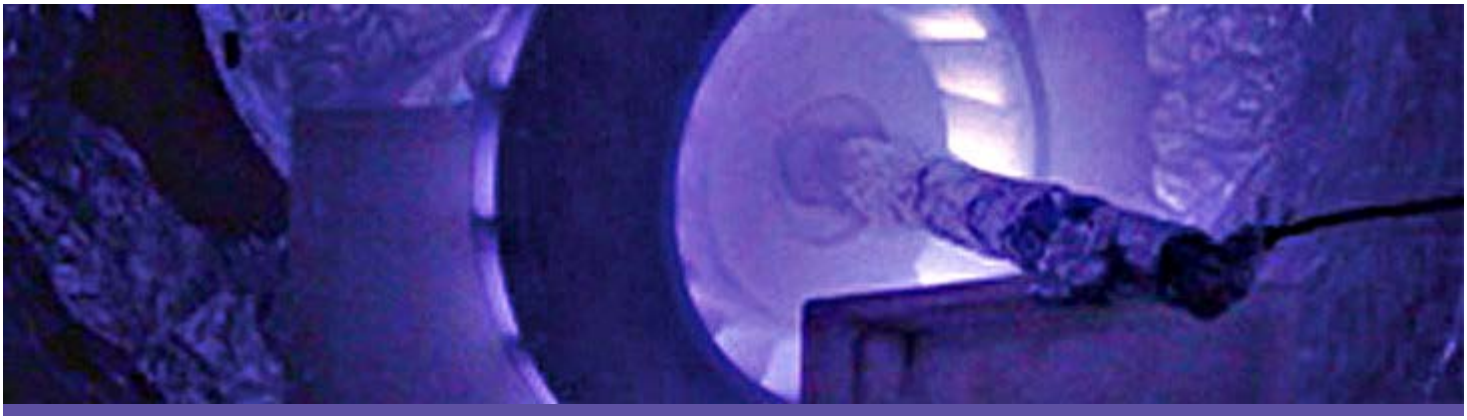

- Crack-Size Effect in Corrosion-Fatigue Crack Growth, 18-R8357
- Development and Characterization of Low Friction-Nanocomposite Films/Coatings for Piston Rings, 18-R8381
- The Development of a Dynamic Finite Element Model of the Temporomandibular Joint (TMJ) and Study of Joint Mechanics, 18-R8386
- NASA Uncertainty Quantification Challenge and Treatment of Multiple Uncertainty Types, 18-R8406
- Development and Evaluation of Corrosion Resistant Alloy Coatings for Inner Surface of Tubes and Closed-end Vessels, 18-R8437
- Design and Development of a New Gripping System and Direct Stress Measurement Method for High Strain Rate Materials Testing, 18-R8473
- Investigation of Computational Methods for Modeling Bird Strike Impacts on Aircraft Structures, 18-R8477
- Developing a Three-Dimensional Model to Estimate Electrical Current Requirement at a Coating Defect Site on Pipeline Segments Installed Using Horizontal Directional Drilling, 20–R8429
- Dynamic Response of Steel-Plate and Concrete Composite Small Modular Reactor Structures Under Explosive and Seismic Loads, 20–R8433
- Development of a Numerical Approach to Modeling Internal Erosion in Embankment Dams and Levees, 20–R8463

SOUTHWEST RESEARCH INSTITUTE®

SwRI IR&D 2014 – Intelligent Systems, Advanced Computer & Electronic Technology, & Automation

- Mobile Persistent Stare Using Unmanned Systems, 10-R8306
- ROS-Industrial® Strategic Technology Development, 10-R8335
- Control of Laser Coating Removal Process, 10-R8385
- Microwave Methods for Enhanced Combustion in Natural Gas Engine Applications, 10-R8408
- Object Ranging and Classification using 3-Dimensional Shapes 10-R8421
- Low Cost Accurate Six-DOF Industrial Robot Localization System Software Modeling and Testing, 10-R8443
- Vision-based Localization, 10-R8452
- Cooperative Control of a Deployable Aerial Sensor Platform, 10-R8462
- Dynamic Transmisson Conductor Measurement, 10-R8466
- Data Management Architectures for Gigabit per Second, Terabit Capacity Non-Volatile Data Storage, 15-R8468

SOUTHWEST RESEARCH INSTITUTE®

SwRI IR&D 2014 – Measurement & Nondestructive Evaluation of Materials & Structures

- Formation Impact Study of Lithium-ion Battery Capacity, Cycle Life, and Safety, 03-R8277
- Development of the MsSR4040 SF Magnetostrictive Sensor Technology, 18-R8328
- Online Monitoring System to Detect Microbial Induced Corrosion, 18-R8445
- Development of a Corrosion Sensor Technology for Buried Piping, 18-R8472

SOUTHWEST RESEARCH INSTITUTE®

SwRI IR&D 2014 – Engines, Fuels, Lubricants, & Vehicle Systems

- Development of a Methodology to Generate On-Board Diagnostic Threshold Selective Catalytic Reduction Catalysts for Heavy-Duty Diesel Applications, 03-R8376
- FOCAS HGTR Design Evolution to a High Pressure Fully Transient System — Creation of the Full-Scale Gas Reactor, 03-R8427
- Feasibility of Detecting Low-Speed Pre-Ignition (LSPI) and Suppressing the Subsequent Knock in High-Performance Spark Ignited Gasoline Engines, 03-R8428
- Identifying and Elucidating Low Temperature Limiters to Catalyst Activity, 03-R8435
- Extension of SwRI's Multidimensional Control Framework to Fueling and Ignition Control of Spark-Ignited Engines, 03-R8438
- Sampling System Investigation for the Determination of Semi-Volatile Organic Compounds (SVOC) Emissions from Engine Exhaust, 03-R8442
- Investigation into the Achievable Load and Misalignment Dynamics of a Crankshaft Bearing Test Rig, 03-R8455
- Dedicated EGR on a Natural Gas Engine, 03-R8457
- Investigation into Engine Wear Map Development with Radioactive Tracer Testing, 03-R8479
- Elucidating the Effects of Lubricant Viscosity, Oxidation and Soot Loading on Total and Component Engine Friction, 08-R8300
- Detecting Piston Ring Instability with Engine Vibration Analysis, 08-R8342

- Investigation of an Oleophobic Coating Effect on Gasoline Direct Injection (GDI) Engine Components to Reduce Carbon Deposits, 08-R8362
- Determination of PAHs in the Tires by GC/MS, 08-R8402

SOUTHWEST RESEARCH INSTITUTE®

SwRI IR&D 2014 – Geology & Nuclear Waste Management

- Testing Frequency-Dependent Geoelectrical Methods and Processing Techniques to Characterize Subsurface Ice, 15-R8422
- Integrity Management of Nuclear Power Plant Components Subjected to Localized Corrosion Using Time-Dependent Probabilistic Model, 20–R8267
- Integrated Physical Analog and Numerical Modeling of Geologic Structures, 20–R8368
- Hypothesis Testing for Subfreezing Mass Movements, 20–R8407
- Landslide Investigations Using Satellite-Based Multitemporal Synthetic Aperture Radar Techniques, 20-R8410
- Developing Methodologies for Gravity-Assisted Solution Mining, 20-R8423
- Evaluating Properties of Chemically-Aged High-Density Polyethylene Piping Material Used in Nuclear Power Plants, 20–R8432
- Assessment of Thermal Fatigue in Light Water Reactors Feedwater Systems by Fluid-Structure Interaction Analyses, 20–R8434
- Detection of Uranium Mill Tailings Cover Erosion Rates and Settlement Using Satellite-Based Radar Interferometry, 20-R8449

SOUTHWEST RESEARCH INSTITUTE®

SwRI IR&D 2014 – Fluid & Machinery Dynamics

- Improvement of Wet Gas Compressor Performance using Gas Ejection, 18-R8327
- Development and Demonstration of Erosion Prediction Capabilities for Oil and Gas Industry Applications, 18-R8338
- Testing and Analysis of Acoustically Induced Vibration Stresses in Piping Systems, 18-R8478
- Efficient Methods for Uncertainty Propagation in Computational-Fluid-Dynamics-Based Fire PRA, 20-R8271

SOUTHWEST RESEARCH INSTITUTE®

SwRI IR&D 2014 – Electronic Systems & Instrumentation

- Development of a Wireless Power Transfer Technique for Quick-Charging Inaccessible Electronic Devices, 14-R8363
- Nanogenerators for Energy Harvesting, 14-R8405
- Artificial Muscle Risk Reduction and Cookbook, 14-R8465
- Design and Analysis of Device to Capture Stratospheric Air Samples, 15-R8446
- Two-Fault-Tolerant Fault Detection and Isolation on a Resource Constrained Platform in Space, 15-R8459

SOUTHWEST RESEARCH INSTITUTE®

SwRI IR&D 2014 – Chemistry & Chemical Engineering

- Humanized Organophosphorus Hydrolase Expressed in Human Embryonic Kidney Cells: Pharmacokinetics in the Guinea Pig Model, 01-R8280
- High Octane Number Gasoline Production from Lignin, 01-R8384
- Development of a Low-Cost Method of Treating Flow-Back Water from Hydraulic Fracturing, 01-R8414
- Investigation of the Rheology and Tribology Properties of Mono-Oleate for Use as an Additive for SAE J1488-10 Emulsified Fuel-Water Separation Test Method, 08-R8389

2014 IR&D Annual Report

Critical Technology for Next Generation Neutral Atom Imaging Instruments for Space Research, 15-R8298

Principal Investigators
Stephen A. Fuselier
Frédéric Allegrini
Robert W. Ebert

Inclusive Dates: 04/01/12 – 03/31/14

Background — The successes of energetic neutral atom (ENA) imagers on the SwRI-led Imager for Magnetopause to Aurora: Global Exploration (IMAGE), Two Wide-angle Imaging Neutral atom Spectrometers (TWINS), and Interstellar Boundary Explorer (IBEX) missions have solidified this measurement technique as a critical component of future NASA heliospheric and magnetospheric missions. Most imagers have an important subsystem that converts an incoming neutral atom to an ion. These conversion systems rely on ultra-thin carbon foils and diamond-like carbon (DLC) surfaces and are the least efficient subsystem in a neutral atom imager, especially at energies below 1 keV. This is because the probability of producing a charged particle decreases dramatically for neutral atom energies below 1 keV. Furthermore, the probability of transmission through a carbon foil also decreases dramatically below about 0.5 keV, making the overall efficiency very low at energies of a few hundred eV.

Recently, a new type of thin carbon surface has emerged — graphene. Graphene is composed of carbon atoms that are packed into a honeycomb crystal lattice. It is a two-dimensional structure (one-atom thick) that, on an atomic scale, is best described as chicken wire. Because they are thinner, these foils may have significantly better transmission for incident particles and produce less scattering, especially at critical energies below 1 keV. In addition, conversion efficiencies for the DLC surfaces used in instruments designed to measure low energy (~0.01 to 1 keV) ENAs are typically below 10 percent and are often 1 percent or less. Small improvements in these efficiencies, especially at lower energies, would result in an enormous improvement in neutral atom imagers. The purpose of this project was to investigate graphene as a potential substitute for current state-of-the-art carbon foils and carbon surfaces used in energetic neutral atom (ENA) imagers for heliospheric and magnetospheric science.

Approach — Project objectives were to:

- Produce and test graphene foils and compare critical properties (angular scattering and charge conversion efficiency) of these foils with properties of state-of-the-art amorphous ultra-thin carbon foils.
- Produce and test graphene surfaces on an appropriate substrate and compare critical properties (scattering and charge conversion efficiency) of these surfaces with properties of the state-of-the-art DLC conversion surface and a "blank" (bare silicon) surface.

Accomplishments — We achieved excellent results for the first objective. In particular, we have shown that the angular scattering of ions passing through graphene foils is reduced by up to a factor of approximately three compared to amorphous carbon foils (see Figure 1). The change exchange efficiencies for ions transiting through graphene and thin carbon foils are nearly identical. These results were published in two separate peer-reviewed journal articles (see references below), and we have results for a third paper that describes the energy loss of ions transiting graphene foils. This work has put SwRI at the leading edge of graphene foil research and their application for space plasma and ENA instrumentation.

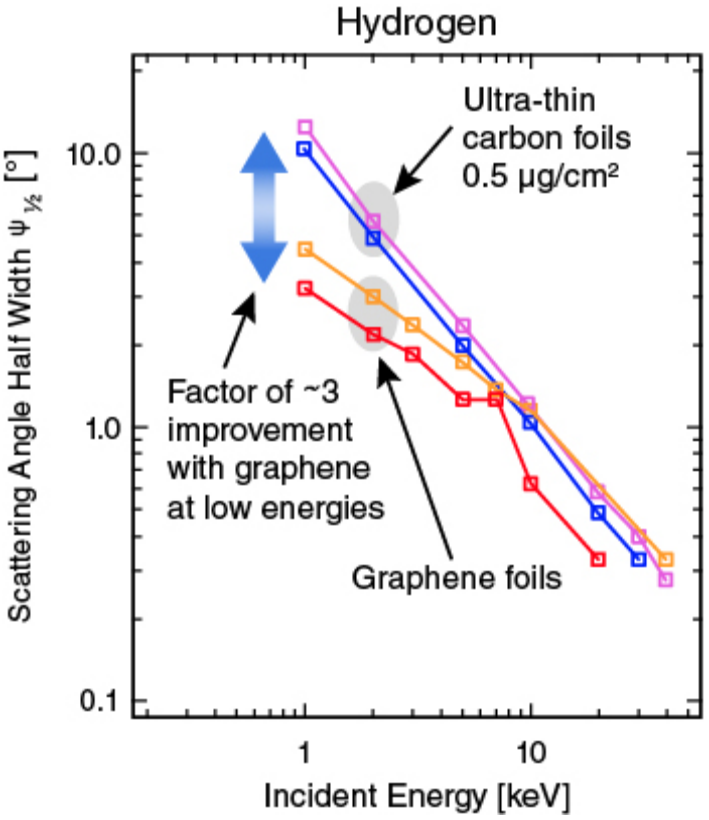

Figure 1: Scattering half-width of H ions after passing through graphene and ultra-thin carbon foils. At low energies, graphene clearly scatters H ions less than ultra-thin carbon foils (from Ebert et al. 2014). The proposed research will make similar comparisons between carbon foils and graphene.

The second objective proved to be more difficult. While we were able to design and build an experiment to investigate the properties of ions and neutrals scattering from silicon, DLC and graphene surfaces, we experienced a number of challenges with the experiment that compromised our ability to make the proposed measurements. The largest issue was the significant background caused by the presence of low-energy particles that were not part of the main distribution of scattered ions and neutrals. We attempted several fixes to this problem (e.g., adding a magnet to deflect low-energy electrons, changing the bias voltages on the MCPs and grid) but the background still remained. This posed a serious problem for the charge exchange measurements. One possibility was that this background was caused by the sputtering of absorbed gases (i.e., water) on the surfaces that can only be removed by heating. We were still able to collect measurements for ions scattering from bare silicon, DLC, and graphene surfaces that provide preliminary results for this interaction. The charge exchange measurements proved to be more challenging and were not achievable within the timeframe of this project. We have made recommendations to address these challenges and will look for a funding opportunity to implement them.

References:

F. Allegrini, R. W. Ebert, S.A. Fuselier, G. Nikolaou, P. Bedworth, S. Sinton, and K.J. Trattner (2014), "Charge State of 1 – 50 keV Ions after Passing Through Graphene and Ultra-thin Carbon Foils," Optical Engineering, 53(2), 024101.

R.W. Ebert, F. Allegrini, S.A. Fuselier, G. Nikolaou, P. Bedworth, S. Sinton, and K.J. Trattner (2014), "Angular Scattering of 1 – 50 keV Ions Through Graphene and Thin Carbon Foils: Potential Applications for Space Plasma Instrumentation," Review of Scientific Instruments, 85, 033302.

2014 IR&D Annual Report

Capability Development for Extreme Ultraviolet Imaging and Calibration, 15-R8322

Principal Investigators
Michael W. Davis
G. Randall Gladstone
Jerry Goldstein
Thomas G. Greathouse
Kurt D. Retherford
Gregory S. Winters
Bill R. Sandel (University of Arizona)

Inclusive Dates: 07/01/12 – 12/31/13

Background — SwRI has a nearly 20-year history of designing, integrating, testing, and launching ultraviolet spectrographs. Beginning with the EUVS rocket in 1993 and continuing through four iterations of the Alice line of spectrographs, SwRI's UV spectrographs have successfully returned data from comets, asteroids, the Moon, planets, and even stars. However, virtually all of these observations were made in the far ultraviolet (FUV) range, longer than 100 nm. The next step in our advancement is to expand our capabilities to even shorter UV wavelengths.

Approach — The objective of this project is to develop the capability to build and calibrate instrumentation that operates solely in EUV wavelengths. We plan to design an improved version of the IMAGE-EUV imager that upon selection by NASA will be built and calibrated at SwRI. Along with a notional design, we plan to reduce some of the technical risks in building and testing an EUV imager, in preparation for the next appropriate NASA mission opportunity. Finally, we will perform a calibration of an existing detector system at EUV wavelengths, going through all of the steps that would be performed in a real flight EUV instrument calibration. By the conclusion of this project, SwRI will be positioned to be the leader in EUV instrument design and calibration.

Accomplishments — We have a baseline imager design that increases the field of view 43 percent while increasing collecting area by 20 percent over the previously built imager. We have found a multilayer mirror coating that doubles reflectivity over the previously built imager, along with a vendor experienced with the coating. We measured FUV-blocking filters and confirmed that their EUV transmission matches the manufacturer specification. We measured the EUV performance of a spare detector.

2014 IR&D Annual Report

An Advanced UV Spectrograph Concept for the JUICE Ganymede Orbiter Mission, 15-R8324

Principal Investigators
Kurt D. Retherford
G. Randy Gladstone
Mike W. Davis
Steve Persyn
Tommy K. Greathouse
John R. Spencer
Andrew J. Steffl
S. Alan Stern
Greg Dirks
John Eterno
Kristian Persson
Brandon Walther
David White
John Trevino
Greg Winters
Maarten Versteeg
Melissa A. McGrath (NASA/MSFC)
Paul D. Feldman (JHU)

Inclusive Dates: 07/01/13 – 01/01/14

Background — Our proposal titled "JUICE-UVS: An Ultraviolet Spectrograph for the JUICE Mission," was selected by the European Space Agency (ESA) as one of 11 scientific instruments. The focus of the project continued with photodiode science tests (Task 6). A Europa-UVS proposal to the NASA Europa Instrument Investigations SALMON-2 AO Appendix O was recently submitted, and was similarly supported by this project work.

Approach — In 2014, a photodiode device was tested in the vacuum chamber with different filter coating materials to assess throughput and sensitivity properties. Tests for sensitivity in the femto-amp range were performed for visible and UV light to determine low brightness constraints.

Accomplishments — The primary project completed several UVS instrument trade studies that resulted in a low technical risk program and provided excellent advantages for the JUICE-UVS concept, leading to its selection for the payload in ESA's JUICE mission. We leveraged these advances to submit a similarly strong concept for a recent NASA Europa Mission payload opportunity. In 2014, the IRD UV detector device AXUVPS7 was purchased for the photodiode tests. The controller test board was designed and built, and basic detector functionalities were tested. This far-UV photodiode instrument prototype lays the groundwork for its inclusion in a future CubeSat proposal.

SOUTHWEST RESEARCH INSTITUTE®

2014 IR&D Annual Report

Carbon Foils Properties for Space Plasma Instrumentation, 15-R8340

Principal Investigators
Frédéric Allegrini
Kent Coulter

Inclusive Dates: 10/01/12 – 09/30/14

Background — Carbon foils are critical components in many space plasma instruments built at SwRI. They are used to detect particles — ions, electrons, or neutral atoms — that pass through by a coincidence measurement and/or to determine their speed with a time-of-flight (TOF) measurement. There are many effects resulting from the interactions of ions with carbon foils, for example, energy straggling, angular scattering, and charge exchange of the ion, and secondary electron emission from the foil. All of these effects have been studied for different parameters, such as ion mass and energy, and for different carbon foil thickness. However, there are still significant gaps in the literature and, in particular, for carbon foils as thin as we fly in our instruments (nominal 0.5 μg/cm^2, which corresponds to about 2 to 3 nm). Moreover, the different characteristics of the interactions of ions with carbon foils have been investigated in most cases for only one variable at a time. Little information is found about energy straggling as a function of angular scattering or charge state of the particle after passing through the foil. This project is about measuring these effects and the relationship between them.

All these effects scale with foil thickness, which is why we use the thinnest practical foils to mitigate the impact of the unwanted effects (e.g., energy straggling, angular scattering) on the performance of our instruments. Ultra-thin carbon foils are difficult to handle and can have intolerable defects (e.g., pinholes, tears). A small increase in thickness reduces the amount of defects and can make a big difference in the handling and robustness of the foils. It is not clear what the impact of a small increase of thickness has on the unwanted effects and on the amount of defects. This project is also about acquiring data to better guide the choice of foil thickness. This will help with selecting the optimal foil thickness for future designs of space plasma instruments.

Approach — We divided the project into four objectives:

- Measure energy loss of ions as a function of exit angle and charge state for different species, energies, and foil thicknesses.
- Measure angular scattering of ions as a function of incident energy and foil thickness for different species.
- Measure foil composition and surface properties using X-ray photoelectron spectroscopy, Fourier transform infrared spectroscopy, Raman spectroscopy, and energy dispersive spectroscopy.
- Measure carbon foils resistance to static pressure.

Accomplishments — We studied the interaction of ~1–50keV ions (H, He, C, N, O, Ne, Ar) with ultra-thin (0.5 to 2.0 μg/cm^2) carbon foils. In particular, we measured the energy loss as a function of exit angle and charge state for different foil thicknesses and the angular scattering as a function of foil thickness. We measured the surface composition and structure of carbon foils using X-ray photo-electron spectroscopy (XPS). We find that most of the foil consists of ~88 percent C and ~12 percent O, forming strong bonds. Finally, we measured the resistance to static pressure of carbon foils. The results are published in the journal Vacuum (Allegrini, F. and M. A. Dayeh, "Thin Carbon Foil Resistance to Differential Static Pressure," Vacuum, Vol. 107, pp. 124-128, September 2014; http://dx.doi.org/10.1016/j.vacuum.2014.04.020). This study shows how robust the carbon foils are and reaffirms that the carbon foil technique is well adapted to space research.

2014 IR&D | IR&D Home

SOUTHWEST RESEARCH INSTITUTE®

2014 IR&D Annual Report

Developing Mission Operations Center Capabilities, 15-R8366

Principal Investigators
John Andrews
Debi Rose
Michael Vincent

Inclusive Dates: 01/23/13 – 07/25/14

Background — Core Mission Operations Center (MOC) capabilities enabling the SwRI Space Operations Team to compete in the mission operations business realm have been successfully developed on this project. Using readily available government-off-the-shelf (GOTS) and commercial-off-the-shelf (COTS) tool sets, the team has successfully implemented and demonstrated the functionality necessary to manage and control spacecraft systems. The team also acquired a spacecraft simulation tool that enabled modeling and operations capability of virtual spacecraft for this project and future work. The experience gained in the configuration and use of the MOC system tools will serve as both a risk reduction to the Cyclone Global Navigation Satellite System (CYGNSS) MOC effort and a foundation for proposing MOC capability on future missions.

Approach — The MOC development effort is based on the selection and use of GOTS and COTS tools to provide the backbone for the SwRI MOC functions. Tools selected to support this effort include:

- Integrated Test and Operations System (ITOS, also known as Galaxy) by the Hammers Corporation, is the tool selected and used to support core CTS functions. This tool has been used on many missions and is available to NASA missions with no licensing fees and was provided to the SwRI team with no licensing fees for use on the project.
- FlexPlan, provided in the United States by MetiSpace Technologies, is the tool selected and used in the project for mission planning system (MPS) functions. This tool has associated licensing and maintenance fees, has been used on several NASA missions, and was provided to the SwRI MOC team in a demo mode, with no licensing fees, to support the project effort.
- Spacecraft Design Tool (SDT) by ADS is the tool selected to provide a spacecraft simulation platform for the MOC and was used in the project to support development and verification efforts for the command and telemetry system (CTS) and MPS capabilities. This tool has associated licensing and maintenance fees and was purchased with capital funding.
- System Tool Kit (STK) by AGI is the tool used to provide the financial data system (FDS) inputs necessary to support the project. SwRI owns several licenses of STK, and these licenses were used to support this effort.

There were three major components for this effort:

- Command and Telemetry System (CTS), which provides the elements used to communicate to a space asset through an antenna network. This system also is responsible for the real-time commanding and processing of telemetered data.
- Mission Planning System (MPS), which allows the operations team to plan long-term and short-term schedules of activities. This includes incorporating requests from the science operations center, and coordinating contact schedules with the ground antenna network.
- Verification and Simulation, which demonstrates correct implementation of the MPS and CTS system with a simulated spacecraft fleet of two LEO spacecraft in a simulated environment.

Accomplishments — Through the course of implementing the MPS, CTS, and simulation environments for the project, the team collected a number of lessons learned including:

- Maintaining configuration control of the master command and telemetry definitions is essential.
- Notifying all teams when changes are made to the master documents is just as critical as controlling the master copies to ensure all products relying on the information are regenerated at the same point in time.
- FlexPlan should be investigated further to see if it is the correct tool to use for missions such as CYGNSS, which consist of a constellation of satellites with a small number of operational options and a single instrument.
- FlexPlan appears to have a lot of overhead that may make it unwieldy in the "simple constellation" environment.
- ITOS has several configurations available to support constellation operations; further investigation should be done to assess which approach will best support a constellation that may have multiple ground contacts occurring simultaneously.
- Databased access to telemetry points will be key when looking at data collected over long periods of time (Note, Hammers has a new tool coming online – DAT – that may fulfill this need).
- A simulated environment provides a powerful tool for the mission operations team.

The MOC team accomplished the project goals to develop core Mission Planning System and Command and Telemetry System capabilities. The work performed on the project will provide a solid basis to build on for the CYGNSS mission, as well as provide a firm foundation to support proposing mission operations work for future projects. The ITOS tool selection for the CTS core has proven to be a solid selection, providing an array of tools and capabilities necessary to support the MOC and a responsive support team at Hammers. FlexPlan as a tool for MPS capabilities may not be a tool that is best matched with our targeted market of constellations of small satellite systems. The team will research this further as they move forward in the MOC development for CYGNSS. The effort in the mission planning area has aided in identifying potential issues with the FlexPlan tool in terms of complexity of use and concerns with support levels from the MetiSpace team. Learning this on the project resulted in a risk reduction for the CYGNSS program.

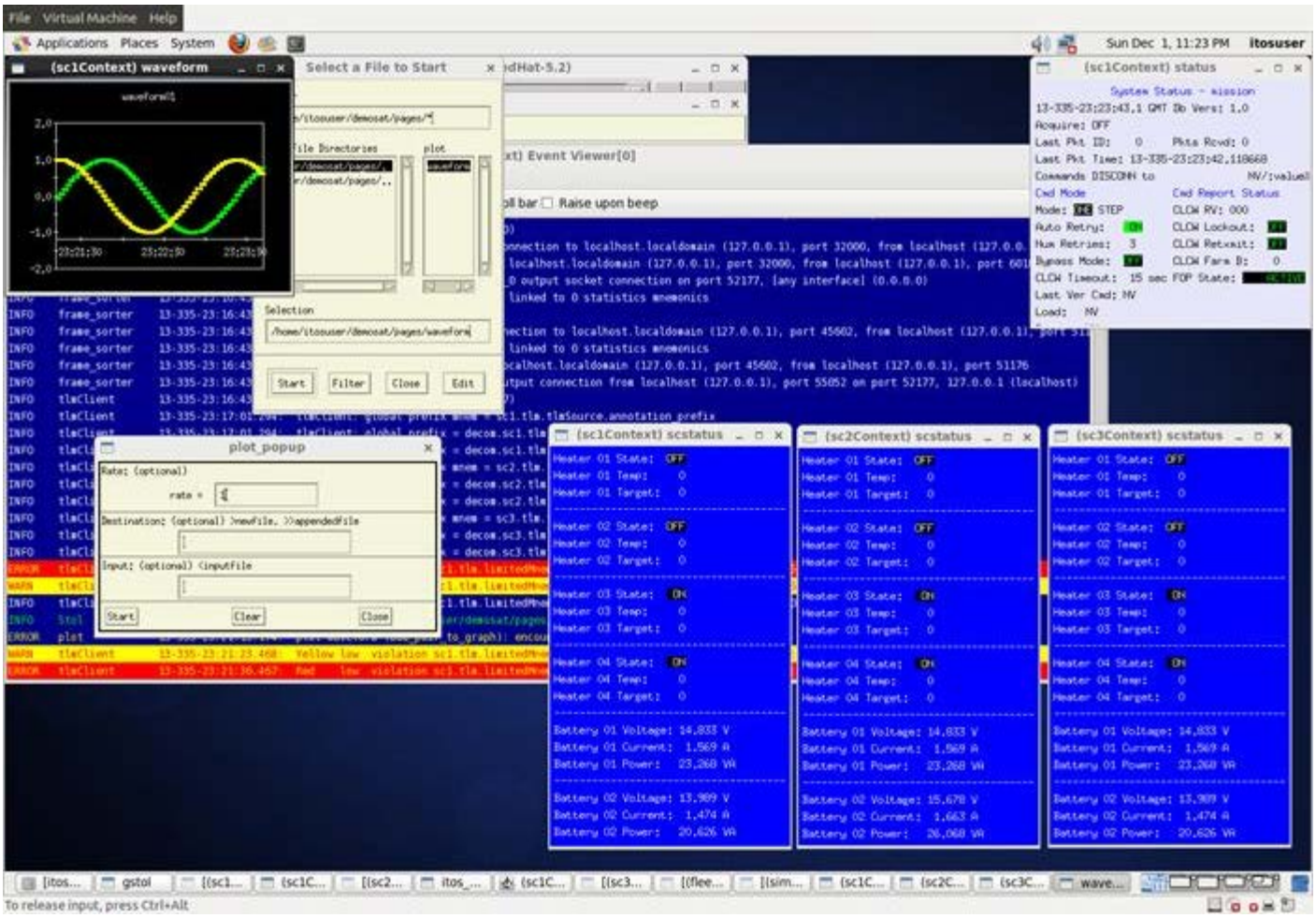

Figure 1. Command and Telemetry System monitoring a fleet of three simulated satellites.

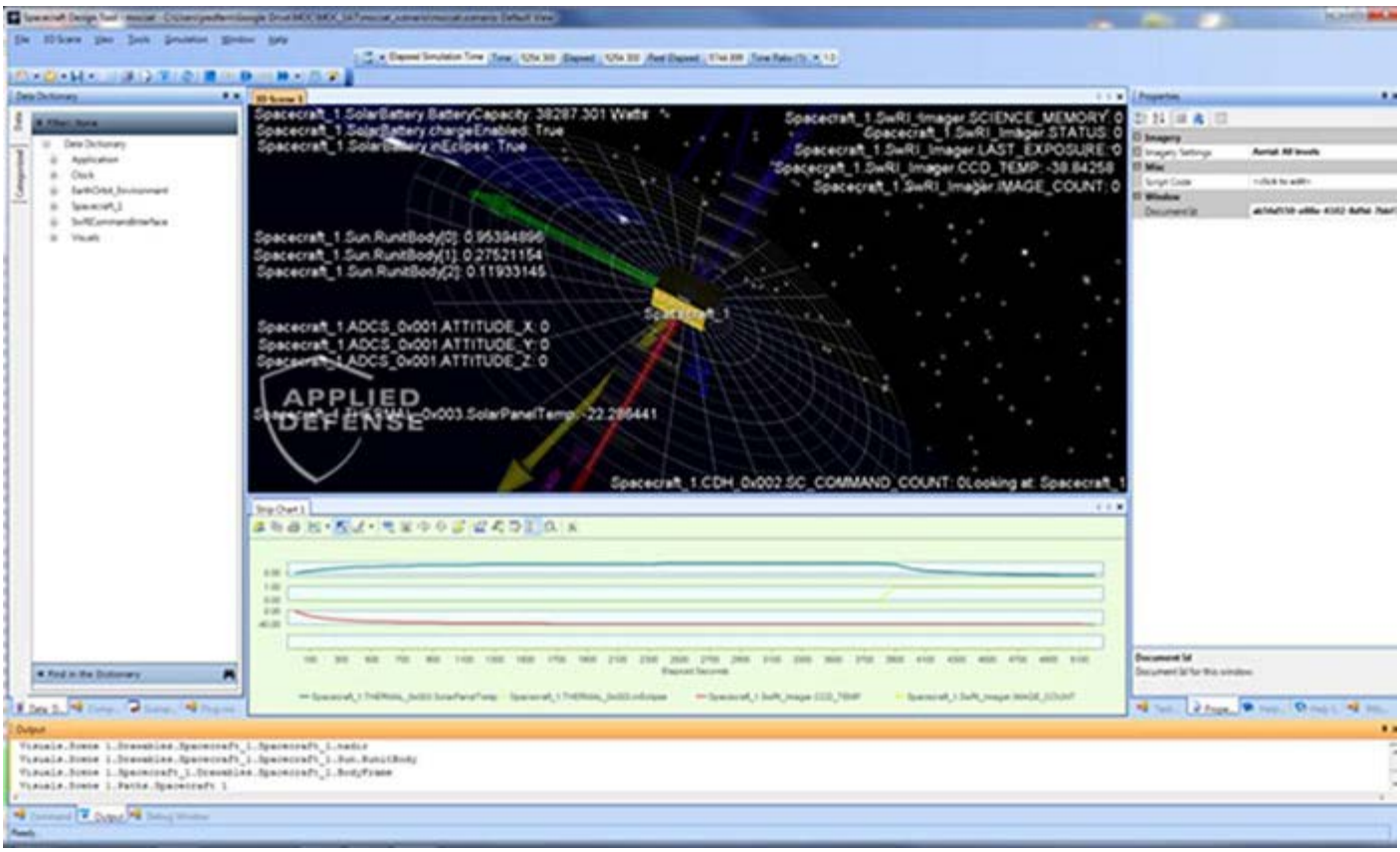

Figure 2. Software satellite simulation using Satellite Design Tool.

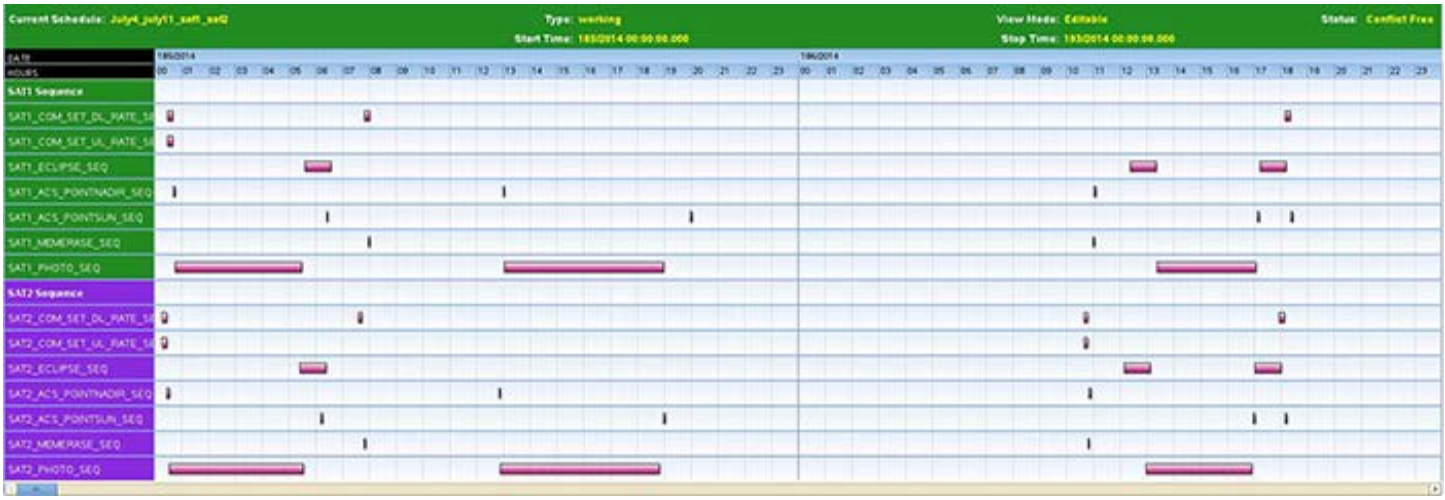

Figure 3. Sample schedule created with Flexplan and the Mission Planning System.

Figure 4. Boulder Mission Operations Center.

SOUTHWEST RESEARCH INSTITUTE®

2014 IR&D Annual Report

Development of High Voltage Optocoupler for Space Applications, 15-R8388

Principal Investigators
Armando De Los Santos
Dennis Guerrero
Matthew A. Freeman
Amanda Richter

Inclusive Dates: 04/01/13 – 10/01/14

Background — SwRI has built a name for itself in the production of high voltage (HV) power supplies for space applications. The HV optocoupler, a component that controls the flow of current in an HV circuit with a low voltage control signal, limits today's supplies. These parts have proven themselves difficult to manufacture and prone to failure, which can render an entire instrument useless. SwRI researchers have vast experience with the challenges of space grade electronics and the principles of high voltage design. This project used those abilities to design a robust optocoupler prototype, the SW1602, suitable for current and future missions. The testing and qualification of these parts continues outside the scope of this project.

Approach — For this optocoupler to succeed where commercially available devices have failed, the prototype needed ample performance to meet mission requirements and it must avoid the problems that plague commercially available parts. To maximize the part's performance, the team researched HV diodes, from standard silicon to state-of-the-art gallium nitride, and paired them with LEDs, which produced the most effective wavelength light. Past failure investigations of commercial parts revealed numerous issues with delaminations and voids in the components. Depending on the delamination and void locations relative to the HV components, electric field stresses occur, causing breakdown or partial breakdown (corona) leading to carbon tracking and other deteriorating conditions across or throughout the part. The SW1602 avoided these issues by design, minimizing any possible leakage paths and ensuring the use of compatible potting compounds with the appropriate surface preparation and cleanliness procedures in place. Once a design was selected, multiple prototypes over a range of environmental conditions were built and tested. After test, the designers reviewed the results and modified the design until the final design of the SW1602 emerged.

Accomplishments — The first year of the project was devoted to testing various HV diode/LED pairings in multiple physical form factors (Figure 1), building 25+ prototypes of three distinct designs. These prototypes then underwent thermal cycling involving more than 500 cycles with temperatures ranging from -50C to +80C. Satisfied with the performance over temperature, the next six months were spent working to overcome two final challenges: bubbles in the passivation coating of the HV diode and contamination issues during the potting process. The team worked with the HV diode manufacturer to produce a custom HV diode fired in a vacuum furnace. This removed the bubbles in the diode coating and with them the chance that those bubbles could lead to the pernicious problem of partial discharge. The cleanliness issues were resolved by setting aside a specific workstation dedicated to silicon potting. A down-draft clean bench protects both the component assembly area and the vacuum chamber where the pour takes place, ensuring no contaminants enter the part body. Additional fabrication of SW1602s and their testing, screening, and qualification for flight use continue outside the scope of this project.

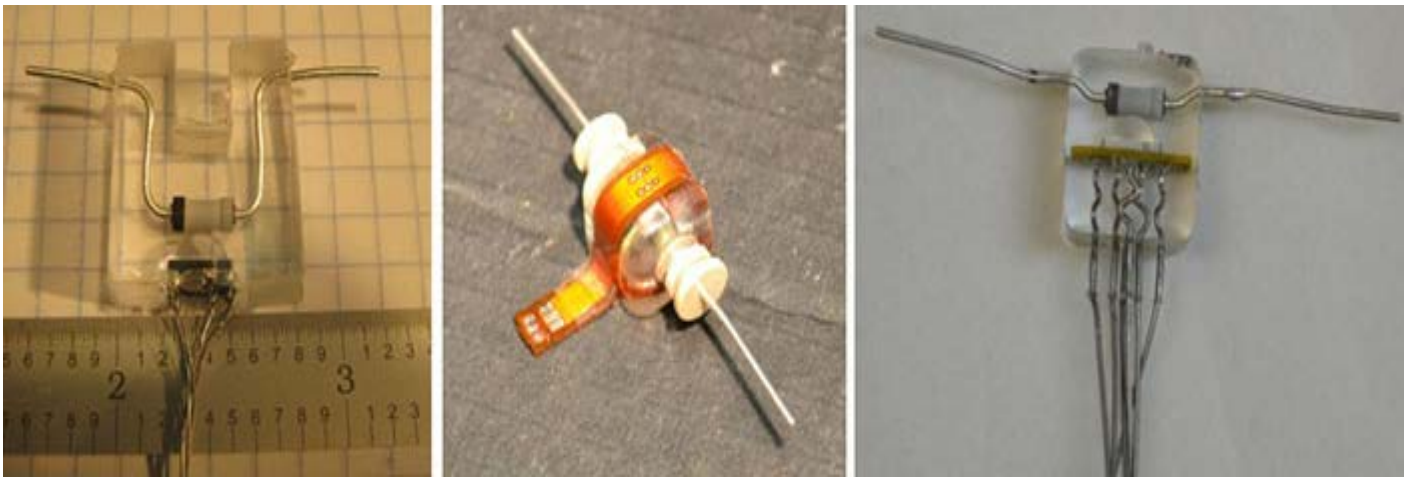

Figure 1. Sample HV diode/LED pairing.

2014 IR&D Annual Report

Development of a Compact Raman Visible Spectrograph Design for a NASA Mars 2020 Rover Instrument Proposal, 15-R8416

Principal Investigators
Greg Winters
Mike Davis
Greg Dirks
Randy Gladstone
Tommy Greathouse
Kurt Retherford
Paul Wilson

Inclusive Dates: 09/09/13 – 01/09/14

Background — In response to a NASA Mars 2020 Rover mission instrument announcement of opportunity requesting remote geological sampling instrument proposals, a Raman spectrograph concept and optical design activity commenced in the fall of 2013. Instrument proposals were due to NASA January 15, 2014. This spectrograph is a major sub-component in the remote geological sampling instrument submitted to NASA named REACH, for "Remote Raman and Laser Induced Fluorescence Emission Spectrograph for the Sample Acquisition and Habitability Assessment." Figure 1 shows the concept and overall spectrograph block diagram, including the intensified charge coupled device detector, and the super notch holographic filter.

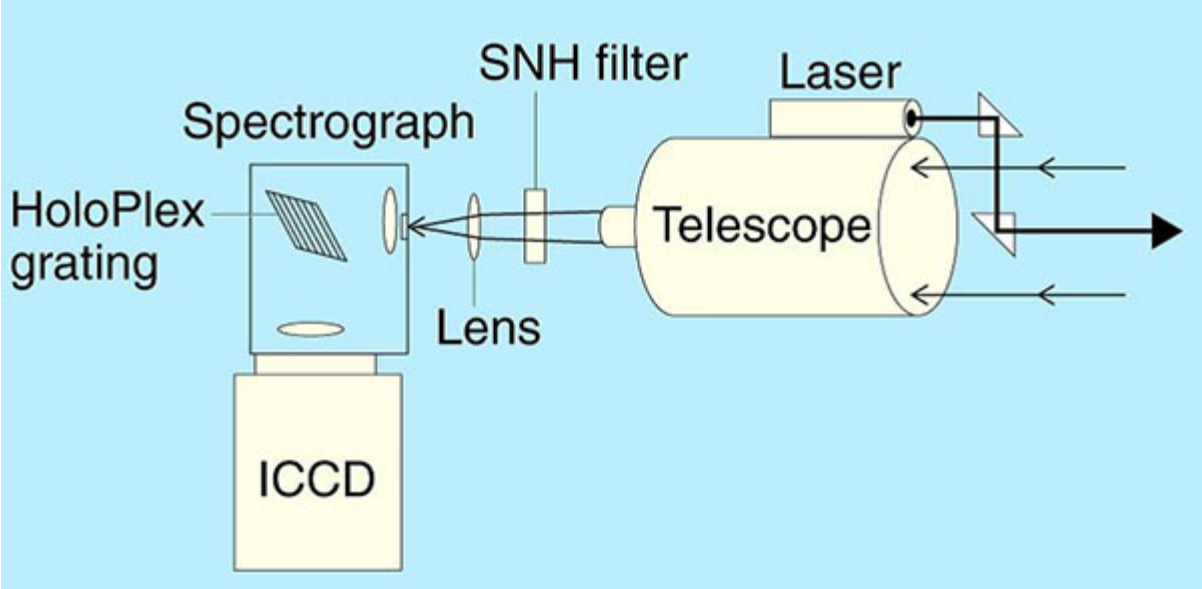

Figure 1. Optical layout of the REACH instrument, showing the Raman spectrograph.

Approach — After spectrograph technical and performance requirements were determined, optical and mechanical design concepts were generated that provide a compact spectrograph solution for the REACH instrument proposed for the Mars 2020 Rover spaceflight and landing/survey mission. Raman spectrograph systems can be used for remote (or stand-off) sampling of geological samples. Raman

spectroscopy uses monochromatic light (usually from a laser) to interact with the sample. A small portion of this incident light undergoes an inelastic, or Raman, scattering event, resulting in the wavelength of this incident light being shifted up or down after it has interacted with the sample. The shift in wavelength yields molecular and elemental information concerning the vibrational modes of the sample. The resulting spectra or "fingerprint" is then used to identify various polyatomic ions and molecules. This spectrograph design covers the 532 to 840 nm spectral range, with a resolution on the detector of 0.15nm/pixel (Nyquist samples 0.3nm), and allows measurement of Raman and fluorescence signals. Figure 2 provides the optical model of the Raman spectrograph. Figure 3 shows the mechanical package and other components.

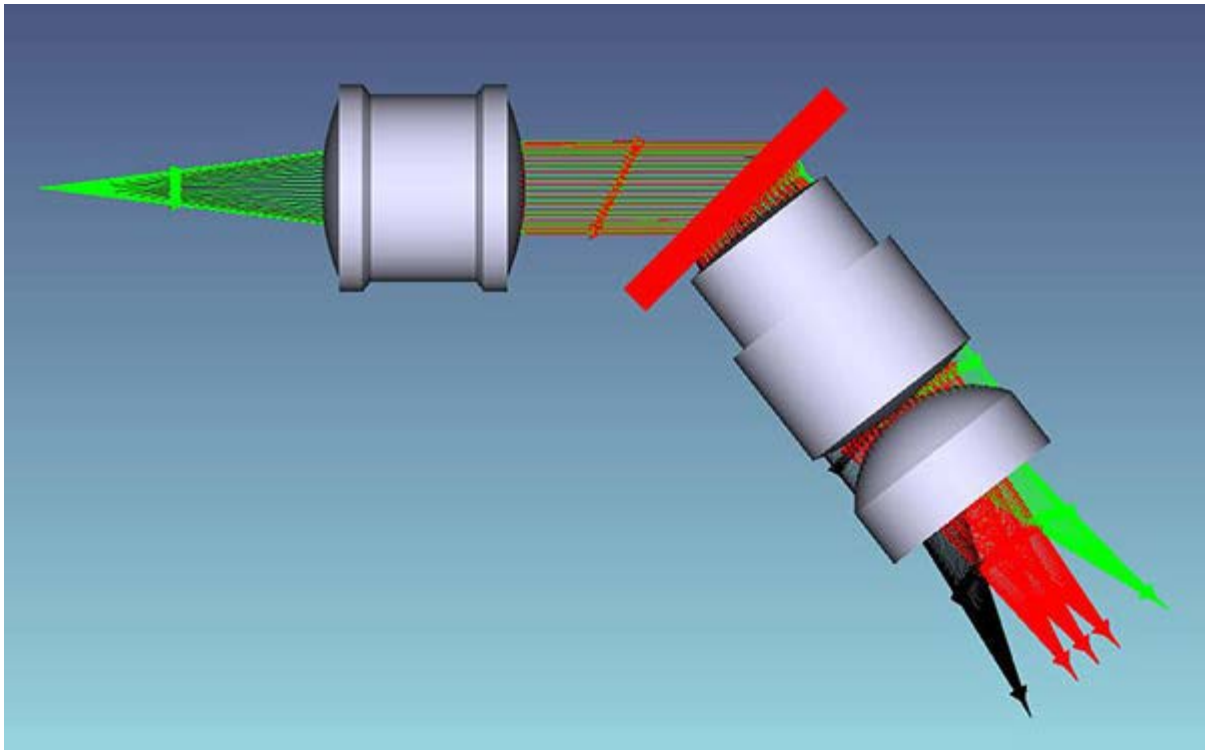

Figure 2. Optical model, showing incoming light (on left) separated into constitute spectra (lower right) after passing through optics and the diffraction grating.

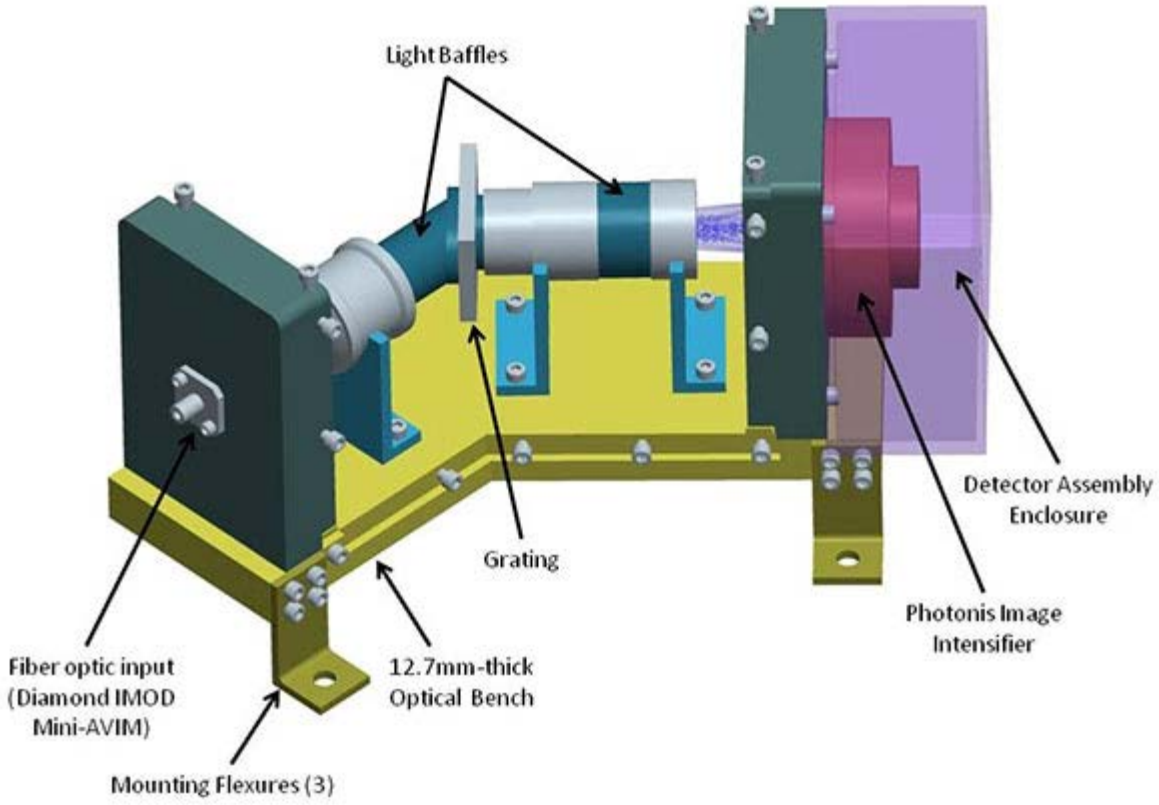

Figure 3. Overall layout of the "REACH" instrument Raman spectrograph (cover removed).

Accomplishments — In response to the NASA Mars 2020 Rover mission instrument announcement of opportunity, a spectrograph design and cost proposal was submitted to the REACH instrument team. Although the REACH instrument was not selected by NASA when they announced winning teams on July 30, 2014, we were able to assist the REACH instrument team with resolving and defining spectrograph optical performance requirements and then generating a conceptual design for a high-performance Raman spectrograph that meets these requirements.

2014 IR&D | IR&D Home

2014 IR&D Annual Report

Validation of SwRI Suborbital Program Experiments Through Zero-g Flight Demonstration of Flight-Ready Hardware, 15-R8417

Principal Investigators
Daniel D. Durda
Constantine Tsang
Eric Schindhelm
Alan Stern
Kimberly Ennico Smith

Inclusive Dates: 09/16/13 – 01/16/14

Background — SwRI is playing a leading role in the burgeoning suborbital research field using next-generation, manned vehicles by becoming one of the first, and quite possibly the first, organization to fly payloads with research payload specialists on these vehicles. This will open up to SwRI a series of new business opportunities including new funded research projects, new hardware development projects, ground and flight system task-order contracts associated with next-generation suborbital work, and the provision of payload specialists for next-generation suborbital work.

Approach — The project's primary objectives were:

- to raise the technical readiness level (TRL) of two SwRI suborbital program payloads (BORE and SWUIS) to TRL5 by flight validating their function in actual zero-g conditions
- to achieve an end-to-end test under relevant flight conditions of the BORE and SWUIS experiments to identify any critical design/operations flaws in a relatively inexpensive flight test environment
- to bring these experiments/payloads to final flight-ready status for XCOR Lynx Mk1 flights
- to provide SwRI payload specialists direct, hands-on experience with the behavior of the BORE and SWUIS equipment in zero-g conditions like those that they will experience during flights on the XCOR Lynx Mk1 vehicle.

The project objectives were met by:

- integrating a new data handling and power sub-system, and fabricating the payload interface hardware
- performing test flight demonstration in the microgravity environment of a zero-g aircraft
- designing the payload interface hardware such that the payload is accommodated in the space available in the XCOR Lynx Mk1 cockpit

Accomplishments — Payload interface hardware design commenced as soon as we were notified this project had been funded. Initial design sketches were completed based on insights gained from a preliminary mockup, followed by more detailed Solidworks drawings. The entire two box structure (BORE payload) is now housed to fit within the XCOR Lynx Mk 1 payload-A compartment, in the form of a trapezoid measuring 15.748 in. × 16.140 in. × 18.75 in. machined from aluminum plating and 80/20 material. There are three subassemblies for SWUIS: optical module, control module, and the two components (laptop and PIB battery) housed inside the BORE payload A. The optical module consists of the Xybion camera, its lens (with lens cap) and a hand mount. A lens cap is tethered to camera body. The control module consists of the PIB, the tablet viewer and its supporting structure, with a hand-mount. A tablet stylus is tethered to the control module supporting structure. We developed a detailed set of checklists to cover flight operations for both payloads. The research flight took place on November 17,

2013. Both the BORE and SWUIS payloads performed flawlessly and as planned during our extensive pre-flight conops development and rehearsal and good calibration data were collected and stored for analysis.

2014 IR&D | IR&D Home

SOUTHWEST RESEARCH INSTITUTE®

2014 IR&D Annual Report

Modeling of an Europan Exosphere with Plumes, 15-R8453

Principal Investigators
Danielle Wyrick
Ben Teolis
J. Hunter Waite
Tim Brockwell
Brian Magee

Inclusive Dates: 02/26/14 – 06/24/14

Background — The recent discovery of a gaseous plume emanating from the south pole of Jupiter's moon Europa by SwRI scientists changed the paradigm for future investigations of the habitability of Europa. These potential plumes support growing evidence of an abundance of liquid water on Europa and the potential for direct sampling of an interior ocean. There were no current models of Europa's sputtered exosphere and plumes for use in a predicative model for future instrument and mission design, and thus this fundamental research project was needed to advance the state of the science for icy moons in the Jovian system. We updated our Europan sputtered atmospheric model with findings from our early proposal efforts and, most importantly, incorporated a new plume model based on plume observations of Europa. Results from this project help provide the scientific rationale for sources of gaseous plumes at Europa and establish SwRI as icy moon exospheric experts for future NASA Discovery or New Frontiers competitions.

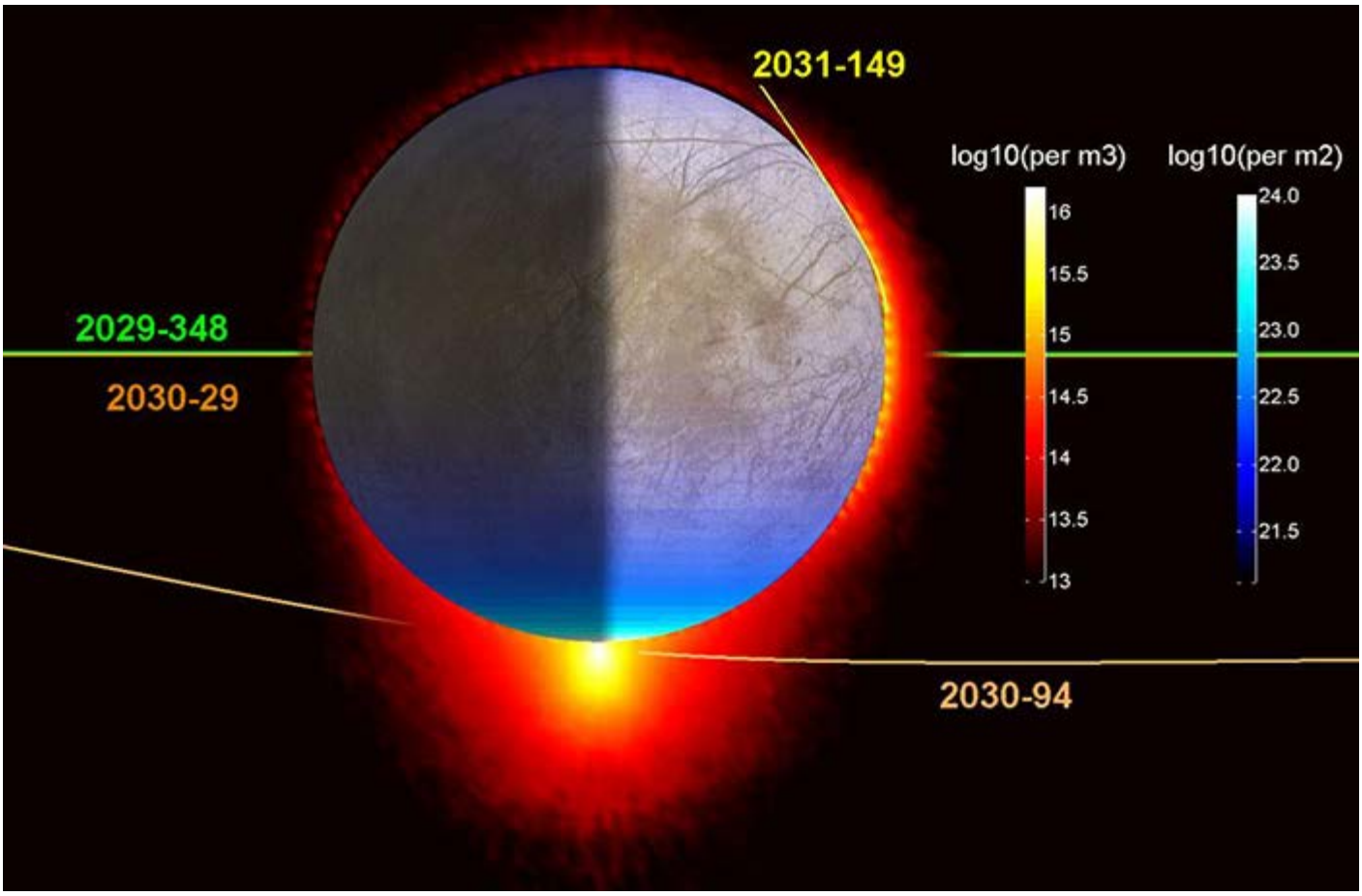

Figure 1. Exosphere simulation showing the H_2O density cross-section (warm-colored logarithmic scale) along noted Europa Clipper spacecraft trajectories under models run with a south polar plume. Blue logarithmic scale shows the H_2O surface column density, including the H_2O diffused into the subsurface regolith. Plume was modeled as a 5,000 kg/s Mach 2 plume with Enceladus-like composition.

Approach — For this project, we developed a Europa exospheric/plume model based on our previous modeling efforts for Enceladus, Dione, and Rhea. Current NASA research modeling of plume structures on Enceladus has illustrated the importance of understanding the source physics and three-dimensional structures of plumes and sputtered exospheres to interpret in situ plume composition. This project consisted of two major tasks: (1) updating our Europan exospheric sputtering model to incorporate the results from earlier Ganymede modeling efforts and (2) incorporating plume modeling. These modeling tasks formed the basis of a new exospheric model of Europa to better understand plume dynamics on icy moons.

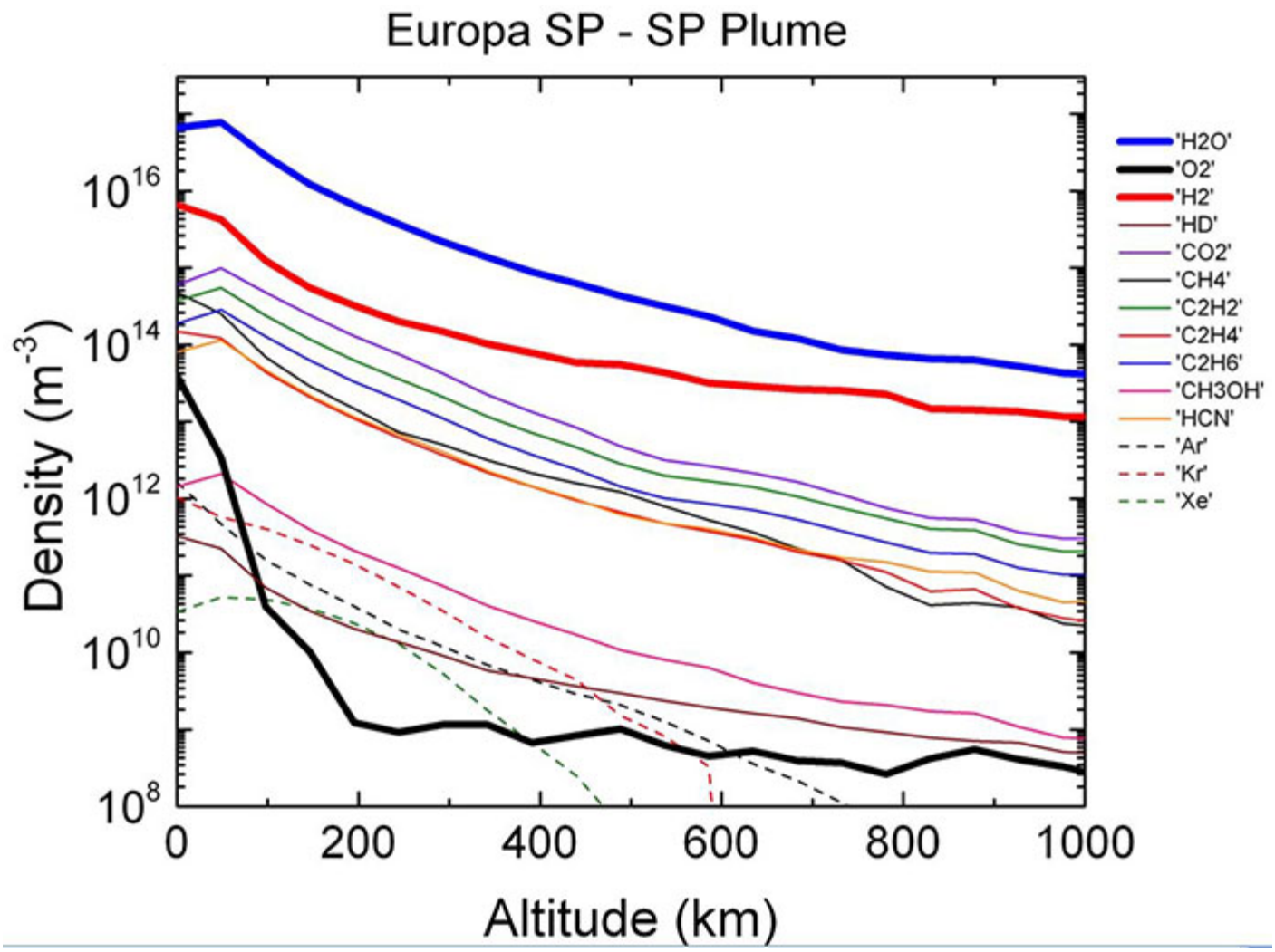

Figure 2. Plot of exosphere compositional density by altitude for select species for the south polar plume model condition, with a direct S/C trajectory through the plume.

Accomplishments — Developing a working model of Europa's exosphere, incorporating both sputtering and plume processes, was the prime metric of success on this project (Figure 2). Our new modeling approach improves upon initial Europa plume models by incorporating an improved sputtering model, a realistic treatment of the exosphere/surface adsorption interaction, and plume geometries and locations that are more realistic (i.e., modeling point source locations rather than a large surface area). Our model incorporates, for the first time at an icy satellite, the interaction between a plume source and the global exosphere, including the spatial and temporal dependence of the gas density and composition distribution. This working model was designed such that it can be easily adapted as new data become available on plume source locations and composition on Europa.

2014 IR&D Annual Report

Space-Based Communications Processing, 15-R8469

Principal Investigators
Jennifer L. Alvarez
Larry T. McDaniel

Inclusive Dates: 05/01/14 – Current

Background — Satellite communications (SATCOM) providers are seeking to expand content distribution, especially of Internet content, to mobile users. Traditionally, SATCOM companies focused on fixed satellite services, which distribute content to users in fixed locations with dedicated, often large, terrestrial equipment. The push to provide mobile satellite services is unsurprisingly motivated by the booming market of smartphones and tablets. SATCOM providers are interested in becoming a part of the mobile data infrastructure by making SATCOM data transmission mechanisms transparent to mobile users. The expansion into mobile satellite services requires the capability to serve large user populations at extremely high data rates. The intent of this research is to develop foundational and cross-cutting technologies that would position us to provide hardware, algorithms, and intellectual property to SATCOM service providers and the spacecraft and component manufacturers that serve the SATCOM industry.

Approach — The project objectives are to develop an end-to-end satellite payload architecture that uses adaptive control algorithms and the next-generation, high-rate signal processing algorithms and hardware needed to achieve the required level of service. These underlying technologies can then be applied to SATCOM technology innovations, including adjustable antenna spot beams, adjustable multi-carrier amplifiers, radio frequency (RF) channelizers, advanced modulation/demodulation methods, and multiple access and routing mechanisms. Each of these technology elements will eventually contribute to space-based systems that can be dynamically optimized based on changing usage profiles over varying geographic area. Our intent is to develop foundational technologies that are applicable to each of the potential SATCOM technology innovations.

Accomplishments — We have developed an initial, high-level model of an intelligent communications manager that uses knowledge of spatial characteristics, communications resources, and data flows to manage communication network resources. The network resources include the signal processing components on the spacecraft. The on-orbit data processing throughput goals of the project require a multi-processor architecture that is flexible and scalable to suit low-cost, low-Earth-orbit satellites, in addition to large, geostationary orbit satellites, and to allow optimization of services over time and market applications. We have developed functional models of the required processing and estimated the necessary performance in operations per second. We have begun to map the processing and throughput requirements against processing architectures and advanced interconnect standards.

2014 IR&D Annual Report

Testing of Prototype Mass Spectrometer for Earth Atmospheric Studies, 15-R8475

Principal Investigators
Kathleen Mandt
Greg Miller
Myrtha Haessig
Jorg-Mich Jahn

Inclusive Dates: 06/18/14 – 10/18/14

Background — The NASA sounding rocket program provides the ideal opportunity to prove the flight-readiness and scientific capabilities of instruments that currently lack the flight heritage required for major NASA missions. The goal of this project was to propose a simplified configuration of an SwRI-built mass spectrometer for in situ measurements in support of a NASA sounding rocket project. The NASA project requires measurements of the total neutral density and the composition of neutrals in the region above 250 km. Neutral composition is poorly understood in this region of the atmosphere due to a serious gap in measurements. At the present time, atmospheric models are the only method for estimating composition at these altitudes, and these models are subject to large uncertainties because no composition measurements have been made since the 1980s. Currently, the predictions for atmospheric density and temperature can only be validated with satellite drag data, which determine the total mass density (in kg/m^3) of the exosphere based on the drag induced by atmospheric particles on a satellite. They do not provide the composition of the atmosphere as a function of altitude. Recent estimates of the composition of the winter polar exosphere have found differences between densities estimated by satellite drag measurements and atmospheric models that ranged between 25 and 70 percent.

Approach — The primary objective of this project was to characterize the operation of a linear time-of-flight mass spectrometer (TOF-MS) for the simultaneous detection of hydrogen, oxygen, nitrogen and carbon dioxide at the range of pressure regimes expected during a sounding rocket ascent and descent stage. This effort was used to establish the required data integration times and leak rates into the analyzer for the measurement of the compounds of interest above 250 km. Completion of this project required four primary tasks:

- Preparing the Multi-Bounce Time of Flight (MBTOF) to be calibrated in linear mode
- Calibrating of MBTOF in linear mode for relevant gas mixtures
- Testing of the pulser under vacuum
- Testing of the power supply under vacuum

Accomplishments — Each of the proposed tasks was completed successfully. We were able to demonstrate that the mass resolution of the linear TOF-MS was clearly sufficient to resolve H, H_2, and He, as well as N_2, O_2 and CO_2. The sensitivities were determined for each of the constituents relevant to the science measurements proposed and were found to be sufficient for the LCAS proposal. Both the pulser and power supply operated successfully under vacuum.

2014 IR&D Annual Report

Crack-Size Effect in Corrosion-Fatigue Crack Growth, 18-R8357

Principal Investigators
Baotong Lu
Stephen J. Hudak Jr.
W. Fassett Hickey
Guadalupe B. Robledo
Carl F. Popelar

Inclusive Dates: 01/01/13 – 06/30/14

Background — Premature failure of steel risers and flowlines caused by corrosion-fatigue in sour environments is a major concern in offshore oil and gas production. In 2010 SwRI developed a joint industry project (JIP) to develop a corrosion-fatigue crack growth (CFCG) model to predict the service life of critical riser and flowline components exposed to sour brine environments. Although the CFCG model is capable of predicting CFCG rates in the intermediate and high growth rate regime, this model results in overly conservative predictions in the low stress regime because it lacks the ability to capture the small-crack effect in which small cracks existing in real structures can grow faster than larger cracks commonly adopted in laboratory tests for CFCG rate measurements. The crack-size effect is of great practical significance in structural integrity assessments because a major fraction of the service life of structures is consumed in the small crack growth stage.

Approach — The objective of this project was to develop the experimental capabilities and corrosion-fatigue crack growth model capable of capturing the crack-size effect in sour environments. The approach was to 1) develop an experimental capability to measure crack growth rate and crack closure from small cracks in sour environments; 2) conduct critical analyses to identify the mechanisms of the crack-size effect; and 3) build a corrosion-fatigue crack growth (CFCG) model based on the fundamental understandings on the crack-size effect.

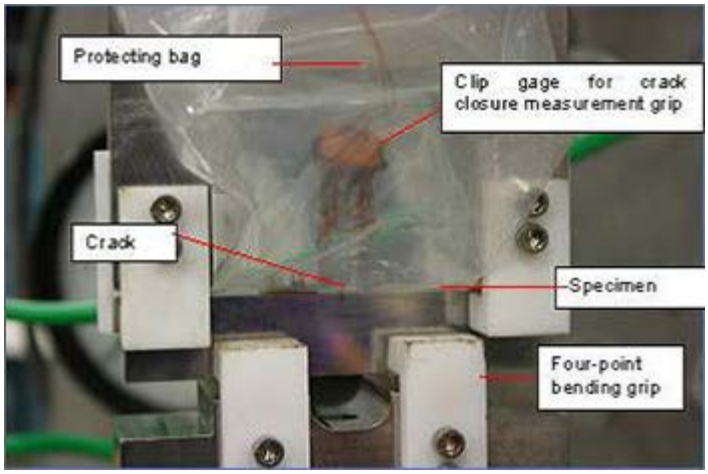

Figure 1. Newly developed small-crack corrosion-fatigue crack growth facility.

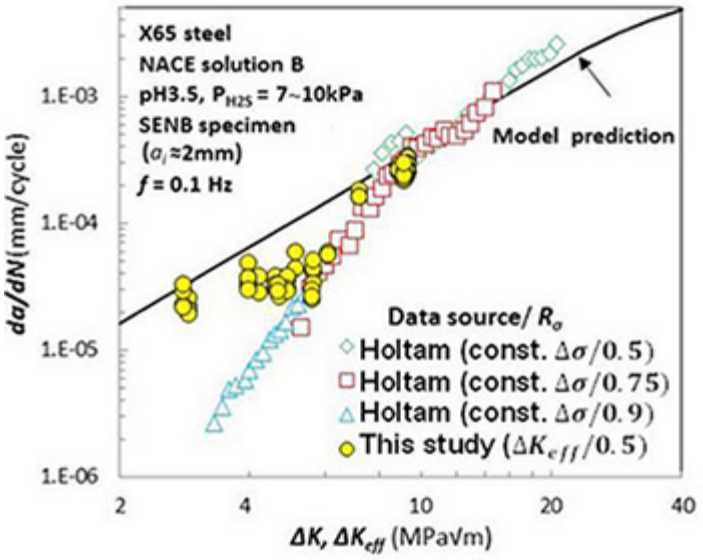

Figure 2. Comparison of the model prediction; da/dN (ΔK_{eff}) obtained in this study and the CFCG rates reported in literature (by Holtam).

Accomplishments — Results of this project demonstrated the ability to quantify the small-crack effects in sour brine environments. A new experimental facility was successfully developed to measure CFCG rates and crack closure of small cracks in sour environments (see Figure 1). Results obtained with the newly developed experimental facility demonstrated that crack closure is the most important mechanism for the crack-size-dependent CFCG behavior and Δ is the proper mechanical parameter to characterize the driving force for CFCG in the near-threshold regime (see Figure 2). A new CFCG model was developed based on the fundamental understandings and experimental findings. This model was capable of predicting the fatigue life of offshore structure steel exposed to sour environments (see Figure 3). Based on fundamental understandings achieved in this project, a technical approach was developed for a second phase of the JIP, which is expected to commence in the first quarter of CY2015.

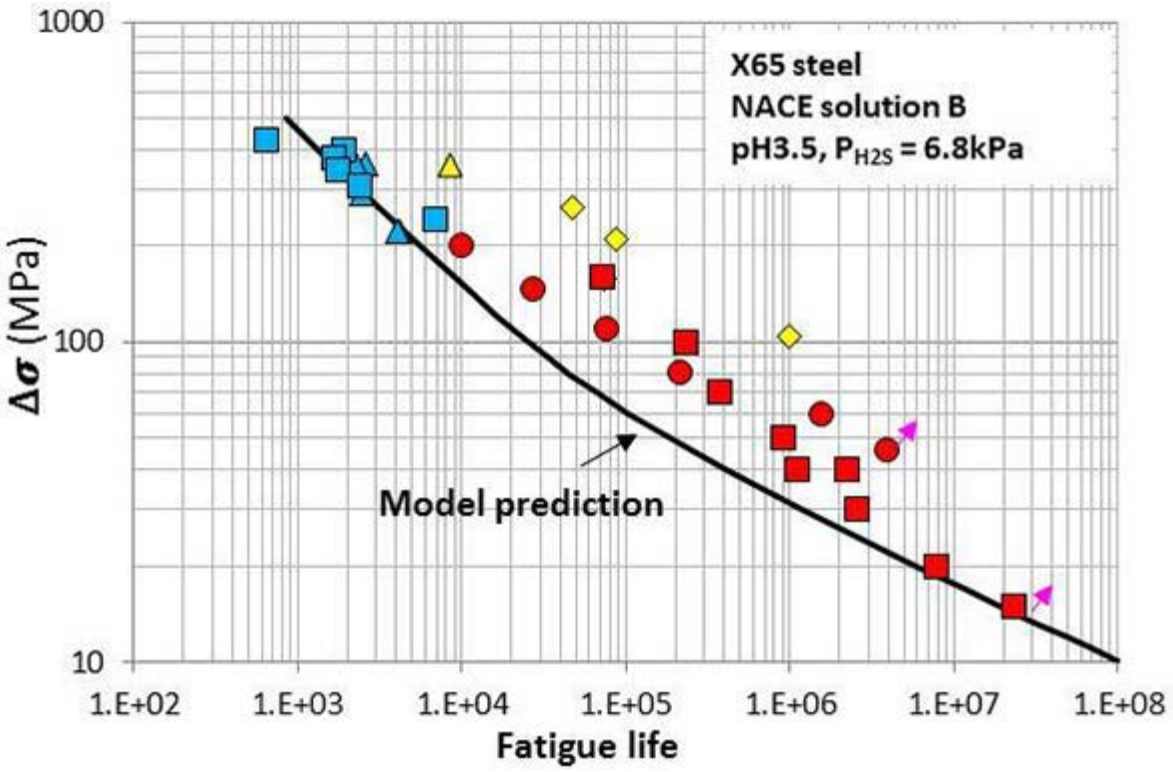

Figure 3. Comparison between predicted fatigue lives with new CFCG model and experimental data. The fatigue lives in sour brine measured with different frequencies are represented by the color of the points: blue - 0.01 Hz, yellow - 0.33 Hz, red - 1 Hz).

2014 IR&D Annual Report

Development and Characterization of Low Friction-Nanocomposite Films/Coatings for Piston Rings, 18-R8381

Principal Investigators
Jianliang Lin
Ronghua Wei
Christopher Bitsis
Peter Lee

Inclusive Dates: 04/01/13 – 09/30/14

Background — To meet future U.S. Corporate Average Fuel Economy (CAFE) standards (54.5 mpg or 4.34 liter/100km in 2025), automobile manufacturers and component makers are making significant efforts to increase the fuel efficiency of vehicles, in which lowering the coefficient of friction (COF) of any moving components including the piston rings is one key area. In addition, efforts are also being made to increase the reliability and sustain the performance including the application of a hard coating on the piston rings. Currently, thick CrN (50 to 70 μm) coatings are commonly used for protecting diesel engine piston rings. However, the relatively high dry COF of CrN coating in the range of 0.4 to 0.7 is deemed insufficient for increasing fuel efficiency. Diamond-like carbon (DLC) coating has also being explored, but it is not commercially accepted because the typical coating thickness of 2 to 10 μm is deemed to be insufficient. Therefore, the aim of this project is to develop low-friction, wear-resistant, thick TiSiCN coatings for piston ring applications. The hypothesis of the project is that nanocomposite coatings containing nanocrystalline TiC_xN_y in a matrix of amorphous diamond-like carbon (DLC) can be deposited on diesel engine piston rings to withstand the severe environment in both improving the wear resistance and reducing the overall friction.

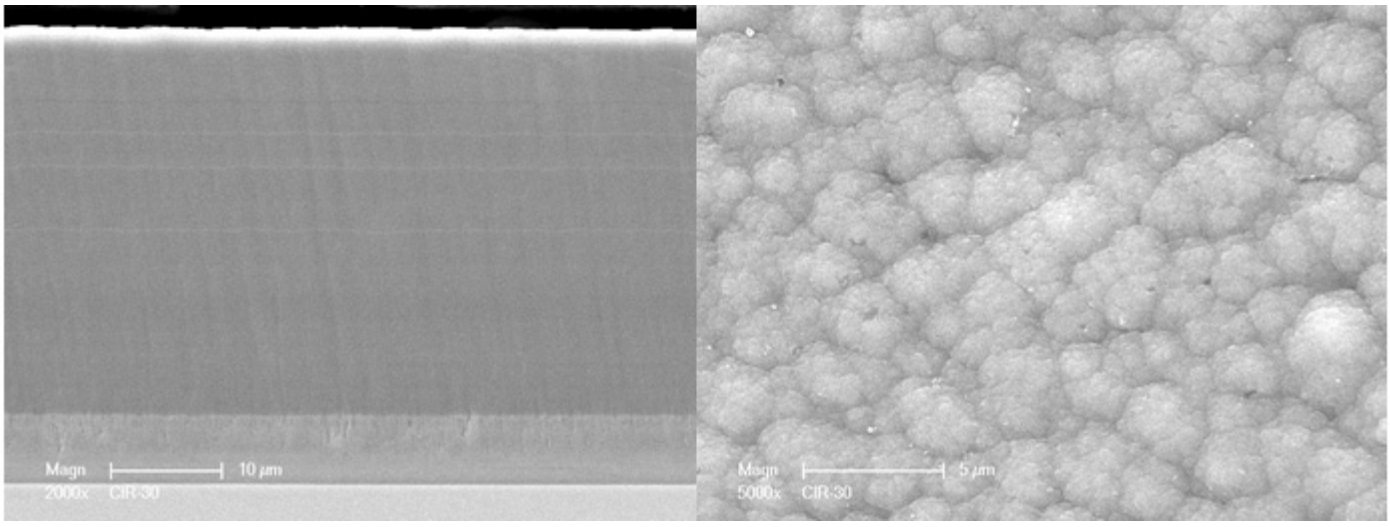

Figure 1 (a) cross-sectional and (b) top view SEM micrographs of a low friction thick (40 μm) TiSiCN nanocomposite coating developed in this project.

Approach — The approach contains three steps. In the first step, TiSiCN nanocomposite coatings with different chemical compositions and microstructures were prepared on coupon samples and piston rings

using a plasma-enhanced magnetron sputtering (PEMS) technique with hexamethyldisilazane (HMDSN) and acetylene (C_2H_2) as sources for Si and C. In the second step, the tribological properties of the TiSiCN coatings were evaluated using dry ball-on-disk test and Plint TE77 test, and then correlated with the microstructure (chemical compositions) of the coatings and the processing parameters. As a result, the composition and structure of the TiSiCN coatings were optimized to achieve high hardness, low friction, good adhesion, and good wear resistance. Finally, an optimized TiSiCN coating was selected and applied onto sets of piston rings, which were evaluated in a single cylinder engine for friction test and in a heavy duty diesel engine for durability assessments.

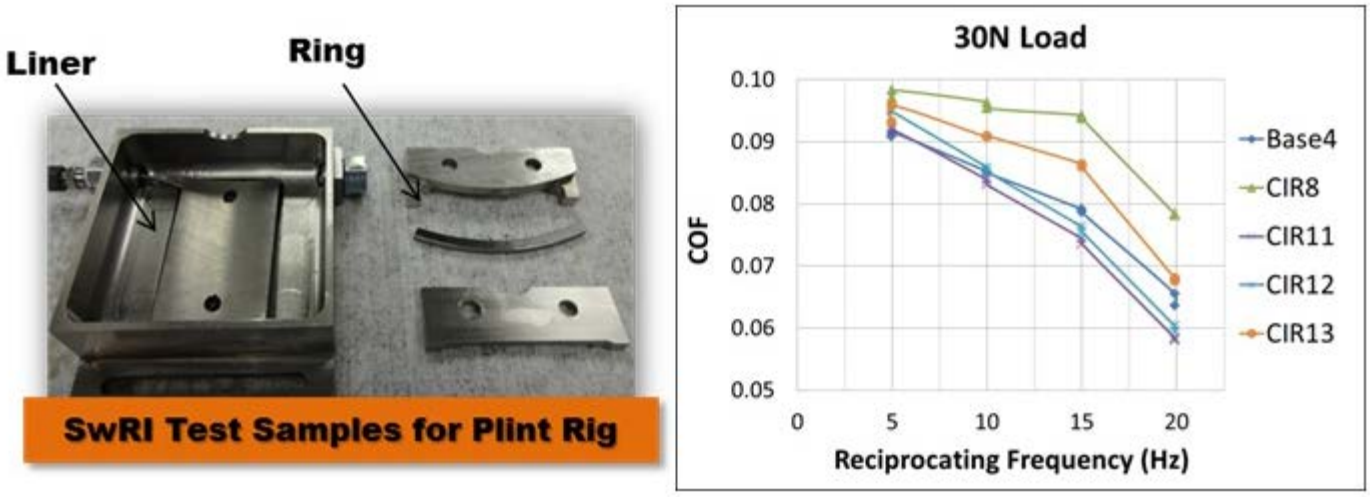

Figure 2. (a) Test sample assembly for Plint TE77 test, (b) COF of TiSiCN coatings measured using the Plint TE77 test. The optimized TiSiCN coating (CIR11) exhibited a 10 percent reduction of the fiction of the coated piston ring (COF=0.058) as compared to the baseline (COF=0.065) at a testing frequency of 20 Hz.

Accomplishments — At the end of this project, low-friction, high-wear resistant TiSiCN nanocomposite coatings were successfully developed for piston ring applications. The chemical composition and microstructure of the coatings were optimized by varying the HMDSN and C_2H_2 flows. HMDSN has been identified as a new precursor for Si and C elements because it is safe for the depositions and can be used for large-scaled production. Microstructure characterization showed that TiSiCN nanocomposite coating contains a nanocrystalline phase of TiC_xN_y and an amorphous phase of SiCN, commonly written as nc-TiCN/a-SiCN. The typical microstructure of a low friction thick (40 μm) TiSiCN coating is presented in Figure 1.

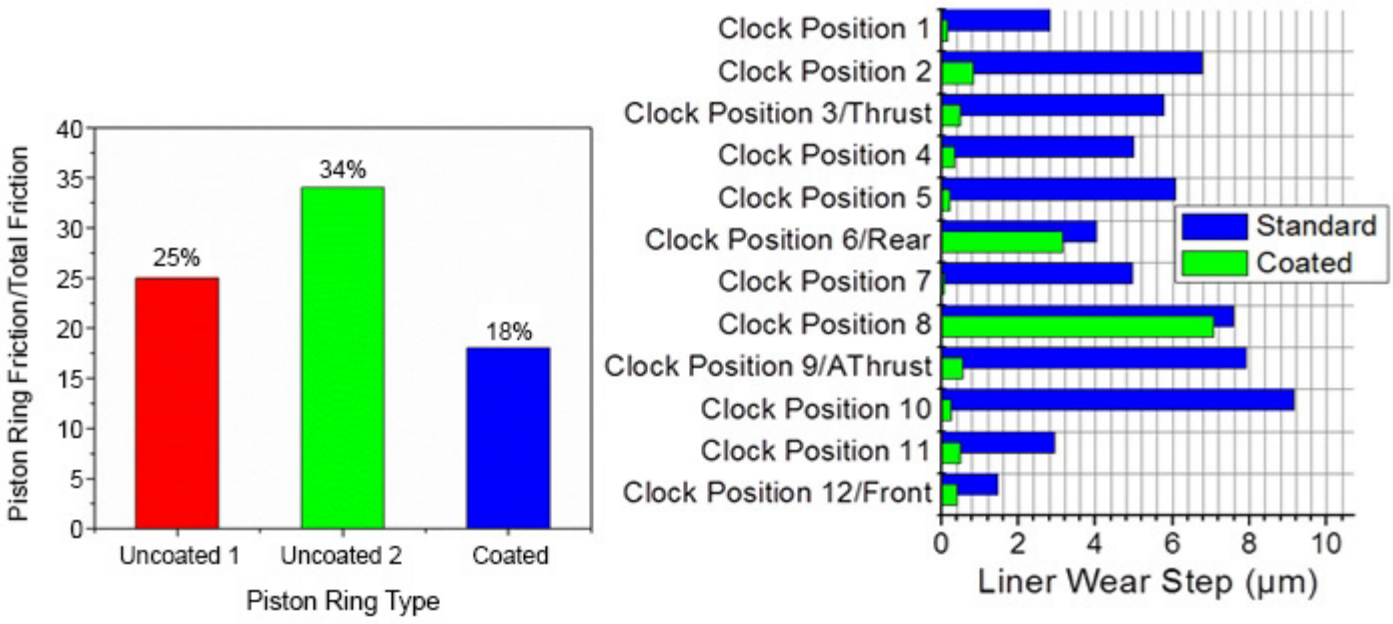

Figure 3. (a) Absolute magnitude of the friction in one engine cycle for coated and uncoated piston rings. The uncoated piston rings contributed to 25 percent and 34 percent of the total COF in two separate baseline tests. In contrast, the coated piston rings contributed to 18 percent of the total COF in the test; (b) Liner wear steps as measured at 12 circumferential points around liner. The cylinder liner showed a 50 percent lower wear than that of the baseline engine test.

The optimized TiSiCN coatings have shown excellent mechanical properties (hardness up to 30 GPa), high H/E ratios (an indirect measure of toughness of the coating), excellent adhesion (rated at HF1, the highest rating from the coating adhesion test standard), low dry coefficient of friction (0.16-0.2), and excellent wear resistance from dry sliding ball-on-disk test. The tribological properties for the TiSiCN coatings were further evaluated on coated piston rings using Plint TE77 test and single cylinder engine test. The Plint TE77 test showed a 10 percent reduction of the fiction of the coated piston ring (COF=0.058) as compared to the baseline (COF=0.065), as shown in Figure 2. The single cylinder engine tests also showed a reduction of the friction of the coated piston rings as compared to the uncoated rings. The uncoated piston rings contributed to 25 percent and 34 percent of the total COF in two separate baseline tests. In contrast, the coated piston rings contributed to 18 percent of the total COF in the test, indicating that the coating on the piston rings reduced the COF by 39 percent on average (Figure 3a). The durability engine test showed a 28 percent and 40 percent lower ring weight loss for the coated top and second rings, respectively, as compared to the baseline. In addition, the cylinder liner, which was not coated, showed a 50 percent lower wear than that of the baseline engine test. The simulation of the project predicted that the coating would not only reduce piston ring friction but also allow a lower viscosity oil to be used without compromising the integrity and durability of the engine.

2014 IR&D Annual Report

The Development of a Dynamic Finite Element Model of the Temporomandibular Joint (TMJ) and Study of Joint Mechanics, 18-R8386

Principal Investigators
Daniel P. Nicolella
Jessica S. Coogan
Travis D. Eliason
Todd L. Bredbenner

Inclusive Dates: 04/01/13 – 10/01/14

Background — Disorders of the temporomandibular joint (TMJ) result in an annual cost of $4 billion and affect approximately 16 to 59 percent of the population. TMJ disorder (TMD) causes pain in the jaw when speaking or chewing that is often associated with clicking and popping of the jaw and can limit a person's ability to open their mouth. Women ages 20 to 40 are the most prevalent suffers of TMD. Various studies indicate that women with TMD outnumber men anywhere from 3:1 to 8:1. While the causes of TMD are not completely understood, it is thought that alterations in joint mechanics due to osteoarthritis (OA) or trauma results in degradation and inflammation of the joint soft tissues (cartilage and disc), which then results in pain and limited motion. In addition, displacement of the TMJ disc is also associated with TMD. The dynamic mechanical environment within the TMJ during chewing or clenching is not well characterized due to the complexity of the anatomy and materials. Within the TMJ research community, the question of how soft tissue properties and geometry of the joint affect the mechanical environment has gone unanswered and is the focus of this project.

Approach — The primary objectives of this program were to:

- Develop a detailed dynamic finite element model of the TMJ and mandible from head CT scans.
- Determine muscle activation timings and magnitude to achieve dynamic mouth opening and closing using a new a proportional–integral–derivative (PID) controller method.
- Perform sensitivity analyzes of TMJ disc properties to determine the importance of those properties in the resulting forces and stresses of the TMJ during normal mandible movements.
- Implement an element erosion or damage material model for the TMJ disc to investigate the effects of disc degeneration on the muscle forces required for normal mandible movements.
- Develop a statistical shape model of the TMJ coupled with the dynamic finite element model.
- Using the FE-coupled statistical shape model, investigate the effect of gender differences on TMJ stress.

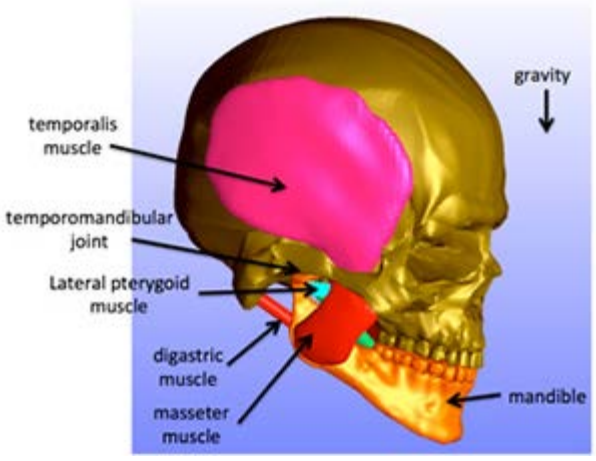

Figure 1. Dynamic finite-element model of the skull mandible, TMJ and associated active muscles. Muscle activation dynamics are determined using a novel feedback controller incorporated directly into the finite element analysis code.

Accomplishments — There are three major accomplishments resulting from this project that significantly advance the field of TMJ biomechanics and will form the basis of a new research project. First, we have developed a high-fidelity, anatomically accurate, finite-element model of TMJ mechanics that is governed by the internal generation of muscle forces to achieve a specific functional goal (such as chewing), paralleling how functional joint motion is produced in vivo (Figure 1). Second, we have modified this new model by incorporating statistical shape modeling methods to efficiently describe variation in human anatomy that occurs between individuals and within populations and to investigate how these variations, particularly anatomical differences between TMD patients and normal individuals, affect TMJ mechanics. Third, we have developed and implemented a new method of determining the time history of internal muscles forces using a feedback model paradigm that improves model efficiency by more than an order of magnitude compared to current muscle force optimization methods. In combination, these new capabilities will allow us to investigate TMJ mechanics both at the length scale of the tissues comprising the joint while simultaneously accounting for anatomical variability at the population level that has been heretofore impossible but nonetheless necessary to understand the link between joint mechanics and disease.

2014 IR&D Annual Report

NASA Uncertainty Quantification Challenge and Treatment of Multiple Uncertainty Types, 18-R8406

Principal Investigators
John McFarland
David Riha
Barron Bichon

Inclusive Dates: 07/01/13 – 06/30/14

Background — Modeling and simulation activities play a key role in decisions associated with design, cost, maintenance, and reliability across a wide range of industries. Nevertheless, the predictions that these decisions are based on are subject to inherent variations in material properties, loading conditions, and other variables, as well as reducible uncertainties attributable to having only limited information or data. The use of probabilistic approaches has seen an increasing level of acceptance as a means for quantifying the impact of such variations and uncertainties on model predictions. However, use of these methods also brings to light new and more challenging questions associated with how different types of uncertainties should be treated. To assess the state of the art and collect proposed approaches in a common problem setting, NASA Langley released a "Multidisciplinary Uncertainty Quantification Challenge," and organized a corresponding special conference session and journal issue to solicit proposed approaches.

Approach — The goal of this research is to develop new methods, build experience, and enhance capabilities for treating multiple uncertainty types in modeling and simulation activities. The approach is to leverage existing SwRI expertise and software tools to develop new capabilities in the areas of sensitivity analysis and model calibration, which are capable of distinguishing between reducible and irreducible uncertainties. The NASA Challenge Problem definition is used both to guide methodology development and also as a testbed to demonstrate the proposed approaches on a realistic engineering application.

Accomplishments — Under this research, new capabilities were developed for calibrating computer simulations using test data, which expand the scope of problems that can be addressed to include additional types of uncertainty. Also, a new approach for sensitivity analysis, referred to as "variance decomposition for statistical quantities of interest," was developed. This approach allows for identification of elements in a model that have the most potential for uncertainty reduction, while accounting for inherent variations that are not reducible. The results were presented at a special session for the Challenge Problem at the AIAA Science and Technology Forum and Exposition, and they were published in a special issue of the Journal of Aerospace Information Systems.

SOUTHWEST RESEARCH INSTITUTE®

2014 IR&D Annual Report

Development and Evaluation of Corrosion Resistant Alloy Coatings for Inner Surface of Tubes and Closed-end Vessels, 18-R8437

Principal Investigators
Jianliang Lin
Erica Macha

Inclusive Dates: 01/01/13 – Current

Background — The internal surfaces of production pipes and process vessels used by the oil and gas industry need protection from corrosion. Generally, corrosion-resistant alloys (CRA) have been widely used. However, the cost for high grade CRA pipes/vessels can be more than 20 times that of commonly used inexpensive stainless steels (e.g. AISI Type 316L stainless steel, SS316) or carbon steel pipes. Furthermore, the main composition of CRA is Ni and Cr with high quantities of molybdenum and tungsten. The increasing demand and cost for non-ferrous metals also drive increases in the price of CRA pipes, and prices for these materials are expected to rise. Additionally, the strength of CRA pipes is usually unsatisfactory compared to carbon steel. One effective way to bring the cost down for CRA pipes/vessels is to use stainless steel or carbon steel as the body material and apply a CRA coating (e.g. Hastelloy® C-276 alloy) onto the inner surface to add protection for the metal surface. The objective of this project is to develop corrosion-resistant C276 coatings for inner surfaces of pipes and closed-end vessels, and to evaluate the performance of C276 coatings under a high-temperature and high-pressure corrosive environment.

Approach — A cylindrical magnetron sputtering (CMS) technique has been developed at SwRI for depositing coatings on the inner surface of tubular structure and closed-end vessels. The C276 coatings were deposited onto stainless steel tubes and vessels using three different magnetron sputtering techniques: continuous dc magnetron sputtering (dcMS), middle frequency pulsed dc magnetron sputtering (PDCMS), and high power impulse magnetron sputtering (HiPIMS). The samples sectioned from the coated tubes have been evaluated in an autoclave for a NACE MR 0175 Level V environment test with a test period up to 90 days. The fundamental relationships between the process, microstructure and corrosion resistance of C276 coatings on the inner surface have been established. Finally, an optimized coating is applied to the inner surface of a closed-end stainless steel pressure vessel, which will be evaluated using the NACE MR 0175 Level V environment test.

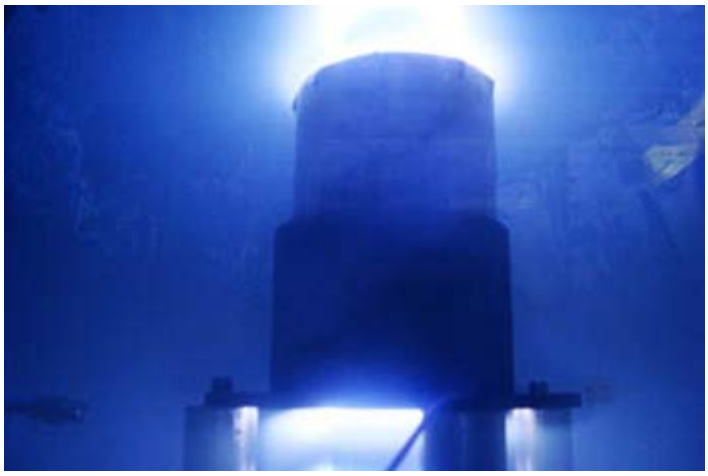

Figure 1. A photo showing the deposition of C276 coatings on the inner surface of an AISI316 tube in the CMS system.

Accomplishments — The new CMS system has been successfully used for depositing C276 coatings on the inner surface of tubular structure and closed-end vessels (Figure 1). The deposited C276 coatings exhibited the same chemical composition as the bulk Hastelloy® C-276 alloy. The C276 coatings with

thickness varying from 1 to 20 μm have been deposited using dcMS, HiPIMS and PDCMS techniques. Several key deposition parameters (including the substrate bias voltage, the working pressure and the target power) have been optimized to obtain C276 coatings with dense microstructure, good uniformity, excellent adhesion and smooth surface. A 90-day test in the NACE MR 0175 Level V environment demonstrated excellent corrosion resistance of the C276 coated stainless steel tube as compared to the uncoated one. The corrosion resistance of the coatings strongly depends on the density of the coating, the thickness of the coating, and the incorporated defects in the coatings. These properties can be controlled by selecting proper deposition techniques (between dcMS, PDCMS and HiPIMS) with optimized deposition parameters. Currently, the on-going project is focusing on optimizing the CMS system design to further improve the uniformity and quality of the C276 coatings on the inner surface of a closed-end vessel.

SOUTHWEST RESEARCH INSTITUTE®

2014 IR&D Annual Report

Design and Development of a New Gripping System and Direct Stress Measurement Method for High Strain Rate Materials Testing, 18-R8473

Principal Investigators
Kathryn A. Dannemann
Nikki L. Scott
Alexander J. Carpenter
Sidney Chocron

Inclusive Dates: 05/22/14 – 09/22/14

Background — A Hopkinson bar test system has been used extensively in our laboratory for determining the dynamic response of various materials (e.g., metals, ceramics, welds, glass, rocks, composites). This is the most widely used method for evaluating the high strain rate behavior of materials at strain rates ranging from 100 s^{-1} to 5000 s^{-1}. A schematic of the SwRI direct-tension Hopkinson bar is shown in Figure 1. For dynamic tension, Hopkinson bar testing of threaded cylindrical specimens is an established method. However, the threaded specimen design is not applicable for tensile testing of thin sheet (≤ 3 mm) materials. High strain rate tension testing of sheet materials presents inherent challenges: i) gripping of the specimen, and ii) a weak transmitted signal. The latter can result owing to the small cross-sectional area of the sheet specimen, especially for low sound speed materials. This poses challenges for extracting the stress signal to obtain the desired stress-strain curves. Further signal loss can result due to an impedance mismatch between the grip hardware and the specimen. A functional grip design with proper impedance is critical for high strain rate tensile testing of sheet materials and for obtaining accurate test data.

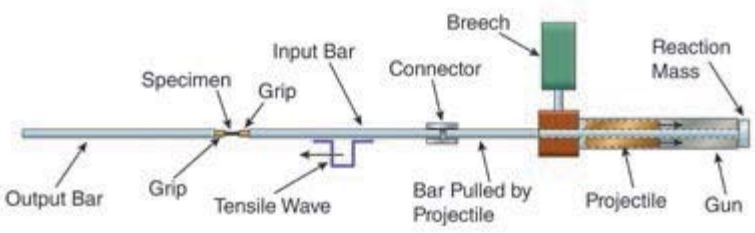

Figure 1. Schematic of the SwRI high strain rate direct-tension test setup. The grip (with tensile specimen) is threaded into the ends of the incident and transmitter bars.

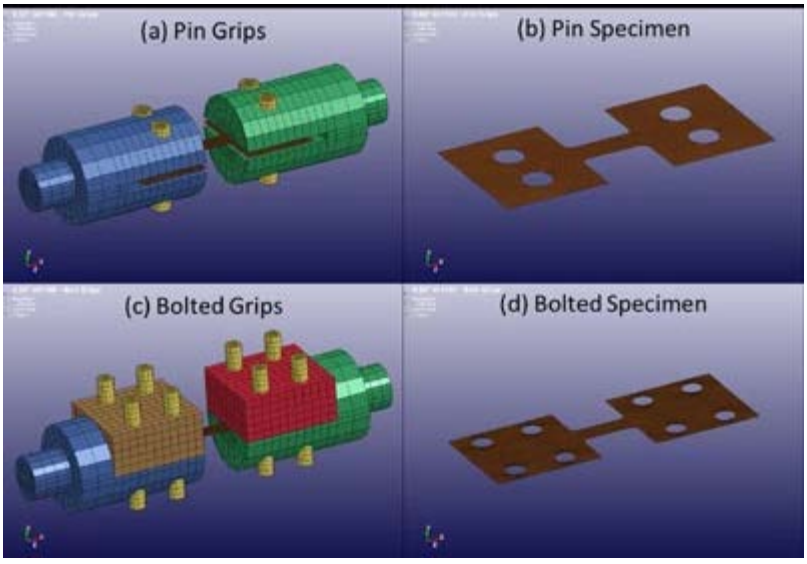

Figure 2. Schematics of the new pin grip and bolted grip. The pinned grip and specimen are shown together (a), and the pinned specimen is shown separately (b). The bolted grip and specimen are shown together (c), and the bolted specimen is also shown separately (d).

Approach — The objective of this project was to design and implement new grips for the SwRI direct tension Hopkinson bar that can accommodate sheet specimens for materials with different strengths and

thicknesses (≤ 3 mm thick). Grip designs with a mechanical means (i.e., pins, bolts) of securing the specimen were utilized to prevent slippage in the grips. High strain rate experiments were designed and conducted to demonstrate the effectiveness of the new grip and specimen designs, and to confirm the reliability and consistency of the measurements. High-speed cameras were used to photograph the progression of damage during tensile loading. Digital image correlation (DIC) software was used to analyze the images and determine strains in the specimen during testing, and for comparison with strains determined from elastic wave analysis as is typically done in Hopkinson bar testing. Numerical simulations of the experiments were performed to aid with interpreting the experiments and to confirm the accuracy of the test results.

Accomplishments — Two new grip and sheet specimen designs were implemented and proven; schematics of these designs are shown in Figure 2. This was accomplished using carefully designed experiments with aluminum and stainless steel sheet specimens. Materials were selected to determine the effectiveness of the grips for a range of conditions (strength, ductility and thickness: 0.125 to 0.5 mm). A slot grip design that incorporated mechanical restraints (pins, bolts) limited the extent of specimen slippage during testing. The size and placement of the grips holes were engineered to limit stress concentrations and minimize the possibility of crack initiation near the holes. Numerous dynamic tensile experiments, conducted at approximate strain rates of 10^3 s^{-1}, demonstrated the reliability and consistency of the data. The results show good agreement for: i) strains derived from strain gages on the incident bar using elastic wave analysis (the usual method), ii) direct strain measurements from gages on the bar, and iii) strains maps derived from DIC analysis. Stresses derived from semiconductor gages, located on the transmitter bar approximately 150 mm from the specimen, provide more accurate stress measurements when the transmitted wave signal is weak. Comparison of the experimental data with numerical simulation results for each test condition confirmed the accuracy of the experimental results for ductile materials. For materials with low ductility, numerical analyses are included to ensure accurate interpretation of the experimental results.

Video of high strain rate tensile test on 0.5-mm thick sheet steel specimen. The strain profile in the upper image was obtained from digital image correlation analysis.

2014 IR&D Annual Report

Investigation of Computational Methods for Modeling Bird Strike Impacts on Aircraft Structures, 18-R8477

Principal Investigators
James Mathis
Sidney Chocron
Joseph Bradley
Andrew Barnes
Matthew Grimm

Inclusive Dates: 07/01/14 – Current

Background — Collisions with bird and aircraft have been a problem since the beginning of aviation. A bird strike during flight can be a major threat to the aircraft depending on the size of the bird, speed of the aircraft, and location of the strike. All aircraft components that are at risk for bird strike are required by regulating authorities to undergo a certification process aimed at demonstrating that a safe landing is possible after a bird strike event. Designers and manufacturers of these components rely heavily on experiments; however, costs to conduct research and development tests are substantial due to the destructive nature of the test and limited production prototypes. In recent years there has been a shift toward the use of computational tools to simulate the behavior of components during an impact event. Unfortunately, the simulations are not always accurate due to the complex composite materials that are often used on forward-facing surfaces in an effort to save weight. Clearly trends are shifting toward the use of numerical simulations for early design efforts and in some limited cases, full certification by analysis. With these challenges in mind, SwRI is conducting a research project aimed at developing and demonstrating SwRI's capabilities to accurately model bird strike impact into aircraft structures using finite element analysis techniques. The intent is to demonstrate this capability through a coupled experimental and computational approach using our existing experimental expertise and computational tools.

Approach — Based on our history in supporting many clients with quality bird strike testing services, combined with our general expertise in computational modeling of ballistic impact and material response, we believe that we are well poised not only to support this emerging market opportunity but also to push the state of the art by generating reliable bird and aircraft structure material models that can accurately predict deformation and failure. We begin with a brief review of current methods used to simulate bird impacts. Sources of existing experimental data will be identified that can be used to aid in validating our simulations. Experiments will be designed and conducted to collect data related to the loading produced by bird strike impacts. Computations will be conducted simultaneously to validate a methodology for reproducing the impact loads measured experimentally. Experiments will also be conducted to determine material constants needed to accurately represent the bird. Actual aircraft material coupon samples will be tested to collect data relevant to understanding the behavior of the materials/structure under the dynamic loading due to bird strike. Computations will then be conducted to demonstrate our ability to accurately model the material and structural response of composites and certain transparencies due to a variety of impact conditions.

Accomplishments — Initial simulations using modeling methodologies including Smooth Particle Hydrodynamics (SPH) and Arbitrary Lagrangian Eulerian (ALE) to represent the bird have been carried out. Simulations were performed to replicate a set of experiments conducted previously on rigid targets instrumented with pressure sensors to measure the loading magnitude and profile due to bird impacts at

various angles of incidence (Figure 1).

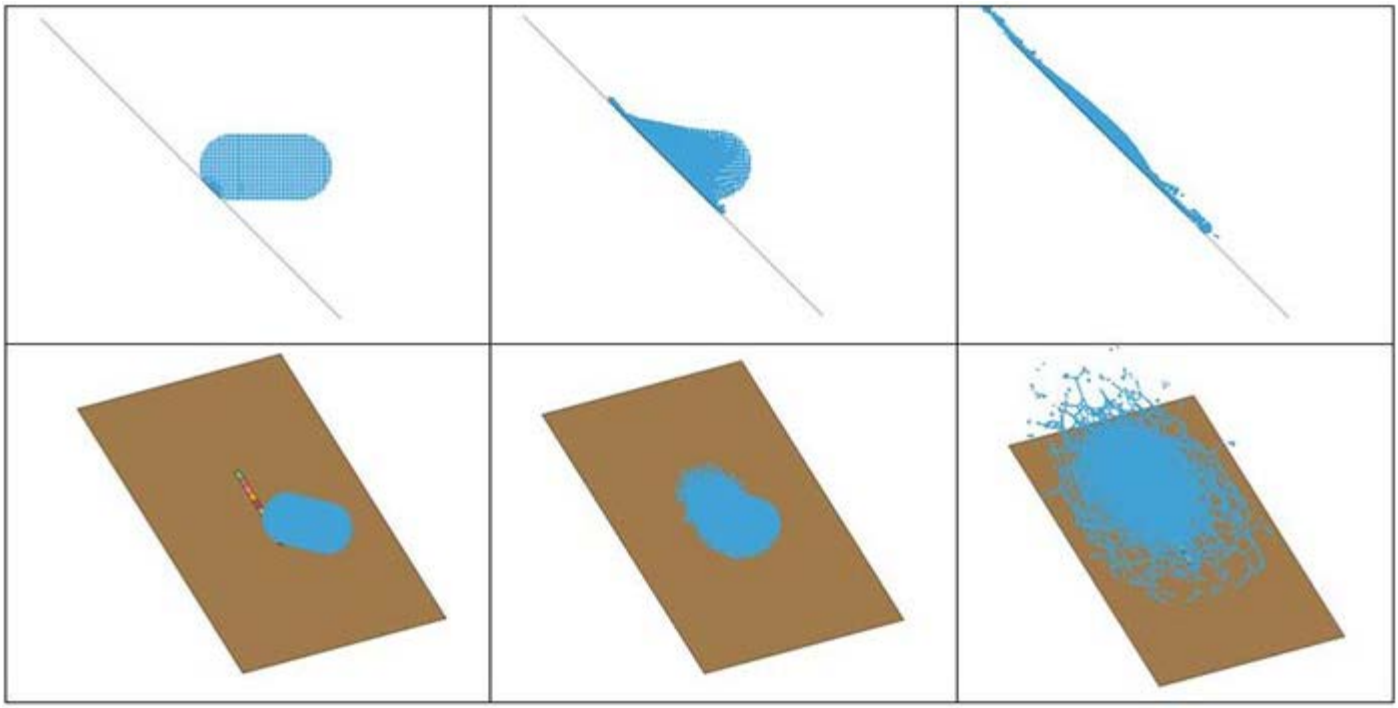

Figure 1. Typical SPH simulation results of a 45-degree bird impact against a rigid surface.

The simulation results using ALE and SPH methods along with bird material models available in literature were compared with the available experimental data. Overall good results have been achieved (Figure 2); however, we look forward to incorporating our bird material characterization experimental data as it becomes available later in this project.

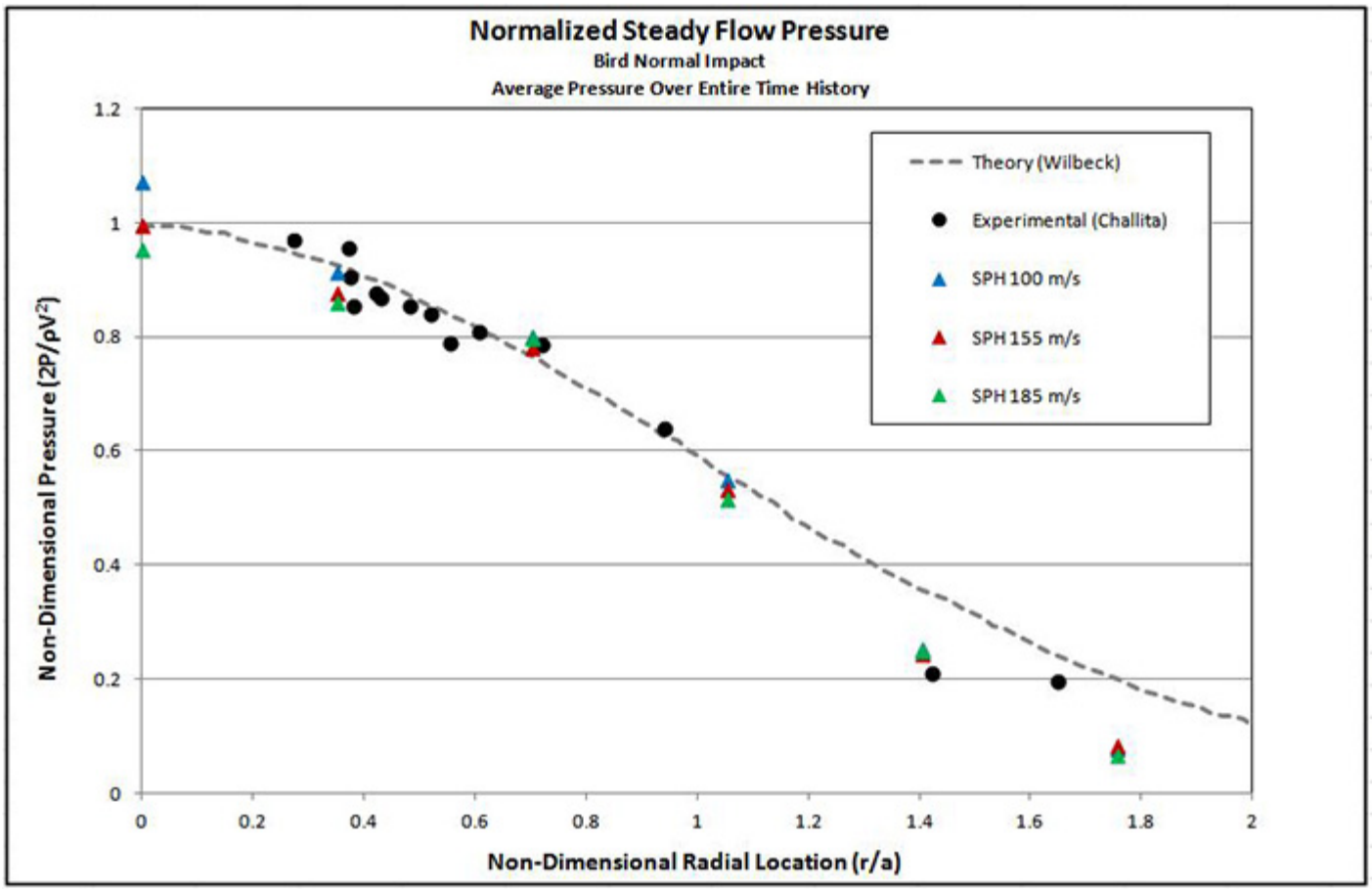

Figure 2. SPH steady flow pressure distribution for a normal impact.

Initial simulations of bird impacts against deformable targets have also been carried out. Experiments were previously conducted by impacting birds against aluminum panels and measuring reaction forces and strains during those impacts. Equally favorable results have been achieved.

2014 IR&D | IR&D Home

SOUTHWEST RESEARCH INSTITUTE®

2014 IR&D Annual Report

Developing a Three-Dimensional Model to Estimate Electrical Current Requirement at a Coating Defect Site on Pipeline Segments Installed Using Horizontal Directional Drilling, 20–R8429

Principal Investigators
Stuart Stothoff
Pavan Shukla

Inclusive Dates: 11/19/13 – 03/19/14

Background — Horizontal directional drilling (HDD) is being increasingly used in trenchless installation of coated pipelines. A schematic of an HDD-installed section is presented in Figure 1. The coating on the pipeline is particularly susceptible to damage during the HDD installation process. A cathodic protection (CP) system is often used to mitigate corrosion of the installed pipeline segments. The objective of this project was to develop the capability to estimate performance of the CP system for the HDD pipeline segments. Such a capability can be used to determine whether computer modeling is a feasible approach for confirming effectiveness of a CP system; assess optimal ground bed types, anodes, and configurations to maximize CP effectiveness at HDD locations; evaluate effects of a resistive rock stratum on CP system performance; develop guidelines for incorporating CP system monitoring hardware and configurations into HDD designs to ascertain protection levels throughout the entire HDD length; determine levels of CP protection when the pipe segment is partially in contact with soil and partially exposed to the air in the gap of the HDD borehole; and correlate in-line inspection metal loss data with CP inspection data. The capability can also be used to analyze field scenarios that cannot be adequately addressed by current CP design equations. This project was sought to develop such a capability and respond to a likely request for proposal from a potential client.

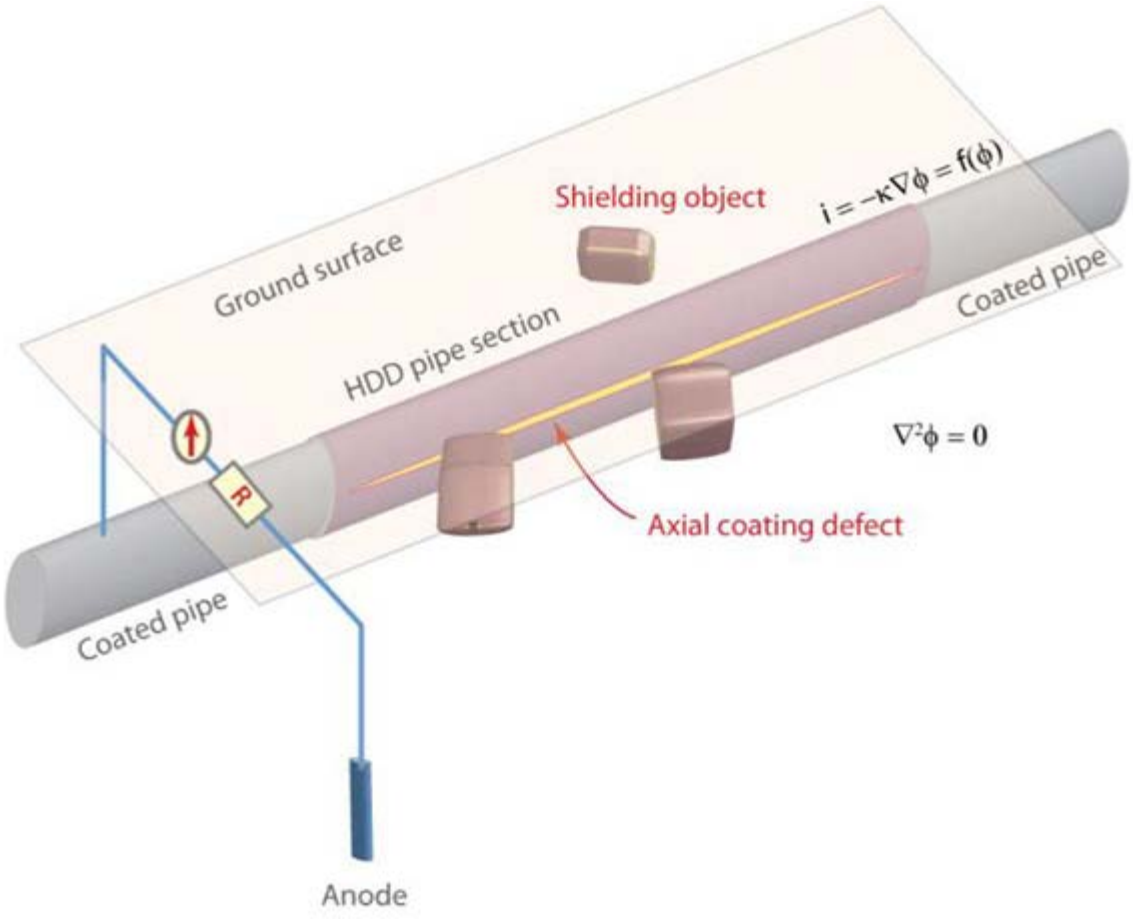

Figure 1. Schematic of the horizontal directional drilling-installed pipeline with axial coating defect.

Approach — A boundary-element-method (BEM) model was developed to simulate CP systems on coated pipeline segments installed using HDD. The BEM model took advantage of specialized surface elements that explicitly account for the shape of the surface, which speeds up computations by orders of magnitude by greatly reducing the number of unknowns to be determined. A single cylindrical element replaces one or more rings of rectangular elements, which are typically used to discretize pipeline surfaces. Verification of the BEM model used a second model, based on finite element method (FEM)-based computational software. The FEM model provides an independent calculation check for specific conditions where both models are accurate.

Accomplishments — The BEM computation model was successfully developed and validated with the FEM-based model. The BEM model can consider an arbitrary number of objects and subzones in an installed pipeline; can consider bare metal, resistive coatings, and nonconductive coatings; has flexible gridding with automated refinement; allows high-order integration of elements near singularities for improved accuracy; and can consider pipelines that are up to several miles long. The capability developed during this project has positioned SwRI well for conducting modeling work in the field of pipeline corrosion. The validation results indicated that the cylindrical elements in the model were correctly implemented and provide guidance on their applicability to field problems. The validation results suggest that the cylindrical elements provide good estimates when the anode is more than two or three pipe diameters from the pipe segment and suggest that an anode can be represented accurately using cylindrical elements unless it is very close to the pipe segment. Further testing is necessary to determine appropriate separations for a given accuracy level.

2014 IR&D Annual Report

Dynamic Response of Steel-Plate and Concrete Composite Small Modular Reactor Structures Under Explosive and Seismic Loads, 20–R8433

Principal Investigators
Asadul Chowdhury
Kevin Smart

Inclusive Dates: 12/13/13 – Current

Background — Conventional reinforced concrete structures for nuclear facilities are designed to the American Concrete Institute code. This code is based on extensive experimental, analytical, and numerical studies, as well as observations of the performance of reinforced concrete structures under actual natural hazards, such as earthquakes, high winds, floods, or tsunamis. There is considerable interest in the United States, Japan, and Korea to build nuclear power plants using steel-plate and concrete (SC) composite structures in which concrete is sandwiched between a pair of surface steel plates and the traditional rebar inside the concrete is replaced by steel members of different shapes, sizes, and spatial distribution. The interest in SC structures stems from their improved performance, reduced cost, shorter modular construction period, and less site work.

Approach — The primary aim of this project is to gain a better understanding of dynamic behavior and responses of shallow-buried SC small modular reactor (SMR) containment dome structures subjected to explosive loads and earthquake ground motion through numerical modeling, starting with an existing constitutive relationship [concrete damaged plasticity (CDP)] and selecting a simplified ABAQUS model without explicit modeling of some steel members embedded inside concrete. A three-step approach is used: (i) numerical simulations of experimental tests of SC structures with explicit inclusion of concrete and steel components and comparison of simulation results with those from the experimental tests, (ii) repeat simulations using a CDP constitutive relationship with a simplified ABAQUS model to capture the overall behavior of the SC structure without explicitly simulating the steel components, and (iii) testing the simplified ABAQUS model against an independent set of experimental tests to gain confidence in the model validity. The simplified ABAQUS modeling technique will be used to study the response of underground SC SMR containment structures subjected to selected explosive and seismic loads, including soil-structure interaction without explicitly modeling each embedded steel and concrete constituent of the SC SMR containment structures.

Accomplishments — Efforts to date have focused primarily on numerical simulations of in-plane cyclic shear tests. Two different test configurations have been analyzed that employ different steel plate thicknesses, stud bolt diameters, and stud bolt spacings. Comparison between numerical simulations and experimental data is based on three load-versus-strain points (concrete cracking strength, steel yield strength, and maximum strength).

2014 IR&D Annual Report

Development of a Numerical Approach to Modeling Internal Erosion in Embankment Dams and Levees, 20–R8463

Principal Investigators
Biswajit Dasgupta
Gordon Wittmeyer
Goodluck Ofoegbu

Inclusive Dates: 04/01/14 – Current

Background — Failure of embankment dams and levees by backward erosion or "piping" is a major safety concern. Internal erosion by piping typically occurs in non-cohesive granular soil (e.g., sand, silt) within the foundation and embankment of the dam or levee initiating at the toe of the dam when the fluid forces from focused seepage are sufficient to suspend and transport sand particles out of the embankment or foundation. The resulting cavity further concentrates seepage, more sand is eroded, and the cavity elongates, forming a pipe or tunnel that propagates upstream. The pipe may grow in size because of internal soil erosion from concentrated internal seepage. The pipe collapses when the pipe walls can no longer support the overburden pressure, causing the overlying earth embankment to fail in modes that range in severity from slight slumping to complete collapse. Observed dam failures from piping have been sudden with little or no prior indications.

Preventing or mitigating internal erosion as a result of piping or backward erosion process is an essential consideration when designing, inspecting, and maintaining levees and dams. Embankment dams with permeable foundations are common in the United States, and there is extensive experience in design, maintenance, and operation of these dams within the civil engineering profession; however, backward erosion remains a poorly understood failure mechanism. Existing internal erosion prediction methodologies, which are based on information acquired from laboratory or field tests, are not adequate for accurate prediction.

Risk assessment of existing dams is gaining importance in the United States and in the rest of the world to ensure safety from aging and from beyond design-basis flood and seismic events. However, the current risk assessment evaluation methodologies for piping failure modes of embankment dams rely on empirical approaches developed based on existing data that may not be applicable to conditions of existing dams. The purpose of this research is to develop a computational approach to model the internal erosion phenomena and develop a process to simulate piping in embankment dams and levees to support risk assessment of existing dams in the U.S. and other countries.

Approach — Internal erosion of the soil embankment or foundation is a complex process that involves continuous three-dimensional (3-D) interactions among seepage forces and intergranular forces wherein piping initiates in the downstream area, erodes backward toward the reservoir, and increases in size, potentially resulting in dam breach and collapse. The research aims at developing a computational methodology for modeling backward erosion in embankment dams and levees by using both micromechanical and continuum modeling approaches. A particle-based micromechanical model will be used to simulate piping at the laboratory scale for a wide range of hydro-mechanical conditions in order to evaluate relationships among hydro-mechanical properties needed for a continuum description of the piping process. The resulting relationships will be applied to develop a continuum modeling approach for coupled fluid-mechanical interaction analysis for simulating backward erosion in full scale dams and levees.

The technical approach for accomplishing the objectives of the research project consists of several steps: (i) extend the capability of a commercially available particle flow code (PFC-3D) with coupled computational fluid dynamics (CCFD) for simulating seepage-induced erosion in a laboratory-scale experiment, (ii) use the model to replicate key physical features observed in small-scale laboratory piping experiments, (iii) establish criteria for the occurrence of piping for a range of particle sizes and particle size distributions, (iv) use the results to develop continuum-scale block or element failure criteria, and (v) simulate small-scale laboratory piping experiments using the continuum-scale code FLAC3D with block failure criteria to simulate backward piping. The simulated backward erosion must initiate on the downstream side of the levee and progress backward to the upstream side, forming a continuous "pipe" through the foundation material.

Accomplishments — Progress has been made in numerical simulation of coupled fluid flow and particle flow using PFC3D and CCFD software to evaluate feasibility of modeling laboratory-scale experiments. Simulation of basic erosion processes was demonstrated for onset of vertical piping due to liquefaction failure, and simulation of horizontal piping in a sand-box experiment is in progress. The simulations also are being used to explore representation of the physical forces involved in particle-fluid interactions to develop failure criteria for continuum damage of internal erosion. Simulation of coupled seepage flow and mechanical response in the granular media of a dam foundation is underway to evaluate the continuum damage concepts using two-dimensional continuum code FLAC.

2014 IR&D Annual Report

Mobile Persistent Stare Using Unmanned Systems, 10-R8306

Principal Investigator
Paul A. Avery

Inclusive Dates: 04/02/12 – 04/02/14

Background — Within the Unmanned Ground Vehicle (UGV) community there have been a number of successful "short-duration" demonstrations, which perform well for 10 to 45 minutes. In order for UGVs to have long-term success in tactical situations, they need to perform missions in duration of 4 to 12 hours. The military has indicated that system "resets" could occur during fueling operations that occur at least every 12 hours. The software for these systems needs to be adaptable and flexible enough to allow the system to "correct" itself over the mission duration. Additionally, most demonstrations have used one of two sensing technologies: Light Detection and Ranging (LIDAR) or Electrical Optical (E/O); SwRI is well versed in both technologies, but fusing the two technologies (cooperatively across platforms) dramatically improves the performance of UGVs. An objective of this project was to add several additional building blocks to the SwRI MARTI (Mobile Autonomous Research Technology Initiative) software platform that are necessary for long-term viability of UGV technology. Groups of unmanned vehicles conducting long-term operations benefit from being linked together to form a cooperative vehicle system, which SwRI demonstrated for traffic scenarios.

Approach — The approach in this work was to develop hardware-agnostic software tools to automatically collect "health" status data from numerous hardware and software components of an unmanned vehicle, which can later be analyzed for long-term operational effectiveness. This tool is integrated into the unmanned vehicle's operating framework, enabling a more rapid identification and notification of system warnings, errors, or failures. With this tool, we were able to conduct endurance autonomy testing with SwRI's fully autonomous HMMWV 1165. A perimeter was identified for a surveillance mission around the SwRI facility. A cooperative perception system framework was developed to allow the integration of sensor and position data from a number of UGVs. We defined and developed tactical behaviors for the cooperative system and integrated these into the assessment for a cooperative vehicle mission.

Accomplishments — Hardware-agnostic software tools were developed using the Robot Operating System (ROS) diagnostic tools for logging data related to the operation and behavior states of an autonomous vehicle platform. The specific vehicle platform that was targeted initially is the SwRI-owned HMMWV 1165. The data logging system functions by subscribing to ROS topics that indicate the status of various subsystems, such as behavior states and health status of all included sensors. This manner of operation allows for the system to operate without modifications to the current vehicle codebase. During operation, the data is periodically saved to a human-readable file called a YAML file, which is later moved to another computer for processing. The data is parsed in a variety of ways, and presented visually, to further facilitate analysis of the performance of the vehicle during the test. A model of a cooperative vehicle system has been developed using agent-based methods, where a simplified UGV model (agent) was combined with other agents in a scenario of perimeter patrol. The behavioral characteristics of individual UGVs when some specified anomaly was either detected or communicated from another vehicle has been investigated regarding their effect on system-level behavior.

SOUTHWEST RESEARCH INSTITUTE®

2014 IR&D Annual Report

ROS-Industrial® Strategic Technology Development, 10-R8335

Principal Investigator
Shaun Edwards

Inclusive Dates: 09/17/12 – 12/11/14

Background — In a previous internal research effort, the principal investigator worked closely with Robot Operating System (ROS) developers at Willow Garage to develop an open-source ROS-Industrial software stack (software suite) to support the use of ROS for industrial applications. The technology developed under this previous effort brought the use of powerful ROS capabilities, such as advanced perception and path/grasp planning, to industrial robotics applications. Since the completion of the previous project, the ROS-Industrial open-source program has attracted significant interest in the industrial robotics community. Two examples of this interest are the growth of the open-source development community and the ROS-Industrial Consortium. The open-source community has grown to include a worldwide network of commercial, independent, and government labs working towards a common goal of enabling advanced industrial robotics and automation through open source development. The ROS-Industrial Consortium, in its second year, now includes 24 members and has expanded with the formation of a European branch. The consortium provides commercial investment and input into the ROS-Industrial program. Specifically the consortium provides funding for technology development through focused technical projects (FTPs). The objective of the ROS-Industrial Strategic Technology Development effort was to continue technology development, expanding the capabilities of ROS-Industrial, while supporting the Consortium and open source community.

Approach — The approach of this ROS-Industrial technical effort was to expand its capabilities through continued software development both at SwRI and through external development teams, as well as demonstrate real-world applications. Specifically this effort:

- Provided guidance to the ROS-Industrial open-source community, outlining development efforts for external teams.
- Expanded the ROS-Industrial driver set, providing compatibility and interoperability with major industrial robot vendors.
- Integrated advanced path planning and perception algorithms with a focus on those that are useful in industrial applications, such as machining and painting.
- Demonstrated ROS-Industrial in multiple real-world applications through cooperation with commercial companies.

The software developed under this internal research effort will be released open source under the ROS-Industrial program.

Accomplishments — The project has completed the following milestones:

- The ROS-Industrial software has grown, with many contributions coming from external development teams in the open source community.
- The ROS-Industrial software now supports most major industrial robot vendor platforms. This capability was demonstrated at the Automate trade show in early 2013.
- Integration of ROS-Industrial with the MoveIt library, which provides advanced path planning capabilities with close integration of 2-D/3-D perception.
- Real-world problems solved with ROS-Industrial under Consortium FTPs.

- Library development for optimizing industrial pick-and-place cycle times.
- Application development for automated deburring, polishing, and finishing of machined aerospace parts is in progress (see Figure 1).
- Application development of a robotic cutting system utilizing a portable measurement device to define cutting paths is in progress.

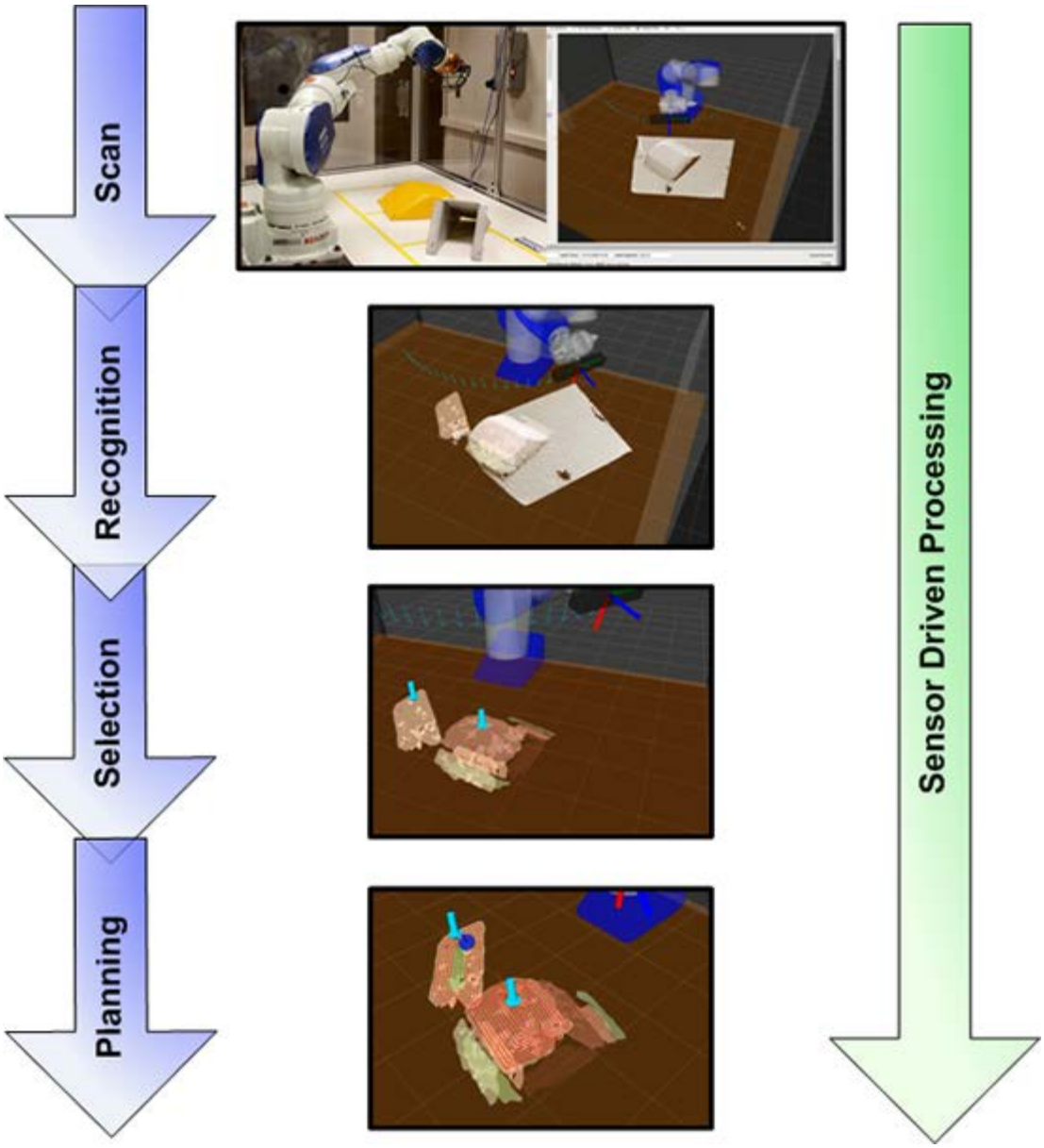

Figure 1. Automated deburring, polishing, and finishing application enabled by ROS-Industrial. Using ROS-Industrial perception and planning capabilities, sensor driven processing is a reality.

SOUTHWEST RESEARCH INSTITUTE®

2014 IR&D Annual Report

Control of Laser Coating Removal Process, 10-R8385

Principal Investigators
Michael P. Rigney
Thomas G. Whitney III
Michael O. Blanton Jr.
Thomas E. Lyons Jr.

Inclusive Dates: 04/01/13 – 09/17/14

Background — Use of high-power lasers for coating (paint) removal from aircraft surfaces offers a significant improvement in process efficiency and reduction of both consumables and waste streams relative to alternate approaches (chemical stripping, media blasting). The ability of lasers to quickly ablate paint from surfaces comes with the challenge of controlling laser power to achieve a selective coating removal goal. A sensing and control system supporting selective coating removal allows for removing the top coat(s) while leaving the primer layer, overlapping processing passes, and minimizing energy input to the substrate. SwRI has long history in the design and deployment of large robotic systems employing media-blasting for coating removal from military fighter aircraft. This research, combined with our capabilities in precision mobile robot systems, supports developing coating removal systems for large military and commercial transport aircraft.

Approach — The objective of this research was to implement a coating state classifier supporting selective coating removal with a high-power laser. The sensing, classifier, and control systems must handle: 1) wide variation in coatings and substrates (thickness, color, laser ablation response), 2) subtle differences between some coatings and substrates, 3) observing a mixture of top coat and underlying material (coating or substrate) within the sensed incremental surface regions during the laser ablation process, 4) the presence of combustion products (flame, smoke, illumination) in the sensed region, and 5) a high process cycle rate (300 Hz).

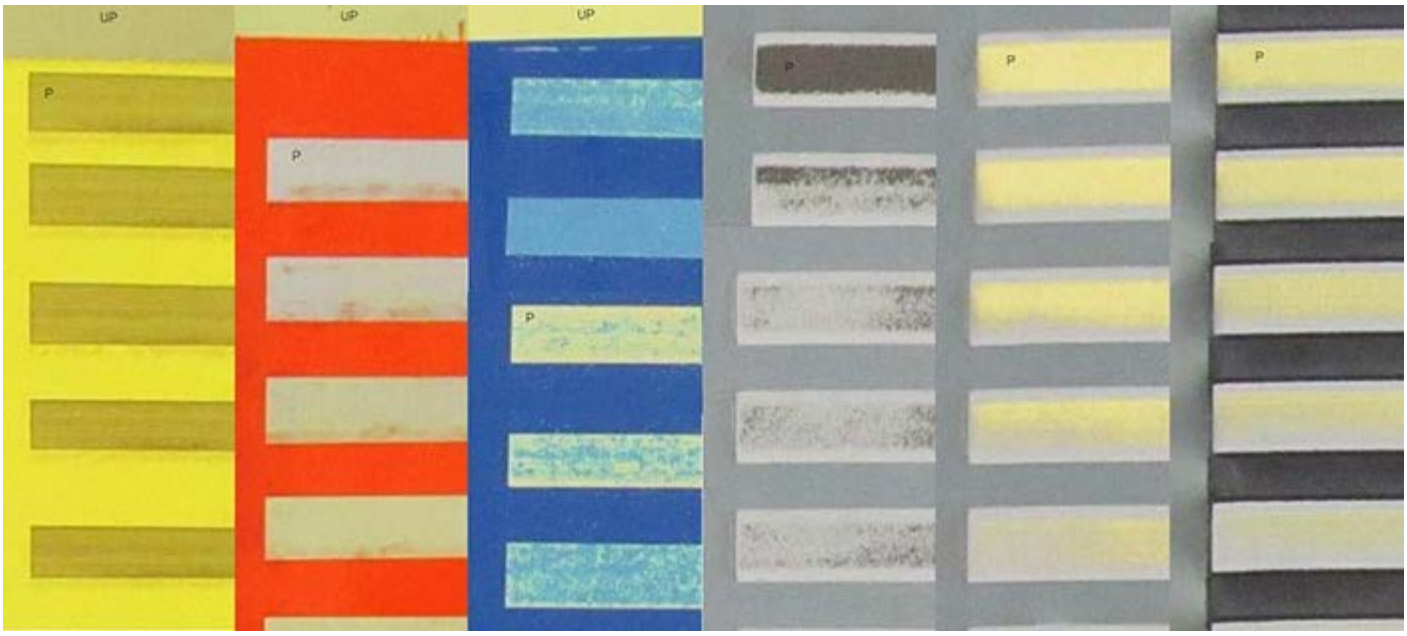

Figure 1. Composite image illustrating three commercial paint systems (left), three military paint systems (right), and coating removal states resulting from different laser power levels.

Test panels representing a wide variety of commercial and military paint systems (primer and top-coat combination) were fabricated or procured. Regions of test panels were processed open-loop by the laser ablation scanner at numerous power levels (Figure 1). Regions were assigned a coating removal state indicating whether insufficient, excess, or the correct amount of coating had been removed. Image data acquired during and subsequent to open-loop processing was used to implement a coating removal state classifier based on features sensitive to image color, intensity gradients, and texture. Numerous features and classifiers were evaluated, followed by feature down-selection to achieve real-time assessment while retaining good classification performance. The output from the coating state classifier fed into a PID control loop to modulate laser power.

Accomplishments — Imaging and illumination system components were refined to obtain improved image quality. Synchronization between image acquisition and the laser scanner was modified to enable laser path measurement, supporting system operation on surfaces with variable curvature. Coating state classifiers provided an RMS error of 1 percent and 3 percent for classifiers trained to evaluate combinations of two- and eight-paint systems, respectively, and provided excellent performance in discriminating between observations representing five or more coating removal states. Image analysis algorithms and coating state classifiers operated in real-time (300 Hz) and successfully provided closed loop control of the laser ablation process (Figure 2).

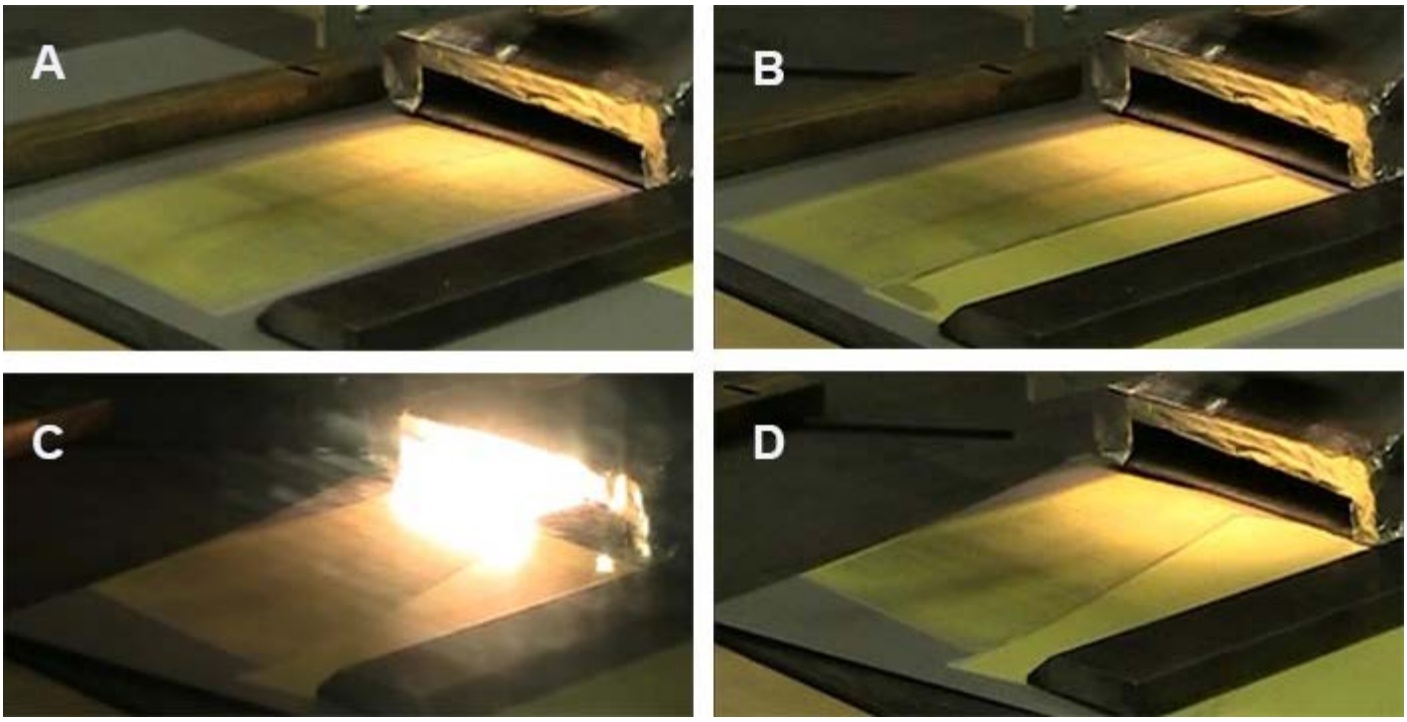

Figure 2. Selective coating removal control with overlapped processing passes. First pass, full swath (a). Second pass with 25 percent overlap of first pass (b). Note reduced laser ablation flame width near third pass completion due to control system response (c). Completed third pass with angled overlap (d).

2014 IR&D Annual Report

Microwave Methods for Enhanced Combustion in Natural Gas Engine Applications, 10-R8408

Principal Investigators
E. Sterling Kinkler Jr.
Christopher Chadwell
Barrett W. Mangold
Russell K. Barker

Inclusive Dates: 07/01/13 – 01/01/15

Background — Internal combustion engines (ICE) are used to convert energy stored in fossil fuels to usable power for transporting people and accomplishing work in an astonishing array of applications and industries. Planes, trains, and automobiles have been the most visible platforms using ICE technologies since the early 1900s, and the energy crises of the 1970s initiated much interest in higher fuel efficiencies. Accompanying the vast growth of operating ICE products, environmental issues are also major concerns. Current and especially future, economic, regulatory, and social pressures are fueling significant research in cleaner, higher efficiency combustion processes. Exhaust gas recirculation (EGR) techniques are frequently found in modern gasoline engines to help reduce harmful emissions and improve efficiency. High levels of EGR dilution can result in slower combustion and related ICE performance problems. Enhanced combustion of gaseous fuels has long been observed when electric fields are applied. Microwave (MW) techniques can produce very high intensity electric fields within an enclosed volume and are often used to develop intense electric fields that accelerate sub-atomic particles to near-speed-of-light velocities for modern physics research. International regulations allocate multiple MW frequency bands for use in industrial applications. Previous work at SwRI coupling MW power into an existing spherical chamber during combustion of gasoline/air mixtures has produced promising experimental results.

Approach — We sought to effectively couple MW power into an enclosed metallic chamber emulating the combustion chamber (CC) of modern ICE products. Design and test of fundamental methods and techniques to develop intense electric fields within a modern ICE CC is an enabling step toward implementation of running ICE platforms that can facilitate performance testing with MW enhanced combustion (MEC) techniques applied. Our approach was to research, fabricate, and test experimental MW coupling methods that can achieve significant MW fields within a CC and accommodate the many constraints imposed by the design and operation of modern commercial ICE products. The ICE CC is generally in the shape of a cylinder with variable height and contains a harsh internal environment, including cyclic high temperatures and pressures. Our research goals included implementation of high intensity internal electric fields for a range of ICE products and operating conditions. The large-bore natural gas ICE class was chosen due to physical and dimensional characteristics and the potential for relatively significant economic and environmental impact of improvements in efficiency and emissions, as engines in this class typically run 24/7 at high loads.

Accomplishments — The team performed research and preliminary design and analysis for a number of experimental MEC implementation methods and selected an initial design using a coaxial MW delivery system coupled to a small circular dielectric-filled MW waveguide. The filled waveguide was intended to couple and excite a desired MW field structure within the CC, maintain the necessary pressure envelope of the CC, and facilitate future MEC integration within commercial ICE products. The team completed design and fabrication of a filled waveguide, including features needed to efficiently transition between a

coaxial MW feed and the waveguide. The team also completed design and fabrication of the laboratory CC fixture that mimics selected commercial CC shapes and sizes, and can facilitate MW system function, performance, and sensitivity experiments. The coaxial-fed filled waveguide and CC fixture have been combined, and system test and refinement completed. An agreement with a major engine manufacturer was concluded, providing the team with design information for current ICE products. Teaming with a large original equipment manufacturer provided realistic constraints on the design of the MEC system to accelerate acceptance of MEC technology in the large bore natural gas engine industry.

2014 IR&D | IR&D Home

SOUTHWEST RESEARCH INSTITUTE®

2014 IR&D Annual Report

Object Ranging and Classification using 3-Dimensional Shapes
10-R8421

Principal Investigators
Douglas Brooks
Edmond DuPont
Christopher Mentzer

Inclusive Dates: 10/01/13 – 10/01/14

Background — Object classification, localization, and ranging are critical objectives in unmanned ground vehicle (UGV) navigation and surveying. The ability to autonomously classify, locate, and determine the distance to various items at any given time aids an autonomous system in understanding the current situation and making calculated decisions regarding its next action. Unfortunately, false classifications or missed classifications of objects continue to be problematic for UGV navigation. Furthermore, manual a priori training of classifiers containing objects of interest requires time and effort that could be better utilized in other areas of implementing autonomous systems.

Figure 1. 2-D image and 3-D object model generated from 2-D image.

Figure 2. Successful feature matching created from a forward facing vantage point.

Approach — The goal of this project was to develop an algorithm and technique for quantifying and mapping three-dimensional (3-D) features to two-dimensional (2-D) features for the purpose of classifying 2-D objects, more efficiently and effectively than the state of the art, during UGV navigation and surveying. The approach incorporated 3-D modeling and a novel method to create a rich set of 3-D features from a single object by way of scanning the object of interest and using texture-based information to generate a method that compares those features to 2-D features obtained from a single camera image. Figure 1 illustrates this approach.

Accomplishments — The results of matching features in 2-D space indicated that there were indeed opportunistic features that exist on the 3-D model. Each of the best performing descriptors tested was able to match a significant number of features from the 3-D model projected into 2-D space and the original 2-D image when the image and projection have a similar orientation. As hypothesized, each descriptor fails to match a significant number of features when the orientations of the objects are drastically different. As a result, one approach to employing this type of system is to create images of the object at fine resolution degree increments from the 3-D model, create a database of feature sets for each defined view of the

model, and perform currently used matching techniques for object detection. This approach ensures a robust dataset that will enable highly accurate recognition of the object during real-time operation. Furthermore, during the data collection process a priori information such as the current range and degree offset from an initial position can be stored in congruence with the projected model, thus allotting for easier determination of the range and pose of the object during real-time operation. Figure 2 illustrates feature matching between a 3-D model projected into 2-D space and the original 2-D image.

SOUTHWEST RESEARCH INSTITUTE®

2014 IR&D Annual Report

Low Cost Accurate Six-DOF Industrial Robot Localization System Software Modeling and Testing, 10-R8443

Principal Investigators
Christopher Lewis, Ph.D.
Paul Hvass

Inclusive Dates: 01/01/14 – Current

Background — Close-range photogrammetry uses multiple cameras to track or measure objects. Digital cameras now are being considered to provide real-time feedback to robotic manipulators and autonomous vehicles. Vision-based tracking systems have the potential to eliminate positioning errors caused by mechanical inaccuracies, loading, wheel slippage, etc. Low-cost, highly accurate positioning opens a wide range of applications to robotic automation. These systems may also replace coordinate measurement machines for metrology. Many factors affect the accuracy of close range photogrammetric systems. One goal is to understand the roles that geometry, lens quality, pixel resolution, calibration procedures, target geometry and other factors play in overall system accuracy. Another goal is to predict the accuracy of the overall system from component characteristics.

Approach — The accuracy of locating objects in images is fundamental to photogrammetric techniques. Therefore, we characterized the accuracy of locating objects using fiducials of various sizes mounted on an optical bench and using motion stages. From this investigation, we verified theoretical predictions relating size and viewing perspective for planar circular fiducials. We also developed a projection model that accounts for the shift between the center of a circle and the center of the observed ellipse. The fiducial localization noise model is the progenitor to both intrinsic and extrinsic calibration accuracy as well as for overall system accuracy. We developed both Monte-Carlo and covariance techniques for predicting accuracy of each phase and then the accuracy of the final system.

Accomplishments — We predicted the accuracy field of a 48-camera system covering the walls and ceiling of an aircraft hangar. The camera system provides localization to a mobile manipulator painting passenger jets. Our work verified the design met system requirements throughout the working volume. We developed a general, configurable calibration framework to automate a variety of robot-camera calibration tasks. This tool interfaces to robots, imagers, and other hardware to automatically collect observations and submits them for optimization. This tool has been used to:

- Precisely locate a 3-D camera mounted on a robot's wrist that scans and processes machined parts.
- Calibrate a network of eight 3-D cameras that scan large parts on a chain conveyor for robotic painting.
- Perform intrinsic calibration using a robot to provide repeatable accurate results.

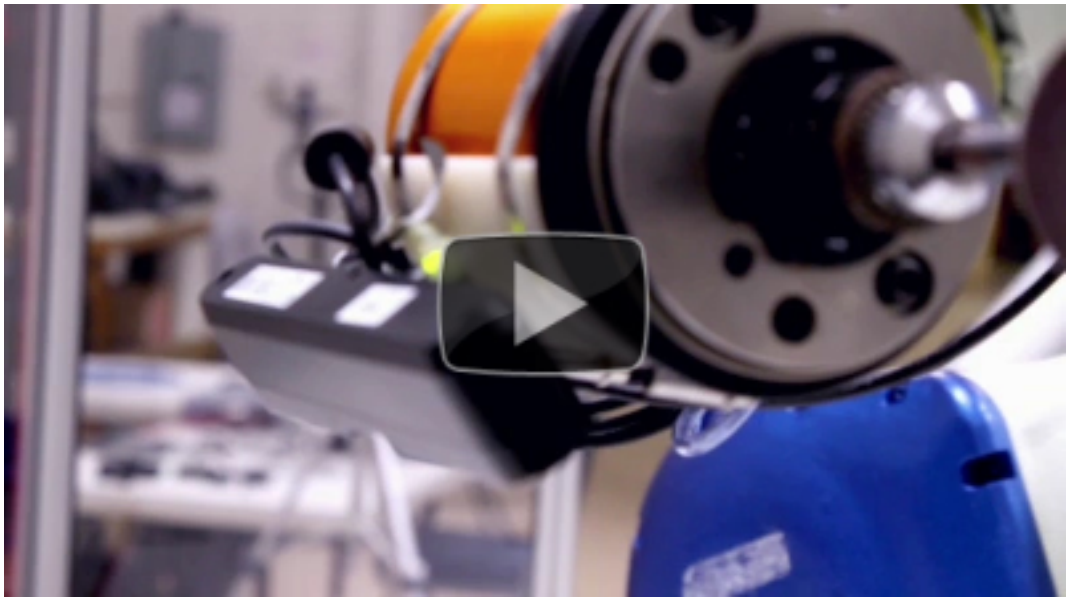

This short video, hosted by ROS-Industrial, describes the calibration framework.

2014 IR&D Annual Report

Vision-based Localization, 10-R8452

Principal Investigator
Kristopher C. Kozak

Inclusive Dates: 02/21/14 – 06/21/14

Background — For many applications that require localization, a Global Positioning System (GPS) receiver serves as an adequate, low-cost solution. However, for some applications, such as automated driving, the limitations and vulnerabilities of GPS make it unreliable as the sole source of localization. For instance, GPS accuracy can fluctuate widely and requires an unobstructed line-of-sight to multiple satellites. In addition, its signals are subject to interference, multi-path, jamming and spoofing. In spite of this, there are essentially no practical alternatives to GPS that are readily available. An alternative/supplement to GPS, which utilizes a downward facing camera, was developed at SwRI under a previous internal research project (10-R8248, 2011-2013). Development of that technology, also known as RANGER, was successfully implemented and demonstrated on a military HMMWV platform. To better address the localization needs of commercial clients, this project was carried out with the goal of porting the RANGER hardware and software to a passenger vehicle.

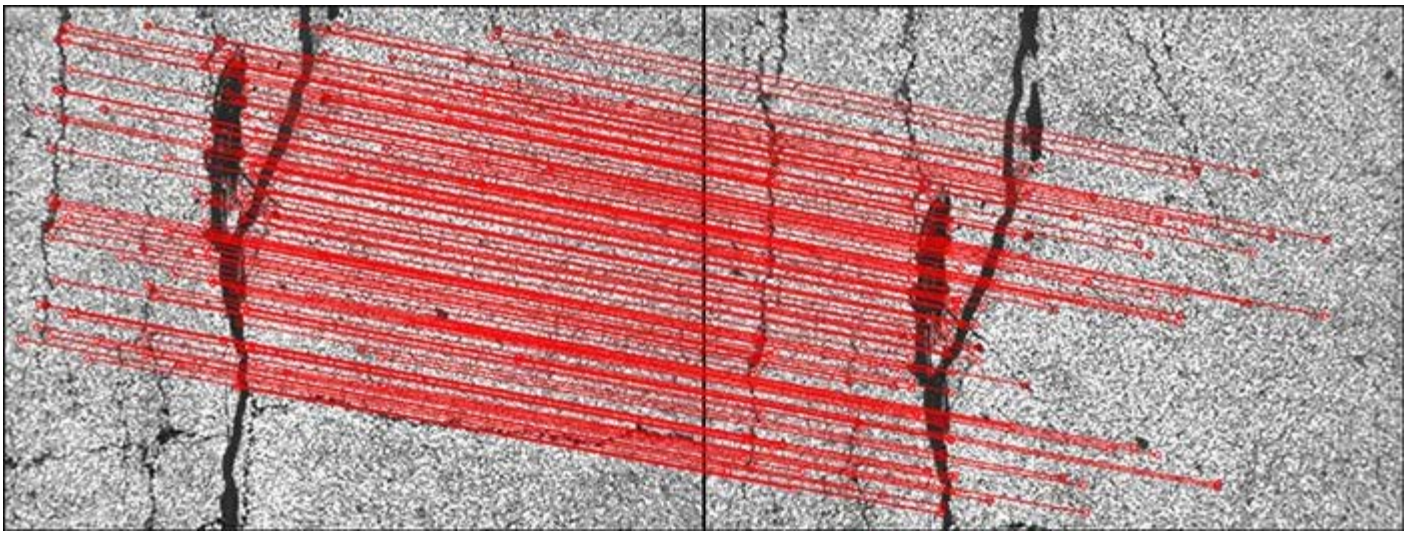

Figure 1. Features of opportunity in ground images are matched by appearance subject to geometric constraints to identify overlapping frames and determine vehicle location.

Approach — The limited ground clearance and electrical power available on typical passenger vehicles made it necessary to change key aspects of the original design. Instead of a large commercial off-the-shelf camera enclosure, a small custom enclosure was designed and fabricated. Instead of a high-powered, rack-mount server, a compact, desktop PC was used. Additionally, a smaller camera and a more flexible illumination system were incorporated into the system. RANGER system capabilities were also split into separate mapping and localization systems, which allowed for compromises on size, cost, field-of-view, etc., for the localization systems, which may be significantly constrained with respect to mounting in a passenger vehicle. Significant improvements to the software were similarly made to accommodate the hardware changes. Among these improvements were changes to image matching methods, and map

optimization methods that allowed the system to operate at frame rates of about 10 fps.

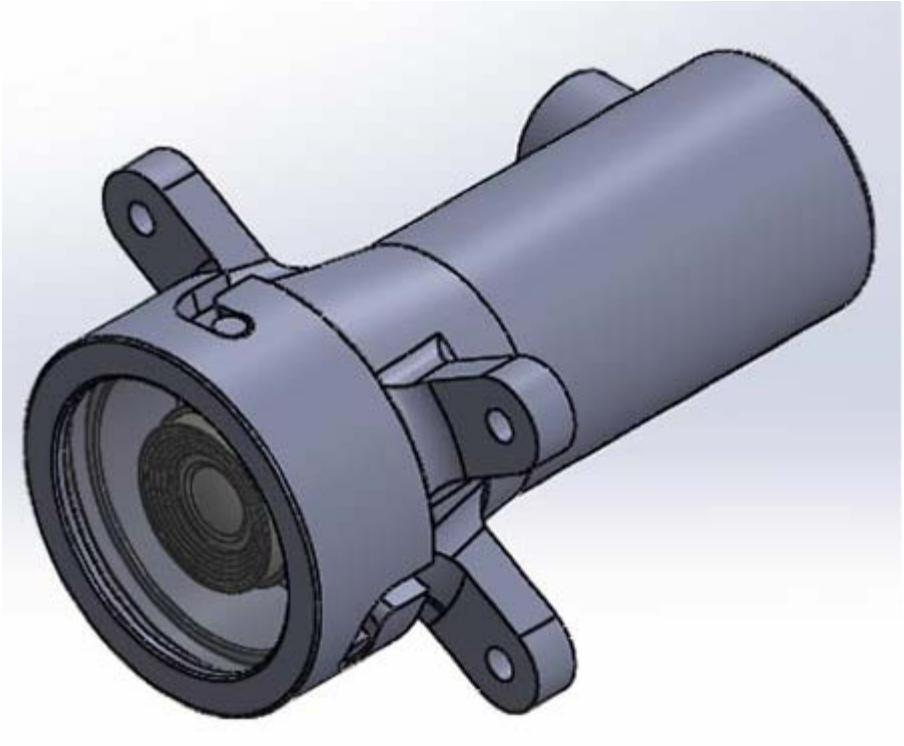

Figure 2: Solid model of custom camera enclosure.

Accomplishments — During this project, not only was the RANGER system successfully ported to passenger vehicles, but also its overall performance and capabilities were greatly improved. The size, power and cost of components for the second-generation prototype were significantly reduced. The camera and lighting hardware was simplified and reduced in size. The image-processing pipeline was streamlined and modified to use new image feature detectors and descriptors, which improved the feature matching performance (both increasing the matching speed and increasing the percentage of inliers per matching frame). The image pre-processing steps were updated to include a dynamic contrast-stretching approach rather than a static normalization map, which significantly reduced over-exposure and harsh shadowing issues with sunlight in the image frames. The updated RANGER system was successfully demonstrated in a variety of real-world conditions including on public roads and freeways (at speeds of up to 70 mph), in locations where GPS was poor or unavailable, and in wet road/rainy conditions.

2014 IR&D Annual Report

Cooperative Control of a Deployable Aerial Sensor Platform, 10-R8462

Principal Investigators
Richard D. Garcia
Jason Gassaway
Jerry Towler
Kristopher Kozak

Inclusive Dates: 04/01/14 – Current

Background — While unmanned aircraft have proven their viability in both the commercial and military market, unmanned aircraft technology continues to suffer from limited payload capacity, limited perception, and dependency on global positioning system (GPS) as a primary localization method. These limitations are significantly compounded on small aircraft (< 10kg) as they cannot sacrifice payload or power to employ large sensor suites or high computational equipment. These limitations quickly become operational failures in obstacle rich environments or where GPS may be unavailable or corrupted.

The primary objective of this research effort is to develop the equations, algorithms, and techniques that will enable an autonomous unmanned ground vehicle to safely and effectively deploy, recover, and navigate an aerial platform. As a result of this work, an unmanned ground vehicle (UGV) will use its own sensors to localize and control an aerial platform, off-loading obstacle detection and avoidance to the ground vehicle. By offloading many of the sensing and computational requirements from the aerial platform to the ground vehicle, the aerial platform can be lighter and simpler in construction, with an emphasis on mission payload. This technique will enable safe and effective flight during extremely low-altitude operation (including under foliage) and enable flight in GPS-denied environments.

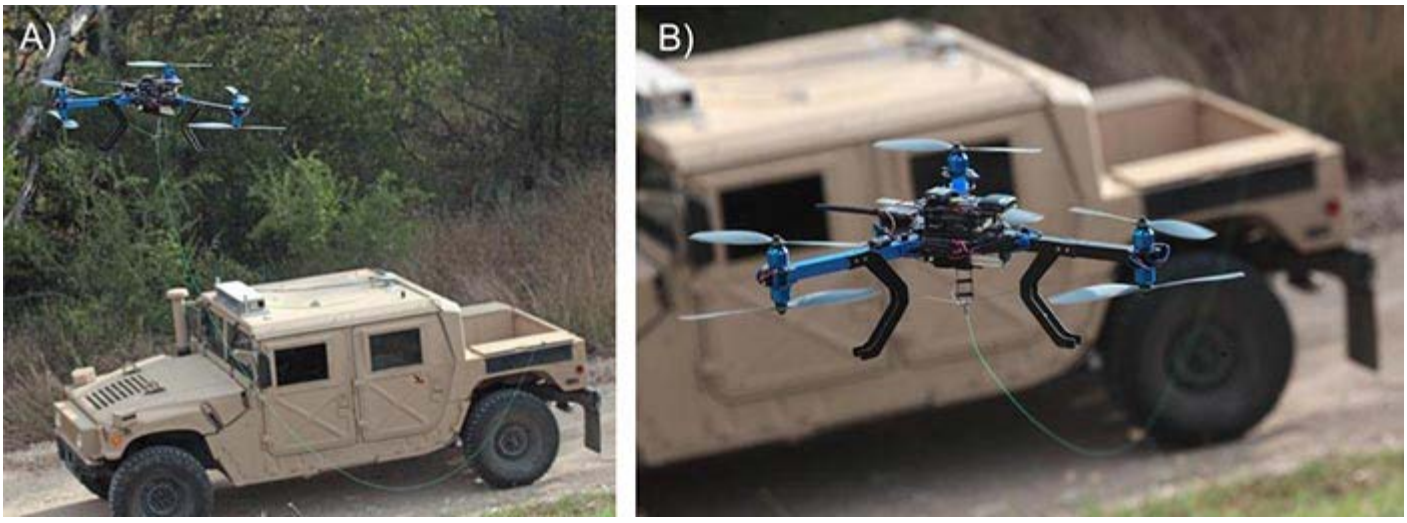

Figure 1. Flight experiment using small unmanned aircraft tethered to an autonomous unmanned ground vehicle (UGV): (a) An active tether system physically links the unmanned aircraft to the UGV while maintaining tether length and tension; (b) close-up of the unmanned aircraft tether attachment mechanism.

Approach — To accomplish the above objectives, we are developing algorithms that allow the UGV to identify and localize the aerial platform using UGV-mounted sensors. Although extensive experience leads

us to believe that a combination of ranging data (provided by a multi-planar laser range finder or radar) and imagery, possibly assisted by light-weight fiducials, will provide accurate localization at close range (~20m), specific sensor configuration will be the result of metrics collected from several manual flights representative of the operational area of the aircraft. Once the appropriate configuration of sensors has been selected, manual flight data can be used to tune basic localization calculations that will be verified for accuracy using a motion capture system.

Accomplishments — During the course of the project, the team has successfully implemented an active tether. This active tether system improves on commercial options by providing active slack control and vehicle reeling capabilities. Autonomous flights including take-off, waypoint navigation, and landing have been performed during the course of the project. ROS command interfaces have also been developed that provide a medium for the unmanned ground vehicle to send navigation commands to the air vehicle.

2014 IR&D Annual Report

Dynamic Transmisson Conductor Measurement, 10-R8466

Principal Investigators
Gary Ragsdale
Patrick Heenan
Jake Casey-Snyder

Inclusive Dates: 04/22/14 – 08/22/14

Background — SwRI was a prominent team member of two DOE-funded projects from years 2009 through 2012: 1) dynamic transmission line rating system demonstration project and 2) demonstrations of wind energy — smart load integration. The DOE projects revealed highly leveraged problems related to determining the characteristics of transmission and distribution power lines in real-time. Specifically, average line temperature can be derived from precise measurements of transmission line reflections. Prior to this research, techniques using direct temperature measurements provided estimates with uncertainties on the order of 20°C. The research summarized herein set a goal of achieving time delay accuracies of 9.8 picoseconds for roundtrip propagation delays on a 640-foot conductor length, i.e., corresponding to an average temperature change of 1°C.

Approach — Precise measurements of conductor lengths were taken using time delay reflectometry (TDR). Using newly devised TDR techniques, a reference signal is sent down the line and the observed reflection is correlated. The correlation is used to calculate the time delay and subsequently derive the length and temperature of the conductor. To provide relevant training data for the new correlative algorithm, measurements were made at a utility-provided industrial training facility. This project developed data processing techniques that increased the resolution attainable by prior transmission methods. New TDR techniques were tested on a medium-voltage, multi-stranded aluminum conductor in a power utility industrial training facility. The data gathered on the conductor provided transmission data in a realistic conductor environment.

Accomplishments — This research created TDR techniques with a demonstrated measured time delay accuracy on the order of zeptoseconds (10^{-21} seconds) for an un-energized conductor under real-world conditions. The measured accuracy is much greater the research goal of 9.8 picosecond (10^{-12} seconds). A contract was awarded for refinement of the SwRI TDR method and its application. This currently funded research will advance the method's accuracy and its ease of use within the noisy, energized, and multipath reflection transmission line environment.

SOUTHWEST RESEARCH INSTITUTE®

2014 IR&D Annual Report

Data Management Architectures for Gigabit per Second, Terabit Capacity Non-Volatile Data Storage, 15-R8468

Principal Investigators
Michael A. Koets
Larry T. McDaniel

Inclusive Dates: 04/16/14 – 08/16/14

Background — There is increasing demand for radiation-tolerant, high-performance data storage systems for spacecraft applications such as synthetic aperture radar (SAR) and image collection missions. These high-performance data storage units (DSUs) require storage capacities of gigabits or terabits and access rates of hundreds of megabits or gigabits per second. Flash memory provides a good solution for providing these capabilities by providing high storage density, non-volatile storage, and low power consumption. However, use of this memory technology is subject to a number of challenges including a command-based interface that limits the flexibility of how the memories can be accessed, highly asymmetric read, write, and erase times, and inevitable localized failures of portions of the devices.

Approach — This project sought to develop a capability for the design of high performance DSUs through two primary investigations. The first investigation developed a framework, methodology, and supporting software tools that accelerate the design of the low-level hardware architecture and interface logic of a DSU. These tools allow an engineer to quickly experiment with memory architectures and design the sequences of control commands that are issued to flash memory devices to achieve high storage capacity and very fast access rates. These tools include the ability to visualize important aspects of the interface sequence, validate that no constraints on the memory functions are violated, and accurately predict the performance of the design. The second investigation explored mechanisms for providing high- level organization of the data stored in a DSU. The high rates of data access and the physical characteristics of flash memory preclude a traditional file-based data organization approach. We developed data structures and a software implementation of a data organization mechanism that is compatible with the low-level flash memory interface while providing a flexible, simple interface to the spacecraft applications that use the DSU.

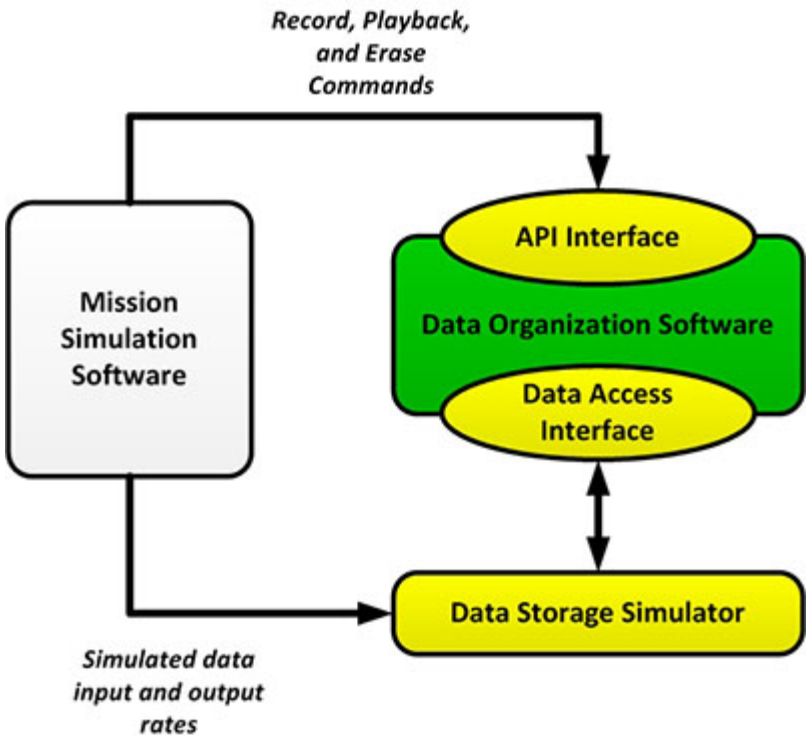

Figure 1. The data organization software emulator is integrated with the low-level data storage simulator and mission simulation software to provide early characterization of overall mission performance.

Accomplishments — The framework and supporting tools for the design of low-level flash memory interface architectures were employed to find solutions to a variety of realistic DSU design problems. One example used the tools to define a DSU providing 128 GB of data storage and simultaneous storage and retrieval of data at more than 256 MB per second each way. The data organization software has been incorporated into a software emulator that allows early, software-based simulation of a DSU within the context of spacecraft mission operations. The emulator incorporates the actual code used in flight, providing high-fidelity simulation of DSU operations. When integrated with a low-level data storage simulator and mission simulation software, the overall performance of the DSU can be evaluated and tailored to meet mission objectives. Figure 1 illustrates the emulator software.

2014 IR&D Annual Report

Formation Impact Study of Lithium-ion Battery Capacity, Cycle Life, and Safety, 03-R8277

Principal Investigators
Jeff Q. Xu
Robert Smith
Jayant Sarlashkar
Vikram Iyengar

Inclusive Dates: 01/01/12 – Current

Background — A "stable" surface film is formed on graphite electrodes upon the first charging of lithium-ion battery cells. This is called formation, which is a critical step during the battery manufacturing process. The formation of this solid electrolyte interface (SEI) layer passivates the graphite surface against further solvent decomposition. The SEI acts to decelerate the cell aging process and improve performance. To date, much of the SEI formation process is still not fully understood and the process is not well monitored during the formation step. Therefore, a direct and effective approach is needed for monitoring the formation process to develop effective and efficient formation protocols.

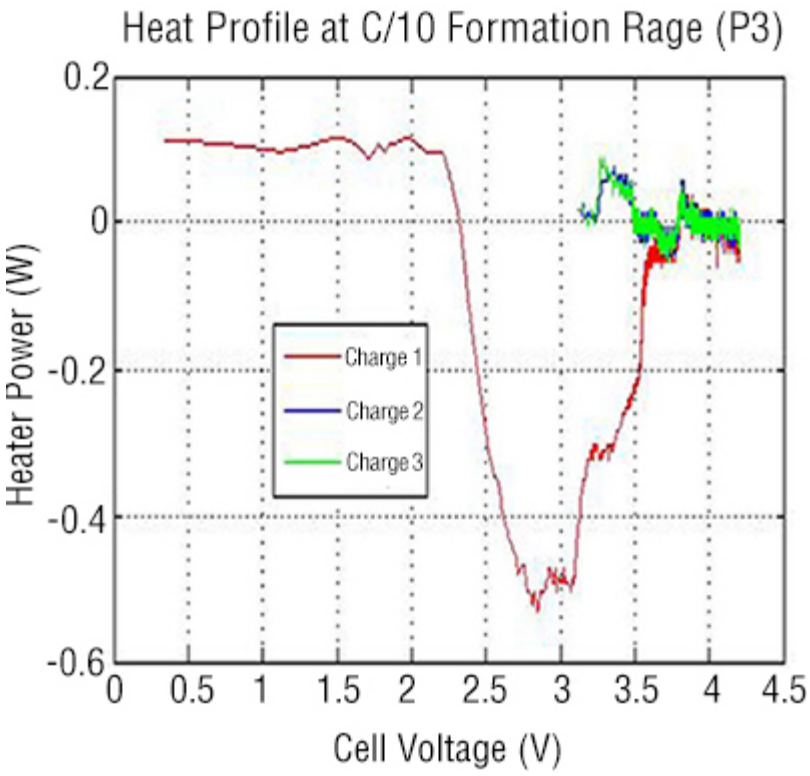

Figure 1. Net heater power change as a function of cell voltage during C/10 formation rate.

Approach — The objective of this project is to develop and evaluate the static and dynamic formation protocol impacts to lithium-ion cell performance such as capacity and cycle life. The approach is to leverage the thermal characteristics of the cell produced when the battery cell is under the first charging or formation cycle. By comparing various thermal or heat profiles at different formation rates, one or more clear voltage transition points can be identified as reference points to guide the changes of formation rates. An illustration of this approach is demonstrated in Figure 1.

Accomplishments — Use of a heat profile measurement/analysis tool during the cell formation stage can offer an insight for developing a suitable dynamic formation protocol for any type of graphite anode chemistry based lithium-ion cell (potentially can be used for silicon or carbon silicon alloy based anodes). The cells formed using the dynamic formation protocol have proved that thermal or heat measurement is effective during the study. The project was able to identify a specific voltage window that is most important to form an SEI layer effectively by using dynamic charge currents to allow reactions to take place with

reduced battery cell degradation. A flexible formation current could be adopted to expedite the process. This tool can be applied to investigate novel electrolyte composition and additive functions, electrode material selection and formulation to the improvement of battery capacity, cycle life, and safety as well. Figure 2a and 2b are examples of the experimental setup.

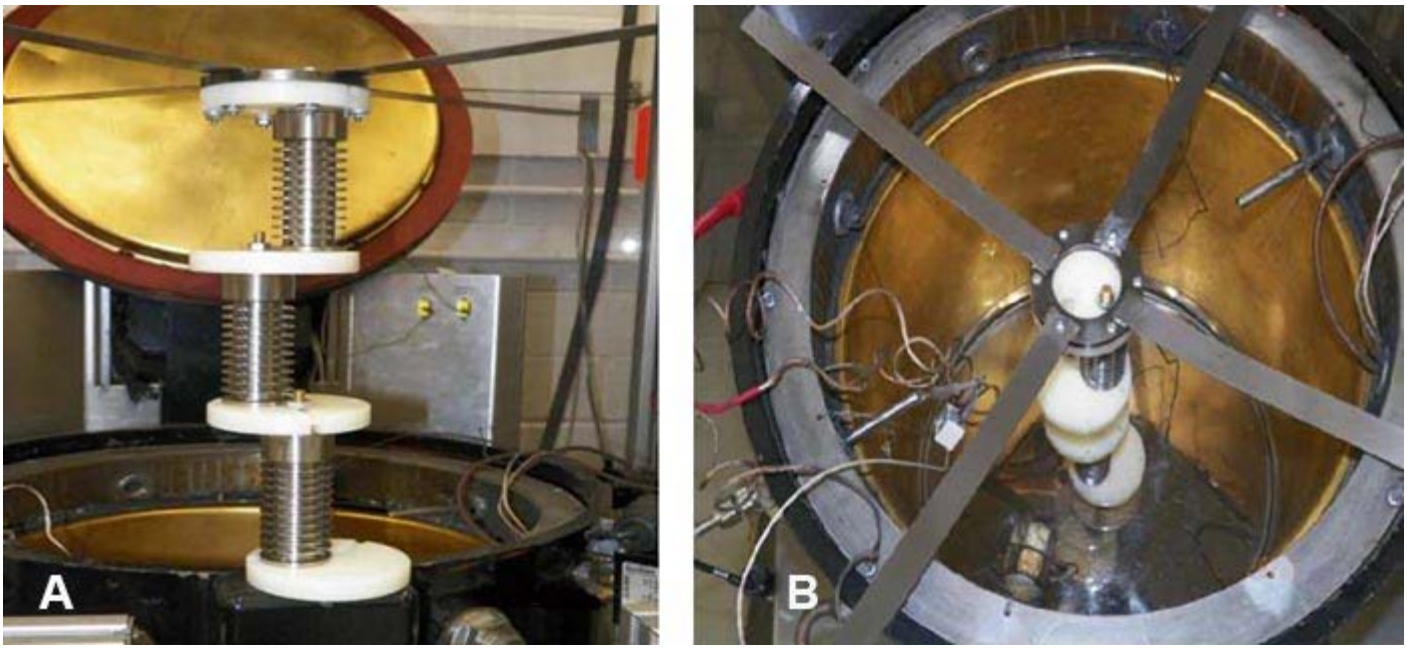

Figure 2. Example of experimental setup for one kind of specific battery cell.

2014 IR&D Annual Report

Development of the MsSR4040 SF Magnetostrictive Sensor Technology, 18-R8328

Principal Investigator
Adam Cobb

Inclusive Dates: 07/23/12 – 02/28/14

Background — SwRI has been very active in developing inspection technology and equipment using acoustic guided waves based on magnetostriction over the past 20 years; magnetostrictive sensing (MsS) technology has accounted for a large amount of contract awards since 2003 and more than 20 U.S. patents. The most recent version of the sensor system, designated the MsSR3030R, was developed before 2006 primarily for pipeline inspection and its technological capabilities are in need of updating to compete with the other guided wave inspection systems. Furthermore, it is becoming increasingly difficult to procure key electrical components of the MsSR3030R. To maintain and expand market position, it is necessary to invest in developing the next generation of the MsS technology.

Approach — The project focus was to design, build and test a developmental system designated as the MsSR4040 SF, the next generation of the MsS technology system. The electronics hardware design was based on recent efforts, leveraging what has been learned in projects related to electromagnetic acoustic transducers and MsS applications for pipelines and plates. Beyond updating the design to use readily available components, the new system has the ability to interface with multiple receive sensors simultaneously, which allows for the axial and circumferential positions of a flaw to be approximated by phasing the received signals together using beam forming principles; the MsSR3030R can only estimate the axial position of a flaw relative to the sensor. Moreover, the MsSR4040 SF utilizes a more power-efficient transmitter circuit design based on an H-bridge network, simultaneously allowing for inspection of more attenuative structures (e.g., buried pipelines) and longer battery-powered operation in the field. To support this new hardware system, custom software suites for data acquisition and analysis are being developed.

Accomplishments — At the conclusion of this project, several major milestones were achieved. For the hardware portion of the system, a modular design approach was followed that divided the electronics into several independent circuits that are combined together to form the system. Each of these circuits (transmitter, receiver, high-voltage converter, digital timing/control and interfacing circuits) and their associated firmware were designed, built, and tested separately and in combination, validating the hardware designs. Additionally, a custom packaging design has been developed and manufactured for ruggedly housing the electronics in a field environment. Also, a new sensor for working with the multiple receiver electronics of the MsSR4040 SF has been designed, manufactured and tested. While beyond the scope of this project, a software suite for both acquisition and analysis is currently being developed that allows all of the underlying functions for analysis, storage and presentation to be performed. The software has been used in conjunction with the hardware system to locate defects both axially and circumferentially in a 16-inch diameter pipe more than 16 meters from the sensor in a laboratory setting. The MsSR4040 SF has been presented at technical conferences and the sales of the system are anticipated within the next year.

2014 IR&D Annual Report

Online Monitoring System to Detect Microbial Induced Corrosion, 18-R8445

Principal Investigators
Todd Mintz
Amy De Los Santos
Spring Cabiness
Larry Miller

Inclusive Dates: 01/01/14 – Current

Background — Microbial-induced corrosion (MIC) is a phenomenon whereby microorganisms presence and activities result in the degradation of a material or component. In particular for the oil and gas industry, various bacteria have been linked to accelerated corrosion. Because of the detrimental effect that MIC can have on infrastructure, pipeline inspection methodologies to monitor this type of corrosion are required. However, current inspection methodologies are time consuming and costly. Thus, online detection systems for MIC are of great interest.

Approach — The objectives of the project are to develop a new in-situ technique to monitor MIC using surface enhanced Raman spectroscopy (SERS). Raman spectroscopy works via a coupling between incident laser light (visible, near infrared, or ultraviolet) with molecules at the surface of a material. Interactions between the laser light and surface molecules result in a shift in wave number of the incident beam that is characteristic of the surface molecules. By this method, the resulting Raman spectra can be used to discriminate between different bacteria strains. By depositing gold particles on the surface of the sample material, the Raman spectra intensity is enhanced (i.e. SERS). The approach to validating the SERS technique includes biological tests in an artificial growth medium, which is required for ideal growth of the bacteria being tested. The sensitivity of SERS compared to standard laboratory and field techniques was examined in this environment. Furthermore, SERS was also conducted in a high pressure gas pipeline environment as shown in Figure 1. The SERS results in the flow loop will be compared to the results obtained in the artificial growth medium.

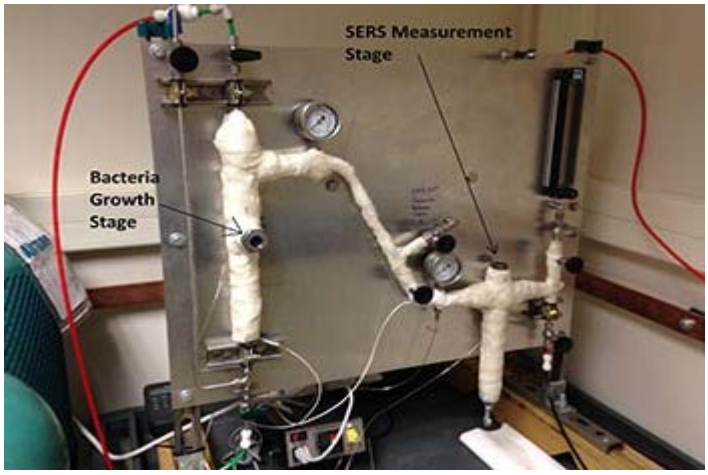

Figure 1. High-pressure flow system.

Accomplishments — Use of SERS to distinguish between bacteria strains can offer an in-situ characterization tool to distinguish the types of bacteria that are growing in a media stream or gas pipeline. During this project, two types of sulfate-reducing bacteria in a biological growth media were grown. It was demonstrated

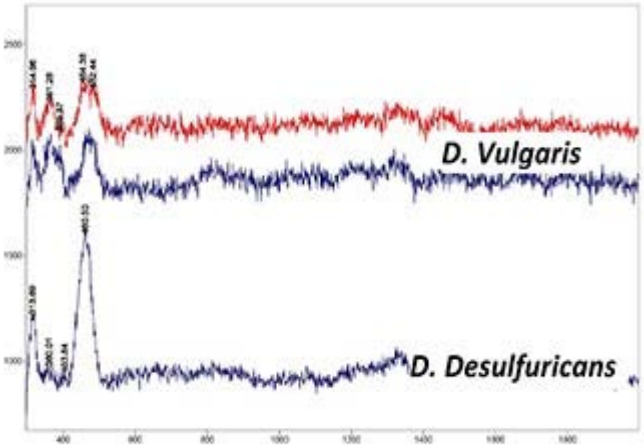

Figure 2. Raman spectra for sulfate-reducing bacteria D. Vulgaris and D. Desulfuricans.

that SERS could be used to distinguish a difference between the two strains as shown in Figure 2. The work conducted showed that the growth of the two strains of bacteria used in this study was not affected by the deposited gold particles. Furthermore, the results also showed that SERS was able to distinguish bacterial growth on the surface of the samples prior to any visual indication of bacteria growth in the media. Finally, bacteria were grown in a flow loop at 1,000 psi and 38 °C and SERS measurements were made on test samples in this flow loop.

SOUTHWEST RESEARCH INSTITUTE®

2014 IR&D Annual Report

Development of a Corrosion Sensor Technology for Buried Piping, 18-R8472

Principal Investigators
Leo J. Caseres
Todd S. Mintz

Inclusive Dates: 05/27/14 – 09/27/14

Background — Due to high regulatory scrutiny, degradation of buried piping is a large concern for numerous industries including nuclear, oil and gas, waste water, etc. Current condition assessment is an important part of the life-cycle management of aging pipelines and includes assessment of the external pipe surface. External corrosion direct assessment (ECDA) for pipelines is a non-trivial task as the pipelines tend to be buried so that inspection is time-consuming and quite costly. Data collection is part of the ECDA process and includes evaluation of soil/environment parameters to determine the level of corrosivity. There are various techniques for making soil property measurements. However, these techniques either measure the general corrosion rate that is not applicable for most soil environment or the time necessary to obtain localized corrosion data is very long. An additional drawback for current measurement techniques is that they are all single parameter measurements, which will limit the ability to illustrate the overall corrosion process occurring in the soil. Thus, the development of a reliable embedded sensor technology, which can: 1) explore the overall corrosion information of soil, 2) meet the urgent needs of life cycle management service companies for real-time field corrosion monitoring, and 3) provide prognostic and structure service life prediction was needed.

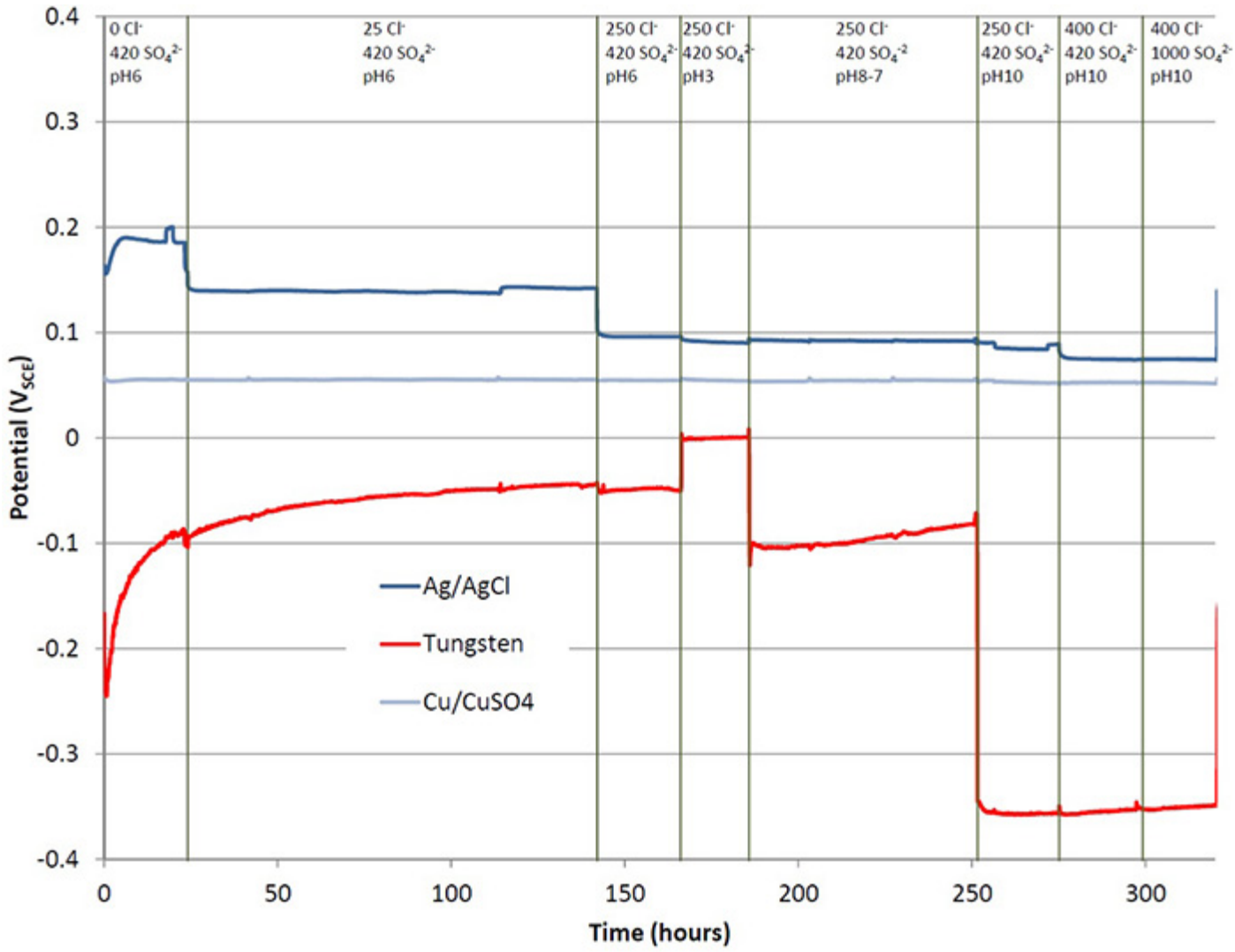

Figure 1. Chloride concentration and pH were successfully measured using the SwRI-developed corrosion sensor technology.

Approach — The objectives of the project was to test and validate a corrosion sensor technology applicable for assessing soil corrosivity and the corrosion rates of metallic components in soils. The project adapted a previously developed SwRI concrete corrosion sensor to detect and quantify the chloride concentration [Cl-], pH, and corrosion rate for monitoring buried pipeline structures in a soil environment. Experiments in simulated soil environments were conducted to select electrode materials and calibrate for pH and [Cl-] concentrations. Traditional [Cl-] and pH measurement techniques were used to calibrate the data acquired from sensors embedded in the soil. Also, long-term metallic coupon samples were exposed to soil environments to be compared with corrosion rate data acquired from a multi-electrode array sensor (MAS) in the same soil environment.

Accomplishments — Use of a multi-parameter corrosion sensor provides a method to obtain data that can be used to support ECDA inspection decisions. During the project, two different experiments were conducted to support the design of the soil corrosivity probe. In both these tests, it was demonstrated that the corrosion sensor electrodes could be used to measure the pH and chloride concentration as shown in Figure 1. The work showed that the Ag/AgCl electrode electrochemical potential was inversely proportional with changes in the [Cl-] in the range from 0 to 400 ppm. This electrode was reversible and could identify both increases and decreases in [Cl-] concentration. The project also showed that the tungsten electrode performed well as a pH monitor. The tungsten electrochemical potential was inversely proportional to the changes in pH and was also reversible. Finally, comparing the MAS corrosion data to weight loss samples showed as positive correlation between the maximum pit depth and the maximum MAS electrode currents.

2014 IR&D Annual Report

Development of a Methodology to Generate On-Board Diagnostic Threshold Selective Catalytic Reduction Catalysts for Heavy-Duty Diesel Applications, 03-R8376

Principal Investigators
Reggie Zhan
Cynthia Webb

Inclusive Dates: 03/15/13 – 03/15/14

Background — The on-board diagnostics (OBD) system monitors engine and aftertreatment components that affect the emissions performance of a vehicle. When the malfunction illumination light (MIL) is illuminated, at least one emission-related problem has been detected, and the driver is notified that vehicle service is needed. The OBD system stores malfunction codes in the engine control unit (ECU) and assists the service technician in diagnosing and repairing the problem. For heavy-duty diesel engine applications, the California Air Resources Board (CARB) mandates that heavy-duty OBD systems be implemented for all on-highway engines offered for sale in California beginning with model year (MY) 2013. Even though urea-based selective catalyst reduction (SCR) technology has been used as a primary means to meet the US 2010 diesel NO_x emissions requirements in North America, technical challenges still exist across the industry. Among them, there was no proven method to consistently create an OBD threshold SCR catalyst in the laboratory environment.

Approach — A novel methodology has been developed through this project to consistently age zeolite SCR catalysts to the OBD threshold level. The approach was to use SwRI's FOCAS® HGTR™ burner technology to thermally age the SCR catalysts to the levels to meet OBD threshold calibration requirements. A US 2010 certified MY 2011 Ford PowerStroke 6.7L diesel engine was used for the project. The heavy-duty federal test procedure (FTP) cycle was measured on the engine and replicated using the FOCAS HGTR system for SCR performance evaluation. An SCR thermal aging cycle was developed for aging SCR catalyst to threshold NO_x levels, while the steady-state NO_x efficiencies were monitored and compared to the simulated FTP tests. At the conclusion of the aging set, the FOCAS HGTR aged SCR catalysts were then emissions tested using the Ford PowerStroke 6.7L diesel engine. These final FTP tests were used to confirm the burner FTP test results.

Accomplishments — The key conclusions from this work included that the OBD aging cycle embedded steady-state SCR efficiency monitoring can be used to accurately guide the aging to a desired level of degradation. OBD threshold level was achieved for the state-of-the-art CuZ SCR as used on the Ford PowerStroke diesel engine. The procedures developed provided a solution to the technical challenges currently imposed by the lack of a consistent method to create OBD threshold SCR catalysts. This method is unique to the burner system and cannot be replicated with currently available industry approaches. A paper has been published at the SAE Emissions Conference 2014. An invention disclosure has been filed.

2014 IR&D Annual Report

FOCAS HGTR Design Evolution to a High Pressure Fully Transient System— Creation of the Full-Scale Gas Reactor, 03-R8427

Principal Investigator
Cynthia Webb

Inclusive Dates: 10/14/13 – 10/14/14

Background — The current emissions certification procedure for heavy-duty engines uses a transient test cycle and a ramped modal test cycle. The certification test cycles run at moderate-to-high loads, and do not weigh the cold portion of the test heavily (US HD-FTP is weighted 1/7 for cold-cycle emissions and 6/7 for hot-cycle emissions). Even with the low relative weighting factor, the emissions from the cold-start cycle still typically account for 40 to 50 percent of the total FTP emission. Due to the low weighting, the standards can be met with little or no emphasis on achieving high catalyst efficiencies at lower temperatures. However, beginning in 2013, the CA ARB funded a program that will focus on cold-start and low-temperature operation. The intended outcome of the study will be lower emissions standards, forcing the manufacturers to address and reduce cold-start emissions.

One major difficulty with studying cold-start emissions is that an engine is capable of only one cold-start a day (or perhaps two with aggressive forced cooling). Additionally, repeatability from day to day may make decisive comparisons difficult. These factors make studying cold-start emissions very time consuming and expensive.

The FOCAS® Hot Gas Transient Reactor (HGTR™) bench is a high-flow, diesel-fueled, burner-based catalyst performance evaluation and aging system that expands the capabilities of SwRI's FOCAS burner technologies. The reactor was sized to accommodate full-sized catalyst systems, allowing independent control of any combination of total exhaust flow, temperature, NO_x, water vapor, oxygen and HC concentration within the operating window of the device. Because the burner system provides independent control of temperature, it can simulate cold-start tests and cold-temperature operation, allowing many cold-start tests to be conducted in a day.

Approach — Through work conducted under two previous internal research projects, 03-R8372 and 03-R8427, the SwRI FOCAS HGTR diesel burner based catalyst evaluation test stand was modified to allow the burner to simulate the transient exhaust conditions generated by a diesel engine operating over a cold-start U.S. HD-FTP test cycle. All the simulated exhaust components were controlled independently, allowing the user to program any combination of variables. The independent control of variables allowed the measured exhaust gas conditions from the engine test to be input as a target cycle for burner, implying that the burner can be used to simulate any engine.

Accomplishments — The HGTR burner control range was greatly extended, and the transient control capability of all independently controlled subsystems was improved, allowing for very close simulation of engine conditions over the transient FTP cycle. This work produced very promising results and demonstrated that the FOCAS HGTR could be used for transient test cycle simulation. Figures 1 through 5 show comparisons to the burner simulation of the engine operation. In each graph, the setpoints (SP) were the data measured from the engine. The feedback (FB) or burner out (BO) conditions were measured from the HGTR simulation of the engine cycle.

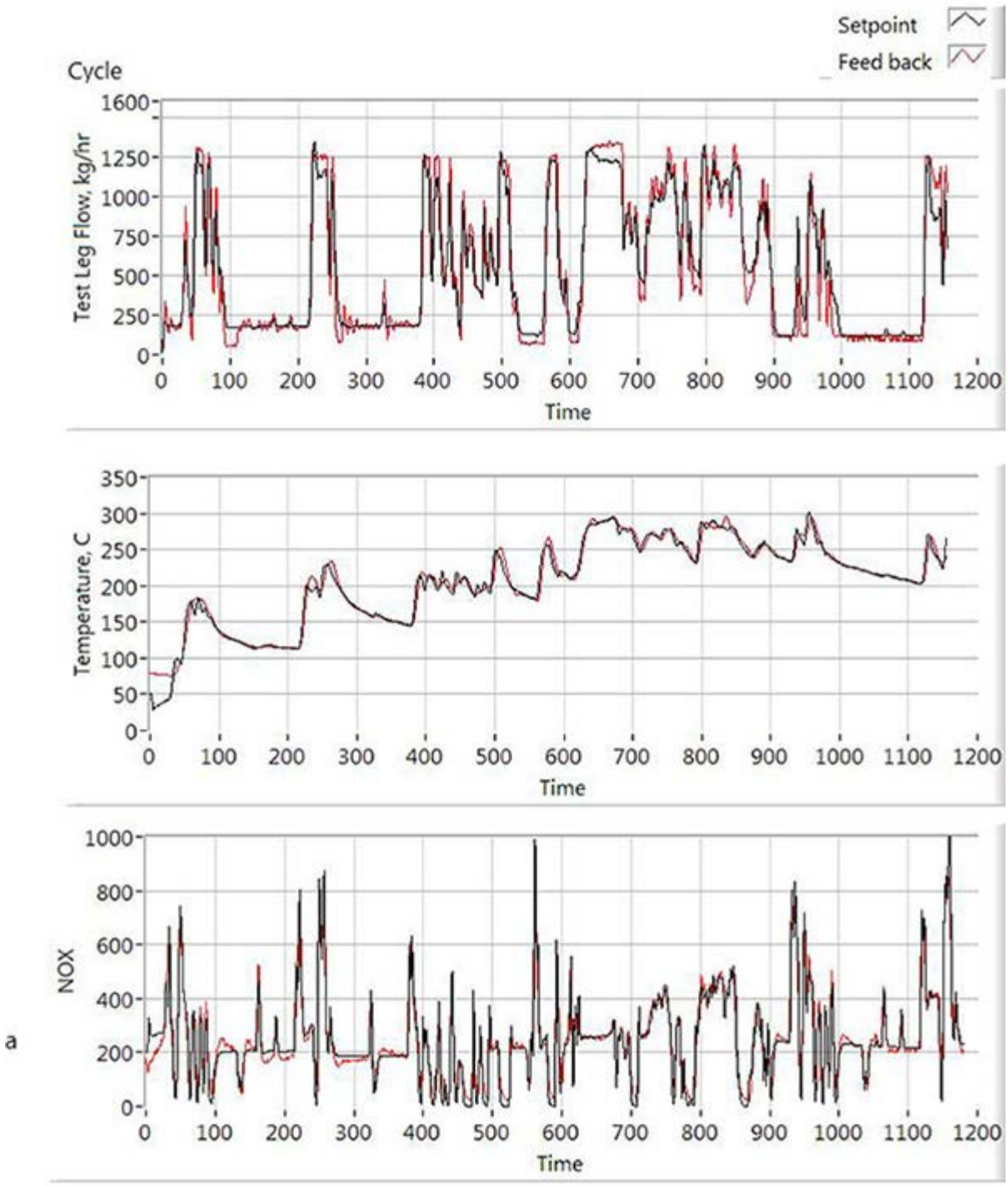

a

Figure 1. Comparison of flow, temperature, and NO_x between the engine and the HGTR simulation.

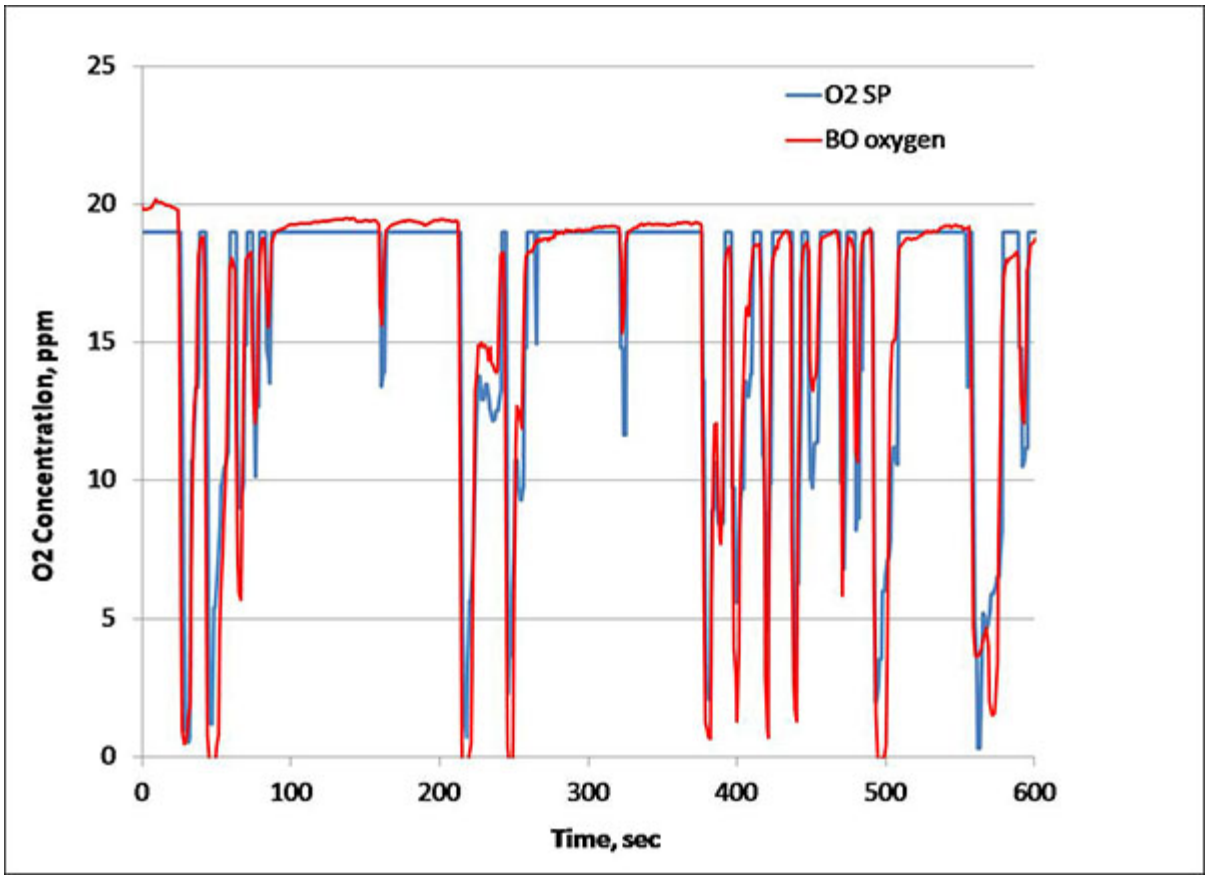

Figure 2. Comparison of measured exhaust oxygen concentration between an engine and HGTR over portion of cold-start FTP test cycle.

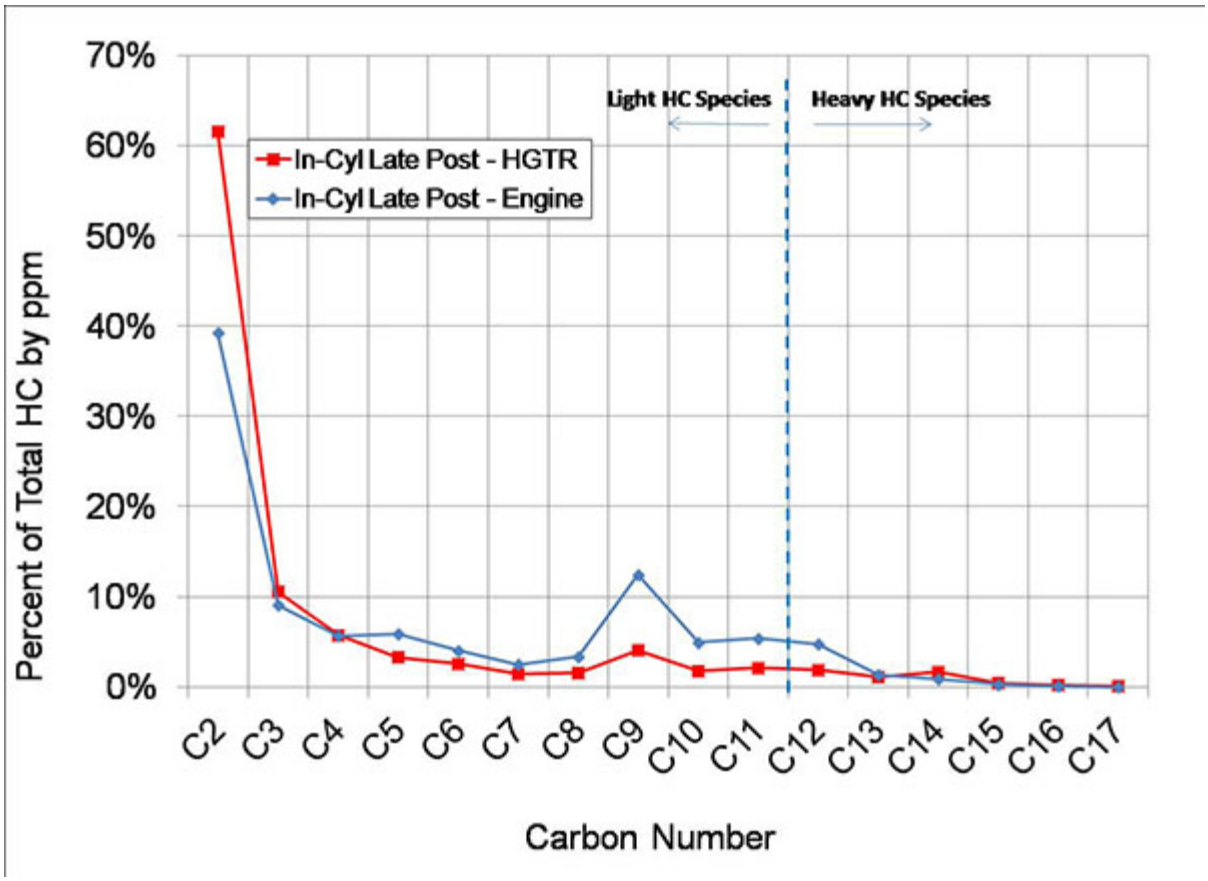

Figure 3. Comparison HC species generated by in-cylinder post injection on engine and in simulation

HGTR.

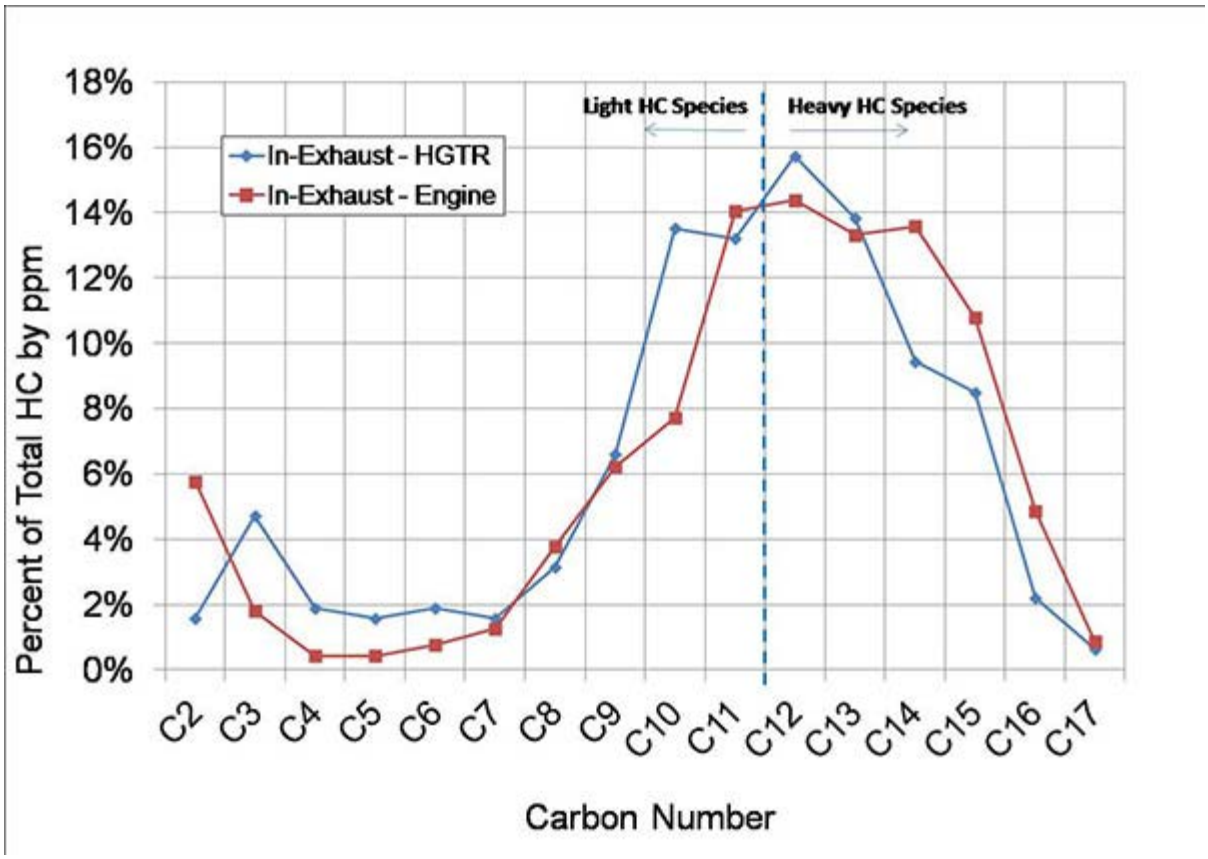

Figure 4. Comparison HC species generated by in-exhaust fuel injection on engine and in simulation HGTR.

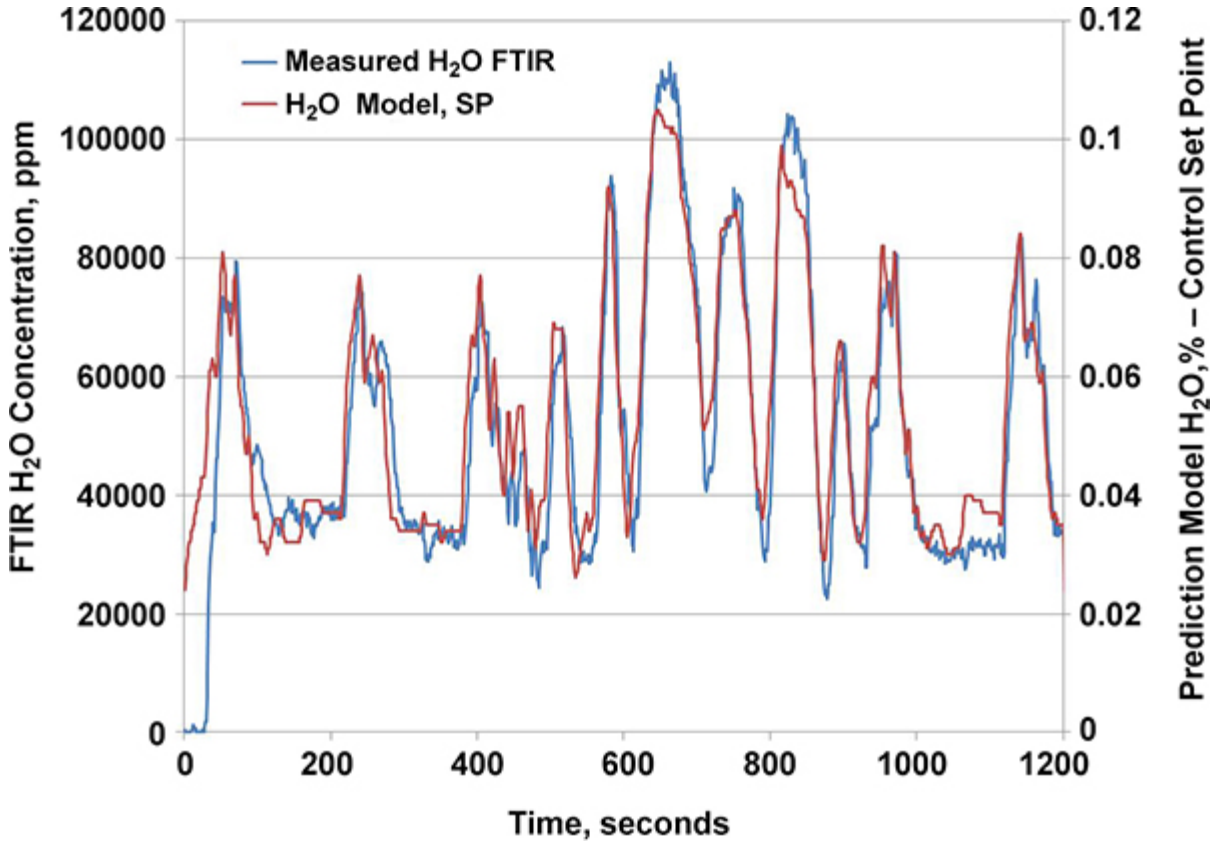

Figure 5. Measured and predicted water vapor over simulated cold-start FTP test cycle.

SOUTHWEST RESEARCH INSTITUTE®

2014 IR&D Annual Report

Feasibility of Detecting Low-Speed Pre-Ignition (LSPI) and Suppressing the Subsequent Knock in High-Performance Spark Ignited Gasoline Engines, 03-R8428

Principal Investigators
Garrett Anderson
Jacob Zuehl

Inclusive Dates: 10/21/14 – 02/20/14

Background — The spark-ignition engine has been known to exhibit several different abnormal combustion phenomena. Most of these abnormal combustion issues have been addressed with improved engine design or control schemes. However, in the next generation of SI engines, where turbocharging and direct injection technology are employed to increase brake power at low engine speeds for improved efficiency, a new phenomenon of abnormal combustion, described as low-speed pre-ignition (LSPI), has been exhibited. Cylinder pressure data and heat-release rates for normal combustion, light knocking conditions and LSPI are shown in Figure 1. Because of the violent nature of LSPI, damage to engine components can occur within only a few engine cycles. However, because LSPI events occur only sporadically and in an uncontrolled fashion, the causes for this phenomenon have not been successfully explained and solutions to suppress or prevent it are desperately needed.

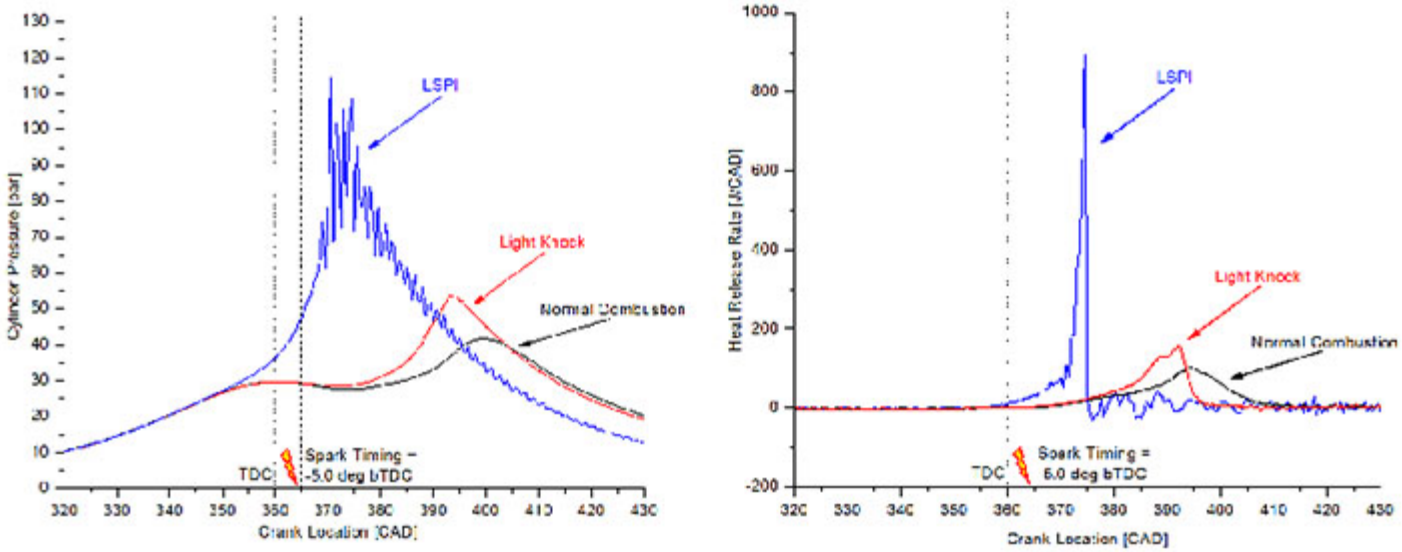

Figure 1: Cylinder pressure and heat release rate for normal combustion, light knock and LSPI

Approach — The approach was to first detect the pre-ignition with cylinder pressure. Once detected, fuel would then immediately be injected with the goal of quenching the flame. This would suppress the severe knock event associated with LSPI. The fuel-air mixture would be reignited late in the cycle to minimize hydrocarbon emissions. This strategy is depicted in Figure 2.

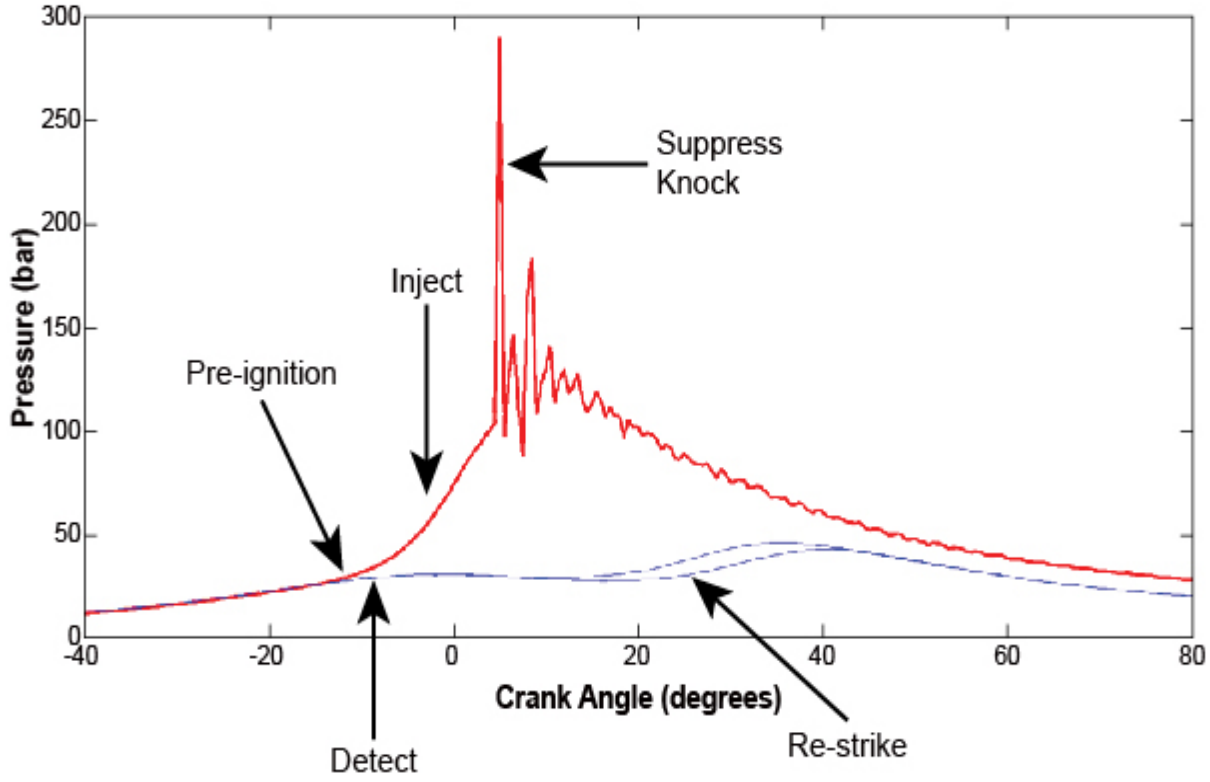

Figure 2. Depiction of knock suppression strategy during LSPI cycle.

Because LSPI is a somewhat random phenomenon, knock was induced by advancing ignition timing. The resulting knock intensity was very consistent. This enabled the resulting knock intensity to be compared with and without the suppression strategy enabled. Using this method, no difference could be found with the strategy enabled.

Accomplishments — While the goal of project was unsuccessful, it was recognized early on in the project before a large portion of the funding was spent. At the same time, other useful knowledge was gained. This project provided experience making control decisions within a fraction of a crank angle degree, which enables same cycle engine control. Typically decisions about injection and ignition timing are done within a loop that executes at a rate of about 10 ms. At 2,000 rpm, this results in decisions being made every 120 CA°. This ability has proved beneficial in other projects requiring triggering for optical equipment based off of combustion metrics. This helped enable combustion to be visualized for LSPI engine cycles.

SOUTHWEST RESEARCH INSTITUTE®

2014 IR&D Annual Report

Identifying and Elucidating Low Temperature Limiters to Catalyst Activity, 03-R8435

Principal Investigators
Gordon J.J. Bartley
Cary A. Henry

Inclusive Dates: 01/01/14 – 01/01/15

Background — The drive to more fuel-efficient vehicles is underway, with passenger car targets of 54.5 mpg fleet average by 2025. Improving engine efficiency means reducing losses such as heat lost in exhaust gases. However, reducing exhaust temperature makes it harder for emissions control catalysts to function because they require elevated temperatures to be active. Addressing this conundrum is the focus of this project.

Figure 1. SwRI's Universal Synthetic Gas Reactor®.

Approach — The primary objective of this project is to identify low-temperature limiters for a variety of catalyst aftertreatments. The goal is to reduce catalyst light-off temperatures, and the knowledge needed is an understanding of what prevents a catalyst from lighting off, why, and how it may be mitigated. Collectively these are referred to here as low-temperature limiters to catalyst activity.

The approach is to determine the low temperature limiters for all major emissions catalysts types, and to consider the mechanisms involved. Mitigation strategies are being considered and investigated, and work is being performed to test out these strategies as time and funding permit. SwRI's Universal Synthetic Gas Reactor® (USGR®) is the primary tool for this testing.

The project is evaluating several relevant catalyst technologies. These are the three-way catalyst (TWC) for stoichiometric gasoline applications; the diesel oxidation catalyst (DOC) now commonly found in diesel applications; ammonia selective catalytic reduction catalysts (NH_3-SCR) that are now the backbone of the diesel NO_x emissions reduction technologies, and of which there are three base formulations; the lean NOX trap (LNT), which is another NO_x reduction technology more useful in smaller engine lean applications, the ammonia oxidation catalyst (AMO_x), which is quite a new technology used to clean up NH_3 released from SCR catalysts, and the natural gas oxidation catalyst (NGO_x), which will become very important as readily available natural gas infiltrates the internal combustion engine market.

Accomplishments — The project work is ongoing. Six formulations have been tested to date. Nitric oxide

(NO) and unsaturated hydrocarbons were found to be significant low temperature limiters to TWC activity. Removal of the NO lowered the carbon monoxide (CO) light-off temperature from 229°C to 174°C, and the propene (C_3H_6) from 257 to 203°C. Conversely, removal of C_3H_6 lowered the CO light-off temperature from 229 to 185°C, but significantly reduced NO activity. Thus, NO and C_3H_6 are limiters to CO light-off, but C_3H_6 is needed to promote NO light-off. This type of complex interaction is common throughout catalysis.

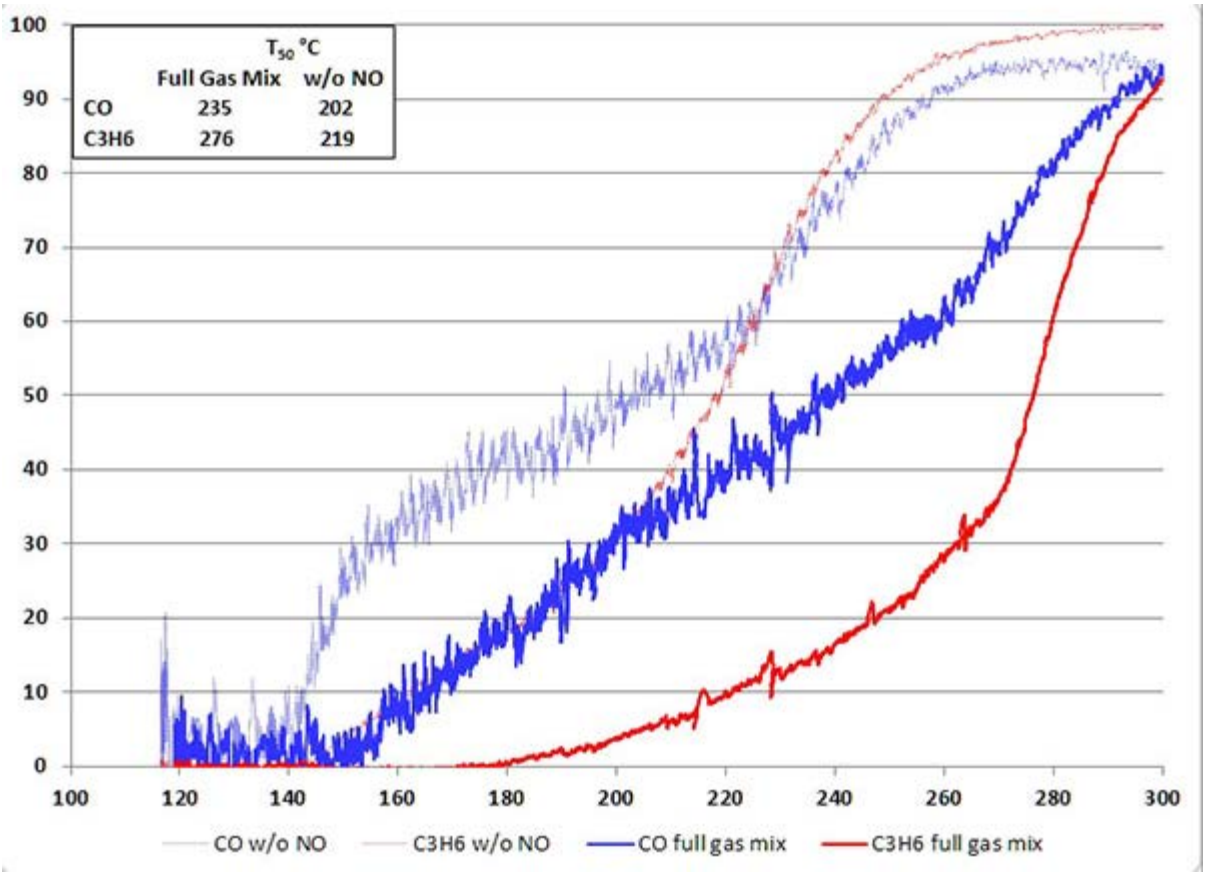

Figure 2. TWC with and without nitric oxide.

For the DOC, removal of NO dramatically improved the light-off of ethene (C_2H_4) from 248 to 179°C. Removal of hydrogen (H_2) slightly hurt C_2H_4 light-off, so NO is a limiter again, and H_2 is a mild promoter.

For the Fe-Z NH_3-SCR catalyst, removal of water (H_2O) slightly improved NO_x light-off, but removal of nitrogen dioxide (NO_2) dramatically increased light-off temperatures. The latter is well known as NO_2, a powerful promoter of the NH_3-SCR reaction. None of the other gases had any marked effect, so lowering of NH_3-SCR catalyst light-off temperatures must be achieved by other means.

For the AMO_x catalyst (NH_3 clean up), removal of C_2H_4 lowered the NH_3 light-off temperature from 281 to 212°C, and removal of CO lowered it to 250°C. In contrast, removal of H_2 raised it to 298°C, so C_2H_4 and CO are both limiters, but H_2 is a promoter.

For the LNT NO_x reduction catalyst, removal of CO lowered the NO light-off temperature from 165 to 107°C. Confusingly, removal of C_3H_6 raised the NO light-off temperature from 165 to 205°C, and removal of propane (C_3H_6) raised it slightly to 170°C, but removal of both C_3H_6 and C_3H_8 dramatically lowered it to 102°C.

For the NGO_x catalyst, removal of H_2O dramatically lowered the CH_4 light-off temperature from 492 to 376°C. Removal of CO, H_2 or NO all raised the CH_4 light-off temperature, such that these are promoters.

To pursue further, H_2 was increased by an order of magnitude and the CH_4 light-off temperature reduced to 469°C, so increasing H_2 exposure may be a mitigation strategy for NGO_x catalysis. SwRI is exploring the possibility of a specialized catalyst for reducing the negative influence of H_2O by collaborating with industry specialists to make and test such a catalyst. If successful, an improved NGO_x catalyst may be introduced to the world in 2015.

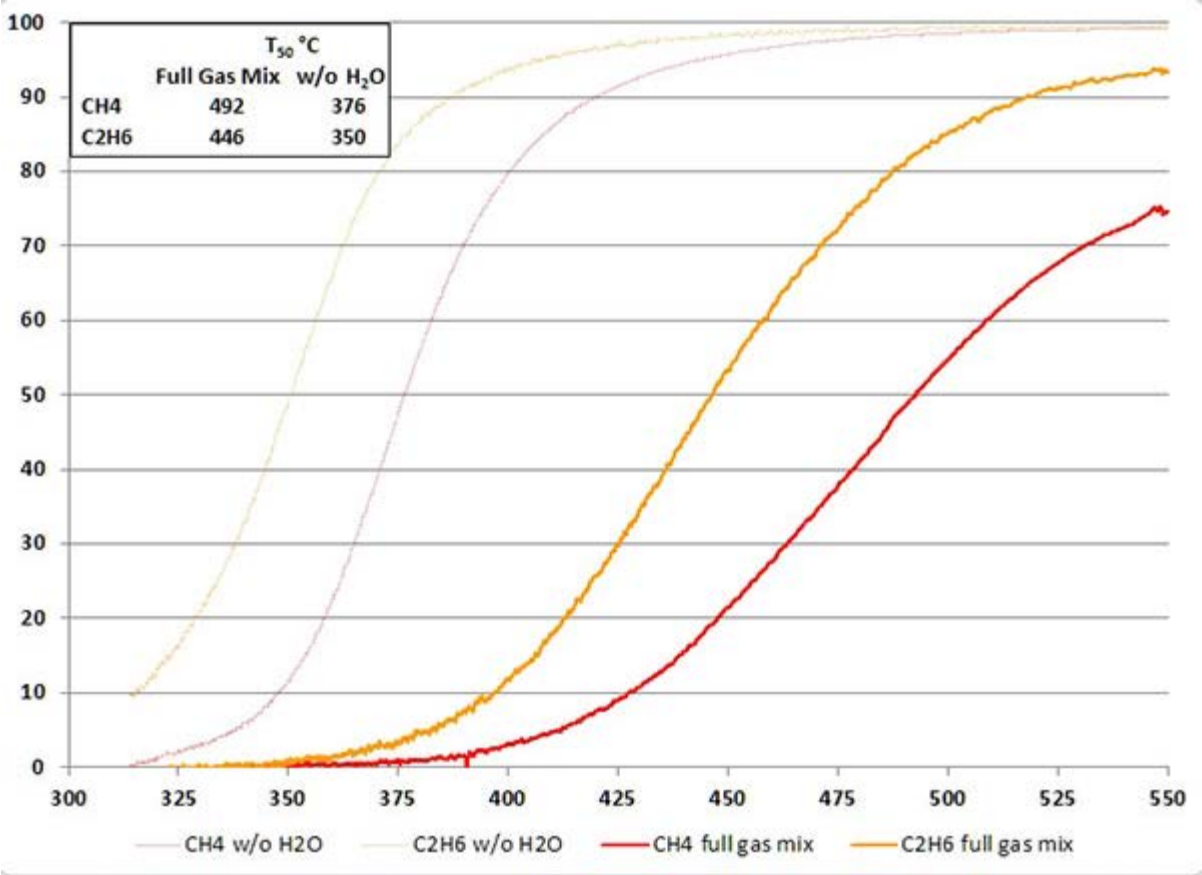

Figure 3. NGO_x with and without water.

SOUTHWEST RESEARCH INSTITUTE®

2014 IR&D Annual Report

Extension of SwRI's Multidimensional Control Framework to Fueling and Ignition Control of Spark-Ignited Engines, 03-R8438

Principal Investigators
Ryan Roecker
Jayant Sarlashkar
Sankar Rengarajan

Inclusive Dates: 01/01/14 – Current

Background — For the past decade or so, SwRI has championed the idea of diesel engine pollution control at source (i.e., in combustion chamber). As a complementary enhancement to this idea, the Institute has pursued over the past six years management of in-cylinder state. This two-pronged approach comprising in-cylinder state-based fueling and active management of in-cylinder state has a solid foundation in physical processes and, generally speaking, extends to all internal combustion engines. SwRI has generated and patented significant intellectual property (IP) in this area, conducted externally and internally funded work, and published results (see internal research project 03-R8179 final report).

Approach — The approach is to apply our control system for the Dedicated Exhaust Gas Recirculation (DEGR) engine demonstrated in internal research project 03-R8329, see Figure 1. While the DEGR engine is relatively simple from a conceptual standpoint (full-time 25-percent EGR), it poses a challenge from a control standpoint because of the additional air handling devices and actuators required. The framework for our control system developed in the previous work should now be extended to the stoichiometric, SI gasoline engine with EGR. What is required to accomplish this is summarized in the following two problem statements:

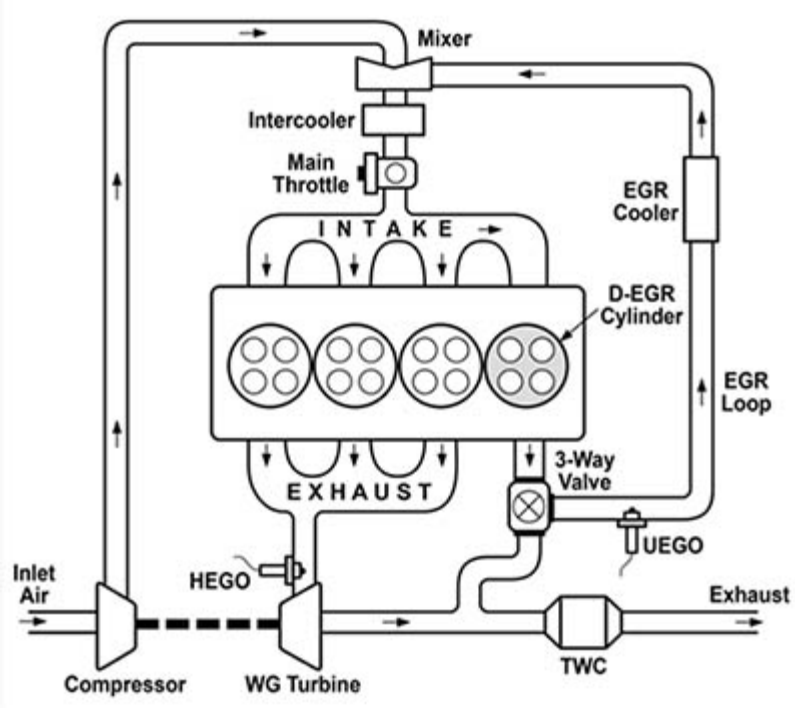

Figure 1. Representation of the DEGR engine.

- In-cylinder state-based fueling for three-way catalyst (TWC) control: The idea of in-cylinder state-based fueling is well grounded in physical principles and has been developed and tested extensively in previously conducted work. The question is whether the idea can be implemented efficiently and uniformly for the lean/rich switching required for TWC control.
- In-cylinder state-based ignition: Control of combustion can be significantly improved by extending the concept of state-based fueling to the control of ignition. The question is how well the concept of determining fueling quantity, timing, pressure, and pattern based on estimated in-cylinder

conditions extends to the determination of ignition timing, duration, and pattern.

The overall control schematic is shown below, see Figure 2. This control structure has been used by SwRI extensively in previous work. This program seeks to add to and refine the portion of the schematic noted in red, namely, fueling and ignition control.

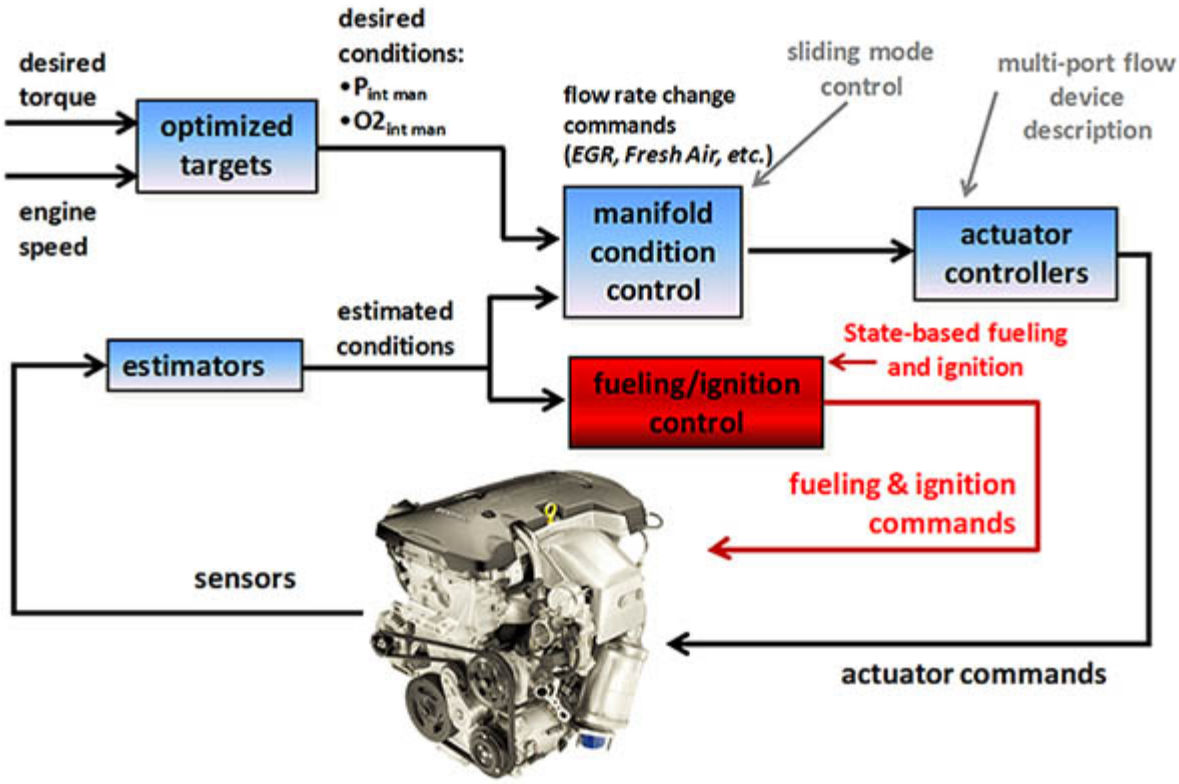

Figure 2. Overall control schematic.

Accomplishments — The effort is on-going and has made progress toward the goals of the project. We are currently testing the multi-dimensional calculation developed for timing, duration and ignition pattern control. SwRI's state-based fueling has been extended to include TWC control. Finally, we have successfully extended SwRI's active management of in-cylinder state to a spark-ignited gasoline engine with EGR.

2014 IR&D Annual Report

Sampling System Investigation for the Determination of Semi-Volatile Organic Compounds (SVOC) Emissions from Engine Exhaust, 03-R8442

Principal Investigators
E. Robert Fanick
Svitlana Kroll
Chris A. Sharp
Shraddha Quarderer
John E. Gomez

Inclusive Dates: 01/01/14 – Current

Background — Semi-volatile organic compounds (SVOC) are a group of compounds that may form during combustion and/or are present in the unburned portion of the fuel and lubricating oil which ultimately becomes part of the exhaust. Many of these compounds are considered toxic or carcinogenic. These compounds are present in very low concentrations in diesel engine exhaust. Engine testing is typically performed using a dilution tunnel method. Experiments were performed to determine the equilibration time and other sampling parameters required for the measurement of SVOC.

Approach — The main objective of this program was to validate and qualify the SwRI dilute sampling procedures for use as a dilute exhaust sampling method. A 2012 Ford 6.7L engine was used to produce the engine exhaust throughout the entire experiment. The testing started with a "clean" dilution tunnel, and engine-out exhaust ("dirty" exhaust) was sampled to determine the equilibration time for the dilution tunnel. Tests using different filter media and trap breakthrough experiments were also performed. The exhaust was then changed to aftertreatment-out ("clean" exhaust), and the equilibration time was determined from a "dirty" tunnel to a "clean" tunnel. Samples were collected periodically throughout the tunnel equilibration period, and these samples were extracted and analyzed by gas chromatography/mass spectroscopy (GC/MS).

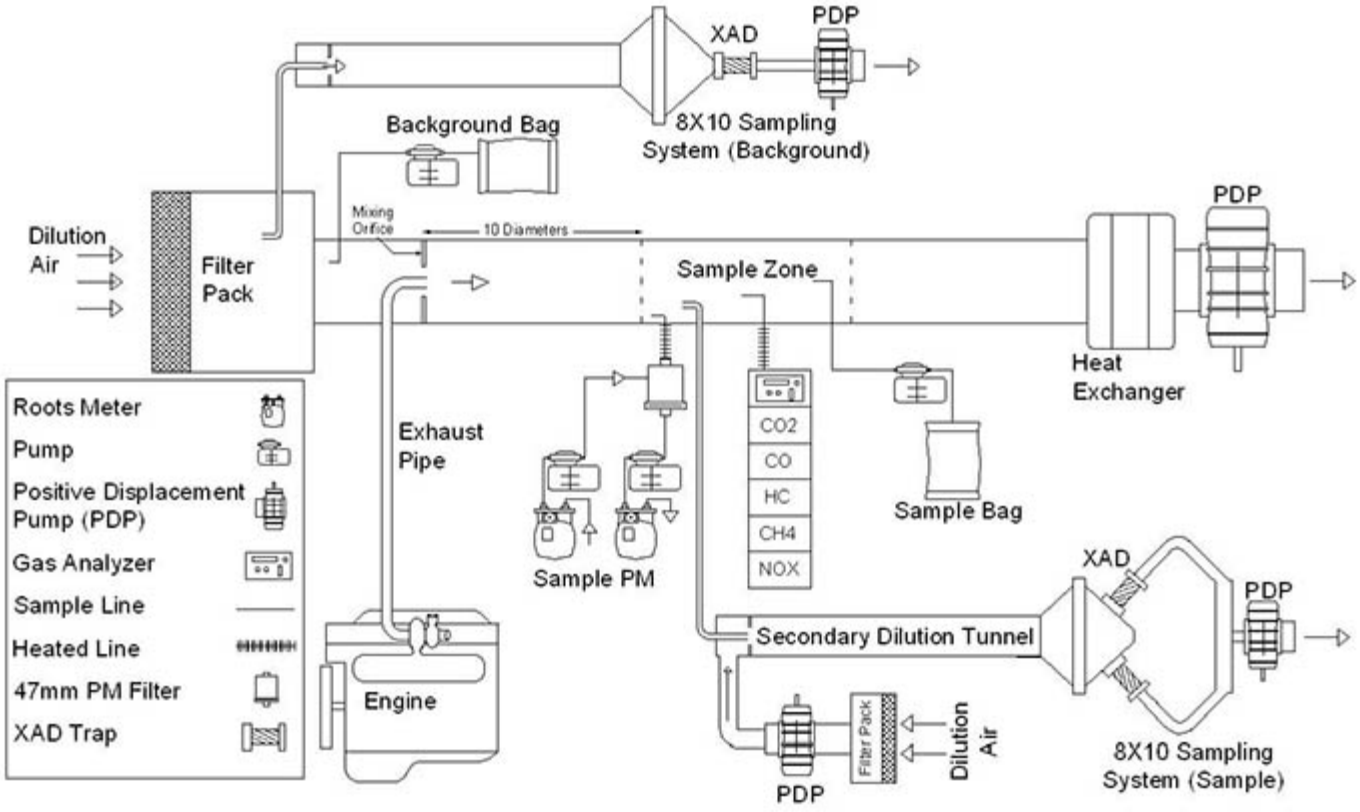

Figure 1. New sample system schematic for dilute exhaust SVOC measurements.

Accomplishments — Several accomplishments and improvements were made to the dilute exhaust sampling system. These improvements included:

- Implementation of a background air SVOC sampling system
- Implementation of closed-loop control to maintain constant flow rate on the dilute exhaust SVOC sampling system
- Implementation of 8x10 inch Zefluor™ filter instead of the traditional 20x20-inch Pallflex filter
- Elimination of polyurethane foam (PUF) in the SVOC sample train (use XAD porous polymer resin only)
- Installation of a heated blanket around the secondary dilution tunnel for the dilute exhaust SVOC sampling system
- Implementation of a field blank procedure for each day of testing to account for ambient air contributions
- Implementation of sampling surrogates and an internal, clean-up, and recovery standard to improve quantitation
- Improvement of solvent extraction techniques for extraction of XAD and filters
- Optimization of the solvent system to reduce losses in surrogate compounds
- Validation of sample media handling for both extraction and collection
- Evaluation of different filter media
- Determination of test-to-test repeatability
- Determination of the tunnel equilibration period
- Determination of trap breakthrough

In addition to the accomplishments listed above, the Environmental Protection Agency (EPA) agreed to allow this method to be introduced for a review and comment period in the Federal Register (FR). This accomplishment will allow the SwRI method to be used as an alternative for sampling and analysis of SVOC in dilute engine exhaust. Several papers will be presented on this topic, and the method will be sent for the FR review period in March 2015.

2014 IR&D Annual Report

Investigation into the Achievable Load and Misalignment Dynamics of a Crankshaft Bearing Test Rig, 03-R8455

Principal Investigators
Kevin L. Hoag
Riccardo Meldolesi (Powertrain Technology, Ltd.)
Anthony Perkins (Powertrain Technology, Ltd.)
John W. Miller

Inclusive Dates: 03/18/14 – 07/18/14

Background — Bearing test rigs, while widely used by bearing manufacturers to compare designs and materials, exhibit poor correlation to engine test results. Engine manufacturers have thus been required to conduct more costly on-engine tests. This project was undertaken to define to what extent it is possible to use a custom bearing test rig to more closely replicate the operating conditions experienced by crankshaft bearings when installed in an engine. Conditions to be replicated included periodically varying (i.e. versus rotation angle) the instantaneous misalignment of the bearing under test while it is being radially loaded. The work provided a background contribution to defining the functional requirements of the rig to be built as part of an industry consortium.

Approach — The bearing test rig is depicted in Figure 1. In this project, several alternative approaches were assessed for achieving the necessary dynamic misalignment and a final approach was selected. One of the critical design requirements was to achieve sufficient stiffness at the bearing-to-shaft interface. The stiffness specifications are based on the dynamic loading requirements the bearing would see in an operating engine. Stiffness analysis was done to assess the contributions along the load and reaction paths summarized in Figure 2. Finally, a dynamic analysis model was constructed as shown in Figure 3, to assess rig controller performance requirements.

Accomplishments — Detailed component design was completed, allowing component and

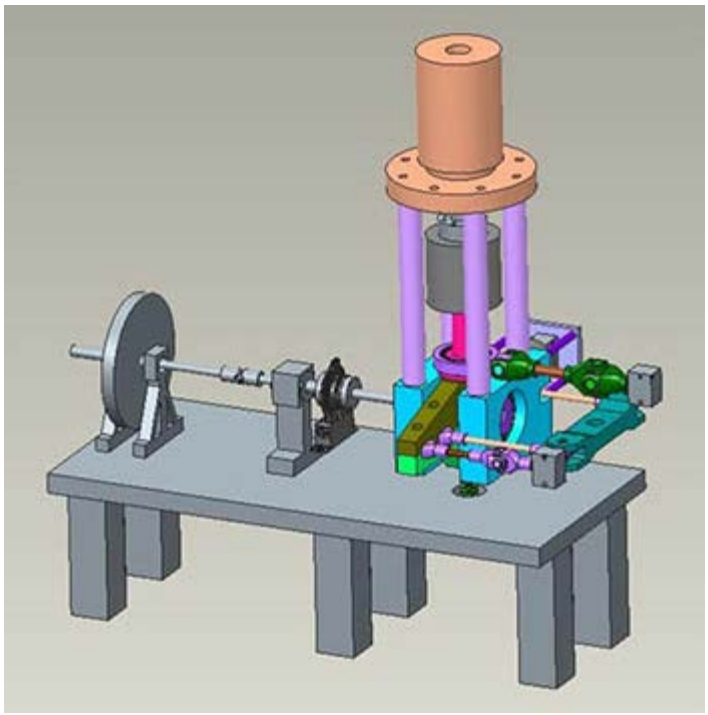

Figure 1. Dynamic bearing test rig.

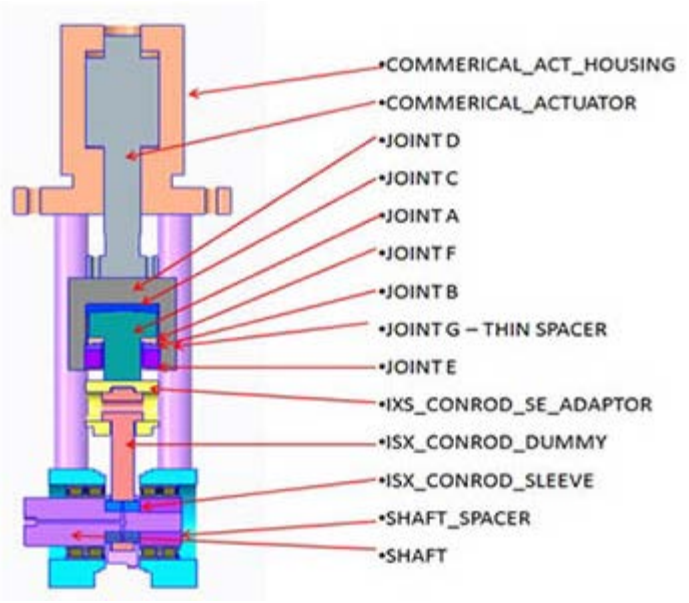

Figure 2. Bearing rig assembly showing each of the components and joints considered in the stiffness analysis..

joint stiffness to be analyzed and dynamic simulation to be conducted. Several possible approaches to incorporate dynamic misalignment between the test bearing and shaft were assessed, and a recommended approach was identified. Component and joint stiffness modeling confirmed that adequate stiffness can be achieved, and performance data was made available to actuator suppliers. A 3-D dynamic model of the entire test rig system was completed and demonstrated.

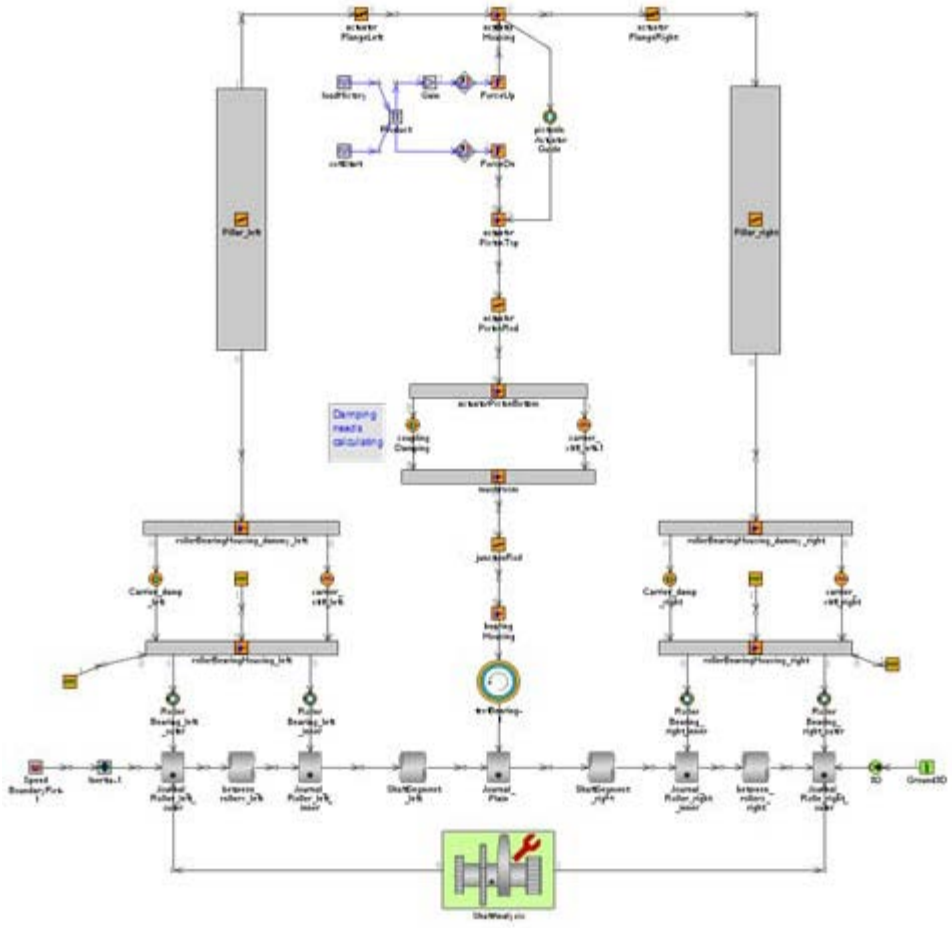

Figure 3. 3-D dynamic model of the bearing test rig.

SOUTHWEST RESEARCH INSTITUTE®

2014 IR&D Annual Report

Dedicated EGR on a Natural Gas Engine, 03-R8457

Principal Investigator
James Chiu

Inclusive Dates: 04/01/14 – Current

Background — The novel solution of SwRI's HEDGE technology with dedicated exhaust gas recirculation (D-EGR™) has shown the potential for significant improvement in efficiency for gasoline engines. Combining the D-EGR concept with a heavy-duty natural gas engine has the potential of matching or exceeding the efficiency of a diesel engine, which has been a goal for many years. D-EGR was initially conceptualized in 2007 as a solution to the combustion deterioration associated with high levels of EGR dilution and to simplify EGR controls for gasoline engines. The concept is to take the exhaust from one or more cylinders of a multi-cylinder engine and route its exhaust to the intake to create the entirety of the EGR for the engine. A closed EGR system enables using combustion temperature and pressure to reform fuel by running fuel rich, but without the conventional chemical energy loss associated with rich operation. With natural gas, a D-EGR engine can take advantage of the high hydrogen-to-carbon ratio and combustion characteristics of natural gas and the potential for greater hydrogen production over gasoline. This brings up the possibility of a six-cylinder engine with two dedicated cylinders with a nominal EGR rate of 33 percent. This configuration is shown in Figure 1.

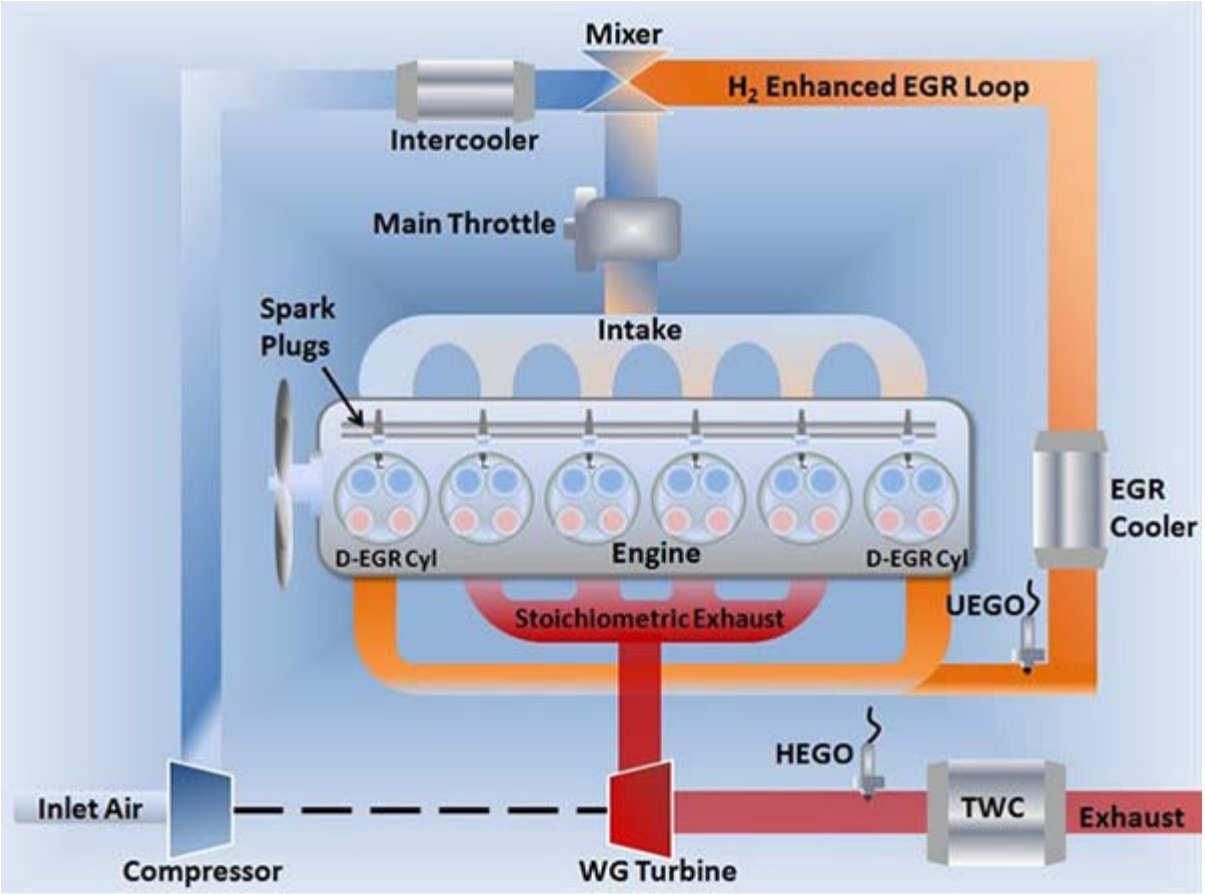

Figure 1. D-EGR configuration on a six cylinder engine with two dedicated cylinders.

Approach — The objective of this project is to investigate the characteristics of a six-cylinder D-EGR engine with natural gas as the fuel. Baseline testing on a Cummins ISX12-G natural gas engine will be conducted at steady-state conditions. The engine will then be converted to a D-EGR configuration with the assistance of a GT-power model and the same steady-state test points will be conducted. Results from the D-EGR configuration will be compared to the baseline of this engine, and change in efficiency will be documented. The goal is to operate at a nominal EGR rate of 33 percent in all cylinders, but other configurations with different EGR rates should be possible with this engine.

Accomplishments — A Cummins ISX12-G was installed in a steady-state test cell, and a baseline test was conducted at steady-state test points. The steady-state test points include the 13 modes used for emission certification along with additional points to obtain a more complete map of the engine. The conversion of the engine to the D-EGR configuration along with a SwRI control system to operate the engine has been completed and testing has started. The GT-power model of the ISX12-G in the D-EGR configuration has been completed and was used to provide guidance for the D-EGR configuration.

2014 IR&D Annual Report

Investigation into Engine Wear Map Development with Radioactive Tracer Testing, 03-R8479

Principal Investigators
Craig Wileman
Peter Lee
Mike Moneer

Inclusive Dates: 07/01/14 – Current

Background — Stoichiometric natural gas engines are becoming more widely used in on-highway transport applications. With reduced natural gas prices, fleet operators may find a move from diesel fuel to natural gas advantageous. Compressed natural gas is a cheaper alternative to diesel and a more energy dense fuel on a mass basis. With U.S. national averages for diesel and compressed natural gas around $3.89 per gallon and $2.11 per diesel gallon equivalent, the upfront vehicle premium of the natural gas fueled engine can be regained in fuel costs. With radioactive tracer testing, there exist a means of quickly evaluating wear rates in these new powertrain units. Developing a test method for engine wear rate mapping will afford SwRI the opportunity to respond to a growing product segment through efficient, short-duration wear testing.

To evaluate long-term durability using currently available methods would require multiple engines to be run over some designed test cycle for hundreds of hours, followed by a complete engine teardown with post-test part metrology to determine the wear incurred on the critical engine parts over the operational period. Even with the current number of manufacturers producing stoichiometric natural gas engines for on-highway usage, a proven method and equipment capable of mapping wear severity across the operating range is a marketable technology.

Approach — The goal of the project is to create a wear map for the Cummins ISX 12G, with the steady-state wear rates collected through a 25-point run matrix across the operating range of the engine. To achieve this goal, a two-stage approach has been outlined utilizing a Plint Te-77 reciprocating, sliding contact tribometer prior to full-scale engine testing. Tribometer testing allows for the systematic separation and combination of operating inputs that affect part wear rates. Results from the Te-77 tribometer work will be applied to construct a method for gathering and interpreting wear rates in the fired engine testing such that the normalized steady-state wear rate observed at one set of conditions is repeatable regardless of the preceding engine condition or day acquired. The Te-77 will be adapted for use with a gamma ray detector intended to monitor the accumulation of radioactive markers in the system while the rig is

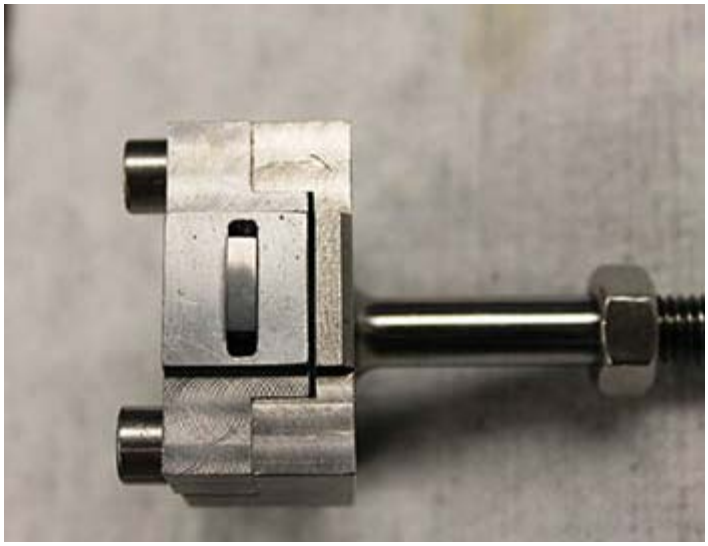

Figure 1. Ring test segment in holder Te-77.

operational. The inclusion of the gamma detector in the system permits monitoring the wear rate response of the parts while altering single inputs such as the applied load and/or reciprocating speed.

Through the simplified loading of ring segments running on liner segments in the Te-77 rig, the project will examine the repeatability of wear rates on single sets of test pieces across varied but controlled and repeatable parameters such as load, speed, lubricating oil flow rate, and lubricating oil temperature. Additional sets of parts will duplicate run conditions to observe the repeatability of wear rates between separate part sets.

Figure 2. Liner test segment in Te-77 reservoir with sample porting and tubes.

Accomplishments — The work within the current project will result in experimental data that defines an operational and statistical approach to engine wear rate mapping. SwRI is currently working on several natural gas engine projects, and has several proposals or pre-proposals for natural gas engine design and development. The market for natural gas on-highway engines, and thus for their design and development, has been expanding rapidly for the past few years. The knowledge and experience obtained from this testing will support current and future natural gas engine projects. There is a potential for intellectual property for predicting high wear operating conditions and subsequent control strategies or features to avoid those conditions.

The project offers other significant benefits to include:

- Developing real-time radioactive wear testing on a Te-77 reciprocating test rig. Figures 1 and 2 depict the tribometer reservoir setup for tracer sampling.
- Investigating correlation between a Te-77 wear test rig and an operating engine.
- Demonstrating the use of radioactive tracer wear testing on a stoichiometric spark-ignited natural gas engine.
- Developing a test methodology to evaluate wear measurement across a range of operating conditions and under a continually changing engine "state-of-wear."

2014 IR&D Annual Report

Elucidating the Effects of Lubricant Viscosity, Oxidation and Soot Loading on Total and Component Engine Friction, 08-R8300

Principal Investigator
Peter M. Lee

Inclusive Dates: 04/01/12 – 01/15/14

Background — Governmental legislation has increased pressure on vehicle manufacturers to reduce exhaust NOx emissions. One way in which this has been achieved in diesel, and now gasoline engines, is the inclusion of exhaust gas recirculation. This technology results in increased soot levels in the lubricant, adversely affecting wear rates and frictional properties of the lubricant. Vehicle manufacturers also are increasing engine loads in an attempt to improve fuel economy resulting in higher operating temperatures, increasing thermal oxidation of the lubricants. In addition, there is a trend towards reduced lubricant viscosities, causing thinner operating films, resulting in increased component contact, which, in turn, results in higher wear rates. There becomes a point where the friction created by component contact outweighs the advantages of lower viscosity lubricants. At this time this is not fully appreciated and is little understood due to the complexities of measuring engine component friction on bench-top rigs. Only measuring the friction of engine components running in an engine will allow direct comparison between results.

Approach — A single cylinder research engine has had all ancillaries removed, ensuring all friction experienced by the engine is caused by engine components only. The engine has been instrumented so total engine friction can be measured. The valvetrain has the cam wheels instrumented to measure instantaneous friction, and the connecting rod has been instrumented with strain gauges to measure piston assembly friction. Bearing friction is calculated by subtracting piston assembly and valvetrain friction from total engine friction. This gives friction for each engine component. The objectives of this project were:

- Elucidate the effect of reduced lubricant viscosity, lubricant oxidation and lubricant soot loading on engine component friction (valvetrain, bearing and piston assembly)
- Validate the results for lubricant viscosity against industry standard tests for fuel economy
- Elucidate the effect of engine load on engine component friction
- Install piston assembly friction on a Cummins ISX in the SwRI clean diesel program
- Generate unique knowledge for SwRI, giving employees more authority when talking with clients
- Create a new and unique capability at SwRI

Accomplishments — The engine, dynamometer and engine control system has been assembled in the test cell and is operational. Four different viscosity lubricants have been supplied and run in the sequence IVD fuel economy test and results reported. Special instrumentation for the engine has been designed, manufactured and successfully used to measure component friction within the engine. Several client tests have been run using this equipment.

SOUTHWEST RESEARCH INSTITUTE®

2014 IR&D Annual Report

Detecting Piston Ring Instability with Engine Vibration Analysis, 08-R8342

Principal Investigator
Craig M. Wall

Inclusive Dates: 10/01/12 – 04/01/14

Background — Engine vibration analysis is a potentially lucrative capability that SwRI is well-positioned to exploit, given the amount of engine testing done annually. In this project, a difficult task was chosen to highlight the sophistication of SwRI sensor technology. Specifically, piston ring instability is a low-energy event that has profound effects on engine performance and emissions. Detecting ring instability without using invasive sensors means subtle mechanical processes can be monitored and recorded without disassembling a client's engine. That is, vibration recording and analysis can be offered as a value-added service at any point during testing, and offers a significant form of analytical insurance when unexpected events require post-test analysis. Other potential benefits include the possibility of developing ring performance monitors that can advise an engine control unit in real time to adjust engine operation and avoid high emission states. This is particularly welcome as engines age, as this capability may well reduce both lifetime emissions and the after-treatment packages required to suppress pollution.

Approach — The initial sensor suite consisted of a combustion pressure transducer in the cylinder head, a crankcase pressure transducer for blow-by gas pulses, and an accelerometer attached to the engine block with an optical encoder referencing crankshaft angle. These were installed on a 500cc single cylinder spark ignition gasoline research engine. Piston ring instability was first sensed by monitoring blow-by gas flow from the crankcase, which rises when the piston rings fail to seal against the combustion gases. This project was not an engine test per se, but was conducted to develop sensing methodology. We used an engine running with a modified piston as a "signal generator" to provide mechanical vibrations for optimizing a non-invasive sensor suite. The initial suite was eventually reduced to only the accelerometer and crank angle encoder. A simple analog device was also developed, which easily displays the vibration information in real time: the accelerometer on the engine block was used to drive an LED light source that illuminated a rotating disk on the camshaft. A mark on the disk was "strobed" similar to the effect of an ignition timing light, but in this case the vibrations are substituted for the ignition event and appear at the characteristic crank angles shown in the accompanying plot.

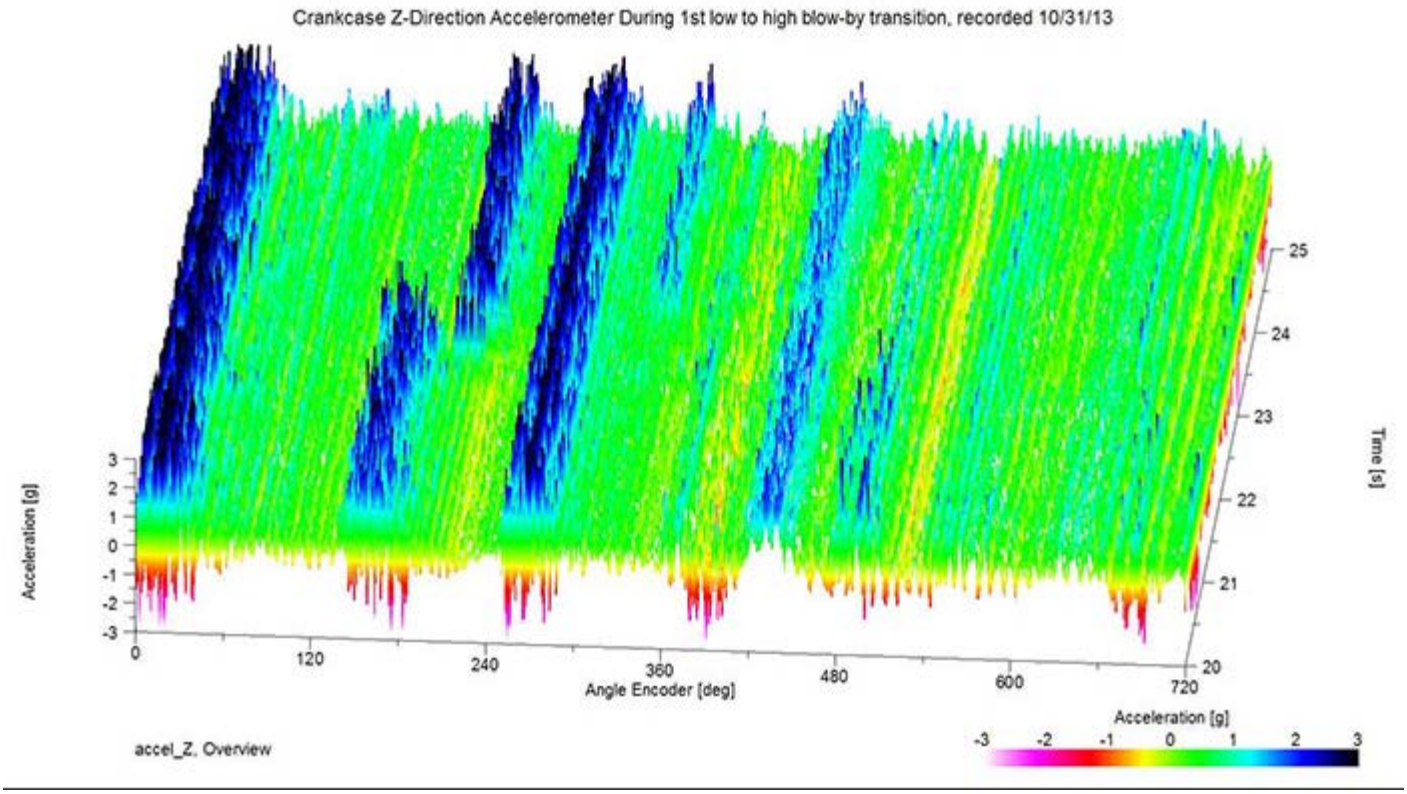

Figure 1. Shift in energy during stable-to-unstable ring operation.

Accomplishments — The technique we evolved used a piston with excessive clearance in the top ring groove. We have managed to arrive at a convenient experimental method that allows us to “turn on and turn off” piston ring instability by independently adjusting rpm and power. Increased rpm decreases ring stability by “throwing” the ring off the lower ring groove seating surface, while increasing power increases ring stability by increasing the gas pressure that holds the ring down against the inertial forces unseating it. Within very narrow limits, we can easily produce instability or stability by a simple turn of a control potentiometer. This is our key ability that provides an opportunity to develop real-time ring stability sensors and eventually an onboard engine control capability to avoid high emission states, even in worn engines. The sensor suite may ultimately consist of no more than the accelerometer attached to the engine block and a crankshaft angle encoder, which can be installed on a client engine in minutes. The following illustrates the shift in energy signature when a transition from stable to unstable ring operation occurs in the middle of a five-second accelerometer recording. These energies are plotted as “G” forces versus crankshaft angle and are the result of repeatedly interrupted high pressure gas escaping past the piston rings as increased blow-by.

2014 IR&D Annual Report

Investigation of an Oleophobic Coating Effect on Gasoline Direct Injection (GDI) Engine Components to Reduce Carbon Deposits, 08-R8362

Principal Investigators
Brent Shoffner
Dr. Terrence Alger II
Dr. Kent Coulter
Carol Ellis-Terrell
Dr. Sylvain Kouame
Eric Liu

Inclusive Dates: 01/01/13 – 12/31/13

Background — Carbon deposits on the backside of intake valves in light-duty vehicle gasoline engines have always been a durability issue for the automotive industry. In traditional carbureted or port fuel-injected engines these deposits have been controlled through the addition of detergent additives to the fuel. Unfortunately, in newer engines using gasoline direct injection (GDI) these additives are ineffective because the liquid fuel is introduced directly into the cylinder, and the detergent-carrying liquid fuel has minimal contact with the backside of the intake valve.

Deposits on the tulip area of the intake valves have the potential to restrict air induction and decrease engine performance. With GDI engines, the fuel additives will have minimal effect on the intake valve deposit (IVD) resulting in an issue that does not have an economic solution at this time.

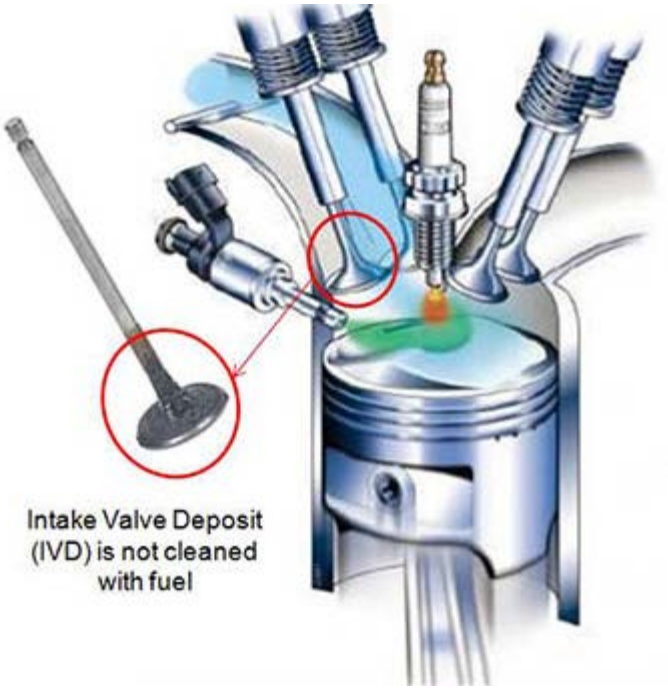

Figure 1: Typical GDI cylinder configuration.

Approach —

- The temperature environment of the intake valves was researched based on previous SwRI data.
- The intake valve surface metallurgy and finish were measured.
- IVD from GDI engines was analyzed.
- Candidate coatings were evaluated for bench properties such as the oleophobic contact angle.
- The original equipment manufacturer (OEM) intake valves and valves with three different coating technologies applied in the "tulip area" were evaluated in a dynamometer-based GDI engine test. The IVD weight was determined for each valve at the end of test.

Accomplishments —

- A dynamometer-based engine test procedure was developed that can be used to evaluate the potential effects of engine oil, fuel, and coatings on the formation of IVD.
- Concentrations of elements in the IVD and the engine oil are similar.
- Interesting IVD formations were observed that relate to intake valve rotation and injector spray pattern.
- The engine test results indicated that the surface (metal or coating) of the intake valve tulip area does affect the formation of IVD. However, none of the coatings evaluated reduced the IVD weight less than the OEM (uncoated) valves.

2014 IR&D Annual Report

Determination of PAHs in the Tires by GC/MS, 08-R8402

Principal Investigator
Joseph Pan

Inclusive Dates: 07/01/13 – Current

Background — In 2007, the European Union issued 1906/2007/EC (REACH), a regulation requiring, as of January 1, 2010, all process oils isolated from the tire treads contain less than 1.0ppm benzo(a)pyrene, BaP, and that the sum of eight specific PAHs be less than 10ppm. ISO 21461, the EU's official method, uses nuclear magnetic resonance analysis to determine whether a tire meets these new standards. The EU regulation states that if the Bay-H NMR signal of the process oil isolated from the tire treads is < 0.35 percent of the total H NMR signal, the tire is regarded as having met the EU's PAH standards for the tires.

Approach — We set out to develop a GC/MS method that would accurately and precisely determine each individual PAH concentration in the process oils isolated from tires. The approaches included:

1. using the GC/MS with isotope dilution technique
2. studying the effects of the sizes of the rubber bits on PAH extraction efficiency
3. comparing various solvents for their efficiencies of extracting the PAHs from the rubber bits
4. fine tuning the sample extract cleanup procedures with liquid-liquid partition and silica gel liquid column chromatography
5. studying the accuracy and precision of the developed GC/MS method.

Accomplishments — Rubber bits of five sizes were tested: 2.8 to 2.36mm, 2.36 to 1.70mm, 1.70 to 1.00mm, 1.00 to 0.425mm, and 0.425 to 0.125mm. No significant differences in PAH extraction efficiency were observed. The solvent extraction efficiencies of the five-ring PAHs from the rubber bits were: toluene > carbon disulfide > acetone = 1,4-dioxane > propionic acid > carbon tetrachloride > cyclohexane. The DMF (N,N-dimethylformamide) or NMP (N-methyl-2-pyrrolidone) each with 10 to 15 percent water extract PAHs well from hexane, separating PAHs from the non-PAH hydrocarbons. The liquid chromatography column packed with activated silica gel also separates target PAHs well from the non-PAH hydrocarbons. The method average accuracy for the determination of 18 PAHs and the five-ring PAHs in the tire oils were 52.1 percent and 48.5 percent, respectively. The method average %RSD for the determination of 18 PAHs and the five-ring PAHs in the tire oils were 15.3 percent and 18.8 percent, respectively.

Forty-three passenger car tires made in 15 countries were purchased locally. These tires were cut up and their treads extracted for PAH analysis. The tire extract oils were analyzed using the developed GC/MS method for quantifying 18 PAHs using 16 deuterated PAHs as internal standards. The split extract oil of each tire was sent to a commercial laboratory for NMR analysis by ISO 21461. A pass/fail decision was made for each tire based on BaP, sum of the eight PAHs, and NMR data.

Results of Commercial Tires Tested for PAHs

- 81 percent (35 tires/43 tires) passed based on NMR data.
- 23 percent (10/43) passed based on the level of Total EU 8 PAHs by GC/MS.
- 7 percent (3/43) passed based on the level of BaP by GC/MS.
- 100 percent (3/3) passed based on the BaP level also passed the Total 8 PAHs level.
- 70 percent (7/10) passed based on the Total 8 PAHs level failed the BaP level.
- 25.6 percent (11/43) agreed between the NMR and GC/MS data on pass/fail decisions, of which 27.3 percent (3/11) agreed on passes (i.e. pass/pass) and 72.7 percent (8/11) agreed on "fails"

(i.e. fail/fail).

- 74.4 percent (32/43) disagreed on pass/fail decisions between the GC/MS and the NMR methods, of which 100 percent passed by the NMR data and 100 percent failed by the GC/MS data.

The data for individually tested tires are given in Table 1.

In conclusion, the NMR method tended to pass tires easily (35/43 or 81.4 percent), many of which (32/35 or 91.4 percent) would be viewed as "false negative" based on the GC/MS (BaP) data.

Method →	Data by ISO 21461	Pass/Fail by ISO 21461	Pass/Fail by GC/MS	Data by GC/MS method	
Tire ID ↓	H-Bay%			BaP, ppm	Sum of EU 8 PAH, ppm
Z1	0.20	Pass	Fail	5.38	17.1
Z2	0.07	Pass	Fail	3.26	8.30
Z3	0.54	Fail	Fail	17.5	91.7
Z4	0.79	Fail	Fail	27.7	115
Z5	0.17	Pass	Fail	4.97	18.2
Z6	0.34	Pass	Fail	9.85	23.2
Z7	0.67	Fail	Fail	19.0	134
Z8	0.29	Pass	Fail	46.3	155
Z9	0.64	Fail	Fail	16.8	138
Z10	0.29	Pass	Fail	12.2	43.6
Z11	0.25	Pass	Fail	2.05	5.80
Z12	0.11	Pass	Fail	25.2	69.7
Z13	0.10	Pass	Fail	2.87	13.2
Z14	0.43	Fail	Fail	37.7	294
Z15	0.08	Pass	Fail	24.0	78.4
Z16	0.52	Fail	Fail	17.4	162
Z17	0.09	Pass	Fail	10.4	29.8
Z18	0.04	Pass	Fail	1.64	5.41
Z19	0.69	Fail	Fail	35.5	443
Z20	0.11	Pass	Fail	2.46	11.4

Tire samples were extracted by Soxhlet extractor with toluene as extracting solvent.

	Indicates a PAH data failing EU std by GC/MS or ISO 21461 method.
Pass	Indicates a "false negative" based on NMR data.
Pass / Fail	Indicates NMR data and GC/MS data agree on the Pass/Fail decisions.

EU standard: Bap <1.0ppm and sum of 8 PAH <10ppm = Pass

EU's Proxy standard by ISO 21461: Bay-H <0.35% = Pass

"Z21" indicates data from re-extraction.

Method →	Data by ISO 21461	Pass/Fail by ISO 21461	Pass/Fail by GC/MS	Data by GC/MS method	
Tire ID ↓	H-Bay%			BaP, ppm	Sum of EU 8 PAH, ppm
"Z21"	0.16	Pass	Fail	4.73	15.8
Z22	0.11	Pass	Pass	0.793	4.18
Z23	0.11	Pass	Fail	4.35	14.0
Z24	0.15	Pass	Fail	4.9	13.5
Z25	0.08	Pass	Fail	2.07	7.39
Z26	0.13	Pass	Pass	0.455	1.69
Z27	0.13	Pass	Fail	5.23	15.2
Z28	0.19	Pass	Fail	3.09	9.7
Z29	0.11	Pass	Fail	9.31	43.3
Z30	0.47	Fail	Fail	3.11	52.5
Z31	0.24	Pass	Fail	48.3	132
Z32	0.14	Pass	Fail	1.12	3.81
Z33	0.15	Pass	Fail	11.5	29.8
Z34	0.05	Pass	Fail	12.2	29.5
"Z35"	0.03	Pass	Fail	3.28	10.7
Z36	0.14	Pass	Pass	0.847	4.19
Z37	0.13	Pass	Fail	32.9	109
Z38	0.09	Pass	Fail	18.6	51.9
"Z39"	0.13	Pass	Fail	6.10	15.6
Z39R	0.13	Pass	Fail	5.73	15.0
Z40	0.16	Pass	Fail	1.76	5.68
Z41	0.21	Pass	Fail	16.6	45.8
Z42	0.05	Pass	Fail	11.9	31.0
Z43	0.16	Pass	Fail	7.42	19.8

Table 1. Comparison of passing/failing the EU regulation over the PAH levels on commercial tires between the GC/MS and NMR (ISO 21461) methods

SOUTHWEST RESEARCH INSTITUTE®

2014 IR&D Annual Report

Testing Frequency-Dependent Geoelectrical Methods and Processing Techniques to Characterize Subsurface Ice, 15-R8422

Principal Investigators
David Stillman
Robert Grimm
Ronald McGinnis

Inclusive Dates: 10/01/14 – Current

Background — The electrical properties of ice are frequency- and temperature-dependent over a bandwidth of 100 kHz to 10 Hz. Our first goal was to determine if noninvasive geophysical techniques such as spectral induced polarization (SIP) can measure this frequency dependence in permafrost. Field SIP measurements are accomplished by injecting current over a broad frequency range (20 kHz to 10 Hz) into the subsurface between two electrodes (steel rods hammered into the ground) and measuring the resulting voltage between two other electrodes. Depth information is found by varying the spatial locations of the electrodes. SIP surveys are very slow; therefore, our second goal was to determine if faster moving techniques such as DC electrical resistivity (DC Res) and capacitively coupled resistivity (CCR) also map subsurface ice concentration, but in a much more economic fashion. While these methods only measure at a single frequency, we use DC Res (8 Hz) to measure the low frequency bound and CCR (18 kHz) to measure the high-frequency bound.

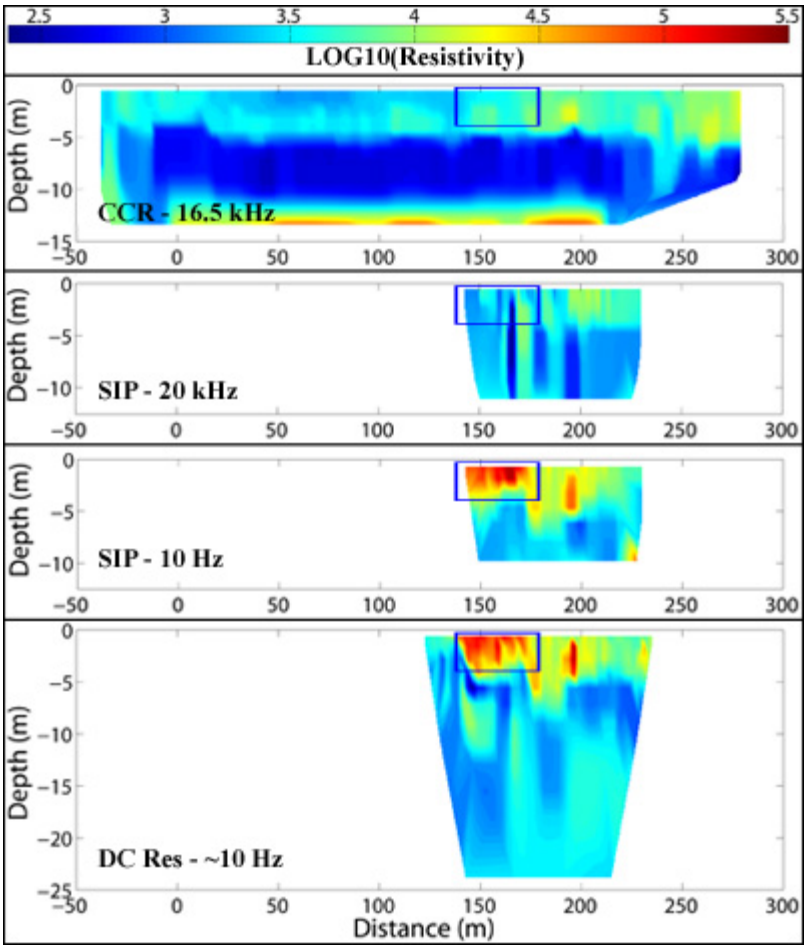

Figure 1. Inverted resistivity (Ωm) of the three Tok geophysical surveys. The SIP spectra within the blue box indicate ice contents >70 percent volume. This could be inferred from just the DC Res and CCR data, because ice-rich permafrost has a high resistivity at low frequency and a much lower resistivity at high frequency.

Approach — Our first task was to determine new inversion techniques that would allow for the multispectral data to be inverted together and then converted into ice content. Our second task was to conduct field measurements at three sites in Tok, Alaska, (eastern Alaska on the Alaskan-Canadian highway) with three geophysical techniques (SIP, DC Res, and CCR) and determine if SIP and the DC Res/CCR method could detect subsurface ice.

Accomplishments — Using SIP data previously acquired, we were able to vastly improve the interpreted results by performing a multispectral inversion. We were then able to exact temperature and subsurface ice composition and published the first peer-reviewed paper of such a method (R. Grimm and D. Stillman, "Field Test of Detection and Characterization of Subsurface Ice Using Broadband Spectral Induced Polarization," Permafrost and Periglacial Processes, accepted). Our Tok field measurements were successful with the three survey types yielding similar absolute resistivity values (Figure 1). We found that while SIP gives the most quantitative results of ice content and temperature, the frequency dependence from the CCR and DC resistivity surveys is all that is needed to determine ice content in permafrost.

2014 IR&D | **IR&D Home**

SOUTHWEST RESEARCH INSTITUTE®

2014 IR&D Annual Report

Integrity Management of Nuclear Power Plant Components Subjected to Localized Corrosion Using Time-Dependent Probabilistic Model, 20–R8267

Principal Investigators
Pavan K. Shukla
Osvaldo Pensado

Inclusive Dates: 11/14/11 – 02/14/14

Background — Nuclear power plant operators are required to periodically inspect components by visual and volumetric examinations to maintain component integrity and ensure safety. As nuclear power plants age, more frequent inspections are expected to ensure component integrity. A framework to define inspection schedules, based on risk considerations, is needed to keep the cost of inspections constrained without compromising safety. The objective of the project is to develop an adaptive-predictive probabilistic model to forecast localized corrosion induced pit population and pit depth distributions. The forecast algorithm is intended to support integrity management programs, including integrity management for nuclear power plant components and dry storage cask systems for spent nuclear fuel. Forecasts of the evolution of corrosion damage and its uncertainty can inform maintenance and inspection program schedules and provide for savings or trigger actions when risk of failure or the extent of damage is not acceptable.

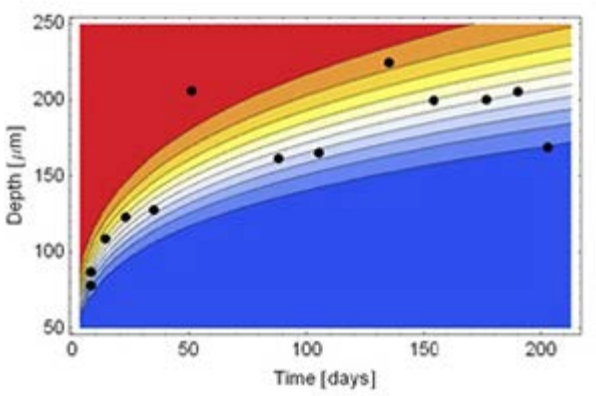

Figure 1. Example of scatter plot of the 0.95 quantile pit depth versus time and contour plot exhibiting uncertainty in the empirical parameter κ' of the power law $d = \kappa' t^{\nu}$.

A model was developed in this project to forecast localized corrosion-induced damage of metallic components based on damage measured at a given time. For example, if a component exhibits pitting corrosion in an environment, the model will be used to estimate the distribution of pit depths as a function of time. The model accounts for previous inspection data, randomness of pit propagation, and pit growth rate as a function of time. The model could be used to estimate probability of component failure due to pitting corrosion and calibrate inspection schedules so that detection of corrosion sites occurs before failure.

Localized corrosion such as pitting commonly exhibits random scatter in the measurable parameters such as corrosion rate, maximum pit depth and time to perforation. The scatter in measurable parameters is hypothesized to arise from metal surface heterogeneities and variations in the corrosive environment over time. This randomness appears to be an inherent and unavoidable characteristic of pitting corrosion. Thus, stochastic models may be better suited to describe pitting corrosion than deterministic ones. This is especially true if the results of pitting corrosion modeling are to be used as inputs to integrity and risk management models, which should account for uncertainty in the decision making.

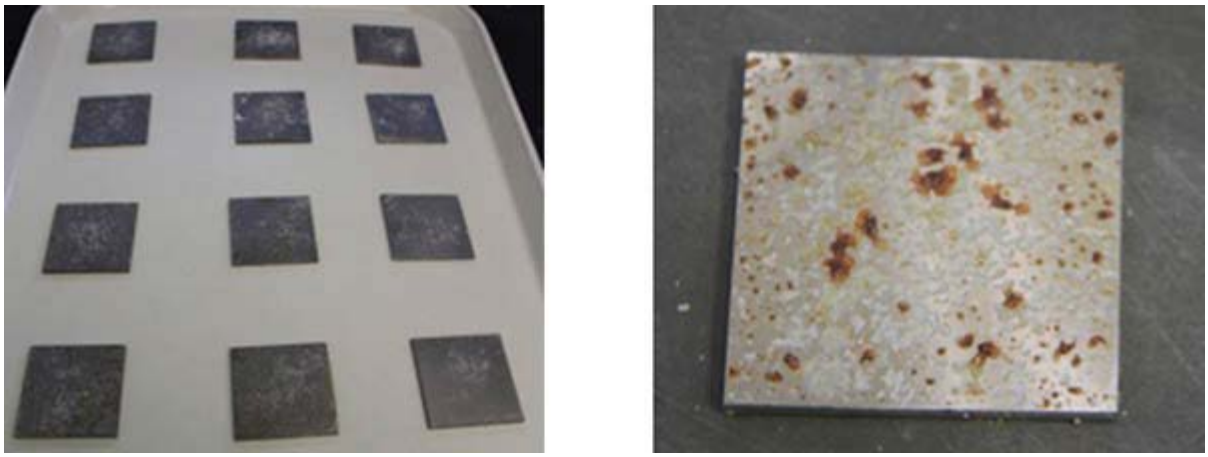

Figure 2. Coupons with salt before exposure and one coupon after 8-day exposure to humidity of 30 g/m³ at 50 °C.

Because measuring pit populations and their depths is time consuming and expensive for a large engineered system, experimental techniques have limited resolution, and the interest has always been in defining failure of a system, only the deepest pits are traditionally studied. There are no general methods to propagate the pit population and depth distributions in time and predict the evolution of corrosion damage. Markov chain models that are tested using Monte Carlo methods and updated with actual data using Bayes theorem have been used elsewhere to study the propagation of corrosion damage. We considered that such an approach has potential and flexibility to define an adaptive method incorporating inspection data to forecast the evolution of the system. Consequently, this method was investigated in this project.

Approach — Model development of the forecast technique consisted of three principal tasks: statistical model development, experiments, and data analysis and integration. In the statistical model, probabilities of transition between discrete states that satisfy Kolmogorov's forward equations for a pure birth process were used to forecast the evolution of depths of a population of pits. The discrete state of a pit is defined as a pit falling in a range of depths (e.g., a pit is in State 1 if its depth falls between 0 and 10 μm; State 2 if the depth is between 10 and 20 μm, and so forth). Thus, pit growth is conceptualized as a pit that transitions from one state to the next. In theory, parameters to define the transition rate between states can be obtained by measuring the average or a quantile (e.g., 95 percent quantile) pit depth as a function of time (see Figure 1). This macroscopic feature (e.g., average pit depth) can be used to quantify microscopic propagation rates.

As part of this project, conditions were selected to induce pitting in 304 stainless steel (SS). An experimental system was designed to monitor pit propagation in time. Small coupons of 304 SS with salt deposits were exposed to controlled temperature and humidity. This environment caused pitting readily after a few hours of exposure (see Figure 2). The 304 SS coupons were systematically removed from the humidity chamber for pitting corrosion evaluation and inspected using laser profilometry. The data collected from coupons were used to estimate pit depth versus time.

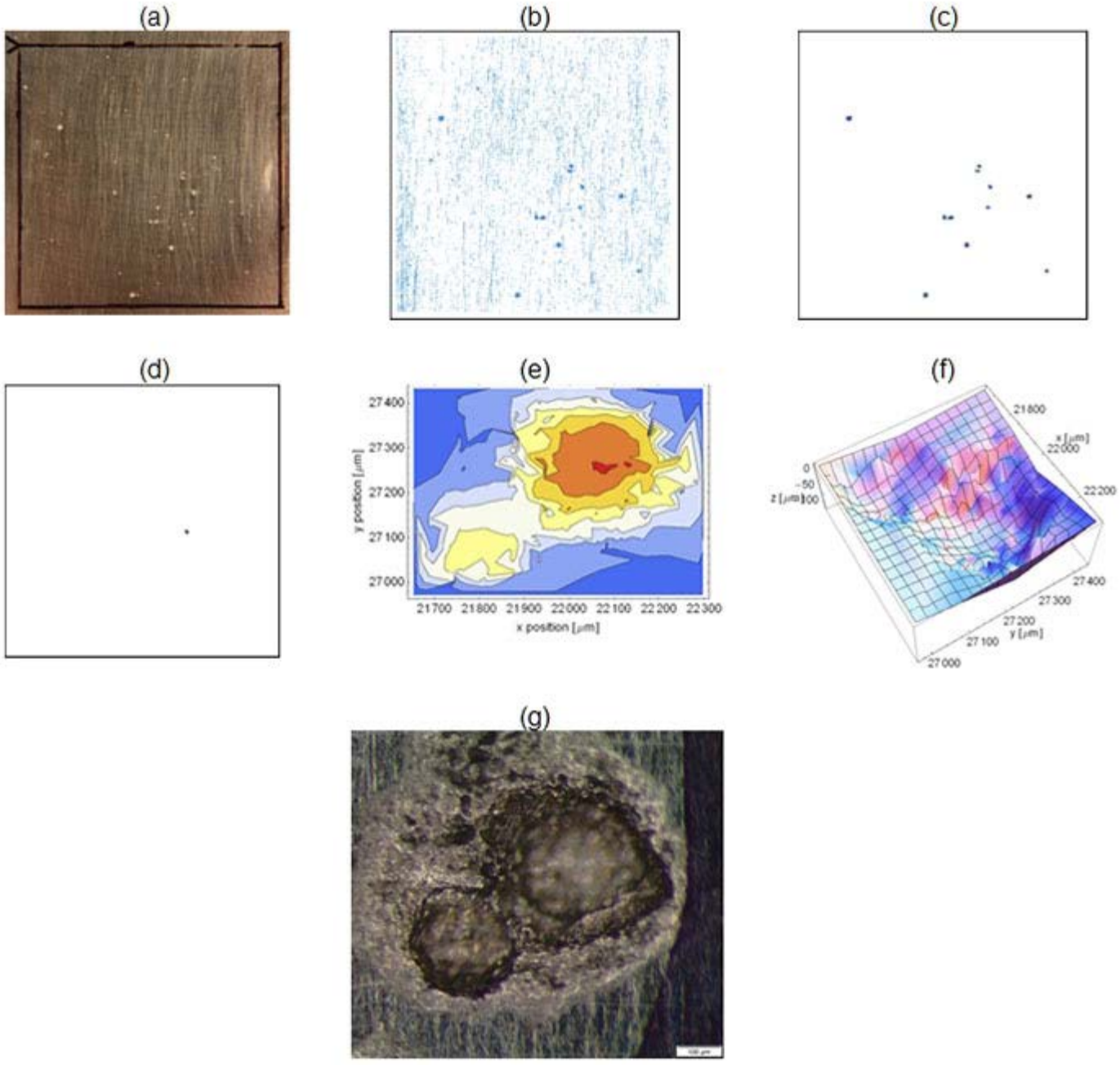

Figure 3. Example of data post-processing approach to identify pitting corrosion features: (a) photograph of metallic sample with pitting corrosion; (b) density plot generated with laser profilometry data; (c) filtered data keeping only pitting corrosion features and removing surface roughness features; (d) identified deepest pit; (e) contour plot of depths of deepest pit, (f) three-dimensional surface plot of the deepest pit; and (g) micrograph of deepest pit.

As part of the data analysis and integration step, the model was used iteratively to forecast the pit depth distribution at the next inspection or detection time. At the next inspection or detection time, the model parameters are updated with the collected data and a Bayesian update algorithm, and the next forecast is performed. A forecast sequence spanning 200 days and longer term forecasts were performed to demonstrate the implementation and use of the forecast model and associated techniques.

Accomplishments — A technique was developed to efficiently identify corrosion pits and measure pit depths using profilometry data. This technique is more efficient than known alternatives because it does not need to manually focus on one pit at a time. The technique automates the process of focusing on individual pits and extracting data for contour plots and two- and three dimensional plots of individual pit depths, as well as counting pixel clusters potentially associated with pits over a given detection area (see Figure 3). The technique allows for quantifying features of pitting corrosion such as the area and volume

of the metal affected by pitting. An invention disclosure on the profilometry data filtering technique was submitted recently.

Based on Markov chain concepts and transition probabilities, a differential model was developed to forecast the evolution of corrosion damage, expressed as a distribution of pit depths. The only inputs to the model are empirical parameters, κ′ and v, of the power law $d = \kappa' t^{v}$ (d = pit depth, t = time) that can be determined from profilometry measurements or alternative techniques. It is demonstrated that the power law $d = k' t^{v}$ directly arises from the propagation algorithm for a given class of transition probabilities or transition rates. The model also can be used to describe damage due to other corrosion modes that exhibit power law propagation.

A forecast algorithm for distribution of pit depths was developed that accounts for uncertainty in those distributions (see Figure 4). The uncertainty forecast employed a Bayesian update algorithm to combine forecasts with measured distributions and correct distributions of the empirical parameter κ′. Figure 4 graphically shows how the parameter κ′ controls the speed of the estimated pit-depth. In the forecast sequence, the κ′ posterior distribution is shifted to the right (i.e., the κ′ magnitude is increased) when the forecasts underestimate the pit penetration depths with respect to measurements, and the posterior distribution is shifted to the left when the forecast depths overestimate the measurements. In other words, the κ′ distribution is the mechanism to slow or accelerate forecasts based on comparisons to depth measurements. The κ′ distributions summarize information on the time propagation and spatial variability of the pits. A κ′ distribution can be interpreted to carry information of the previous forecast cycles. The algorithm is a method to combine and average measurements taken at different times, and extrapolate in time distributions of depths based on previous trends. As part of the project, longer-term forecasts were executed to demonstrate how the method would be applied to estimate the lifetime of components subject to pitting corrosion.

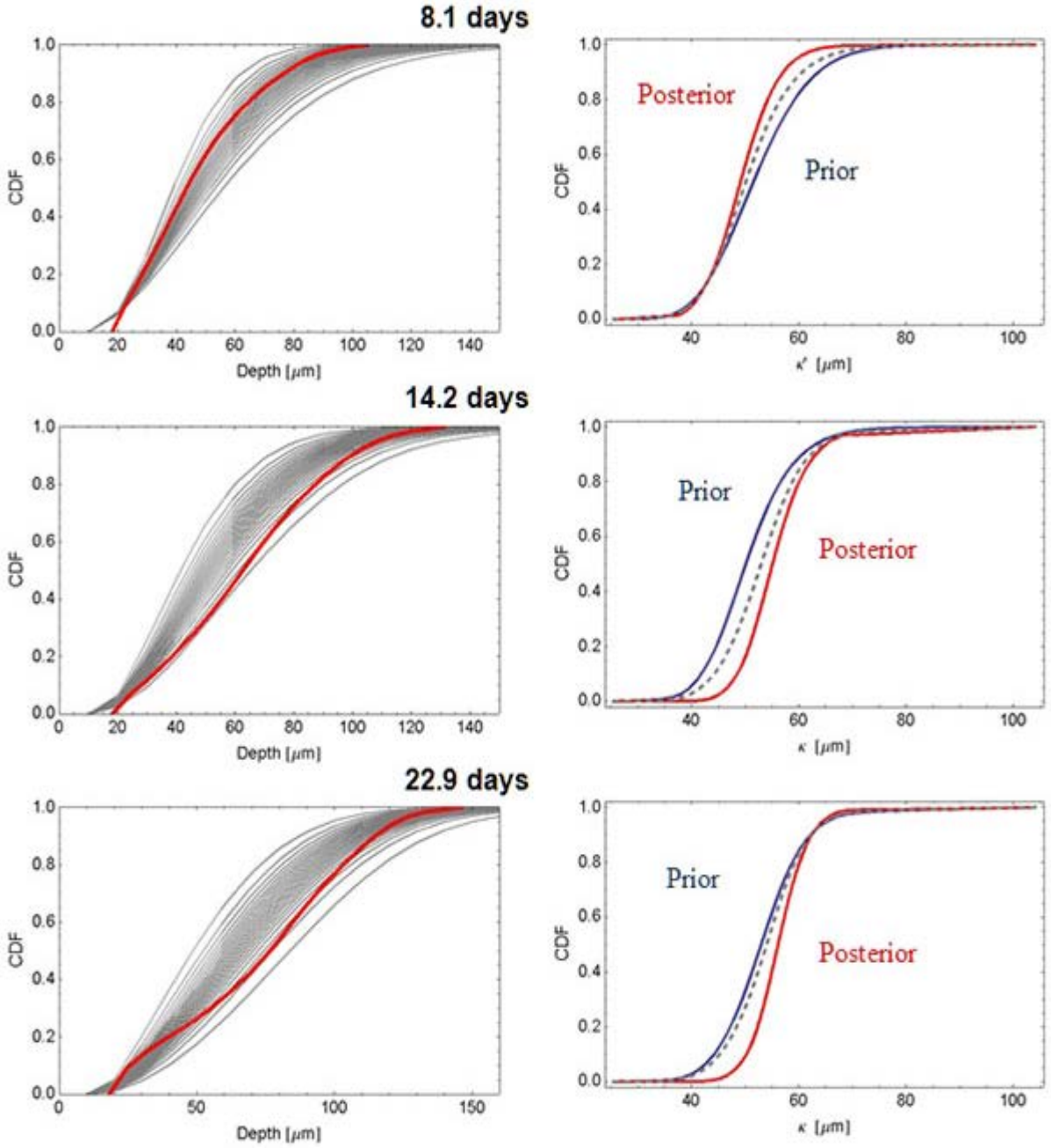
8.1 days
CDF
Depth [μm]
Posterior
Prior
κ' [μm]
14.2 days
CDF
Depth [μm]
Prior
Posterior
κ' [μm]
22.9 days
CDF
Depth [μm]
Prior
Posterior
κ' [μm]

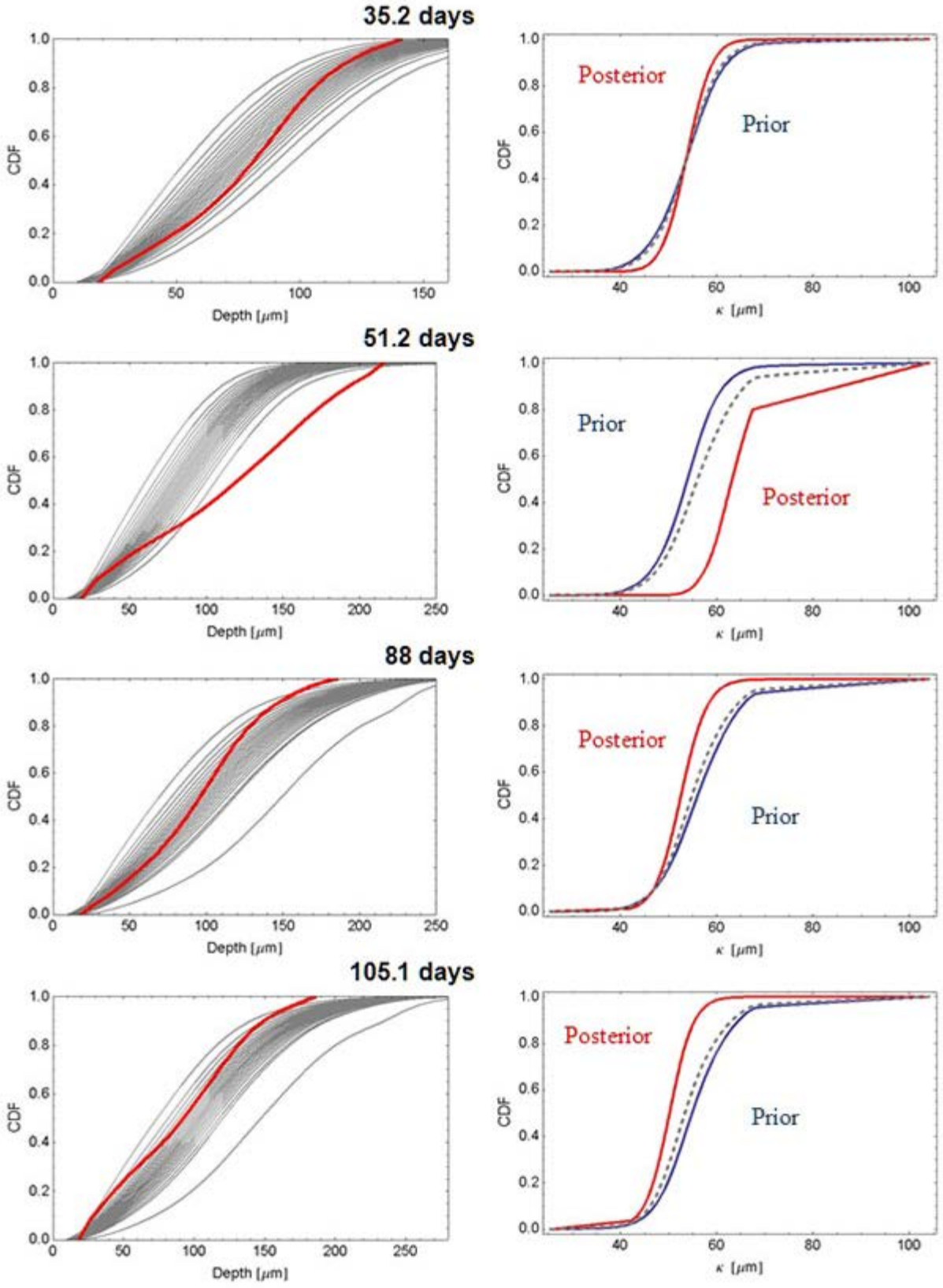
35.2 days
51.2 days
88 days
105.1 days
CDF
Depth [μm]
κ [μm]
Posterior
Prior

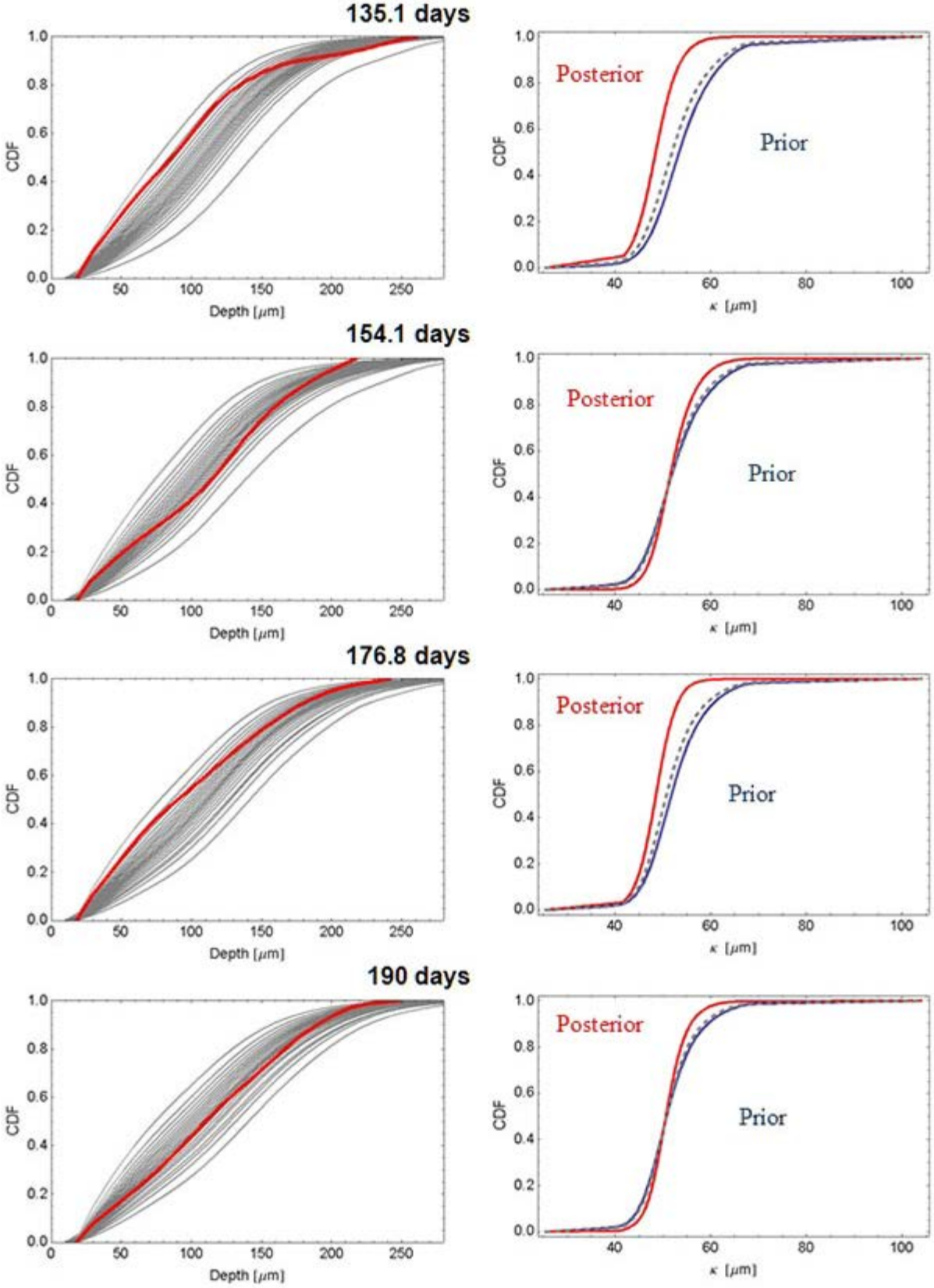
135.1 days
CDF
Depth [μm]
Posterior
Prior
κ [μm]
154.1 days
CDF
Depth [μm]
Posterior
Prior
κ [μm]
176.8 days
CDF
Depth [μm]
Posterior
Prior
κ [μm]
190 days
CDF
Depth [μm]
Posterior
Prior
κ [μm]

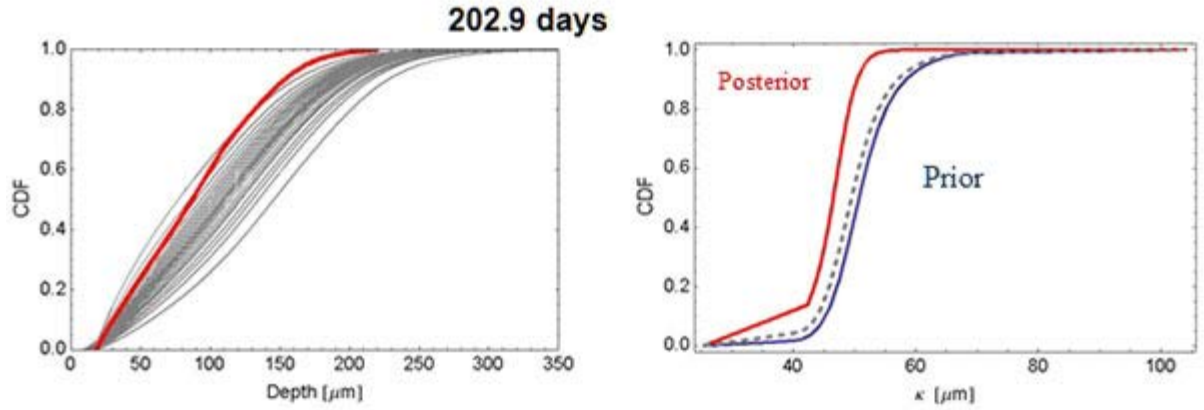

Figure 4. 200-day forecast sequence. The forecast is on plots on the left, gray curves. The red curve on the left is the measured cumulative distribution of pit depths. The plots on the right show the prior cumulative distribution function (CDF) for the rate constant parameter k', the posterior CDF computed with the forecast outputs and the measured pit depth distribution, and the weighted average (dashed line curve) to be used as prior in the next forecast cycle.

SOUTHWEST RESEARCH INSTITUTE®

2014 IR&D Annual Report

Integrated Physical Analog and Numerical Modeling of Geologic Structures, 20–R8368

Principal Investigators
Kevin J. Smart
Danielle Y. Wyrick

Inclusive Dates: 01/21/13 – 01/21/14

Background — One of the major hurdles in structural geology and geomechanics is the ability to accurately model the evolution of complex geologic structures in a reproducible and efficient manner. Whether modeling large-scale crustal deformation or outcrop-scale localized deformation, the ability to create realistic, predictive models remains constrained by the limitations of the modeling approach. Typically, complex geologic problems have been characterized by one of two modeling approaches: physical analog modeling or numerical modeling. Physical analog modeling is currently better suited to simulating three-dimensional structural complexity, including discontinuous deformation such as faulting. However, analog modeling is cumbersome for conducting multiple parametric analyses and is not amenable to extraction of quantitative stress information. In contrast, finite-element-based numerical modeling can record complex stress and strain fields during model evolution, but still struggles with accurately capturing discontinuous processes such as fracturing and faulting. In particular, finite element models are often "too perfect" (lacking inherent flaws) to model natural geologic structures with accurate geometries.

Approach — The objective of this research is to couple physical analog and finite element modeling approaches to leverage the strengths of one approach against the weaknesses of the other, and to quantify the differences in data inputs and outputs between the approaches. To reconcile the inherent limitations in the two modeling approaches, a suite of experiments was conducted using both modeling approaches with the goal of testing and informing both. This project sought to perform calibrated, identical (or as near as practical) physical analog and numerical modeling of complex geologic phenomena to quantify and cross-inform these modeling approaches. This project focused on three fundamental areas: testing and selecting of appropriate physical analog modeling materials for simulating mechanical stratigraphy, constructing and analyzing of physical analog and numerical models to simulate deformation due to fluid/magma injection, and constructing and analyzing of physical analog and numerical models to simulate regional contraction.

Accomplishments — A material properties database was compiled to augment both the physical analog and numerical modeling components. Analog modeling materials must conform to known scaling laws, yet many materials reported in the literature have not been thoroughly tested for strength characteristics. For the numerical models, a mathematical description of the stress-strain behavior is selected that requires input values for material properties. Dry quartz sand has traditionally been used in analog modelings and its material behavior is well-documented. However, to impart heterogeneity to our layering, alternative analog materials need to be identified that can mimic the scaling behavior of weaker and stronger intervals. A number of promising materials including aluminum oxide, silicon carbide, and crushed glass were tested to find potential materials that scale appropriately to weaker and stronger rocks. Material testing included measuring the density, grain size distribution, angle of repose, friction angle, and cohesion.

The fluid-injection models performed under this project showed similar patterns of growth and deformation,

although the effects in the numerical models were more subtle than in the physical analog models. These results illustrate that changes in the mechanical stratigraphy can directly influence initiation and propagation of induced hydraulic fractures. The regional contractional models illustrated that both physical and numerical modeling approaches can capture the fundamental behavior of this geologic process, including the impact of mechanical stratigraphic layering. More importantly, the project results suggested that future efforts toward better integration of physical analog and numerical modeling should be focused on acquiring and testing additional analog materials, numerical mesh refinement, and testing and calibrating of constitutive relationships used to represent the behavior of the analog materials.

2014 IR&D Annual Report

Hypothesis Testing for Subfreezing Mass Movements, 20–R8407

Principal Investigators
Donald M. Hooper
Cynthia L. Dinwiddie

Inclusive Dates: 07/01/14 – Current

Background — Debris flows, some seasonally recurring, are known to be present on dune slopes in several mid- to high-latitude dune fields on Mars. Mass movement signatures are among the best records of historical and ongoing geologic activity on Mars, and seasonally recurring debris flows on Martian sand dunes therefore imply modern, ongoing alluvial activity. We observed analogous debris flows consisting of a sand and liquid water mixture that cascaded down leeward dune slopes under subfreezing conditions in March 2010 at the Great Kobuk Sand Dunes (GKSD), Alaska. For this project, field work was conducted at Great Sand Dunes National Park and Preserve (GSDNPP) in Colorado to examine subfreezing debris flow initiation and development.

Approach — Project team members conducted field work at GSDNPP during February 10–19, 2014, to test the hypothesis that relatively dark sand lying on bright snow may cause local hot spots to form where solar radiation can be absorbed by the sand and conducted into the snow, enabling meltwater to form at subfreezing air temperatures and sand to mobilize through alluvial processes. The team chose to focus instrumentation and data collection on a sinuous transverse-to-barchanoid dune at a site that the National Park Service calls the "Sand Pit." A thermal properties analyzer was used to measure thermal conductivity, specific heat capacity and thermal diffusivity of the principal depositional units in situ. A thermal infrared imaging camera was used to obtain surface temperature distribution measurements across portions of the dunes as well as an experimental grid of snow/ice, dry sand, moist sand and darkened (with aluminum oxide) sand. A network of 35 digital thermometers recorded the spatial and temporal temperature distribution across the Sand Pit. SwRI meteorologic and hydrometeorologic stations were also deployed to measure air temperature, multilevel subsurface temperature, barometric pressure, relative humidity, precipitation, net radiative flux, carbon dioxide levels, wind velocity and direction with a 3D sonic anemometer, and subsurface unfrozen water content at three depths. Also mounted on the stations were a pyranometer for measuring solar irradiance and a saltation flux sensor for recording sand particle impacts at a set height. Sand transport was also measured by an additional pair of sediment samplers, including one developed by SwRI.

Accomplishments — Field team members did not observe any naturally occuring debris flows at Sand Pit. Dry sand avalanching on the slip face was common, especially when the wind was from the west or southwest. An artificial debris flow was initiated on the dune brink by pouring measured volumes of water down the slip face. This man-made debris flow closely resembled those observed at the GKSD. During February 2014 field work, our network of digital thermometers recorded spatial and temporal distributions of surface temperature that allow us to describe dune response to solar insulation, shadow, and microtopography. Granulometric analysis was completed on all aeolian samples and reveals that the sand is (i) fine grained, (ii) well sorted to very well sorted, (iii) finer at dune crests than in interdune corridors, and (iv) better sorted in active aeolian samples than bulk samples. To supplement our data collection from GSDNPP, the thermal properties analyzer was used in the laboratory to measure thermal conductivity, specific heat capacity, and thermal diffusivity of sand samples previously collected at the GKSD. These data are being input into a meteorology-driven, cryo-hydrologic numerical model to achieve our goal of understanding how debris flows, fed by liquid water, form at sub-freezing air temperatures.

2014 IR&D Annual Report

Landslide Investigations Using Satellite-Based Multitemporal Synthetic Aperture Radar Techniques, 20-R8410

Principal Investigators
D. Marius Necsoiu
Ronald N. McGinnis
Leslie D. Gergen

Inclusive Dates: 07/29/13 – 01/15/14

Background — SwRI is actively promoting its capabilities in the area of remote sensing and geoinformatics. The requested support for this research was motivated by a number of proposal opportunities related to detecting and monitoring landslides using satellite-based remote sensing technologies. Landslides represent one of the most common natural hazards, threatening and influencing the socio-economic conditions of many countries. Because preventing landslides or mitigating their impacts is difficult, a deep knowledge of landslide distribution and state of activity is required, especially for situations where property, infrastructure and human lives are at risk.

Approach — This research investigated the feasibility of using high-resolution multitemporal interferometric synthetic aperture radar (InSAR) techniques (i.e., mm-resolution techniques) to monitor slow landslide movement and developed a work-flow that maximizes the accuracy of high resolution multitemporal InSAR techniques (i.e., mm-resolution techniques) and minimizes the number of synthetic aperture radar (SAR) datasets that are required. The results provided an estimated rate of change over two decades; a unique capability to determine the extent of the affected area; an assessment of change at a significantly higher density of locations with similar or greater accuracy than the previous cited studies; and an in-house multitemporal InSAR capability to process SAR imagery.

Accomplishments — The results of this project place SwRI in a position to pursue government and commercial clients with direct interest in natural hazard mitigation and earth process investigations by:

- Strengthening SwRI's presence and complementing capabilities developed in the field of natural hazards assessment and mitigation over the years; i.e., differential InSAR (DInSAR), Corner Reflector InSAR (CRInSAR), wireless sensor technologies.
- Expanding our exposure within the natural hazards community by publishing a peer-reviewed journal article titled "New Insights on the Salmon Falls Creek Canyon Landslide Complex Based on Geomorphological Analysis and Multitemporal Satellite InSAR Techniques" (Necsoiu, M., McGinnis, R.N., and Hooper, D.M., 2014, in Landslides, DOI 10.1007/s10346-014-0523-8).
- Exploring new areas of business development, including the insurance industry, by contacting several private insurance companies.

2014 IR&D Annual Report

Developing Methodologies for Gravity-Assisted Solution Mining, 20-R8423

Principal Investigators
Amitava Ghosh
Gary R. Walter

Inclusive Dates: 10/01/13 – 09/30/14

Background — The objective of this project is to develop a numerical approach to model the evolution and fate of horizontal solution cavities in solution mining projects. The approach combines a cavity evolution model that considers dissolution dynamics in a cavity and a geomechanical model that predicts the onset and extent of caving resulting from the ongoing cavity evolution. This combined model can be used to design and optimize undercut solution mining projects in bedded evaporates, particularly for trona deposits like those in the Green River Basin of Wyoming. This new tool will help mine operators design and operate solution mining projects using a simulation-based tool to augment intuition and experience gained from conventional underground mining.

Approach — The project uses a simplified cavity evolution model to simulate the gross aspects of the solution cavity geometry, and uses the evolving cavity geometry as input to a geomechanical model that considers the caving process. The cavity evolution model assumes the fluid is well mixed at each cross section of the cavity, calculating the fluid flow rate from the known injection-extraction rates and the evolving cross-sectional area of the cavity. The model uses the one-dimensional advective-dispersion equation to calculate average concentrations across each cross section. Changes in cavity geometry due to evaporite dissolution are simulated using published empirical relationships between fluid concentrations and dissolution rates, combined with geometric relationships considering cavity wall geometry. The caving model simulates the gross aspects of caving initiation and collapse front progression. The caving model discretizes the evaporite mass above the cavity into Voronoi blocks. These blocks can undergo gravity-driven deformation and collapse, as well as creep-related deformation due to viscoplastic material properties.

Accomplishments — Results from this project were presented at the Solution Mining Research Conference held in San Antonio in May 2014. These modeling results addressed the initial project scope, which considered evaporite beds featuring an insoluble overlying confining bed. Other evaporate configurations lack an insoluble overlying confining bed, such as potash deposits in Canada that occur within a thick sequence of other evaporite deposits like halite. In these geologic settings, economic-mineral extraction procedures seek to prevent dissolution of the overlying evaporite beds in order to minimize contamination of the high value solution and avert a potential collapse of the cavity and overlying land surface if the cavity were to penetrate too far into the overburden. Common practice uses an oil cap, formed by injecting a liquid hydrocarbon such as diesel fuel, to prevent dissolution of overburden beds. On-going work is extending the cavity evolution model to consider the more complex effects of an oil cap on cavity development.

2014 IR&D Annual Report

Evaluating Properties of Chemically-Aged High-Density Polyethylene Piping Material Used in Nuclear Power Plants, 20–R8432

Principal Investigators
Pavan Shukla
Mike Rubal
Mohammed Hasan

Inclusive Dates: 12/13/13 – Current

Background — The principal objective of this project is to evaluate the material properties of chemically aged high density of polyethylene (HDPE) piping used in nuclear power plants (NPPs). In nuclear power plants located in the United States, HDPE pipes are increasingly being used in safety-related components, such as essential service water (ESW) systems including buried and above-ground sections. Because carbon steel piping in the ESW system corrodes with age, carbon steel piping requires costly maintenance and has become a safety concern. To mitigate corrosion risks, nuclear power plant operators have begun to replace carbon steel ESW piping with HDPE. There are regulatory and safety concerns regarding the use of HDPE pipes in safety-related components. Even though there is a generalized belief that HDPE pipes have service lives of 50 years or more with minimal degradation and thus are safer compared to carbon steel pipes, there is limited evidence supporting this assumed service lifetime and associated performance. Therefore, this project work includes evaluating properties of the material as it ages and estimating its remaining service life.

The available methods for testing HDPE pipe failures and service lifetime have limitations, as they do not account for both chemical and mechanical degradation. The available testing methods are solely based on the mechanical strength of HDPE materials. These methods show two types of pipe failures: (i) ductile pipe rupture occurring with ballooning of the pipe specimen and yielding of the HDPE material and (ii) nonductile, slit and pinhole failures. In the available test methods, the allowable service life (i.e., for 50 years or more) is dependent on the level of stress applied at the pipe wall. HDPE materials undergo chemical degradation in the form of oxidative degradation due to the chemical environment in contact with the external and internal surfaces of the HDPE pipe. For the HDPE pipes, the internal environment is service water, which contains oxygen and radical generating disinfectants, such as chlorine or chlorine dioxide (ClO_2). The external environments are generally soil or air. The presence of oxidizing species in the service water leads to the oxidative degradation. The oxidative-degradation resistance of HDPE is increased by adding antioxidants, such as stabilizers and carbon black. When these antioxidants are significantly depleted from HDPE, the dissolved oxygen and other chemical species degrade the polymer at the pipe inner surface. This degradation leads to reduced molecular weight and diminished mechanical strength of HDPE. When degradation of the inner surface material is severe enough, an embrittled surface layer develops cracks, which tend to propagate through the pipe wall, driven by internal pressure.

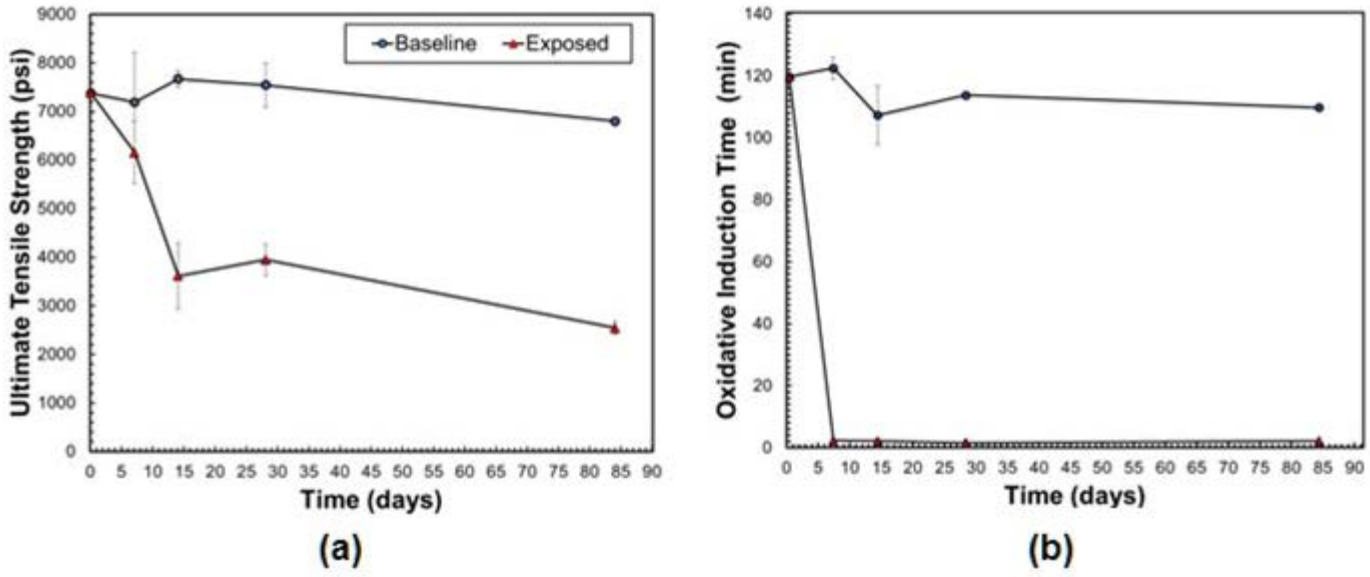

Figure 1. (a) Average ultimate strength for high density of polyethylene (HDPE) dog bone samples exposed to the baseline solution and the ClO_2 solution versus exposure time. (b) Oxidative induction time measurements of HDPE dog bone samples exposed to either the baseline solution and the ClO_2 solution versus exposure time.

Approach — The overall technical approach consists of the following four elements: mechanical testing, chemical treatment under oxidative conditions, developing a model for estimating antioxidant concentration and depletion with time, and designing a method for in-situ measurement of the antioxidant level and extent of oxidative degradation in the in-service HDPE pipes. In the overall approach, mechanical testing is used to correlate the antioxidant level and oxidative degradation to mechanical properties. The mechanical testing data will be used as a master curve for predicting the service lifetime of HDPE pipes. For the third objective, which involves predicting the evolution of the antioxidant concentration in the HDPE pipes, a model is being developed based on diffusion theory. The sample data will be used to estimate model parameters. It is important to develop a model because antioxidant concentration in HDPE pipe will vary in the radial pipe direction, and this variation is difficult to measure. Finally, a tool to measure the antioxidant concentration as a function of depth from the external surface of the pipe will be developed. The measured antioxidant level will help determine the antioxidant concentration profile in the pipe and overall antioxidant level to quantify the extent of oxidative degradation.

Accomplishments — The project accomplishments include insight gained on the mechanical and chemical properties of the HDPE piping materials as it ages in oxidizing solution. Two types of samples were prepared for the aging tests. The first type consisted of "dog bones" of a HDPE (TUB121) prepared by injection molding and aged at 40 °C in either a baseline solution (pH = 2) or a solution containing an oxidant, chlorine dioxide (ClO_2) (average concentration of 82 ppm for duration of exposure experiment) at a pH of 2. The second type consisted of four-inch thick blocks of HDPE exposed at 40 °C from one side with a solution 90 to 140 ppm of

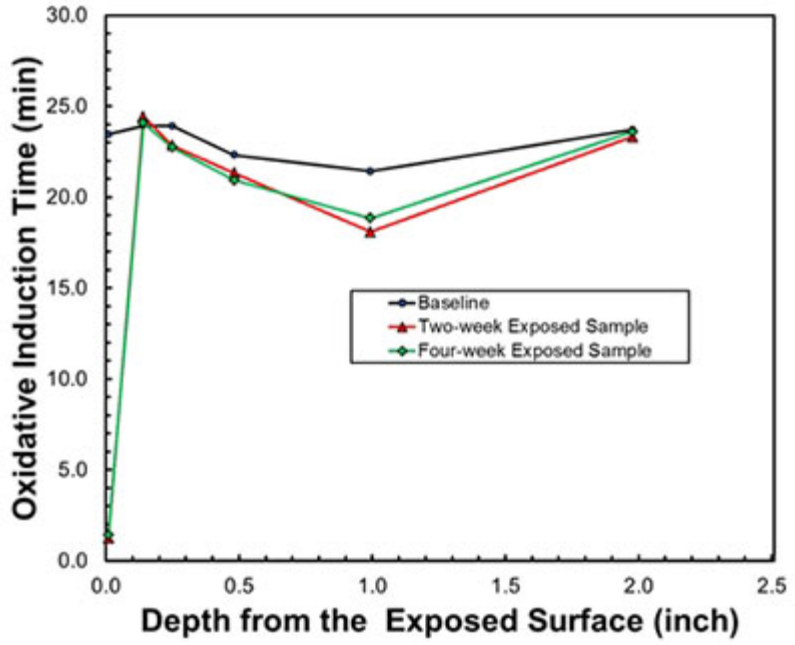

Figure 2. Oxidative induction time comparison between high density of polyethylene block samples exposed for various times and the effect of exposure on the depth from the exposed surface.

ClO_2 at pH of 2. For the HDPE blocks, samples were later machined into dog bones or discs over a series of depths from the surface so as to ascertain a correlation between the depth and material properties. After exposure tests, samples were analyzed by tensile, oxidative induction time (OIT), Fourier Transform Infrared spectroscopy, creep, and dynamic mechanical analysis for molecular weight.

Figure 1 compares the tensile results and OIT data for the first type of samples (dog bones made of TUB121). It is found that mechanical and chemical properties of the exposed samples decreased rapidly with exposure to the ClO_2 solution. For example, the ultimate tensile strength decreases by 50 percent after two weeks of exposure to ClO_2 solution. This correlated with the loss of antioxidant in the HDPE, as exhibited by the dramatic reduction of the oxidative induction time after a week of exposure. These data indicate that both mechanical and chemical properties of HDPE significantly change for the samples after exposure to the ClO_2 solution.

Initial analysis of the second type samples (four-inch thick blocks) also shows a rapid decrease in OIT values; however, as shown in Figure 2, these phenomena are limited to the exposed surface. As seen in Figure 2, the OIT values for samples prepared from the bulk of the HDPE remained more or less unaffected by the exposure. This surface limiting aspect is also noticed in the mechanical properties. For example, the ultimate tensile strength of the samples directly from the exposed surface shows significant reduction in mechanical properties compared to the bulk and unexposed material. However, the ultimate tensile strength of the samples at a small distance from the exposed surface is the same as the bulk and unexposed material, and remains unchanged.

The experimental data suggest that mechanical and chemical properties of the HDPE piping material are correlated. The data also suggest that the degradation in the HDPE material properties due to exposure is expected to be limited to certain depth from the exposed surface. Additional work is underway to further verify the later observation.

2014 IR&D Annual Report

Assessment of Thermal Fatigue in Light Water Reactors Feedwater Systems by Fluid-Structure Interaction Analyses, 20–R8434

Principal Investigators
Kaushik Das
Debashis Basu
Hasan Mohammed

Inclusive Dates: 12/13/13 – Current

Background — In a nuclear reactor, thermal striping, stratification and cycling take place as a result of mixing pressurized hot and cold water streams. The fluctuating thermal load generated by such unsteady mixing may result in fatigue damage of the associated structures. The mixing is often caused by faulty valves and can potentially affect safety-related lines such as the pressurizer surge line, emergency core cooling injection lines, reactor clean-up systems and residual-heat removal systems. Generally, thermal fatigue is classified as a long-term degradation mechanism in nuclear power plants. This is significant especially for aging power plants, and regulators need improved screening criteria to reduce risks of thermal fatigue and methods to determine the potential significance of fatigue. Though fluid mixing and thermal fatigue have been studied separately, a number of issues related to complex interaction between turbulent mixing and the mechanical structure of the Light Water Reactors (LWR) have not yet been resolved. Key uncertainties in this area include the effects of solid walls on variations in the thermal load amplitude and frequency (often referred to as filtering). These effects determine the temperature spectrum transmitted from the fluid to the structure. In addition, the effects of the mixing configuration, leak size and temperature differences between fluids are parameters that subsequently determine failure threshold and need to be explored. Expected project accomplishments include using advanced numerical techniques, especially fluid-structure interaction (FSI) methods, for studying turbulent mixing induced thermal fatigue in LWRs.

Approach — The work addressed in this project is fundamentally an FSI problem, which requires a computational fluid dynamics (CFD) solver to simulate the thermal mixing and a finite element model (FEM) solver to perform the stress analysis. Initially, the flow and structural temperature response will be calculated using a CFD solver. At this stage the flow solution will be compared against available experimental data for model confidence and benchmarking. Subsequently, temperature fluctuations on the structure will be calculated using a conjugate heat transfer solver and the thermal stress will be calculated from the temperature fluctuations. Later, a two-way FSI calculation will be performed, where the thermal mixing will be simulated using the CFD solver and simultaneously the FSI solver will be used to calculate the thermal stress. Based on the calculated stress, fatigue lifetime of the structure will be determined through the fatigue curve from the pressure vessel and piping design code.

Accomplishments — Numerical simulations were conducted for the T-junction experiment carried out at the Älvkarleby Laboratory of Vattenfall Research and Development AB and the experiment was selected to validate the numerical simulation results. The experiment consisted of two perpendicularly connected pipes with diameters of 0.1 m (D_{hot}) and 0.14 m (D_{cold}) for the hot flow (vertical direction) and cold flow (horizontal direction), respectively, forming a T-junction. The unsteady Reynolds averaged Navier-Stokes (URANS) turbulence models were used for turbulence. The URANS simulations are not able to predict the fine scale structures in the velocity field for the mixing region; these simulations give average results for the velocity. Furthermore, the URANS simulations are unable to predict the complex flow characteristics in

the T-junction mixing region that involve flow separation, recirculation and reattachment zone. The URANS solution approached a steady-state solution in terms of velocity and temperature fields. Based on the preliminary simulations using the URANS turbulence model, it will be necessary to use higher fidelity turbulent models, such as detached eddy simulation (DES) and large eddy simulation (LES) for subsequent simulations. The computational grid will be refined to capture the fine scale structures, mixing, and other complex flow features (e.g., circulation, reattachment) using DES and LES.

2014 IR&D Annual Report

Detection of Uranium Mill Tailings Cover Erosion Rates and Settlement Using Satellite-Based Radar Interferometry, 20-R8449

Principal Investigators
D. Marius Necsoiu
Gary R. Walter

Inclusive Dates: 01/20/14 – 06/20/14

Background — The Institute is actively expanding work related to land disposal sites with the U.S. Nuclear Regulatory Commission and other clients. Closure of uranium mill tailings impoundments requires construction of earthen covers that limit radon emissions and dispersal of radionuclides to the environment. NRC10 CFR Part 40 requires reasonable assurance that control of radiological hazards will be effective for at least 200 years. and for 1,000 years to the extent reasonably achievable.

This project investigated the feasibility of using synthetic aperture radar (SAR) coherence analysis, differential radar interferometry (DInSAR) and multitemporal interferometry, in particular the small baseline subsets (SBAS) technique to monitor the performance and stability of soil covers at uranium mill tailings sites and other land disposal sites with earthen covers. The methodology promises to provide a low-cost means for routinely monitoring changes across the entire site, infeasible with groundbased methodology.

Approach — Archived satellite SAR data were acquired to include two uranium mill tailings sites in northwestern New Mexico: the Bluewater site and the Grants Homestake site. Mill tailings covers may consist of vegetated soil, rock mulch (a mixture of rock and soil), or rip rap. These various cover conditions affect the strength of the SAR signal and may affect its coherence, which in turn affects the ability to use InSAR techniques in estimating surface displacement measurements. For the Bluewater site, the DInSAR and SBAS analyses provided consistent centimeter-scale changes in ground surface displacements, mapped over the entire tailings impoundment. The displacements correlate with variations in the slope of the tailings impoundment cover and nature of the underlying tailings. At the Grants site, only the rock-covered side slopes maintained sufficient coherence to perform quantitative SBAS InSAR analysis because reclamation activities disturbed the surface soil of the impoundment cap during the time period covered by the SAR data.

Accomplishments — This project provided a proof of-concept that InSAR techniques can be used to monitor the performance and stability of soil covers at uranium mill tailings sites and other land disposal sites with earthen covers. The research also advanced the understanding of how rip rap (coarse rock) affects the SAR signal response. Although the extent of the analysis was limited by the availability of archived data, the results demonstrated that future monitoring using on-demand SAR data acquisitions should yield reliable measurements of ground surface displacements.

2014 IR&D Annual Report

Improvement of Wet Gas Compressor Performance using Gas Ejection, 18-R8327

Principal Investigator
Grant Musgrove

Inclusive Dates: 07/13/12 – 01/2/14

Background — During upstream production of natural gas, the gas brought to the surface is compressed so that it can be injected into a pipeline and transported elsewhere. Sometimes the gas brought to the surface is a mixture including a small amount of liquid hydrocarbons, up to 5 percent volume fraction. Because a compressor is designed for dry gas only, the mixture of gas and liquid degrade the performance of the compressor to require much more power. By requiring more power, large drivers are needed that increase the cost and footprint of the compressor system. The current state of the art in wet gas compression in the oil and gas industry is characterizing compressor performance under wet gas conditions through experimental testing. However, it is becoming clear from the growing dataset of available test data of wet gas compressor performance that a fundamental understanding of wet gas effects on the compressor flow path is needed, as well as a solution to recover lost compressor performance.

Figure 1. An open-loop wind tunnel was developed to measure lift and drag for an airfoil placed in wet gas flow at Re = 700,000.

Approach — The goal of this project is to design and test a concept to eject air from an airfoil to remove liquid from the surface. Airfoil performance is evaluated from measured lift, drag, and surface pressure along the airfoil in wet-gas flow, including images of the gas-liquid flow near the airfoil. This project is conducted in two phases using computational predictions and experimental measurements. In the first phase, the effects of airfoil performance with wet gas over a range of operating conditions are studied with experimental measurements and computational predictions using a lattice-Boltzmann (LB) fluid solver, whereby the computational predictions can be directly compared to measurements. In the second phase, a gas ejection concept is implemented using the results from Phase 1, and studied experimentally for comparison to the baseline configuration without gas ejection.

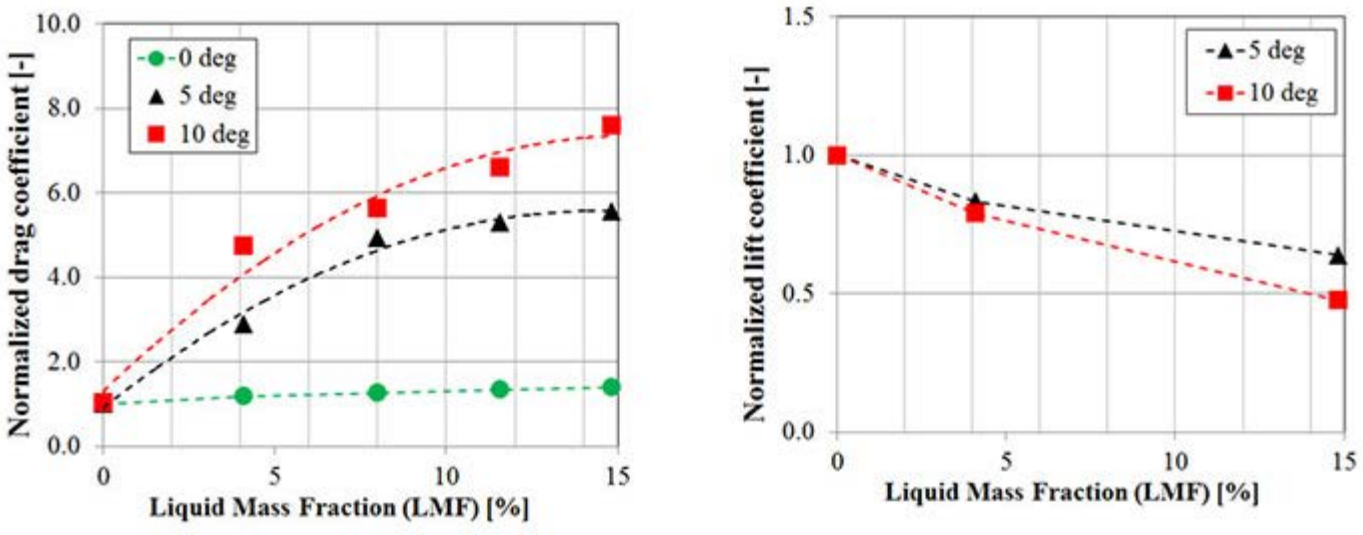

Figure 2. Wet gas flow increased the drag and reduced the lift of the airfoil over a range of attack angles.

Accomplishments — The work in this project has provided a first step towards quantifying compressor aerodynamic performance under wet gas conditions and a proof-of-concept to recover lost compressor performance. The aerodynamic effect of wet gas was quantified by placing an airfoil in an open-loop wind tunnel (Figure 1) in which liquid water was injected into the flow to provide a liquid mass fraction consistent with oil and gas applications. The results showed that aerodynamic lift was reduced and drag was increased (Figure 2) as the amount of liquid in the air flow was increased. The lift and drag coefficients for wet gas conditions were increased up to eight times the value for dry conditions and were shown to be dependent on the airfoil angle of attack. A method to recover lost aerodynamic performance was developed and tested using air ejected from the airfoil surface through a row of holes placed near the airfoil leading edge. With gas ejection, it was found that aerodynamic drag was significantly reduced in wet conditions compared to without gas ejection (Figure 3). A patent application (14/092976) for the gas ejection method has been filed.

In addition to experimental testing, an unconventional computational method to predict wet gas aerodynamics was undertaken. Instead of using a conventional Navier-Stokes computational solver, a Lattice-Boltzmann (LB) fluid solver was developed and used to predict air flow at the tested conditions. An LB solver was developed because the current capabilities of open-source and commercial LB solvers cannot simulate the multiphase conditions of wet gas flow around an airfoil. The developed solver was successful in predicting single-phase, turbulent flow around the tested airfoil with good agreement of surface static pressure distribution to test data. The multiphase capability of the solver was developed enough to resolve the complex gas-liquid interface during agglomerations of a two-phase mixture. Multiphase capability needed for wet gas simulation is not yet possible with the LB solver, but the work completed in this project sheds light on future areas of focus needed for wet gas simulation with the solver.

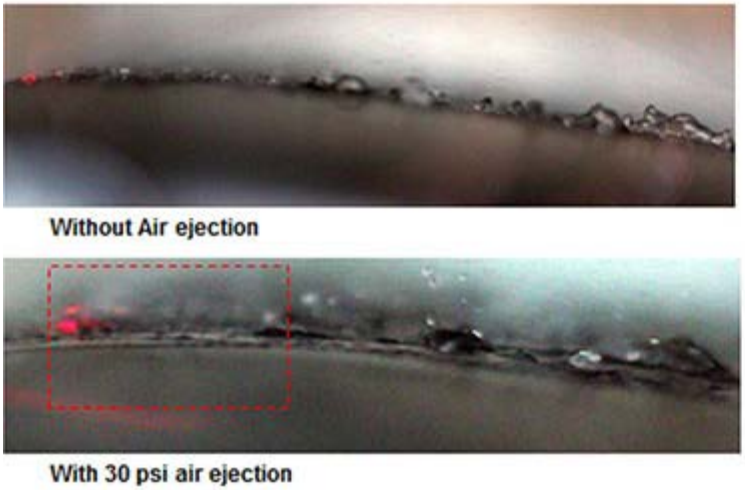

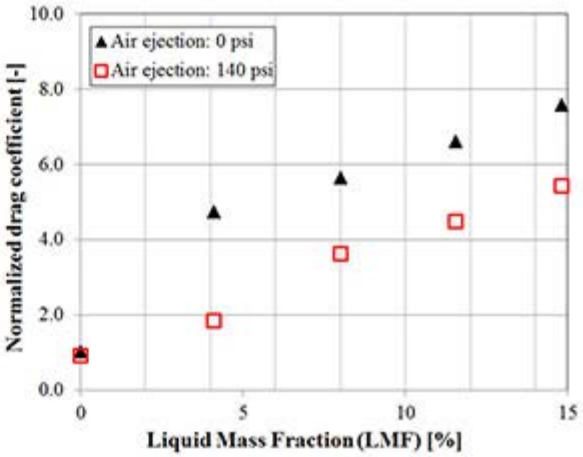

Figure 3. The use of the gas ejection method to remove the liquid film from the airfoil surface was successful to recover performance by decreasing the airfoil drag under wet gas conditions.

2014 IR&D | IR&D Home

SOUTHWEST RESEARCH INSTITUTE®

2014 IR&D Annual Report

Development and Demonstration of Erosion Prediction Capabilities for Oil and Gas Industry Applications, 18-R8338

Principal Investigators
Rebecca A. Owston
Steven T. Green
Ronghua Wei

Inclusive Dates: 10/01/12 – Current

Background — Equipment erosion is a major problem for the oil and gas industry, resulting in many millions of dollars in capital and labor expenditures each year. In addition to the economic aspects of erosion, safety and environmental risks are also matters of concern. A combination of testing and computational modeling is used for estimating erosion rates in industry. Testing is generally expensive, time-consuming, and limited in terms of maximum flow rates/sand concentration that a facility can handle. Computational modeling of erosion is a low-cost alternative to testing for preliminary design analysis. Current erosion models are generally semi-empirical in nature though, and caution must be exercised in their application to practical cases. From a survey of the literature, only a limited number of computational fluid dynamics (CFD) erosion studies have been conducted on oilfield equipment considering realistic fluids. These studies generally do not report the functional relationships of their model coefficients or systematically consider the effect of different geometries, sand concentration, flow rates, etc.

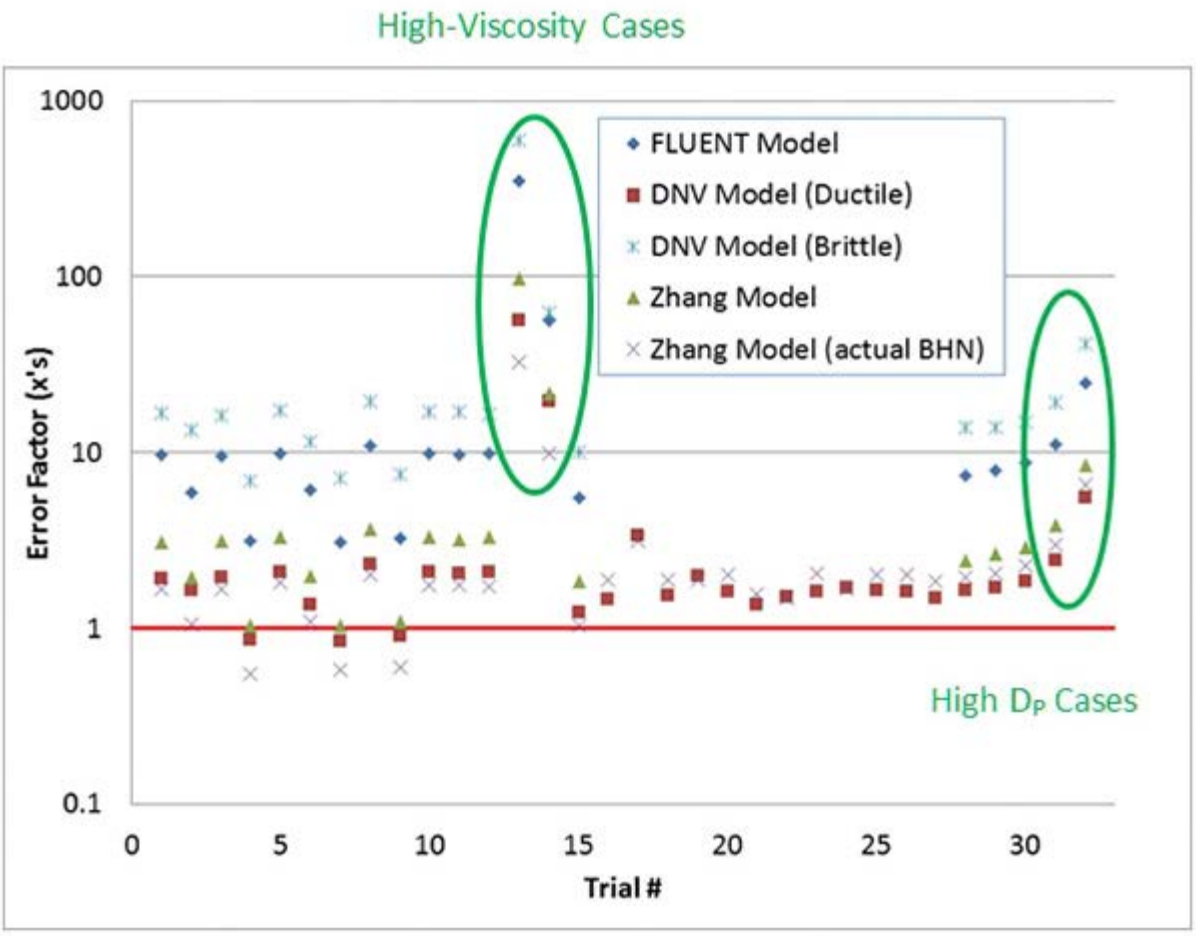

Figure 1. Erosion submodel comparison to experimental data. DNV (Ductile) and Zhang (BHN-adjusted) models show the most promise, demonstrating ~50 percent or lower (factor of 2) error for most cases.

Approach — The objective of this project is to develop and demonstrate capabilities for accurate prediction of erosion using a two-fold approach: computational modeling and experimental testing. Data from each area are intended to complement and enhance the value of the other. Specific goals for the project include:

- Validate common flow-coupled erosion submodels against existing experimental data for water and low-concentration (<10 percent) proppant flowing through simple geometries,
- Use experimental data obtained as part of this project to extend and/or validate CFD submodels for a range of fluid viscosities, concentrations, material hardness, and particle sizes,
- Demonstrate the ability to effectively model erosion in oilfield equipment using CFD.

Accomplishments — Five existing submodels were incorporated into a CFD software package and experimental erosion testing of coupons was conducted over a wide range of conditions. Comparison of modeling and empirical data has shown that two of the submodels exhibited 50 percent error or lower for the majority of cases. As shown in Figure 1, cases with high fluid viscosity or large particle size had the greatest level of error compared to experimental data. Thus, efforts were turned towards creation of a submodel to lower uncertainty over a wider range for these two parameters. Validation of this submodel is currently underway. In parallel to the submodel development, simulation of erosion of a Venturi meter is proceeding, and results will be compared against existing experimental data. This geometry is representative of oilfield equipment prone to erosion failure and demonstrates the applicability of erosion modeling for "real-world" applications.

2014 IR&D Annual Report

Testing and Analysis of Acoustically Induced Vibration Stresses in Piping Systems, 18-R8478

Principal Investigators
Neal Evans
Tim Allison
Nathan Poerner

Inclusive Dates: 07/01/14 – Current

Background — Acoustically induced vibration (AIV) is the phenomenon of high-frequency piping vibration downstream of a high-amplitude noise source, which can potentially lead to fatigue failure of the piping at a branch or welded support. Although AIV has long been a concern in high-capacity gas piping systems, recent capacity increases to aging systems and debottlenecking operations, as well as the development of new higher-capacity systems have led to renewed interest in AIV mitigation strategies. Existing methods of AIV analysis used to predict if a weld failure is likely to occur are based on an incomplete historical dataset that does not properly address the fundamental physics of AIV, the high flow rates and pressure ratios encountered in modern blowdown systems, or the increasingly larger pipe sizes that are being implemented. In many cases, these methods are considered to be overly conservative and costly. Furthermore, AIV mitigation options are limited for existing systems that are predicted to fail.

Approach — Testing will be performed at SwRI's gas blowdown facility to obtain dynamic pressure and stress measurements to validate models of the noise source, internal piping acoustics, and piping stress response for several representative configurations of gas blowdown piping. Several AIV remedies will also be tested for existing piping to characterize the stress reductions of these remedies. Application of associated stress reductions to existing analysis methods will enable SwRI to offer AIV analysis services with improved accuracy. Test data for various remedies will increase the pool of available design and retrofit options.

Accomplishments — The project began during the fourth quarter of 2014. Work completed to date has consisted of hardware procurement, test section assembly, and detailed experimental planning. Testing began in November 2014, and will continue through January 2015, with detailed data analysis to follow. Data analysis and reporting will conclude with an investigation of an updated AIV analysis procedure based on the program results and effectiveness of the AIV treatments.

2014 IR&D Annual Report

Efficient Methods for Uncertainty Propagation in Computational- Fluid-Dynamics-Based Fire PRA, 20-R8271

Principal Investigators
Sitakanta Mohanty
Marc Janssens

Inclusive Dates: 11/14/11 – 12/16/13

Background — U.S. Nuclear Power Plants (NPPs) have recently been allowed to transition from a deterministic fire protection licensing basis to a risk-informed performance-based program. The transition requires a full Fire Probabilistic Risk Assessment (FPRA) to quantify the effect of fire incidents on core damage frequency and large early release frequency. Realistic FPRA involves an accurate evaluation of the performance of critical components for a range of design fires (heat release rates). Ideally, this process heavily relies on the use of computational fluid dynamics (CFD) codes [i.e., Fire Dynamics Simulator (FDS)]. Because CFD codes are computationally intensive (a single run may take days or even weeks), fire modeling is currently limited to point estimates, which do not explicitly account for uncertainties in input parameters and forces the analyst to make conservative assumptions in lieu of full quantification of uncertainty. The traditional Monte Carlo approach for propagating uncertainty requires a large number of CFD simulations (several hundred), which makes uncertainty quantification intractable. There is a strong need for developing an uncertainty quantification method that can propagate uncertainty without sacrificing computational accuracy in FPRA.

Approach — The approach adopted in this project is to propagate input uncertainties in FPRA using a small number of Monte Carlo realizations (a few tens to hundreds as opposed to thousands), which would improve computation time by at least an order of magnitude compared to a pure Monte Carlo method. The methods explored are reliability-based methods that minimize the need for a large number of Monte Carlo realizations to construct a cumulative distribution function (CDF) from the model outputs. The approach involves constructing an approximate CDF from a few Monte Carlo realizations by applying mean value and advanced mean value methods and refining the approximate CDF to the desired level of accuracy by applying an importance-sampling approach. The method involves careful selection of a number of estimation points on the approximate CDF, constructing a CDF through these points, and then repeating the process until the CDF is obtained with the desired level of accuracy for various statistical moments. The results from this method are compared against the regular Monte Carlo method using the stratified sampling method to gauge improvement in computational efficiency. The methods are then tested using a variety of realistic fire scenario examples.

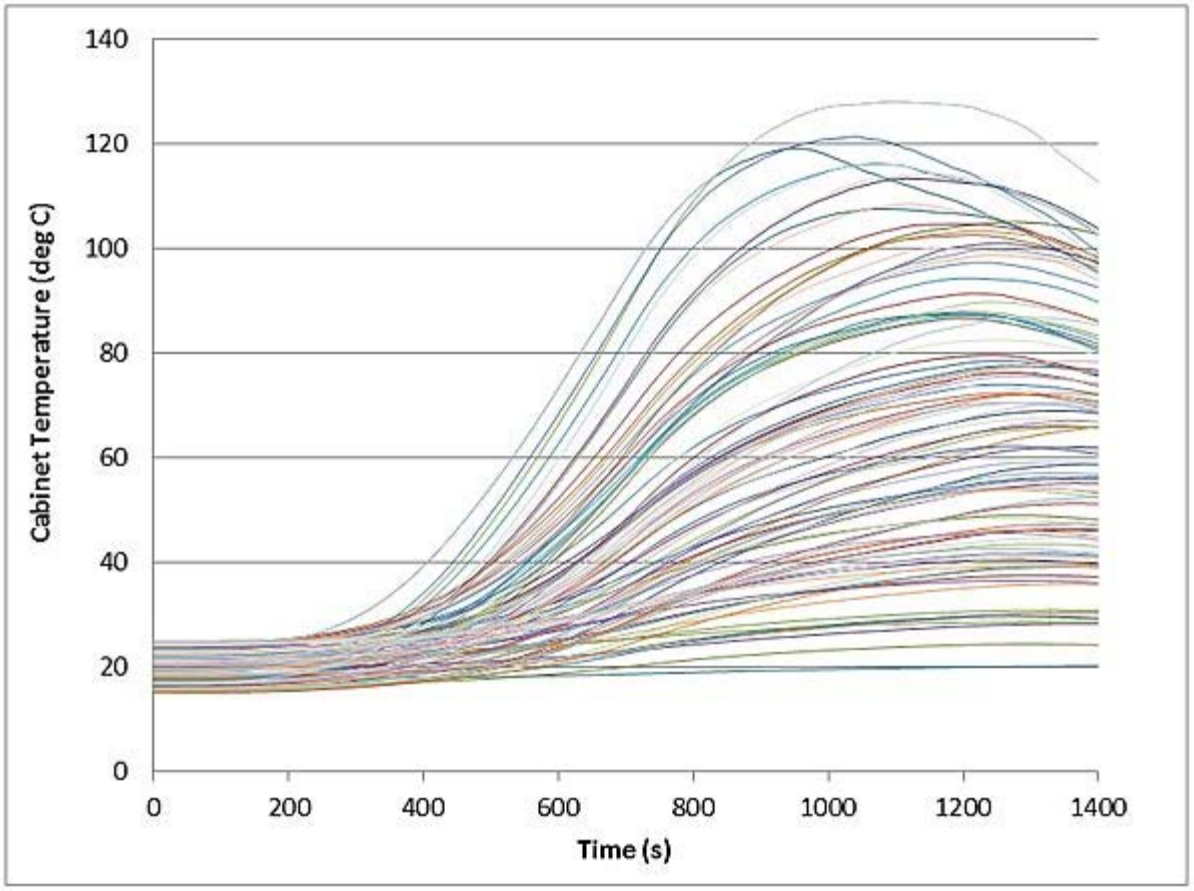

Evolution of temperature in one cabinet from a fire in a neighboring cabinet in the switchgear room. The figure shows 100 of a 1000-realization simulation carried out using a large array of processors on a computer cluster.

Accomplishments — A Monte Carlo (and stratified sampling) FDS model has been developed for benchmarking that will be used once the reliability-based methods are developed. The Monte Carlo FDS code is capable of running the FDS code repeatedly after sampling from input parameter distribution functions (i.e., probability density functions or PDFs), correlating parameters if needed, and propagating one "vector" of input values to a processor on the parallel computer cluster, and collecting FDS code outputs for constructing the model output CDF. An example study of NPP control room abandonment in response to Switchgear Room electric-cable cabinet fire scenario has been explored. Parameters for which uncertainties are to be represented in these test problems and performance function output uncertainties of interest have been identified. Uncertainty is represented via PDFs and propagated through the model for 18 parameters. For a computationally intensive model such as FDS, this is considered to be a relatively large set. Special considerations have been given to time-dependent parameters, such as the heat-release rate curves. Because developing the reliability and Monte Carlo methods requires a large number of trial runs during the model development phase, a faster Monte Carlo CFAST code has been developed to serve as a surrogate for the time-consuming Monte Carlo FDS code. Figure 1 shows a spectrum of temperature evolution curves from which the probability of failure of cables is determined based on a temperature threshold criterion. Reliability-based calculations have been effectively used to extend the failure time prediction to four standard deviations around the mean.

SOUTHWEST RESEARCH INSTITUTE®

2014 IR&D Annual Report

Development of a Wireless Power Transfer Technique for Quick-Charging Inaccessible Electronic Devices, 14-R8363

Principal Investigators
Monica Rivera Garcia
Richard D. Garcia
Joseph N. Mitchell
Grahm C. Roach
Jeffrey L. Boehme

Inclusive Dates: 01/01/13 – 07/01/14

Background — Many system- or mission-critical electronic devices are located off the electrical grid and, as a result, on-board energy storage units in the form of batteries are typically used to supply power to the devices. Due to finite energy storage limits, the energy storage units within these devices must be periodically replaced or replenished. Although the completion of this task is relatively straightforward for devices that are easily accessible, difficulties arise when the devices are located in areas that are inaccessible due to work force limitations, inhospitable terrain, adverse weather, hazardous environmental conditions, mission constraints, or the presence of hostile adversaries. While energy-harvesting systems are often incorporated into off-grid system-critical devices, the magnitude and consistency of the energy generated by these systems are still a concern. The primary objective of this research effort was to develop a wireless power transfer technique capable of quick-charging electronic devices located at inaccessible locations. To accomplish this goal, we developed a portable wireless power transfer technique, determined the appropriate design parameters to minimize charge time while maximizing power transfer efficiency, demonstrated the feasibility of quick-charging electronic devices from a mobile delivery platform, and generated credible data about the wireless transfer process and overall system performance.

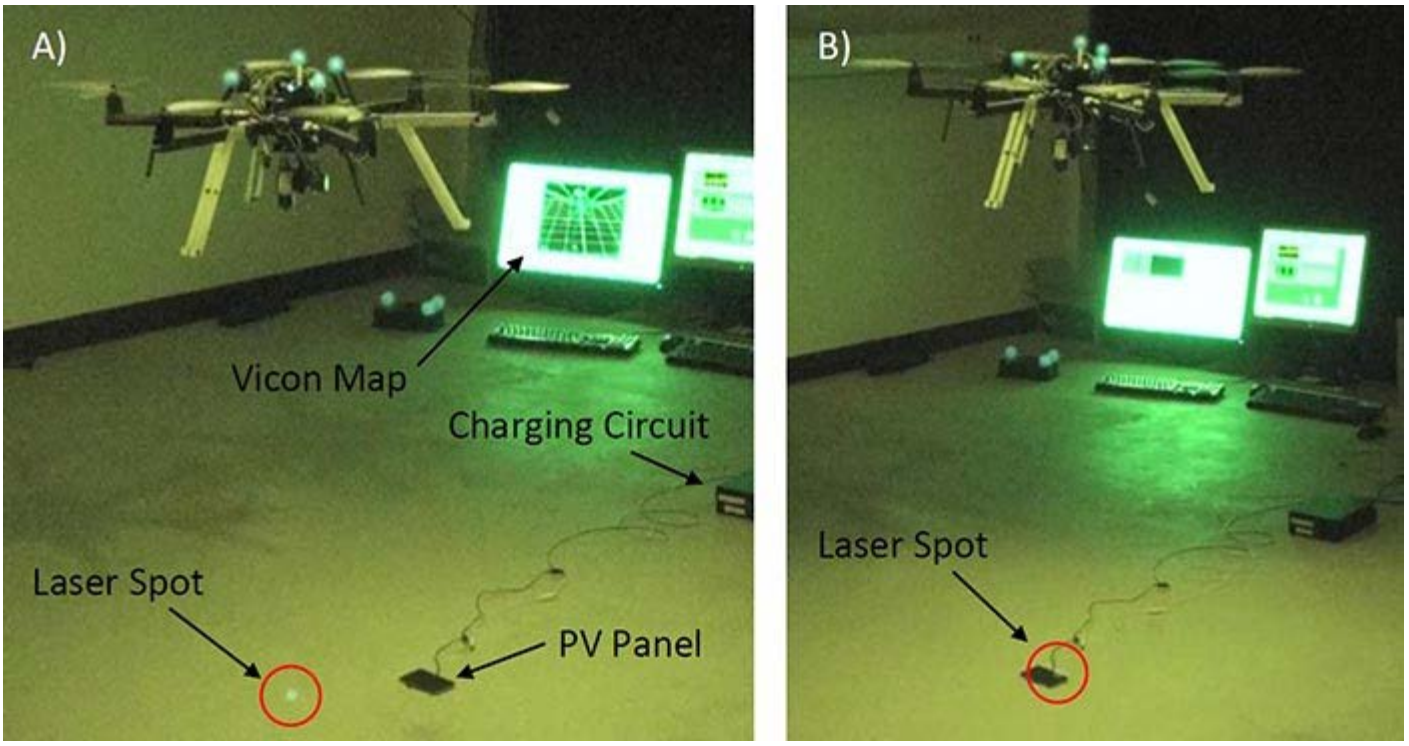

Figure 1. Photos obtained during wireless power transfer flight tests: (a) this photo demonstrates payload functionality. The laser spot is clearly identifiable on the floor mats; (b) this photo demonstrates alignment capability. While the laser spot is visible, the properties and orientation of the photovoltaic (PV) panel make the spot less discernable in the video.

Approach — In this project, power was transferred wirelessly to an inaccessible electronic device via a narrow-band light source. The wireless power transfer process is unique from existing light-based wireless power transfer systems in that it can supply power to electronic devices in a recurrent, non-continuous fashion, store the delivered energy quickly in supercapacitors for abbreviated charge durations, and enable power transfer beyond the operator's line-of-sight via the use of an unmanned aerial system (UAS).

Accomplishments — During the project, the team successfully transferred power via a laser-based system over a separation distance of one meter. In an effort to expedite the charging process, the team also designed and constructed a multi-phase supercapacitor charging circuit and investigated the parameters that influenced overall charge time. To facilitate power transfer beyond the operator's line-of-sight, the research team designed and constructed a wireless power transfer payload compatible with a small commercial off-the-shelf UAS. The UAS and gimbaled payload were modified to increase the hovering and pointing stability of the platform and payload during autonomous flight modes. The program culminated with indoor flight tests of the complete wireless power transfer system.

SOUTHWEST RESEARCH INSTITUTE®

2014 IR&D Annual Report

Nanogenerators for Energy Harvesting, 14-R8405

Principal Investigators
Jerome A. Helffrich
W. Royall Cox
John D. Harrison

Inclusive Dates: 07/02/13 – 12/31/14

Background — In the evolving field of piezoelectric material technology, fabrication methods have been developed to make arrays of long, thin piezoelectric fibers. Such fibers present interesting new opportunities for energy harvesting from incidental motion (walking, vibration, wind, etc.) by the piezoelectric conversion of mechanically generated stress to electric current. Because the piezoelectric material can be made flexible, strands may be woven into clothing, incorporated into shoes, or imbedded in randomly moving systems such as rubber vibration isolators. These "nano-generators," consisting of arrays of high-aspect-ratio, aligned nanowires are fabricated on flexible substrates, so that current may be produced by simply bending or stretching them.

Approach — Our objective is to advance nanogenerator fabrication technology by developing processes for making dense arrays of nanowires over larger areas with current outputs sufficient to run very low power devices that can be imbedded onto clothing. We have chosen PZT (lead zirconate titanate) for the piezoelectric material because of its relatively high electromechanical conversion efficiency. To fabricate arrays of PZT nanowires, we have used a process called "electrospinning." Here droplets of a precursor fluid containing the requisite elements are ejected from a needle that is maintained at a high electric potential (10 to 30 kV) relative to collection electrodes located some distance below it. As each droplet emerges from the needle it is elongated into a wire shape and pulled toward the grounded electrodes by the strong electrostatic field. The alignment of these nanowires to each other is achieved by using, for collection substrates, arrays of parallel chromium strips fabricated by magnetron sputtering onto quartz wafers. The electrospinning is done inside a dry box to insure evaporation of solvents from the droplets in flight. After electrospinning, the nanowire arrays are annealed at a high temperature (650°C) to drive out the organic components. Then they are electrically poled (4 kV/mm at 130°C) to enhance growth and alignment of the crystals within the nanowires.

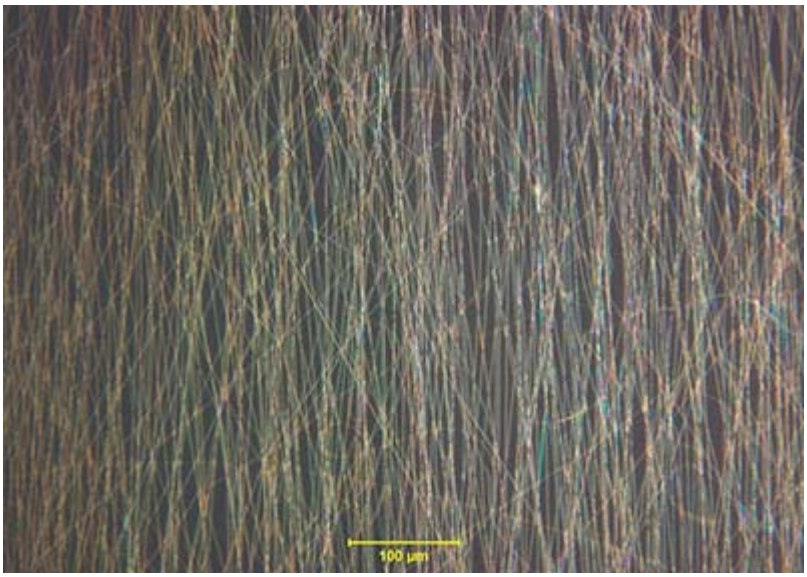

Figure 1. Array of 2 mm long PZT nanowires aligned vertically between two horizontal chromium electrode strips (not shown) just above and below photo.

Accomplishments — We have been able to electrospin dense arrays of highly aligned PZT nanowires 2 mm in length, which is believed to be approximately four times longer than that achieved previously by other researchers. We have also developed processes for annealing and poling these arrays, and we plan to demonstrate the current generation in the near future.

2014 IR&D Annual Report

Artificial Muscle Risk Reduction and Cookbook, 14-R8465

Principal Investigators
Andrew Moore
Alexis Prust
Grahm Roach

Inclusive Dates: 04/03/14 – 10/18/14

Background — Artificial muscles have applications particularly in robotics and aerospace, where compact, lightweight and high-strength actuators are needed to perform many tasks. Electric motors are insufficient in some cases, particularly when a high-strength actuation is performed at slow speeds, but artificial muscles have had limited success as a replacement. This is due to a variety of factors, including high hysteresis, expensive or exotic material composition, and limited actuation ranges. In February 2014, Haines et al., published an article in Science entitled "Artificial Muscles from Fishing Line and Sewing Thread." The article described a low-cost temperature actuated polymer artificial muscle (TPAM) that is stronger than human muscle, linear with temperature, and has a greater actuation range than nickel-titanium shape memory alloys. The device appeared to address many of the downsides of previous artificial muscles, but a formal investigation was needed to determine whether these artificial muscles might be practical for future designs.

Approach — Over the course of this two-phase effort, the following tasks were attempted:

Phase I:

- Develop procedures for manufacturing artificial muscles from fishing line.
- Replicate the behaviors described in the original Science article.
- Integrate an artificial muscle into a proof-of-concept mechanical assembly.

Phase II:

- Model the actuation behavior of an artificial muscle as a temperature-dependent ideal spring.
- Perform an in-depth materials analysis on the fishing line.
- Build an empirical dataset to refine the ideal spring model.
- Build reference designs to validate the spring model.

Accomplishments — The tools to manufacture and characterize coiled nylon artificial muscles were acquired or built, and procedures were honed experimentally. Muscles were formed through a three-step process of twisting, coiling, and annealing a length of fishing line. Once annealed, the muscles were characterized in a custom vertical tube oven instrumented to measure muscle length under a constant load. The muscle length, when plotted over a range of temperatures, was consistent with the behavior shown by the original researchers, but there was insufficient data in the original paper to directly compare our results to theirs, and they did not respond to direct inquiries.

The initial attempt to model the muscles as temperature-dependent springs was not successful because the muscle elongated for several minutes at a constant temperature and load. This creep made it difficult to characterize the muscles under dynamic loads. Figure 3 shows the creep in a muscle at a constant temperature over a seven-minute period after being loaded with a 200g weight. Two-thirds of the overall elongation occurred almost instantaneously upon loading the muscle, but it continued to stretch slowly for several minutes afterward. This indicated that TPAMs could not be modeled as ideal springs as originally

proposed.

To refine the actuation model, remaining resources were dedicated to better understanding the dynamic behavior and thermal performance of the muscles and to characterize the chemical makeup of the fishing line. In parallel with the TPAM characterization, an electrically controlled TPAM was integrated into the body of a small unmanned aircraft and successfully actuated the rudder. This system was intended as a tool to visually illustrate TPAMs to clients. The TPAM weighed less than 1g, generated more than 200g of force, and served as a direct replacement for an electric motor.

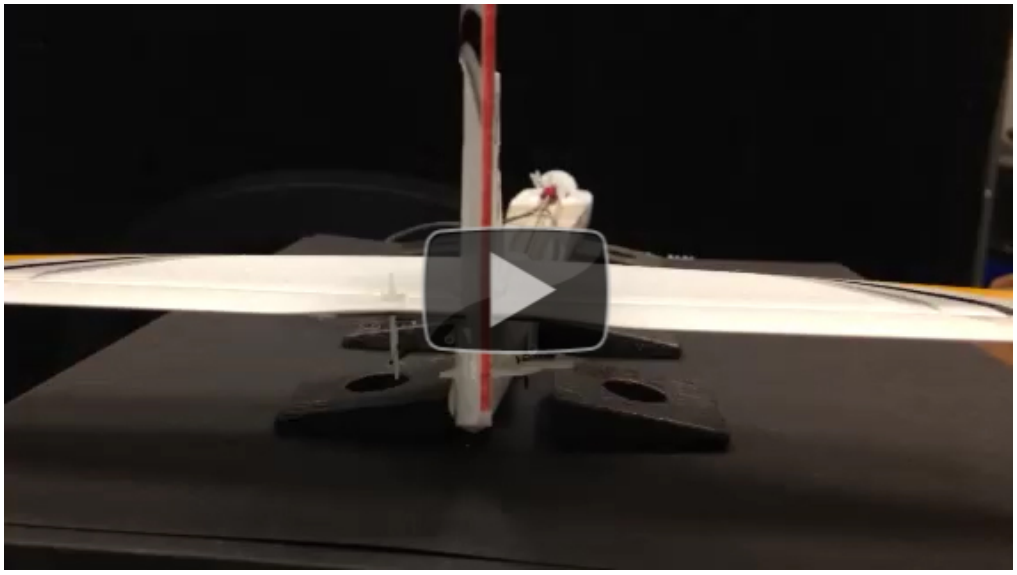

Video of a TPAM demonstration.

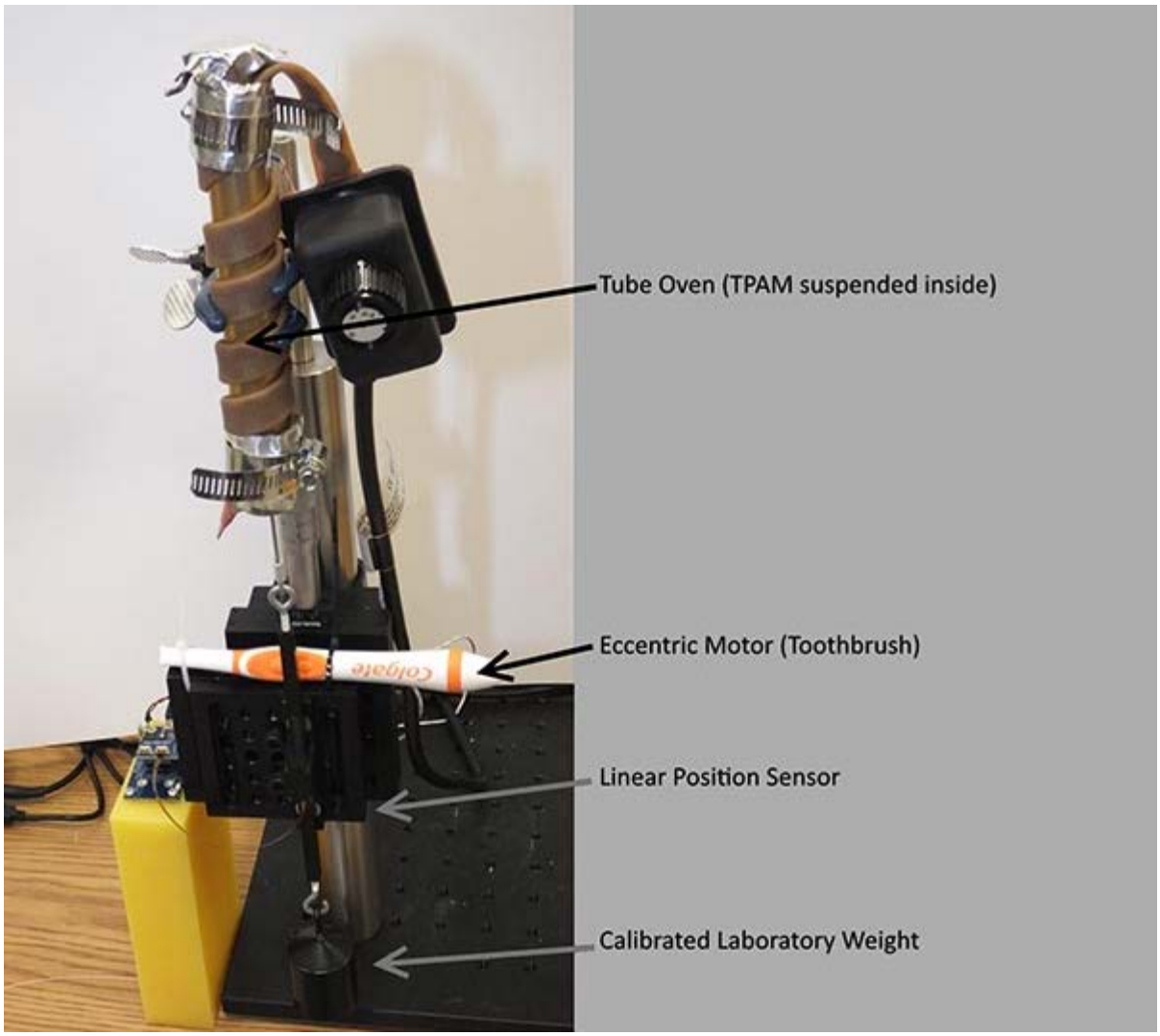

Figure 1. Test oven for characterizing artificial muscles.

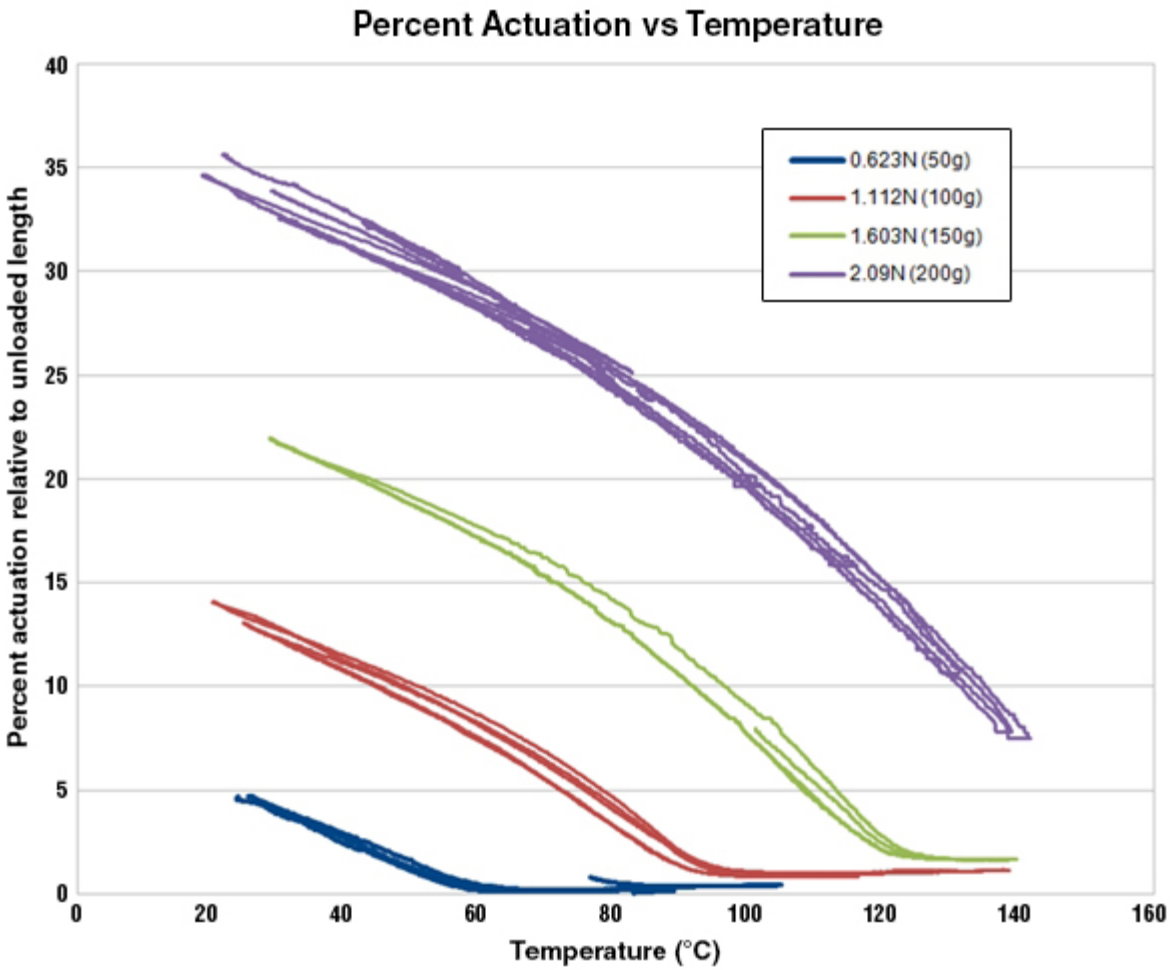

Figure 2. Temperature actuation of an artificial muscle under a variety of static loads.

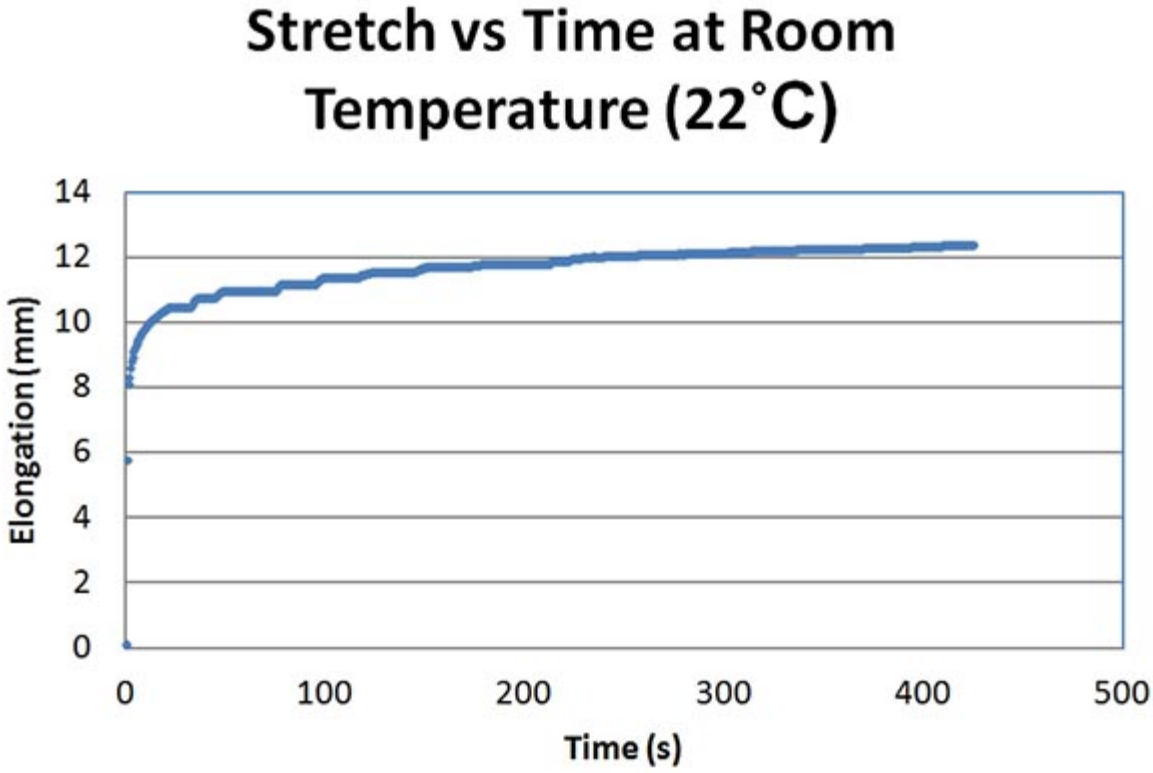

Figure 3. A muscle slowly elongates for several minutes when loaded.

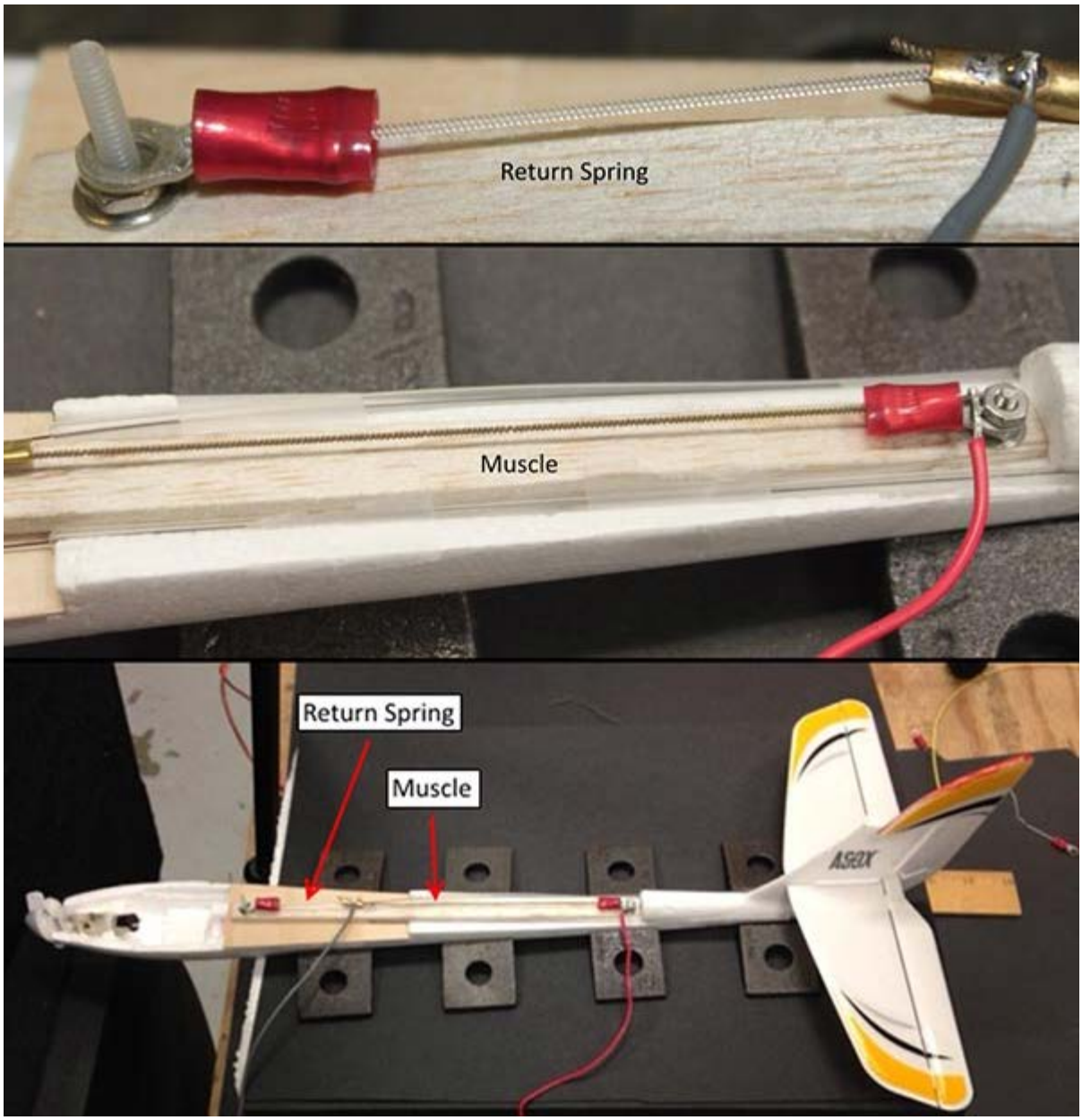

Figure 4. An artificial muscle is integrated into an unmanned aircraft.

2014 IR&D Annual Report

Design and Analysis of Device to Capture Stratospheric Air Samples, 15-R8446

Principal Investigators
Kathleen Mandt
Edward Patrick
Ryan Blase
Wendy Tseng
Kristin Favela
William Williamson

Inclusive Dates: 01/01/14 – Current

Background — This work is a collaborative effort between two SwRI technical divisions to design and analyze a device to collect atmospheric samples in the Earth's upper atmosphere. The purpose of this device is to address a serious gap in Earth atmospheric measurements needed to understand the energy balance, transport and chemistry in the upper atmosphere. The device will include two components. The first is the commercially available AirCore®, which collects columns of air during descent from high altitudes in a manner that preserves an altitude profile of constituents such as carbon dioxide, methane and nitric oxide. This device has been proven up to altitudes as high as ~30 km. The second component is a discreet sampling device that will collect air samples of 1L in volume for laboratory analysis of isotopic composition.

Approach — The project had four questions to address:

- What is the upper altitude (or lower pressure) limit of AirCore?
- What is the amount of fractionation that takes place as air enters and within the AirCore tube as a function of pressure?
- What is the upper altitude limit for collecting a discrete sample as a function of flight vehicle descent velocity?
- What other greenhouse gases can be measured using the device?

Accomplishments — We completed the initial setup of the system for evaluating the AirCore and conducted tests to characterize the system. In the process of characterizing the system, we found preliminary evidence for mass fractionation in the column and have determined the fill time for the column under static conditions. Further tests have shown signs of significant diffusion suggesting that there may be a lower pressure limit for use of AirCore. We are investigating this further.

2014 IR&D Annual Report

Two-Fault-Tolerant Fault Detection and Isolation on a Resource Constrained Platform in Space, 15-R8459

Principal Investigators
Meredith B. Lecocke
Justin Blount

Inclusive Dates: 04/01/14 – Current

Background — Two-fault-tolerant avionics provide critical command and control capabilities for not only manned space programs in which personal safety of the crew is at stake, but also robotic spacecraft featuring time-critical quick response sequences, such as close rendezvous operations, in which a single fault could jeopardize the spacecraft. Complex distributed systems in space are susceptible to multiple sources of faults, including sensors, actuators, processors, transient radiation-induced errors (single event upsets, or SEUs), communications links, and timing faults. To be two-fault-tolerant, the system must be able to withstand any two of these faults occurring simultaneously. This complex and multivariate problem of failure detection, isolation, and recovery (FDIR) takes on additional complexity when constrained by the unique environment and resources available to space-based systems. The goal of this project is to produce an over-arching two-fault-tolerant architecture combining state-of-the-art fault tolerance approaches that execute within the resource constraints of space-based platforms.

Approach — Our technical approach for a two-fault-tolerant architecture combines decades of research within the aerospace, networking, and drive-by-wire industries. Our novel architecture combines the techniques of group membership protocols, reconfiguration tables built with formal methods, message voting (Byzantine fault tolerance), distributed time synchronization, and analytical redundancy. Since these methods must work within the resource constraints of space, we must also produce an efficient embedded implementation of this new architecture with reasonable functional and time-critical performance.

Accomplishments — During this first half of the performance period, we made progress on three of the five fault tolerance algorithms. The main emphasis was developing a mature system model in Answer Set Prolog to prove two-fault tolerance of the system and automatically generate lookup tables for efficient embedded implementation of fault detection and fault response. This work has been accepted for publication in the IEEE Aerospace Conference in March 2015. In addition, we developed a testbed in which nodes pass messages in several rounds to collaboratively determine the system time tick. Results from the message voting algorithm showed consensus can be obtained within tolerable limits with three rounds of messaging. This testbed laid the groundwork for the evaluation of the remaining fault-tolerant algorithms, to be completed in the second half of this project.

2014 IR&D Annual Report

Humanized Organophosphorus Hydrolase Expressed in Human Embryonic Kidney Cells: Pharmacokinetics in the Guinea Pig Model, 01-R8280

Principal Investigator
Tony E. Reeves

Inclusive Dates: 01/02/12 – 07/31/14

Background — Current proteins under consideration for use as prophylactic drugs in the treatment of organophosphorus nerve agent intoxication lack sufficient circulatory half-life to afford reasonable in vivo protective efficacy for extended periods of time. Most are cleared from circulation rapidly and possess half-lives on the order of hours. The vast majority of proteins found in the blood/plasma are glycosylated, meaning they have carbohydrates (sugar molecules) covalently linked to their surface. Using exogenous or "non-self" proteins with dissimilar glycosylation, or entirely lacking this glycan surface modification, makes them susceptible to clearance from the blood stream by multiple mechanisms, and it is generally accepted that this rapid clearance results from the carbohydrate decoration on the surfaces of these proteins and not the protein sequence itself.

Of those proteins under investigation, the most promising are of nonhuman origin (bacterial) or use nonhuman expression systems for their production (bacterial, plant, transgenic animals). To extend the circulatory half-lives of these molecules to days rather than hours, it is necessary to modify their surface decorations. Using an expression system that can accomplish this during expression is a significant cost saving measure over post-purification modification by chemical means.

Approach — To address the issue of "non-self" carbohydrates, this project is using human embryonic kidney cells (HEK 293) to express a protein encoded by a gene of bacterial origin. This protein has been successfully expressed and glycosylated in transgenic corn.

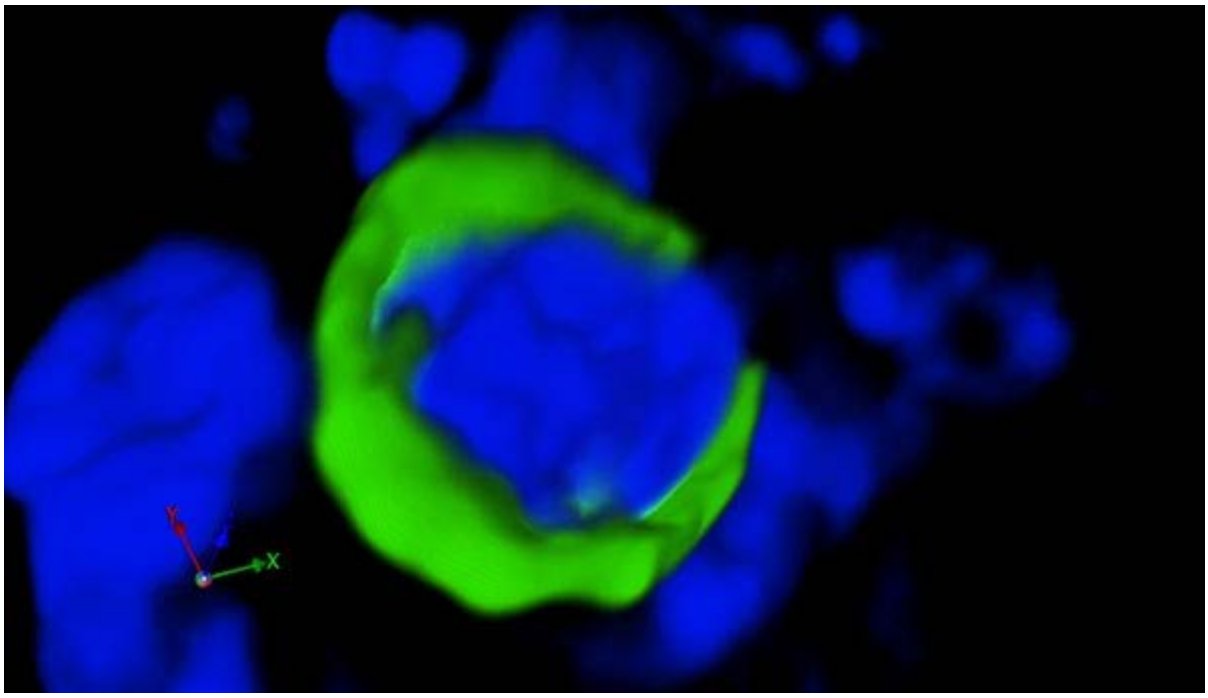

Three-dimensional confocal image of a human kidney cell expressing OPH. The nuclei are stained blue and the fluorescently labeled OPH appears green in the cytoplasm.

Accomplishments — The genetic information encoded by the bacterial organophosphorus hydrolase (OPH) gene has been optimized for expression in human cells. To achieve this, the codons for each amino acid of OPH were modified to maximize translation efficiency for high levels of protein expression. The humanized OPH gene was used to generate transient and stably transfected HEK cell lines and these transgenic cell lines express functional humanized OPH at a constant level over time. Preliminary data indicates the protein hydrolyses the pesticides paraoxon and demeton-S, as well as the nerve agent VX, but is not glycosylated as expected. It has not been determined if the cells initially fail to glycosylate the protein or if the carbohydrates are subsequently removed by cellular processing. Detailed mass analysis is planned for peptide fragments to determine if there is carbohydrate remains on the amino acid attachment sites to answer this. New gene constructs are being developed to have the expressed protein secreted from the cell into the media as it is being expressed to alleviate intracellular processing.

SOUTHWEST RESEARCH INSTITUTE®

2014 IR&D Annual Report

High Octane Number Gasoline Production from Lignin, 01-R8384

Principal Investigators
Maoqi Feng
Darius Daruwalla

Inclusive Dates: 04/01/13 – 09/30/14

Background — Biofuels production from lignocellulosic biomass would reduce the nation's reliance on imported fossil fuels while yielding economic benefits. Of the three major components in lignocellulosic biomass — celluloses, hemicelluloses, and lignin — lignin is the most difficult to convert. This project worked to develop chemical methods for processing lignin through the steps of dissolution, depolymerization, deoxygenation and separation to yield hydrocarbons in the gasoline boiling point range.

Approach — Ionic liquids were used as solvents, and lignin was catalytically depolymerized in a hydrogen environment generated in situ from formic acid decomposition to prevent repolymerization of the fragmented molecules. There were two steps in the process: the oxygenates produced by depolymerization in Step 1 are not good fuels, the subsequent Step 2 catalytic hydrodeoxygenation of the substituted phenolic compounds in hydrogen was used to produce hydrocarbons.

Two kinds of lignin were used as the feed: kraft lignin from a commercial source and organosolv lignin extracted from wood chips. Three ionic liquids, 1-n-butyl-3-methylimidazolium chloride, 1-ethyl-3-methylimidazolium chloride, 1-n-butyl-3-methylimidazoline trifluoromethanesulfonate, and two deep eutectic solvents, were used as solvents in the study. Figure 1 shows the reactor for Step 1 tests.

Figure 1. A batch reactor for lignin depolymerization

Figure 2. A continuous reactor for catalyst development on oligomers hydrogenation

Accomplishments — Kraft lignin was successfully depolymerized to phenols, anisole, and substituted phenols at reasonable yields (~60 percent) at 200°C in ionic liquids. Organosolv lignin (acid soluble) extracted from pine wood was successfully depolymerized to phenols and substituted phenols at higher yields (more than 70 percent) in ionic liquids. Different catalysts were evaluated, possibly by facilitating the decomposition of formic acid to hydrogen and CO_2. The depolymerized products were extracted by organic solvent and used as feed for hydrogenation study.

In the hydrodeoxygenation catalyst development, both model compounds and lignin depolymerized oligomers were used as the feed stocks. The reactor is shown in Figure 2. Three model compounds, phenol, anisole and a substituted phenol, were first studied. A series of catalysts, including Pd/alumina, Ni/alumina, Ni-Mo/alumina, and some proprietary catalysts prepared in the lab, were tested for the catalytic hydrodeoxygenation activity. Phenol and substituted phenol were converted to benzene quantitatively. A mixture of benzene and phenol was produced from anisole. Two catalysts were found to be very active and contaminants-tolerant for hydrogenation of the model compounds and the oligomers for depolymerized lignin. Overall thermal efficiency of the process was estimated to be 86.9 percent, which compares favorably with the Fischer-Tropsch process.

2014 IR&D Annual Report

Development of a Low-Cost Method of Treating Flow-Back Water from Hydraulic Fracturing, 01-R8414

Principal Investigator
Maoqi Feng

Inclusive Dates: 09/01/13 – 08/31/14

Background — Water consumption in hydraulic fracturing is substantial, and water resources are scarce for most shale plays in the U.S., thus water recycling is preferred. Flow-back water from hydraulic fracturing is difficult to treat because of high concentrations of dissolved inorganic solids and organic hydrocarbons. Use of current technologies, such as reverse osmosis, electrodialysis, and membrane technologies, for treating oil and gas produced waters has been limited by the presence of large amounts of total dissolved solids (TDS) and hydrocarbons in these waters, which can cause rapid and severe deterioration of membranes. Also, most current technologies are costly and often unable to meet the new, rigorous water quality standards. New, low-cost, and readily implemented approaches are needed for managing water associated with developing conventional and unconventional oil and gas reserves. The present work advanced the development of a sustainable, low-cost sorbent process for treatment and management of flow-back and produced waters. This technology will make it possible for on-site water reclamation and reuse, as well as waste minimization.

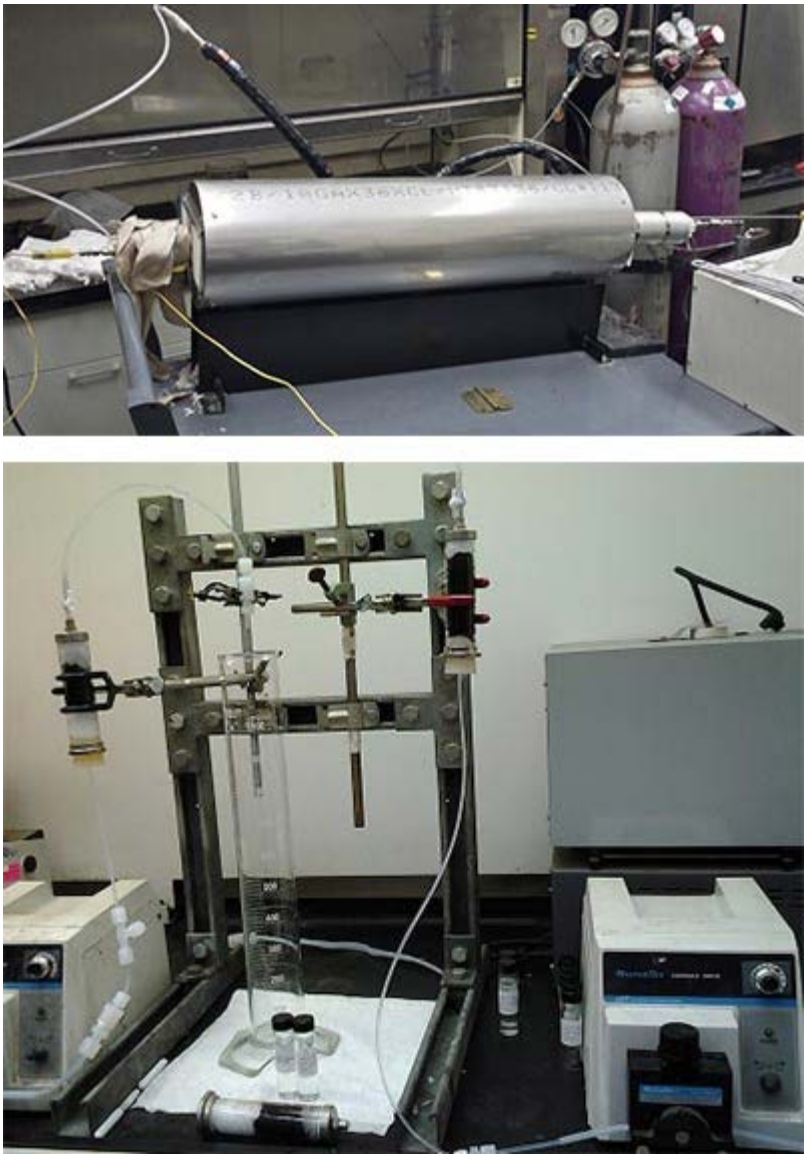

Figure 1. Top: biochar production reactor; Bottom: sorbent bed evaluation under continuous flow.

Approach — This project used a low-cost biochar, an adsorbent produced from forestry and agricultural wastes, that can significantly reduce the cost for treating hydraulic fracturing wastewater and similar water tailings. The scope of the work included 1) producing biochar samples, 2) testing biochar produced under several conditions as a cost-effective method for flow-

back water cleanup, and 3) evaluating the efficiency of major contaminants removal by the biochar thus produced, e.g. total dissolved solids and hydrocarbons.

The study focused on removing typical hydrocarbons, colloids, and the ions of Na, Ca, Mg, Sr, K, Cl^-, CO_3^{2-} from solutions of known concentrations; these ions are commonly found in produced water from tight shale fractured wells. Commercial activated carbon, coconut char and biochar produced from pine and oak wood at different pyrolysis temperatures, were used as the adsorbents (see Figure 1). Two types of batch studies, stagnant and mixed, and one continuous flow study in packed columns were used to investigate adsorption capabilities.

Accomplishments — The major achievements for this project are:

- Biochar preparation and characterization: Biochar was prepared from different woodchips (pine and oak), cellulose, lignin and plant husks, at different temperatures: 350°C, 450°C, and 550°C.
- Biochar characterization: Biochar was characterized by elemental analysis and several surface analysis techniques, including scanning electron microscopy and energy dispersive X-ray.
- Biochar for inorganic salts removal (adsorption capacity for each individual salt). The inorganic salts, including NaCl, K_2CO_3, CsCl, $MgCl_2$, $CaCl_2$, and $Sr(NO_3)_2$, were tested in both batch and continuous mode. The adsorption capacity data was obtained for these ions.
- Ocean water desalination study: The total salt removal and selectivity adsorption of NaCl and $MgCl_2$ versus the other solutes were observed.
- Hydrocarbons removal (total adsorption): Biochar was found effective for hydrocarbon adsorption from a water solution/suspension.
- Removal of solid fines simulated with clay was evaluated.
- Biochar regeneration with steam was tested with notable success.

In summary, the technology developed in this project makes it possible for on-site water reclamation and reuse, as well as waste minimization for flow-back water treatment from hydraulic fracturing. This technology could be used as a stand-alone method (see Figure 2), or a pretreatment unit or polishing step to be combined with other technologies, such as membrane technology or biotechnology. The method has great potential to reduce substantially the overall costs and environmental impacts associated with gas and oil production by many other methods.

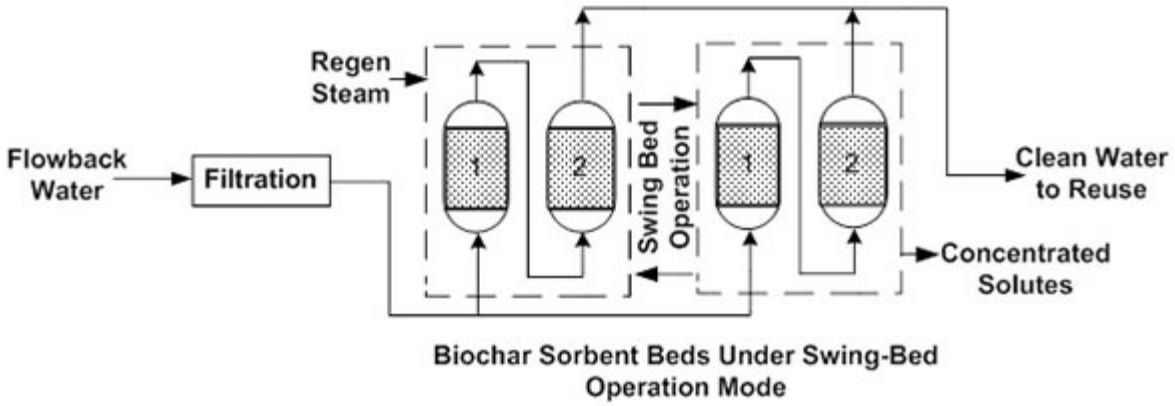

Figure 2. Process flow diagram for flowback water treatment with biochar.

SOUTHWEST RESEARCH INSTITUTE®

2014 IR&D Annual Report

Investigation of the Rheology and Tribology Properties of Mono-Oleate for Use as an Additive for SAE J1488-10 Emulsified Fuel-Water Separation Test Method, 08-R8389

Principal Investigators
Gary Bessee
Dr. Andrew Clark
Dr. Peter Lee
David Herrera

Inclusive Dates: 04/01/13 – 04/01/14

Background — Diesel fuel-water separation is a major process for protecting the fuel system and engine components in any vehicle or machine. The water separation process becomes increasingly more difficult with the addition of alternative fuels (biodiesel) and other various additives. Multiple joint industry programs (JIP) and internal research projects have been performed addressing these issues over the past few decades; however, none has investigated the rheology and tribology properties and the resulting fuel water separation characteristics. The objective of this project was to investigate these properties as well as new gas chromatography techniques to better understand fuel water separation, particularly with biodiesel fuels, and how SwRI can assist the industry with improving and standardizing the testing process.

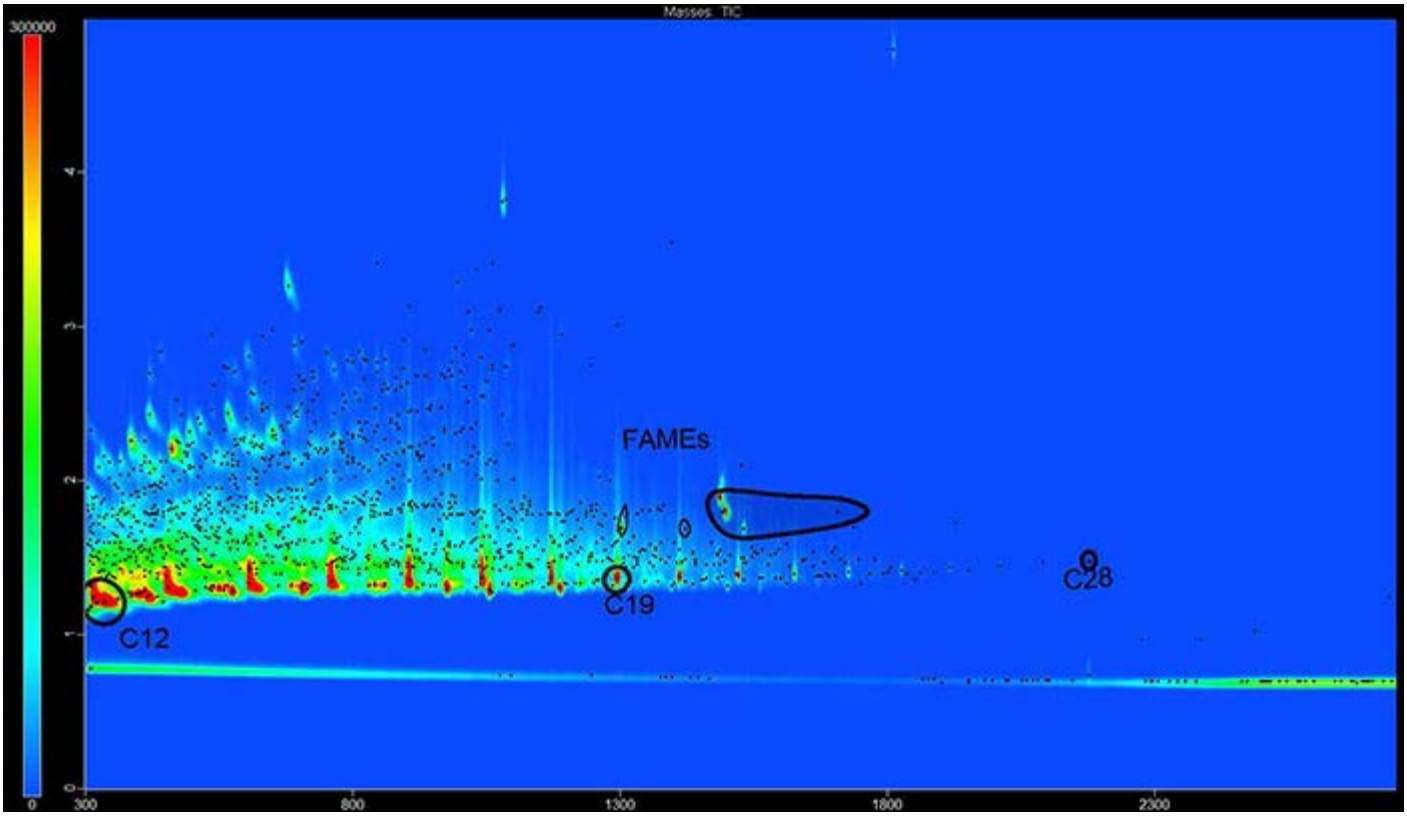

Figure 1. Example of GCxGC/MS data from biodiesel fuel sample.

Approach — The technical approach for this project was to use mono-oleates to provide a "standard" compound to simulate biodiesel fuels. Both new technologies and instrumentation were used for evaluating "stable" emulsions in an attempt to add some science to the understanding of fuel water emulsions. Since variability of the mono-oleate is the major issue, mono-oleates from many manufacturers and suppliers were obtained to determine the variability of the products both at a compositional and performance application. Some of the proposed analytical tools/instrumentations to be used for this project include environmental electron microscope (ESEM), GCxGC/MS, water droplet characterization, strain-controlled rheometer, tensiometer, water separation test stand and a laser diffraction particle sizer.

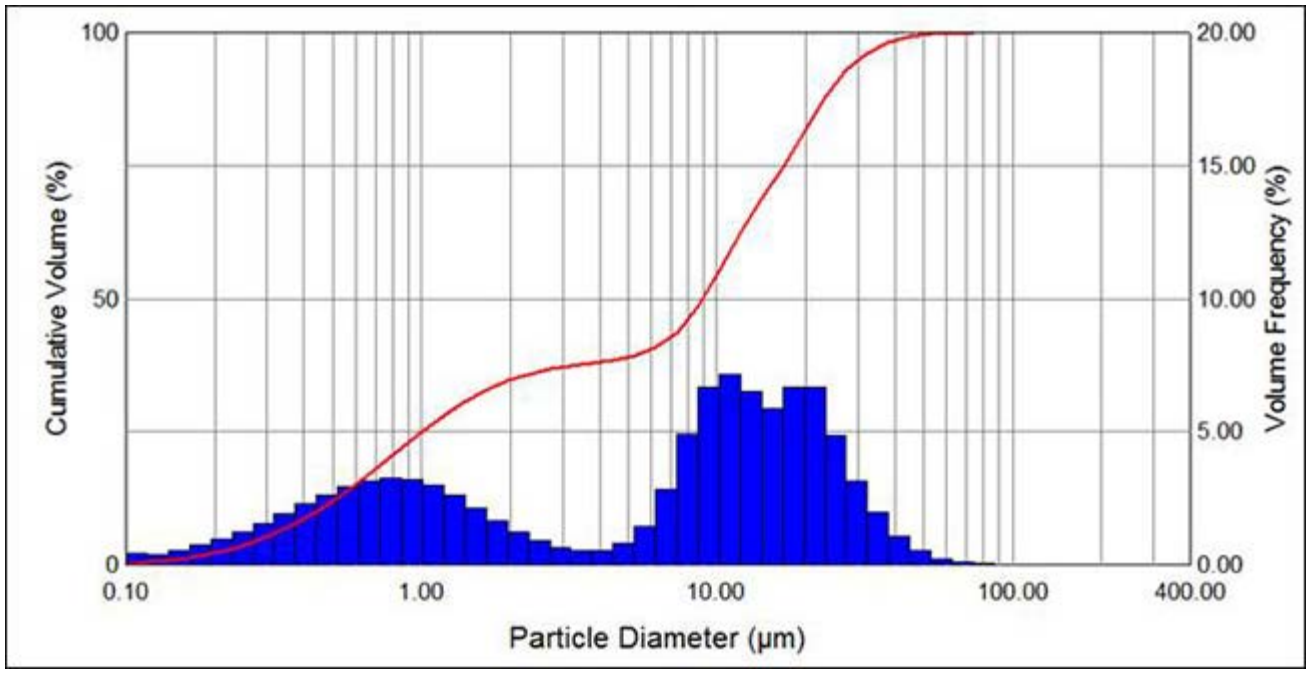

Figure 2. Typical water droplet distribution for biodiesel with an interfacial tension of 15 mN/m.

Accomplishments — The GCxGC/MS analysis determined that the selected mono-oleates, at least compositionally, are different; see Figure 1. Although claims that mono-oleates are 50 to 98 percent purity, this analysis illustrates many foreign materials of various quantities that are not in all the samples. The rheology and tribology results did generate some interesting data, but due to the nature of the emulsion, e.g., low viscosity, there was difficulty making the measurements. The cone and bob device was able to differentiate between the mono-oleates, and shows potential for better understanding water separation characteristics. The laser diffraction instrument provided significant data, demonstrating the water droplet distributions generated by each mono-oleate; see Figure 2. The water droplet distributions provided important data to allow us to better understand the impact of different biodiesel fuels and why fuel water separators do not perform as well with biodiesel as compared with just diesel fuel. The data generated from this project has resulted in a joint industry program, and improvements in the industry water separation test method.